UNIVERSITAT DE BARCELONA

Metabolic vulnerabilities of rhabdomyosarcoma: insights into the role of ASS1

Paola Monaco

Universitat de Barcelona

Facultat de Farmàcia i Ciències de l'Alimentació

Programa de Doctorat en Biomedicina

METABOLIC VULNERABILITIES OF RHABDOMYOSARCOMA: INSIGHTS INTO THE ROLE OF ASS1

Memòria presentada per Paola Monaco
per optar al títol de Doctora per la Universitat de Barcelona

Tesi realitzada al Grup de Recerca en Sarcomes de l'Institut d'Investigació Biomèdica de Bellvitge sota la direcció del Dr. Òscar Martínez Tirado i la Dra. Cristina Muñoz Pinedo, i la tutoria del Dr. Albert Tauler Girona

Paola Monaco

Dr. Òscar Martínez Tirado **Dra. Cristina Muñoz Pinedo** **Dr. Albert Tauler Girona**

Barcelona, 2022

IDIBELL Institut d'Investigació Biomèdica de Bellvitge

Universitat de Barcelona

Rhabdomyosarcoma (RMS) is the most prevalent soft tissue sarcoma (STS) in children and adolescents. RMS Alveolar subtype (ARMS) is driven by PAX3-FOXO1, a fusion protein originated from a chromosomal translocation. Metabolic reprogramming is considered one of the main hallmarks of cancer. To sustain enhanced cell proliferation and build new biomass, many metabolic requirements must be satisfied by tumor cells through the activation of gene expression and protein regulation programs. The main objective of our research project is to analyze the effects of PAX3-FOXO1 expression on RMS metabolic landscape. Starting from transcriptomic analysis of publicly available data, we identified the Argininosuccinate Synthase 1 (ASS1), an enzyme of the urea cycle involved in the *de novo* synthesis of arginine, as a putative transcriptional target of PAX3-FOXO1. It has been described that ASS1 plays a role in enhancing tumor progression and invasion in different cancer types. Despite all the evidence that describe other STS as ASS1-deficient, we found that RMS cells overexpress ASS1. Particularly in ARMS, PAX3-FOXO1 silencing results in ASS1 mRNA downregulation, confirming that the fusion protein could regulate ASS1 transcription. CRISPR-Cas9-mediated ASS1 knockdown impair ARMS migratory capability *in vitro* without affecting cell proliferation, suggesting that arginine metabolism rewiring could be promoting ARMS metastatic phenotype. Furthermore, *in vivo* tumorigenesis resulted to be notably delayed in mice injected with ASS1-silenced ARMS cells, confirming the oncogenic role of the enzyme in these cancers. Finally, we performed a microarray to study the transcriptional signature induced by ASS1 knockdown. The elongation factor EEF1A2, extensively described in literature to display oncogenic activity in cancer, resulted to be transcriptionally downregulated upon ASS1 silencing. Consequently, AKT phosphorylation was also found to decrease, together with the activation of S6K1 and S6 downstream effectors. Further experiments are needed to better describe the upstream signaling involved and the precise mechanism that links ASS1 to EEF1A2 downregulation. In conclusion, our work suggests that ASS1 upregulation could be involved in sustaining the tumorigenesis and metastatic process of ARMS. Thus, the inhibition of this pathway could represent a promising tool to target RMS metabolism, hopefully leading to the potential development of more effective targeted therapies.

TABLE OF CONTENTS

LIST OF ABBREVIATIONS

ARMS	Alveolar rhabdomyosarcoma
ASS1	Argininosuccinate synthase 1
ATP	Adenosine 5′-triphosphate
cDNA	Complementary DNA
CM	Conditioned media
DNA	Deoxyribonucleic acid
ERMS	Embryonal rhabdomyosarcoma
FBS	Fetal bovine serum
H&E	Haematoxylin & Eosin
LC-MS	Liquid chromatography-mass spectrometry
Luc	Luciferase
miRNA	Micro RNA
mRNA	Messenger RNA
NADPH	Reduced nicotinamide adenine dinucleotide phosphate
NO	Nitric oxide
PBS	Phosphate-buffered saline
PCR	Polymerase chain reaction
PRMS	Pleomorphic rhabdomyosarcoma
qPCR	Quantitative real-time PCR
RMS	Rhabdomyosarcoma
RNA	Ribonucleic acid
RT	Room temperature
SCR	Scrambled
siRNA	Small interfering RNA
SpRMS	Spindle cell/sclerosing rhabdomyosarcoma
STS	Soft tissue sarcoma
UC	Urea cycle
WB	Western Blot

INTRODUCTION

1. Soft tissue sarcoma

Soft tissue sarcomas (STS) are rare tumors of mesenchymal origin that account for less than the 1% of all adult cancers[1]. In 2021, the American Cancer Society estimated that 13.460 new cases of soft tissues tumors were diagnosed in the United States[2].

Almost 50% of STS occurs in the extremities, although the anatomic distribution can also involve the trunk, the head and neck regions, the gastrointestinal tract, the retroperitoneal area and the uterus, arising in skeletal and smooth muscles, fat, connective, vascular and lymphatic tissues[3].

One of the main features of this group of malignancies is the heterogeneity: the fifth edition of the World Health Organization (WHO) Classification of Tumors of Soft Tissue and Bone describes more than 100 subtypes of these cancers, the majority of which are STS[4]. Each histological and molecular subtype presents a wide range of molecular and cellular characteristics and displays different clinical behaviour; therefore, STS diagnosis is a crucial and complex process that requires a multidisciplinary approach[5]. Immunohistochemical staining of biopsies and fluorescence in situ hybridization (FISH) are usually performed for STS diagnosis and tumor staging. According to the complementary molecular classification, two main sarcoma subtypes are distinguished: 1) sarcomas characterized by specific genetic alteration, such as the presence of fusion genes as *SYT-SSX* for synovial sarcoma, or simple genetic mutations, as the mutation in the *c-KIT* gene that characterizes gastrointestinal stromal tumors, and 2) sarcomas with complex karyotype, characterized by multiple genetic abnormalities, such as leiomyosarcoma[6]. The combination of the histological and molecular criteria is the most widely used approach for STS diagnosis and to determine the correct clinical strategy.

The overall relative 5-year survival of STS patients is approximately 50%. However, following metastatic disease, the 3-year survival rate decreases to only 20-25%. Metastatic spreading usually involves the lungs, but bones, liver, lymph nodes and brain can also be affected[7]. The standard treatment for these tumors includes surgical resection, with or without radiation and standard chemotherapy. However, for metastatic patients, there is the need for more effective targeted therapy based on an individualized approach[8].

STS may also affect children and young adults: in people under 20 years of age these cancers represent the 7% of all primary tumors[9]. Our research group is particularly interested in the study of childhood sarcomas and this thesis work is specifically focused on the most common pediatric STS, the Rhabdomyosarcoma (RMS).

2. Rhabdomyosarcoma

RMS is the most common STS in children and adolescents, with an overall incidence rate of approximately 4 patients per million individuals under 20 years of age[9]. Although for children with localized disease, the cure rates are up to the 80%, the prognosis for patients that show metastasis is extremely poor[10]. Despite the incredible effort of basic and clinic research during the last decades, that has improved notably the biological understanding of this tumors, it is still essential to find successful targeted approaches for the treatment of children with advanced disease.

2.1 Historical aspects

In 1854, Dr. C.O. Weber identified for the first time a tumoral mass located in the tongue of a 21-year-old patient as derived from striated muscle cells. Only 90 years after, Dr. A. P. Stout published the first manuscript in which RMS was finally described as a tumor originated from skeletal muscle cells that could affect both sexes at all ages, in a variety of soft tissue districts throughout the body[11]. In 1958, a first classification of RMS was published, and four major subtypes were distinguished, according to their histologic features: alveolar (ARMS), embryonal (ERMS), pleomorphic and botryoid[12]. Since then, one of the most significative step forward has been the molecular characterization of these cancers: the identification of specific genetic abnormalities, including the t(2;13)(q35;q14) translocation, were associated to the ARMS subtype[13,14], and finally the genes *PAX3* or *PAX7* (Paired Gene Box 3 or 7) and *FKHR/FOXO1* (Forkhead Box Protein O1) were found to be involved in the chromosomal translocations t(2;13)(q35;q14) and t(2;13)(q35;q14)[15,16], originating the fusion protein PAX3-FOXO1 and PAX7-FOXO1 that characterize the ARMS subtype.

2.2 Epidemiology and prognosis

In the United States, approximately 350 new cases of RMS are diagnosed each year, accounting for almost the half of all pediatric STS[17,18]. According to a study based on 59 cancer registries from 19 different countries, the incidence of these tumors in Europe is reported to be slightly superior, with 5.4 cases per million in children under 15 years of age[19].

Age is one of the factors that determine RMS incidence rates: ERMS subtype is more commonly diagnosed in very young patients under 4 years of age, while ARMS incidence does not seem to vary significatively throughout childhood[9]. More in general, ERMS diagnosis is reported to be approximately 2.5 times more frequent than ARMS[20]. On the

other hand, pleomorphic RMS is more common in young adults[21]. Biological sex also influences RMS incidence, with a slight predominance in male children compared to female (male: female ratio of 1.5:1)[22].

The prognosis for children with localized disease is usually favorable , with more than 70% survival rate 5 years after the diagnosis[23,24] and uncommon relapses, that are more frequently registered in patients that present unresectable tumors, located in unfavorable sites, or metastatic disease at diagnosis[25]. Other factors that can influence patients prognosis are the primary tumor localization and subtype, with a survival of 80% for ERMS versus 40-60% for ARMS patients[26], but most importantly the presence and number of metastatic lesions: survival rates may decrease up to a 20% in metastatic RMS patients[27]. Regarding age, children up to 12 years of age present better outcome when compared to adolescents up to 19 years of age, with a 5-year survival rate of 67% versus 45%. For young adults, the prognosis is worst, and the 5-year survival can decrease up to 29%[28].

2.3 Risk factors

2.3.1 Non-Genetic risk factors

Environmental and prenatal factors can contribute to RMS etiology[29]. It has been demonstrated that parental habits as drug use[30] or maternal smoking[31], as well as the exposure to X-ray[32] may affect RMS development, while no association with maternal and paternal age has been reported[33].

No clear association between birth weight and major chromosomal and non-chromosomal genetic defects has been identified[33,34]. Further studies are needed to clarify the role of other factors that emerged as potentially associated with increased RMS risk, as children immunization[35], breastfeeding[36], and exposure to chemicals[37].

2.3.2 Genetic risk factors

Various studies report that children affected by specific genetic disorders are more prone to develop RMS[38]. The most common syndromes associated with RMS diagnosis are Li-Fraumeni Syndrome, caused by germline mutation of the tumor suppressor gene *TP53* (Tumor Protein P53)[39], Costello Syndrome, caused by activating mutations in *HRAS* gene[40], Neurofibromatosis Type I, associated to the inactivation of *NF1* gene, that is involved in the RAS pathway[41], as the mutations that lead to the Noonan syndrome[42], also associated with increased RMS risk. Other syndromes that were described to

represent risk factors for RMS development are the DICER1 Tumor syndrome[43], Rubinstein–Taybi Syndrome[44], Retinoblastoma, caused by the inactivation of *RB1* gene[45] and the Beckwith–Wiedemann Syndrome (BWS), associated with the epigenetic modifications of chromosome 11[46].

2.4 Clinical presentation

RMS patients typically present an asymptomatic mass, or signs and symptoms that depend on the primary site in which the tumor arises: cranial nerve palsy can be caused by parameningeal tumors, or intra-abdominal masses may lead to swelling and bowel obstruction[47]. When the cancer originates in the bladder or in the prostate, urinary tract obstruction and hematuria can be observed. Vaginal and vulvar lesions are often associated with inflammation, bleeding, and local protrusions formation[48]. Pain is not considered to be a consistent symptom and it is usually associated to the compression generated by the growing mass upon the adjacent structures[47].

Ideally, RMS can originate in any anatomical site[38], in or near skeletal muscle districts as well as in other areas that lack muscular tissue. Approximately the 40% of all RMS originate in the head and neck regions: commonly, it can arise in the parameningeal area (15%), near to the base of the skull and the meninges, including nasal cavities and nasopharynx, and the orbit (10%)[49]. A 20% of these tumors occurs in the genitourinary tract, including the bladder, the prostate, the paratesticular tissues, as well as the vagina, the vulva and the uterus (**Figure I1**). Another 20% of all RMS arises in the extremities, with a more common involvement for the lower part of the body. The remaining percentage of tumors may occur in different regions, as the trunk, the biliary tract and the retroperitoneum[48].

2.5 Diagnosis

The correct diagnosis and classification are pivotal to determine the specific treatment of RMS patients, as well as the long-term follow up and the early detection of metastasis and recurrence.

The physical examination of the mass allows to assess the size of the primary tumor, as well as its proximity to vital structure, therefore determining whether the tumor can be completely resected. Laboratory evaluation is then performed, including complete blood count, renal and liver function tests and urine analysis[50]. The following imaging investigation of the primary site includes magnetic resonance imaging (MRI), that allows cross-sectional analysis of the mass and regional lymph nodes, and the computed

tomography (TC), to detect small pulmonary nodes and metastatic lesions[51]. Metastasis detection and nodal involvement at diagnosis are crucial for patient management and the main technique for the evaluation of these two parameters is the whole-body [F-18]2-fluoro-2-deoxyglucose positron emission tomography (18F-FDG PET)[52].

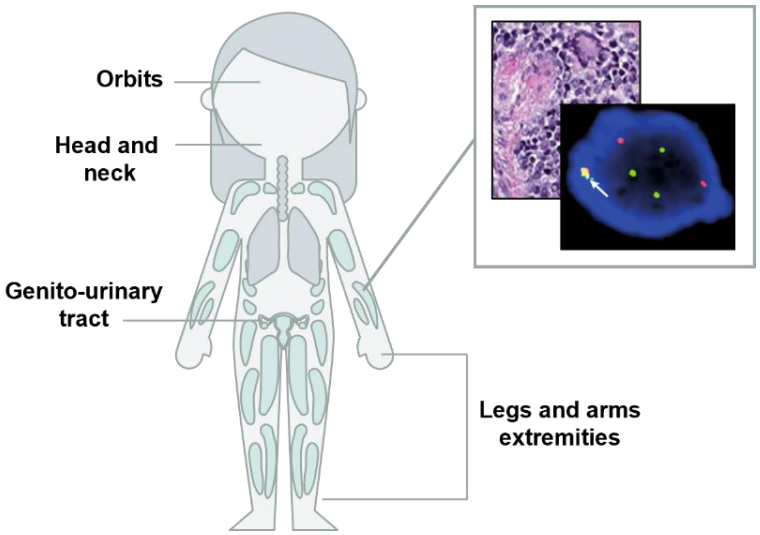

Figure I1: Schematic representation of the main body parts affected by RMS, with the histological and molecular criteria for its diagnosis and classification. Created with Slidesgo.com[53] using images from Skapek *et al*., 2019 and Agaram *et al*., 2022 [54,55].

RMS diagnosis is confirmed by biopsy of the tumor. Bone marrow samples as well as lymph nodes tissues are usually also collected[56]. The histopathological appearance as well as the immunohistochemical and molecular features guide RMS characterization (**Figure I1**). Typically, RMS cells resemble undifferentiated skeletal myoblasts, with scant cytoplasm and large round or oval nuclei. Polynucleated fused cells are also observed[57]. Based on the histological analysis, four subtypes are recognized: two main variants, ARMS and ERMS, and two less common subtypes, the pleomorphic and the spindle cells/sclerosing RMS. The specific histological description of each subtype is reported in the section 2.6 of this chapter.

RMS immunohistochemical analysis includes the evaluation of a panel of specific muscular markers, as desmin, myogenin and Myogenic Differentiation 1 (MyoD1). Positive nuclear staining is employed not only for the identification of rhabdomyoblasts, but also as a criteria to distinguish between the different RMS subtypes[57]. Other molecular markers recently identified to be associated with RMS prognosis are P53, BCL-2, MDR-1 and Ki67[58,59].

Molecular diagnosis and genetic assessment of RMS subtypes are recognized to be essential for patient management[60]. The molecular classification of RMS is based on the identification of the chromosomal translocations t(2;13)(q35;q14) and t(1;13)(p36;q14) that lead to the formation of PAX3/7-FOXO1 fusion proteins, therefore determining the distinction between fusion-positive and fusion-negative RMS[61,62]. PAX3/7-FOXO1 presence is detected through fluorescence *in situ* hybridization (FISH) or RT-PCR assays[63,64] and its state is one the most meaningful prognostic factors for RMS patients stratification[65,66]. In the section 2.7 of this chapter, RMS molecular classification and fusion proteins features are further introduced.

2.6 Histological classification

The most recent WHO classification identifies four main RMS subtypes: ARMS, ERMS, pleomorphic RMS (PRMS) and spindle cell/sclerosing RMS (SpRMS)[67]. In addition to the ones described in the previous classification, novel subtypes have been included, as RMS with *EWSR1/FUS-TFCP2* fusion genes, grouped under the SpRMS subtype, and RMS with *MEIS1-NCOA2* fusion gene.

2.6.1 ARMS

ARMS tumors represent approximately the 20% of all RMS, more commonly affecting adolescents and young adults than children[68]. Histologically, these cancers appear as round cells that cluster together to form cellular nests, separated by fibrovascular tissue, conferring the characteristic “alveolar” aspect[55] (**Figure I2A**). Multinucleated giant cells are also frequently observed. Furthermore, ARMS tumors typically show strong positivity to MyoD and myogenin staining[69].

2.6.2 ERMS

ERMS is the most common RMS subtype, accounting for almost the 60-70% of all cases. It is more frequent in children than young adults, with a peak incidence between 0 and 4 years of age[22]. The histology of these tumors resembles the one of the embryonic skeletal muscle: it is possible to distinguish round undifferentiated cells organized in low-cell density regions, localized in a myxoid submucosa, and high-cell-density regions, more in proximity to blood vessels[57] (**Figure I2B**). The botryoid RMS subtype is recognized by the WHO as an ERMS variant. It is characterized by specific histologic features, as the formation of the so-called cambium layer, that appears as a linear cell aggregation located under the epithelium. Another variant of ERMS is the anaplastic, characterized by the presence of large atypical, polymorphous cells with hyperchromatic

nuclei. Immunohistochemical analysis of ERMS shows strong positivity to desmin, while the staining observed with MyoD and myogenin is variable[55].

2.6.3 PRMS

PRMS represent only the 1% of all RMS cases and most frequently occurs in young adults[21]. Clinically, they appear as an aggressive rapidly growing mass, in most of the cases located in the lower extremities[70]. The histological analysis describes these tumors as formed by undifferentiated round cells with eosinophilic cytoplasm and pleomorphic nuclei (**Figure I2C**). Focal positivity to MyoD, myogenin and desmin is observed at the immunohistochemical analysis. Genetically, PRMS are characterized by a complex karyotype, with frequent chromosomal rearrangements and amplifications[71]. The prognosis associated to these tumors is generally poor[72].

2.6.4 SpRMS

As PRMS, SpRMS represent a very rare subtype, most observed in adults than in children[73]. The prognosis associated to these cancers is usually favorable[74]. Regarding the histology, SpRMS subtype includes tumors formed by spindle cells with eosinophilic cytoplasm that resemble fibrosarcoma morphology, as well as the sclerosing variant, which main feature is the extensive deposition of hyalinizing extracellular matrix that can confer to these tumors a chondroid appearance[75] (**Figure I2D**).

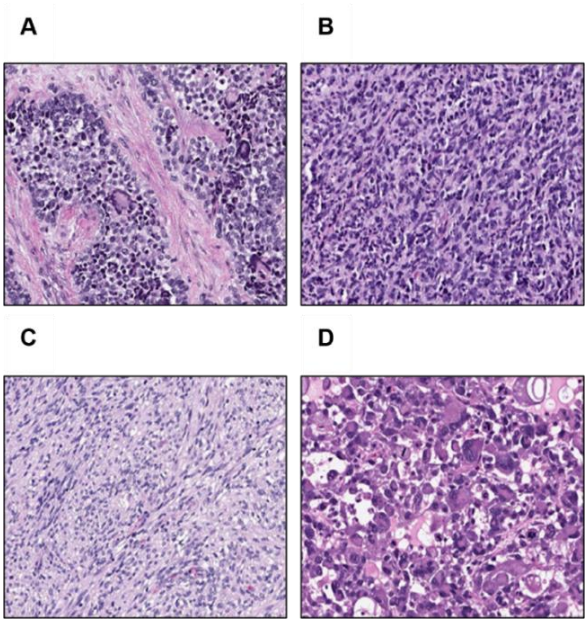

Figure I2: Representative images of Haematoxylin and Eosin (H&E) staining of RMS histological subtypes. **A.** ARMS; **B.** ERMS; **C.** PRMS; **D.** SpRMS. Modified from Agaram *et al.*, 2022[55].

2.7 Molecular classification

Historically, the Children's Oncology Group (COG) risk stratification criteria have relied on the histologic features of RMS, basing the clinical assessment of RMS patients on tumor size, local or distant metastatic spreading and tumoral mass localization[76]. In the last decades, PAX3/7-FOXO1 fusions status has been recognized as meaningful biomarker for the prediction of patients prognosis[77]. Indeed, the poorer outcome associated with ARMS subtypes relates more to the fusion protein detection than the histological appearance: Williamson and collaborators showed that in a cohort of 210 patients, the clinical and molecular characteristics of fusion-negative ARMS and ERMS tumors, including the overall survival and the gene expression signature, were indistinguishable, while the differences observed with the fusion-positive cases were significative, underlying the need to include PAX3/7-FOXO1 fusions state as a molecular marker for RMS classification and management[78].

2.7.1 Fusion-positive RMS

Approximately the 80% of RMS histologically classified as ARMS present a fusion protein originated from a chromosomal translocation; at the same time, more than the 95% of tumors defined as ERMS on histological bases, do not show any fusion gene[79]. The chromosomal translocations t(2;13)(q35;q14), observed in the 60% of ARMS[80] and t(1;13)(p36;q14), observed in the remaining 20%, respectively lead to the formation of PAX3-FOXO1[15,16] and PAX7-FOXO1[81] fusion proteins. Based on the identification of these transcripts, RMS tumors can be distinguished into fusion-positive (FP-RMS) and fusion-negative RMS (FN-RMS), independently from their histological features[82].

PAX3 and *PAX7* genes encode members of the paired box transcription factors family that are expressed in myogenic precursors and play an important role in the early development of neural and muscular tissues[83,84]. On the other hand, FOXO1 (originally referred as FKHR) is part of the FOXOs (Forkhead Box-containing proteins, O subfamily) transcription factors family, being involved in essential metabolic functions as well as cellular differentiation[85]. The molecular analysis of the translocation events shows that the N-terminal DNA binding domain (DBD) of PAX3 or PAX7 are fused to the C-terminal region of FOXO1 Transactivation domain (TAD) (**Figure I3**), originating an aberrant potent transcription factor that alters gene expression and contributes to the oncogenic initiation of RMS[86].

PAX3/7-FOXO1 fusion proteins present enhanced transcriptional activity compared to PAX3 and PAX7, due to their constitutive nuclear localization[87] and since FOXO1 TAD

lacks the inhibitory effect of the wild type N-terminal domain of the two proteins[88]. Furthermore, the fusion proteins expression levels result to be higher than the original proteins, due to the increased transcription and amplification of the fusion genes[89]. In ARMS cells, PAX3-FOXO1 activity is also associated with the tumoral epigenetic reprogramming: the fusion protein is able to bind proteins that interact with chromatin as the bromodomain-containing protein 4 (BRD4) and the chromodomain helix DNA-binding protein 4 (CHD4)[90,91], leading to the epigenetic remodeling of these tumors.

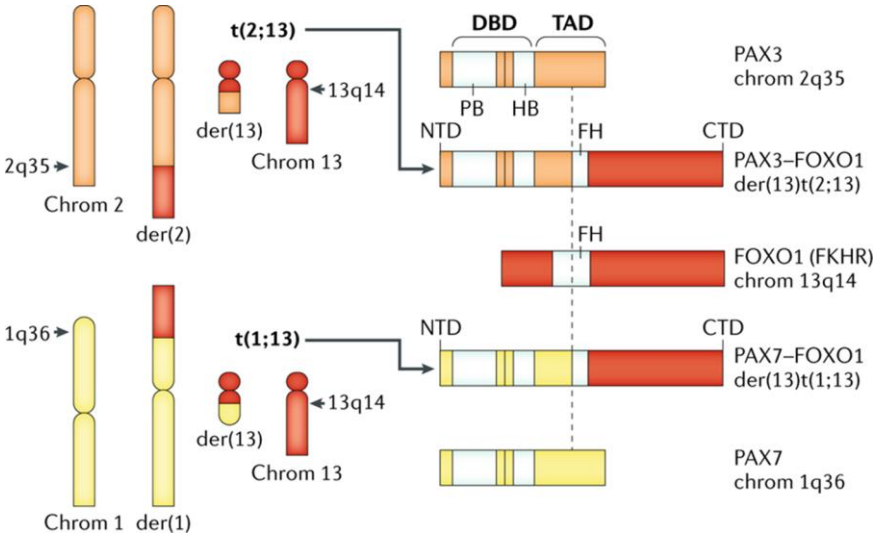

Figure I3: Schematic representation of chromosomal translocations t(2;13)(q35;q14) and t(1;13)(p36;q14) to originate PAX3-FOXO1 and PAX7-FOXO1 fusion proteins. The N-terminal domain (NTD) of PAX3 or PAX7, containing the DNA Binding Domain (DBD) with the Paired Box domain (PB) and the Homeobox domain (HB), is fused together with the C-terminal domain (CTD) of FOXO1 (originally designated as FKHR). From Skapek *et al*., 2019[38].

PAX3/7-FOXO1 fusion proteins act as main drivers of ARMS tumorigenesis, mainly dysregulating gene expression to stimulate cell proliferation, promote cell survival and block terminal differentiation[92]. Increasing research effort has been put in identifying PAX3-FOXO1 target genes, considering that this fusion variant results to be present in most ARMS cancers. Experiments of transcriptomic profiling of fusion-positive cells as well as the ectopic introduction of PAX3-FOXO1 in human or murine cells have allowed to spot the specific changes in gene expression induced by the fusion protein[93–95]. One of its main direct transcriptional targets is the oncogene *N-MYC*: several studies have

confirmed its overexpression upon PAX3-FOXO1 introduction in ERMS cells[62,96], as well as its downregulation upon the fusion protein silencing in ARMS cells[97].

MET proto-oncogene receptor tyrosine kinase (*MET*) and the CXC-Chemokine Receptor 4 (*CXRC4*) are other two PAX3-FOXO1 target genes identified to be key in ARMS tumorigenesis[98,99]. In particular, these two receptors are described to contribute to the metastatic process by inducing cell migration in a synergistic way[100]. Furthermore, both factors have been found to correlate with ARMS histology, advanced disease stage at the diagnosis and poor prognosis[101].

Other PAX3-FOXO1 target genes described to be relevant for ARMS oncogenesis are the Transcription Factor AP2β (*TFAP2β*), that mediates the fusion protein anti-apoptotic role in these cells[97], as well as the Fibroblast Growth factor Receptor 4 (*FGFR4*), which enhanced transcription, together with activating mutations of the kinase domain, are described to promote tumor proliferation and survival[102].

Although PAX3/7-FOXO1 are considered the main modulators of ARMS genetic background, other mutations cooperate to the establishment of the malignant phenotype in these tumors. Indeed, the fusion protein introduction or silencing are respectively described to induce or inhibit the oncogenic transformation[103–106]. Nevertheless, in this sense, the maintaining a specific expression level is key: if introduced in murine cells at higher levels compared to what observed in ARMS cell lines, PAX3/7-FOXO1 can exhibit toxic effects and promote cell death[61,107]. Moreover, it has been described that PAX3-FOXO1 transfection in cells alone is not sufficient to induce oncogenic transformation in mice[108,109], confirming the hypothesis that other genetic events and a specific cellular background of the tumoral progenitors are required to induce ARMS tumorigenesis.

Among the numerous genetic alterations described to collaborate with fusion proteins to ARMS transformation, it is worth mentioning TP53 loss, required for tumor formation *in vivo*[110,111], and the amplification of chromosomes 2, 12 and 13[112,113]. These specific genetic events lead to the increased expression of genes as the TP53 regulator Mouse Double Minute 2 (*MDM2*), the zinc finger transcription factor *GLI1* and the cell cycle regulator Cyclin-Dependent Kinase 4 (*CDK4*)[114], the *C13ORF25* gene[115], that encodes the miR-17-92 microRNA cluster, and *GPC5* gene, which upregulation leads to the consequent increase of tumor proliferation, mediated by the Fibroblast Growth Factor 2 (FGF2), the Hepatocyte Growth factor (HGF) and the Wnt Family member 1A (WNT1A)[116].

2.7.2 Fusion-negative RMS

Genetically, FN-RMS are driven by a combination of events that confers to these tumors a complex karyotype. The most common alteration observed at genetic level is the Loss of Heterozygosity (LOH) at the chromosome 11[117], registered in the 77% of FN-RMS[27]. The LOH at Chr11p15.5 leads to the overexpression of the Insulin Like Growth Factor 2 (*IGF2*) gene[118], that results to be upregulated in these tumors also due to another genetic mechanism that occurs in these cancers: the Loss of Imprinting (LOI)[119].

RAS family member alteration represents another frequent genetic event associated with FN-RMS: *HRAS*, *KRAS* and *NRAS* have been found to be the most commonly mutated genes in ERMS[120], with the consequent aberrant activation of the RAS signaling pathway[121].

TP53 and MYOD have been identified as key players in FN-RMS tumorigenesis as well as established risk predictors: the 13% of FN-RMS shows *TP53* mutations and is associated with worst overall survival[122]; on the other hand, *MYOD1* mutations are associated with SpRMS cell phenotype and are predictive of poor prognosis[123,124].

2.8 Risk stratification and standard treatment

RMS diagnosis, classification and management have been under constant evolution in the last decades. To promote collaboration and improve these fundamental processes, the International Soft Tissue Sarcoma Consortium INSTRuCT was initiated in 2018, with the aim to bring together the advances of the main clinical studies groups of Europe and United States, including the COG and the European Paediatric Soft Tissue Sarcoma Group (EpSSG)[125].

The current risk stratification is based on the Intergroup Rhabdomyosarcoma Study (IRS) trials I-IV[126]. According to IRS I and II, patients are classified after the surgical resection of the tumor into four clinical groups, based on the extension of the disease, metastatic spreading and lymph node involvement (**Table I1**).

IRS III and IV included a staging system based on the pre-clinical treatment of the patients, independently from the surgical outcome, based on the localization and the size of the primary lesion, the presence of distant metastasis and the regional lymph nodes involvement (**Table I2**)[126,127].

Table I1: Post-surgical clinical groups established by IRS. Modified from Haduong *et al*., 2022[127].

Group	Description
I	Localized disease, completely resected with no signs of lymph nodes involvement
II	Localized disease, grossly resected with: A. microscopic positive margins and no regional lymph nodes involvement B. Regional lymph nodes involvement, completely resected with no microscopic positive margins C. Regional lymph nodes involvement, grossly resected with evidence of microscopic residual disease
III	Localized disease, incompletely resected with residual disease
IV	Distant metastatic disease present at diagnosis

Table I2: TNM staging system. T: Tumor. N: Regional Nodes; N0: No regional lymp nodes involvement; N1: Regional lymph nodes clinically involved; Nx: Lymph nodes status unknown. M: Metastasis; M0: No presence of distant metastasis; M1: Presence of distant metastasis. PM: Parameningeal. GU: Genitourinary. Modified from Haduong *et al*., 2022[127].

Stage	T Site	T Size	N	M
1	Orbit, head, neck (non-PM), GU (non-bladder, non-prostate), biliary tract	Any	N0, N1 or Nx	M0
2	Bladder and prostate, extremities, PM, others	≤ 5 cm	N0 or Nx	M0
3	Bladder and prostate, extremities, PM, others	≤ 5 cm	N1	M0
		> 5 cm	N0, N1 or Nx	M0
4	Any	Any	N0 or N1	M1

Based on tumor histology, fusion status, stage and group previously assigned, risk group stratification is determined (**Table I3**)[127].

Table I3: RMS patients risk stratification proposed by the COG. FN: Fusion-negative; FP: Fusion-positive. Modified from Haduong *et al*., 2022[127].

Risk group	Stage	Clinical group	Age	Fusion status
Low	1	I, II, III	Any	FN
	2	I, II		
Intermediate	1,2,3	I, II, III	Any	FP
	1	III	Any	FN
	2,3	III		
	3	I, II		
	4	IV	< 10 years	FN
High	4	IV	≥ 10 years	FN
			Any	FP

The standard treatment for all RMS patients is based on a multi-modal approach that includes surgical resection of the tumor, chemotherapy and/or radiotherapy[128]. The administration of Vincristine, Actinomycin D and Cyclophosphamide (VAC) is the standard treatment for RMS patients[129,130], adjusting cycles duration and dosage according to the risk stratification. The addition of Doxorubicin to the VAC regimen did not show any significative benefit to RMS patients[131], as for the addition of Topotecan and Irinotecan[132]. Many recent clinical trials with the combination of various chemotherapeutic agents did not report a strong improvement in RMS patients outcome[133]. As clinical trials can be performed only on a small number of patients, it is important to choose accurately among the combinations and targets that can produce the best clinical benefit on most RMS patients[128].

2.9 New therapeutic approaches

The recent advances made in understanding the molecular basis of RMS have led to the identification of new diagnostic biomarkers and therapeutic targets that hopefully will provide more effective strategies for the treatment of these pediatric cancers (**Figure I4**).

Given the key role played by RTK/RAS pathway in both FP- and FN-RMS[82], many different trials are currently investigating the possibility of targeting the activators of this axis. In this sense, the multi-kinase inhibitor Regorafenib is currently being tested[134].

FGFR inhibition with Ponatinib in preclinical mouse models has also shown promising results[135] as well as the combination of IGF-1R and MEK inhibition using Trametinib[136].

Another interesting strategy for RMS treatment is to target DNA repair mechanism in cancer cells, for example through the use of poly (ADP-ribose) polymerase (PARP) inhibitors. It has been demonstrated that PARP1 inhibitors Olaparib, Iniparib and Veliparib induce cell cycle arrest in STS cell lines[137]. Moreover, a pre-clinical study shows the synergy of Olaparib and the DNA-damaging agent Temozolomide in inhibiting tumor growth in a zebrafish RMS model[138].

Incredible research effort has been put in the last years for the specific targeting of PAX3/7-FOXO1 in FP-RMS, being the true oncogenic drivers of these cancers, only expressed in tumoral cells. Fusion proteins have been defined as “undruggable” targets, due to their intrinsic features and structures as well as their nuclear localization[139], although several strategies are currently being tested to specifically target these proteins. The direct inhibition of PAX3-FOXO1 has been achieved *in vitro* and *in vivo* using liposome-protamine-siRNA (LRP) particles, with the consequent block of tumor growth[140]; however, the off-target effects induced by the siRNA technology do not encourage its translation into clinics. To overcome this limit, CRISPR-Cas9-based genetic editing could represent a promising alternative to selectively target RMS fusion proteins with increased efficiency[134]. In alternative to directly targeting the fusion proteins, modulators of their activity can be addressed, as the histone deacetylase HDAC, which inhibition with Entinostat results in PAX3-FOXO1 destabilization and decrease[141].

Lastly, another interesting approach for RMS treatment is immunotherapy: PAX3/7-FOXO1 vaccines[142], chimeric antigen receptor (CAR) T-cells therapies for specific antigens expressed by RMS tumoral cells, as the Epidermal Growth Factor Receptor (EGFR) and FGFR[143], as well as the immune checkpoint blockade strategies are continuously under investigation as promising tools to explore for the improvement of RMS patients outcome (**Figure I4**).

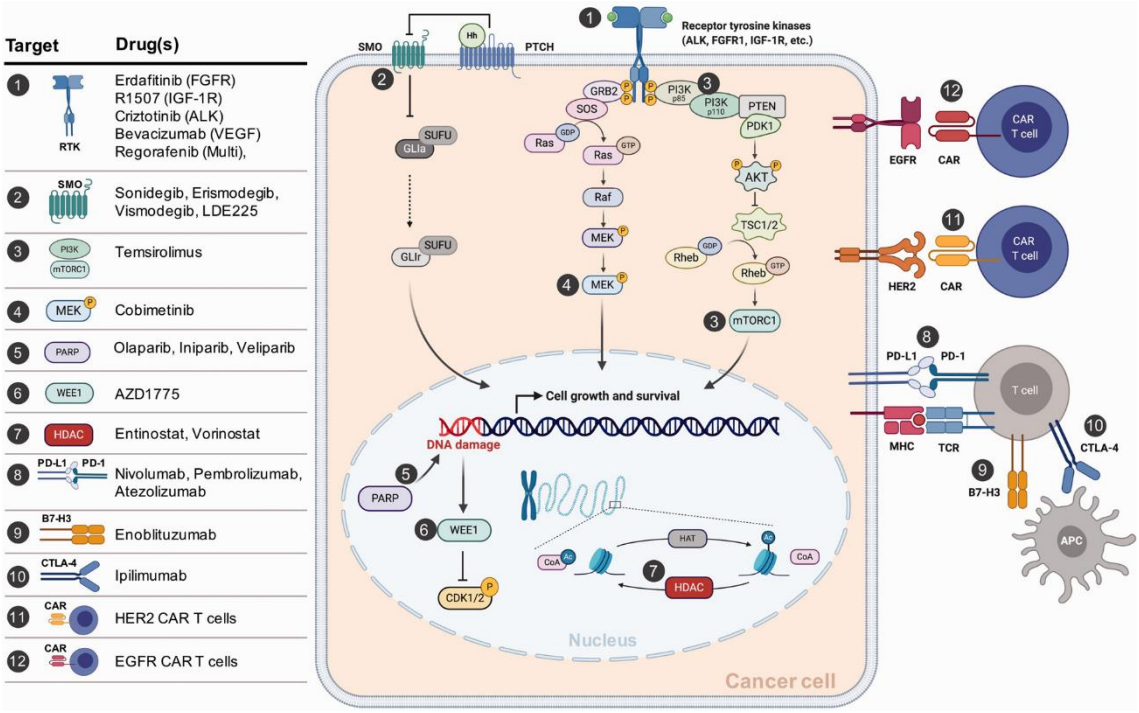

Figure I4: Schematic representation of promising therapeutic options currently explored in clinical trials for RMS treatment. Modified from Giannikopoulos and Parham, 2021[134].

3. Cancer metabolism

Reprogramming energy metabolism has been recognized as one of the emerging hallmarks of cancer[144]. The very first observations of altered energy metabolism in cancer cells by Otto Warburg led to the definition of “aerobic glycolysis”, according to which malignant cells can increase their glucose uptake regardless of oxygen availability[145]. Since this first example of metabolic reprogramming in tumors, the research field has grown considerably, and the new insights gained during the last decades have provided promising therapeutic strategies to target cancer metabolic vulnerabilities.

To meet the increased energetic demand and sustain biosynthetic pathways required to proliferate, tumor cells need to re-shape three fundamental steps of their metabolism: 1) increase the uptake of nutrients from the environment, 2) reprogramming the use of these nutrients and reaction intermediates in metabolic pathways and 3) induce global and long-term changes through metabolism, that can affect the cancer cell itself as well as the interaction with other components of the tumor microenvironment[146].

Glucose is one of the major energy sources for cells: through glycolysis, pyruvate generation contributes to acetyl-CoA production, for the fatty acids and lipid biosynthesis, as well as other non-essential amino acids, as asparagine and aspartate. Other pathways that require glucose-derived intermediates are the pentose phosphate oxidative pathway, from which NADPH and ribose for nucleotide synthesis are generated, as well as the hexosamine pathway for protein glycosylation, among others[147,148]. After glucose, glutamine is the second most consumed substrate by cancer cells, providing the nitrogen required for purines, pyrimidines and other non-essential amino acids synthesis. Through glutaminolysis, the glutamate produced from glutamine is converted to α-ketoglutarate, that fuels the TCA cycle to sustain cell survival and growth[149]. Indeed, TCA cycle intermediates are used by cancer cells as precursors in biosynthetic reactions, to generate “building blocks” and reducing power needed for the sustained expansion[150].

Metabolic changes in tumors do not only favour cancer growth, but also its metastatic potential. During the distal colonization process, cancer cells need to adapt to changing environments, frequently characterized by hostile conditions, as hypoxia and nutrient deprivation[151]. In this sense, the activation of specific metabolic pathways as well as the establishment of complex interactions with the extracellular compartment are key for the successful invasion of distant tissues[152]. For instance, tumoral cells can secrete factors

for the creation of a permissive microenvironment, the pre-metastatic niche, in which cancer seeding is favoured through mechanisms of metabolic priming[153]. An example is the release of exosomes containing miR-122 by primary breast cancer cells, that can suppress the glucose transporter GLUT1 expression on resident cells in lungs and brain, to increase glucose availability for tumoral metastasizing cells[154]. To date, no common metabolic pattern has been identified to characterize metastasizing cells: the tissue of origin, the genetic mutations that drive the tumor, as well as the features of the metastatic niche that characterize the organ to invade are important factors that shape the metabolism of metastasis[155].

The clear connection between tumorigenesis and cancer metabolism has led to the progressive increase of research interest in the field, with the final aim to identify new diagnostic and therapeutic opportunities for cancer treatment. However, the complex metabolic networks that characterize each different cancer type, as well as the heterogeneity of the metabolic status in patients, suggest that the most promising approach for metabolic cancer therapy should be based on the "personalized medicine" concept[156]. According to this principle, standard care of therapy with radiation, chemotherapy or immunotherapy to induce cytotoxicity in cancer cells, should be combined with the identification and targeting of specific driver mutations that induce a metabolic vulnerability in a particular cancer type[157].

4. Arginine metabolism in cancer

L-Arginine is a conditionally essential amino acid: although it can be synthetized *de novo* by the adult organism, its dietary intake becomes essential during fetal and neonatal development, as well as under certain stress conditions, as renal or intestinal disfunctions[158]. Its concentration in the plasma goes from 95 to 250 µmol/L, while inside the cells it is approximately 1-2 mmol/L[159]. *De novo* synthesis of arginine takes place in the kidneys: the citrulline produced in the small intestine reaches the kidneys through blood circulation via the intestinal-renal axis[160], where it is metabolized by the Argininosuccinate Synthase (ASS) to produce argininosuccinate, further converted to arginine by the Agininosuccinate Lyase (ASL)[161] (**Figure I5**). Physiologically, arginine plays a key role in a variety of cellular and molecular pathways, including cell proliferation, hormonal balance, neurotransmission, immunity, muscle contraction as well as cell signaling and other amino acids synthesis[162].

Numerous studies show that this amino acid and the products that originate from its metabolism are crucial also for cancer cell proliferation and tumor progression[163]. Experiments of arginine starvation on 26 different tumor cell lines showed that less than the 10% of the cell populations tested was able to survive[164]. Accordingly with tumor cells increased arginine demand, the expression of its transporters has also found to be upregulated in many different cancer types[165–167]. Following its uptake, arginine can modulate tumor metabolic state by regulating important pathways: together with glutamine and leucine, it can directly activate mTOR[168], therefore increasing protein, lipid and nucleotide synthesis; furthermore, by binding the G-protein coupled receptor GPRCA6, arginine can induce RAS/ERK and PI3K/AKT pathways[169,170]. Recently, arginine has also been described to modulate cancer epigenetics[171] inducing histone acetylation and the consequent upregulation of metabolic and DNA repair genes. Furthermore, arginine is also involved in maintaining the cellular nucleotides pool: glutamine, proline and serine derived from arginine metabolism are direct precursors of pyrimidines, therefore contributing to genome integrity[172].

One of the main arginine-derived metabolites involved in cancer is the nitric oxide (NO), synthetized from arginine by the Nitric Oxide Synthases enzyme family (NOS)[173] (**Figure I5**). NO has been described to present a dual role in cancer[174]: from one side it can suppress neuroblastoma cell proliferation by inhibiting c-Myc expression[175] and its high levels can contribute to induce apoptosis in tumor cells[176], on the other hand it can act as a oncogenic metabolite, activating mTOR pathway in melanoma cells[177] as well the Wnt/β-Catenin pathway, to promote proliferation and migration of breast and colon cancer cells[178]. Finally, arginine-derived NO has also been described to promote angiogenesis[179] and induce epithelial-to-mesenchymal transition[180].

Polyamines are other important products of arginine metabolism that are described to be involved in sustaining cancer proliferation and metastatic process[181]. Indeed, inhibitors of the ornithine decarboxylase (ODC), one of the enzymes involved in the synthesis of putrescine, have been described to exert anti-proliferative effects on lung cancer and neuroblastoma[182,183].

Agmatine is produced from arginine by the arginine decarboxylase enzyme (ADC). This compound has been described to exert an inhibitory effect on tumor cell proliferation in different cancer types[184,185], due to its role in modulating polyamines metabolism: indeed, agmatine interacts negatively with ODC, therefore inhibiting polyamines synthesis and modifying cell cycle progression; moreover, agmatine is involved in decreasing polyamines uptake and favouring their catabolism[186]. Due to this mechanism, arginine

has also been defined as a “two-faced” metabolite in cancer[187]: several studies suggest that arginine supplementation may be beneficial against tumorigenesis, also considering its role in modulating T cell metabolism and supporting the immune response[188,189].

Since arginine exhibits a pivotal role in cancer, the dependency of several tumor types on its availability has been recognized as a vulnerability to exploit for metabolic therapeutic strategies. New treatment approaches that involve arginine metabolism are further reviewed in the section 6 of this chapter.

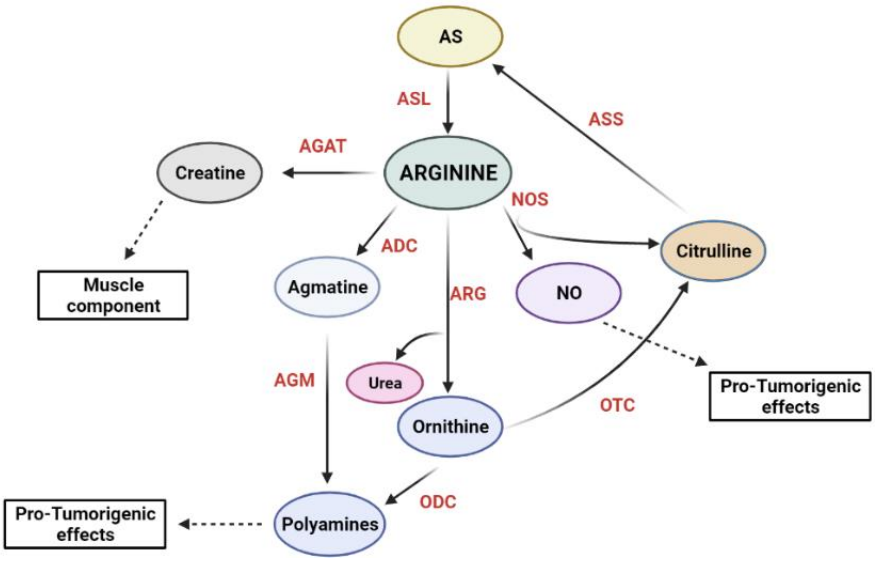

Figure I5: Schematic representation of arginine metabolism main reactions. AS: Argininosuccinate; NO: Nitric Oxide; ASL: Argininosuccinate Lyase; ASS: Argininosuccinate Synthase; NOS: Nitric Oxide Synthase; ARG: Arginase; ADC: Arginine Decarboxylase; AGAT: Arginine/Glycine Amidinotransferase; AGM: Agmatinase; ODC: Ornithine Decarboxylase; OTC: Ornithine Transcarbamylase. Created with BioRender.com[190].

5. Argininosuccinate Synthase 1

The Argininosuccinate Synthase (ASS, commonly referred as ASS1) is the enzyme that catalyses the reversible ATP-dependent formation of argininosuccinate from citrulline and aspartate. It was described for the first time in the liver as one of the enzymes involved in the urea biosynthesis[191–193].

ASS1 gene is located on the long arm of chromosome 9, within 9q.34.11–9q34.12 and is composed by 16 exons[194]. It was first cloned in 1981 from human carcinoma cells[195] and it is notably conserved across species[196]. At least 14 pseudogenes have been identified, dispersed across 11 human chromosomes[197], although the sequence located on chromosome 9 is the only one described to encode the functional enzyme[198]. Two mRNA isoforms have been identified[199], but no biological function has been yet addressed to the splicing variants. The gene product is a homo-tetramer composed of 45-kDa subunits of 412 amino acids[200] and its crystal structure shows that the enzyme is formed by three domains: the nucleotide-binding domain, that displays an N-type consensus sequence for ATP pyrophosphatase, the synthase domain and a C-terminal domain[201,202].

5.1 ASS1 function

As above mentioned, ASS1 catalyses the reaction that converts citrulline and aspartate into argininosuccinate, consuming ATP and producing AMP and pyrophosphate. ASS1 activity has been detected in many tissues[203], therefore it is recognized as an ubiquitous enzyme. However, depending on the cell type in which is expressed, the biological meaning of its function can vary: in the liver, argininosuccinate formation represents an important step of the urea cycle (UC) for ammonia detoxification; in the kidney, argininosuccinate is mainly used for arginine *de novo* synthesis; in most extra-hepatic tissues, where the so-called arginine-citrulline cycle takes place, ASS1 main function is related to NO production (**Figure I6**).

The UC consists of a series of enzymatic reactions that lead to conversion of the toxic excess of nitrogenous compounds derived from protein metabolism into urea, a product that is excreted with the urine[204,205]. As already mentioned, UC takes place in the liver; however, the enzymes involved in the cycle are expressed in different tissues for the synthesis of UC intermediates, including arginine and NO. The Carbamoyl Phosphate Synthase 1 (CPS1) and the Ornithine Transcarbamylase (OTC) are expressed inside the mitochondria, and respectively transform ammonia into Carbamoyl Phosphate (CP) and CP and ornithine into citrulline; following its formation, together with aspartate, citrulline is metabolized by ASS1 to produce argininosuccinate, that is then transformed by the Argininosuccinate Lyase (ASL) into arginine and fumarate; finally, the Arginase (ARG) converts arginine into urea and ornithine, that can be metabolized by the first enzyme of the cycle or support polyamines synthesis outside the mitochondria[206] (**Figure I6**).

Thus, ASS1 reaction is a recognized rate-limiting step for arginine and NO production[207,208]. Hepatic developmental ASS1 expression is controlled by hormones, as insulin and glucagon, that modulate the glucocorticoids response[209], as well as by the nutritional status, especially the protein intake[210,211] as well as fatty acids availability[212]. ASS1 expression and regulation in cancer are further addressed in the section 5.3 of this chapter.

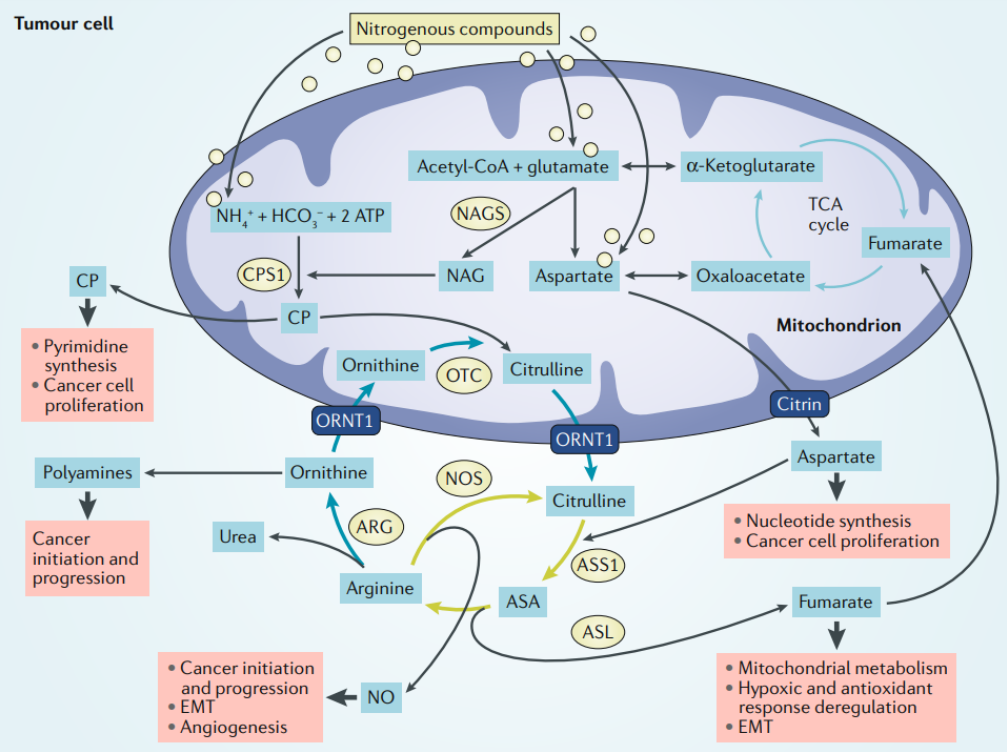

Figure I6: Schematic representation of nitrogenous compounds metabolization through UC (light blue arrows) and the arginine-citrulline cycle (green arrows). The interaction with the TCA cycle is also showed. ASA: Argininosuccinate; NO: Nitric Oxide; CP: Carbamoyl Phosphate; NAG: N-Acetyl Glutamate; CPS1: carbamoyl phosphate synthase 1; NAGS: N-acetyl glutamate synthase; ASL: Argininosuccinate Lyase; ASS: Argininosuccinate Synthase; NOS: Nitric Oxide Synthase; ARG: Arginase; OTC: Ornithine Transcarbamylase; ORNT1: mitochondrial ornithine transporter 1; EMT: Epithelial-to-Mesenchymal Transition. In the pink boxes, the impact of the reaction intermediates at metabolic level is shown. From Keshet *et al*., 2018[206].

5.2 ASS1 mutations and Citrullinemia Type I

Urea cycle disorders (UCD) are a group of pathologies resulting from a deficiency in any of the enzymes or transporters involved in the UC[213]. Approximately, the incidence of

these diseases is 1:35000 births[214] and their clinical characteristics and severity depend on the pathway step involved in the pathogenesis. As UC is the only metabolic pathway for ammonia clearance, UCD lead to the accumulation of this product and other metabolites, with the consequent generation of the associated symptoms: although immediately after birth, the child may not present any sign of the pathology, after few days, failure to feed, somnolence and loss of thermoregulation may appear and progress to seizure episodes and coma[215,216].

The genetic disorder caused by ASS1 deficiency is named Citrullinemia type I (CTLN I, MIM#21570)[217]. Since the first time it was cloned[195], 87 different mutations have been identified across *ASS1* gene, throughout exon 3 to exon 15, with the G390R in exon 15 being the most common one[198]. The highly conserved aminoacidic sites of the protein, as the binding sites for ATP and citrulline, are the main interested in amino acid loss and exchange[198]. CTNL I incidence is estimated to be 1:250000 births[214] and the clinical manifestation of the disease can be notably heterogeneous, due to the high number of genetic variants that can be produced. The main symptoms shown at birth are associated with low arginine plasmatic levels and hyperammonemia, that in the most severe cases can lead to cognitive functions impairment or even be lethal[218]; however, patients affected by mild forms of CTLN I may not present any sign of the disease until adult age[219].

The management of patients that show acute hyperammonemia includes dialysis and pharmacological therapy with nitrogen scavenger agents, to rapidly lower ammonia plasma levels, as well as dietary protein restriction, that is maintained lifelong as part of the chronic therapy[220]. Liver transplantation is the only definitive curative option, and it is recommended for patients above 5 kg of weight[221].

The diagnosis is based on the measurement of ammonia, citrulline and amino acids concentration in plasma, together with the intracranial pressure and the evaluation of the neurologic state of the patient. Following the biochemical analysis and ASS1 enzymatic activity evaluation[222,223], genetic testing is performed, including the sequencing of *ASS1* gene and a multigene panel analysis to identify mutations in genes of interests for the differential diagnosis[220].

5.3 ASS1 in cancer

ASS1 is differentially expressed in a variety of tumor types, when compared to the correspondent healthy tissue[224] (**Figure I7**). Given its fundamental role in arginine and

NO synthesis, this enzyme is strictly regulated in cancer through several different molecular mechanisms, at epigenetic, transcriptional and post-translational level.

Most of cancer types are described as ASS1-deficient[225]: in pancreatic ductal carcinoma (PDAC), ASS1 low expression is associated with worst prognosis[226]; renal cellular carcinoma and pleural mesothelioma also show ASS1 loss, associated to increased sensitivity to arginine starvation[227,228]; melanoma has also been extensively described as susceptible to arginine deprivation, due to ASS1 deficiency[229,230], as well as invasive bladder cancer[231,232], clear cell renal cell carcinoma[233], hepatocellular carcinoma[229,230,234,235], small cell lung cancer[236] and prostate cancer[237]. Bean and collaborators performed an immunohistochemical screening of more than 700 specimens across 45 different sarcoma subtypes and found that the 87.2% of bone sarcoma and the 86.4% of STS were negative for ASS1 expression, defining a common alteration of these cancers[238]. Moreover, ASS1 reduced expression has been associated with increased pulmonary metastasis in osteosarcoma patients, describing this protein as a predictive prognostic biomarker[239].

Oncogenic regulators as P53 and c-MYC regulate ASS1 expression, respectively promoting its activity under genotoxic stress or arginine deprivation[240,241]. Epigenetic silencing is the main mechanism by which ASS1 enzyme is downregulated in cancer. The CpG islands methylation of its promoter, described in multiple tumor types[228,242,243], leads to the establishment of a crucial dependency of these cancers on extracellular arginine, a metabolic mechanism known as arginine auxotrophy. This vulnerability has been defined as the “Achille’s heel” of many tumors[244], giving rise to a series of clinical trials based on the administration of arginine-deprivation agents to target cancer cells that are incapable of synthesize this amino acid. Therapeutic strategies related to arginine metabolism are further discussed in the section 6 of this chapter.

Although the somatic silencing of ASS1 in tumors is still poorly understood, one of the most recent hypotheses describes ASS1 downregulation as a mechanism to favour pyrimidine synthesis: the accumulation of aspartate leads to the carbamoyl-phosphate synthase 2, aspartate transcarbamylase, and dihydroorotase complex (CAD) activation, identifying this multifunctional enzymatic complex as a putative target for ASS1-deficient cancers[245].

Despite most commonly described as downregulated in cancers, ASS1 has also been found to be overexpressed in several tumors: ovarian cancer cells show increased ASS1 expression when compared to healthy tissue, due to the TNF-α-mediated upregulation of the enzyme[246]; in colorectal cancer, ASS1 high expression is associated to increased

tumorigenesis and cancer cell motility[247,248]; in gastric cancer cells, where ASS1 upregulation defines worst patient prognosis[249], it also promotes migration and metastatic spreading by activating STAT3, broadly recognized to promote cancer proliferation and invasion[250]. In breast cancer, ASS1 upregulation has been found to be induced by the inflammatory cytokine interleukin-17 (IL-17), that also regulates NOS and arginine availability for NO synthesis[251]. These findings, together with the evidence of TNF-α-mediated regulation of the enzyme[246,252] and novel studies that describe ASS1 as a key regulator of the pro-inflammatory microenvironment[253], suggest an interesting link between this metabolic enzyme and the inflammatory response that could be further explored for a better definition of ASS1 role in cancer.

6. Therapeutic strategies targeting arginine metabolism

Metabolic profiles and biomarkers have been successfully described for many tumor types, offering an increasing number of therapeutic opportunities. However, it is important to consider that the inhibition of specific metabolic pathways could be systemically toxic if the therapeutic blockade of a certain enzyme or metabolic route interferes with its physiological function[254]. For this reason, the most promising option to selectively target cancer metabolism is represented by the identification of mutations in genes that encode for metabolic enzyme in tumors, producing an increased amount of specific products that in this case are named “oncometabolites”[148,255]. The first described oncometabolite is the 2-hydroxyglutarate (2HG): oncogenic mutations in the isocitrate dehydrogenase enzyme (IDH) lead to the excessive accumulation of 2HG, that contributes to tumorigenesis and progression[256].

Even in the absence of genetic mutations, other mechanisms can lead to the expression loss or gain of metabolic enzymes, inducing specific metabolic needs in cancer. These nutrient dependencies can be exploited for cancer therapy through different strategies, as dietary interventions, direct metabolites elimination and uptake or utilization blocking[257]. One of the best example of clinically exploited tumor dependency is the depletion of asparagine in serum through the administration of L-asparaginase, included in the first-line therapy for the treatment of pediatric and adult acute lymphoblastic leukemia[258,259].

The 70% of tumors show ASS1 decreased expression[172]. Consequently to their inability to synthetize arginine, these cancers are auxotrophic for arginine and develop a strict dependency on the uptake of this ammino acid from the extracellular compartment[260].

Indeed, while arginine deprivation induces reversible cell cycle arrest and quiescence in normal cells, in the tumoral counterpart the activation of cell death pathway has been described, including caspase-dependent or -independent apoptosis[243,261,262], necroptosis[238] or autophagic cell death[263] (**Figure I7**).

Different strategies to induce arginine deprivation have been employed to selectively target ASS1-deficient tumors: the establishment of dietary restriction, demonstrated to be effective only in a small subset of colon carcinoma studies, the inhibition of arginine sensing and uptake, and the enzymatic removal of arginine from the extracellular media[264], being this last option the most exploited. Indeed, an increasing number of preclinical studies have focused on the use of recombinant enzymes for arginine deprivation, as a monotherapy or in combination with classic chemotherapeutic agents as Cisplatin, Docetaxel and Gemcitabine[172].

Polyethylene glycol (PEG)-modified Arginine Deiminase (ADI-PEG20) is a mycoplasmal enzyme that catabolizes arginine into citrulline and ammonia[265]. More than 20 clinical trials testing its efficacy in 12 different cancer types are completed or ongoing[172], showing anti-proliferative effects and promising correlation with patients survival in many ASS1-deficient cancers as hepatocellular carcinoma[266], melanoma[267], acute myeloid leukemia[268,269], and interestingly, STS, in combination with Gemcitabine and Docetaxel (NCT03449901, phase II).

The administration of Pegylated Recombinant Human Arginase I (PEG-rhARG1) is another effective strategy to induce arginine deprivation in tumors. These enzymes catalyse urea and ornithine production from arginine, therefore impacting on polyamines metabolism. As for ADI-PEG20, the use of PEG-rhARG1 have been extensively studied in preclinical and clinical assays for the treatment of ASS1-negative cancers, with interesting advances collected in hepatocellular carcinoma[270,271], melanoma[272] and in different pediatric solid tumors (NCT03455140, Phase I/II).

Mechanisms of resistance towards arginine-deprivation-based therapies have been described[273] (**Figure I7**). The main molecular reason of failure for these treatment options is ASS1 re-expression: in tumors that repress ASS1 expression through the methylation of its promoter, demethylation mechanisms have been reported[274,275]. HIF-1α and c-MYC have also been identified as factors involved in ASS1 re-expression following arginine starvation[241]. Moreover, molecular pathways associated with c-MYC activation, as the RAS-activated ERK/PI3K/AKT cascade, have also been described to be involved in these resistance mechanisms. This data suggests that the combination of ADI-based therapies with RAS-induced signaling inhibition may represent a potential strategy to

improve arginine metabolism targeting[276]. The development of neutralizing antibodies against ADI-PEG20 and the rapid recovery of plasma arginine levels have also been recognized as possible reasons for tumor relapses[277,278].

Finally, the use of small molecule inhibitors of ASS1 may also represent an effective strategy to lower this enzyme expression in tumors. ASS1 specific inhibitor N-methyl-DL-aspartic acid (MDLA) have shown effectiveness in blocking colorectal cancer cell proliferation, affecting glycolytic capacity and lipid metabolism in these tumors[247]. ASS1 inhibition also impairs serine and glycine synthesis, therefore affecting purines production, with the consequent improvement of the response to immune checkpoint inhibition therapy[279].

The encouraging safety profiles and the solid results collected in the clinics indicate that targeting arginine dependency represents a promising strategy for cancer treatment. However, considering the heterogeneity of tumor response towards metabolic stress, as for example the differentially regulation of ASS1 expression, further research effort is needed to build a more personalized approach to target arginine metabolism in cancer and explore the potential use of ASS1 as a biomarker for treatment response.

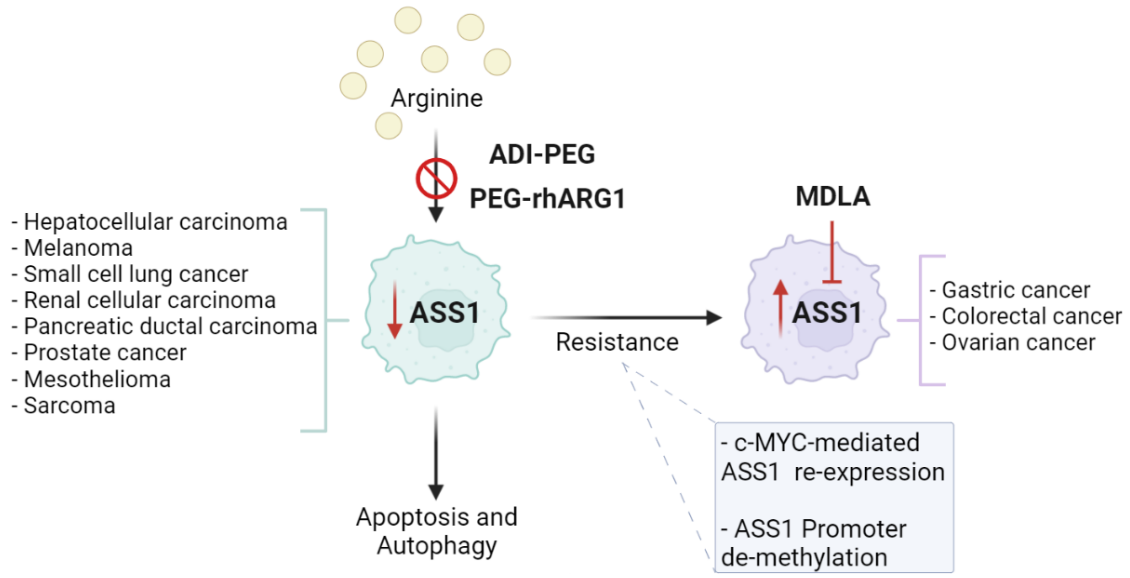

Figure I7: Schematic representation of arginine deprivation-based therapeutic strategies: ADI-PEG and PEG-rhARG1 induce extracellular arginine depletion to target ASS1-deficient tumors (listed on the left). Resistance mechanisms induce ASS1 re-expression in these tumors, that therefore become able to synthetize arginine, NO and polyamines as ASS1-expressing tumors (listed on the right). Created with BioRender.com[190].

HYPOTHESIS AND OBJECTIVES

1. Hypothesis

PAX3-FOXO1 has been recognized as the main driver of ARMS tumorigenesis and metastatic disease, as well as a predictor of poor prognosis in patients[77,111]. Its role in orchestrating major oncogenic events of these tumors, as the differentiation block and the transcriptional and epigenetic remodeling, have been extensively characterized. Nevertheless, very few evidence about PAX3-FOXO1 impact on ARMS metabolic rewiring have been collected to date[280].

Unraveling the metabolic landscape of tumors have emerged as a pivotal step to design new therapeutic strategies to effectively target specific vulnerabilities of cancers.

We propose the hypothesis that PAX3-FOXO1 may act as a key regulator of ARMS metabolic profile, impacting on the tumorigenesis and metastatic potential of these pediatric tumors through the transcriptional regulation of metabolic genes, inducing specific vulnerabilities that may be exploited for the treatment of these young patients.

2. Objectives

The main objectives of this thesis are:

I. Establish cellular models for the study of the effects induced by PAX3-FOXO1 overexpression on ARMS metabolism.
II. Identify key players in ARMS metabolic rewiring.
III. Characterize ASS1 expression in RMS upon PAX3-FOXO1 silencing or introduction.
IV. Elucidate ASS1 role in sustaining ARMS tumorigenesis and metastatic spreading.
V. Explore the molecular mechanism underlying ASS1 pro-oncogenic function in ARMS.

MATERIALS AND METHODS

1. Cell culture

1.1 Cell lines

All cell lines used for this study are listed in the **Table M1**. The validation and authentication were provided by qGenomics (Esplugues de Llobregat, Barcelona). Laminar flow hoods were used to maintain a sterile environment for cell culture.

To test for Mycoplasma presence, cells were periodically grown on coverslips, fixed, and stained using Hoechst 33342 to detect bacterial contamination through DNA staining.

Table M1: List of the cell lines used for this study. Tumor type, cellular origin, acquisition and karyotype information are detailed.
[a]Greehey Children's cancer Research Institute, San Antonio, USA; [b]Leibniz Institute DMSZ – German Collection of Microorganisms and Cell Cultures, Braunschweig, Germany; [c]Department of Oncology and Children's Research Center, University Children's Hospital, Zurich, Switzerland; [d]St. Anna Kinderkrebsforschung, Wien, Austria; [e]ATCC American Type Culture Collection, Manassas, Virginia, USA; [f]CLS Cell Lines Service GmbH, Eppelheim, Germany. ARMS: Alveolar Rhabdomyosarcoma; ERMS: Embryonal Rhabdomyosarcoma; ES: Ewing Sarcoma; LMS: Leiomyosarcoma.

Cell line	Tumor subtype	Acquisition	Cellular origin	Cariotype
RH4	ARMS	Dr. Peter Houghton[a]	7-year-old patient	t(2;13)(q35:q14) PAX3-FOXO1
RH41	ARMS	DSMZ[b]	Xenograft lung metastasis from the same patient as RH4	t(2;13)(q35:q14) PAX3-FOXO1
RMS13	ARMS	Dr. Beat Schäfer[c]	16-year-old patient (not confirmed)	t(2;13)(q35:q14) PAX3-FOXO1
RH28	ARMS	Dr. Beat Schäfer[c]	17-year-old patient metastatic axillary nodule	t(2;13)(q35:q14) PAX3-FOXO1
RH30	ARMS	Dr. Peter Houghton[a]	16-year-old patient metastatic bone marrow (probably same patient as RMS13)	t(2;13)(q35:q14) PAX3-FOXO1
RH36	ERMS	Dr. Beat Schäfer[c]	15-year-old patient paratesticular relapse	Unknown

RD	ERMS	DSMZ[b]	7-year-old patient pelvic mass	Hyperploid
A673	ES	Dr. Heinrich Kovar[d]	15-year-old patient	t(11;22)(q24:q12) EWS-FLI1
RD-ES	ES	DSMZ[b]	19-year-old patient humerus	t(11;22)(q24:q12) EWS-FLI1
SK-ES	ES	DSMZ[b]	18-year-old patient bone	t(11;22)(q24:q12) EWS-FLI1
SK-LMS1	LMS	ATCC[e]	43-year-old patient uterine mass	Hypotriploid to hypertriploid with abnormalities
SK-UT1	LMS	CLS[f]	75-year-old patient uterine mass	Hypodiploid to hyperdiploid
293FT	Embryonal human kidney	DSMZ[b]	Derivative of 293 cell line	SV-40 large T-antigen expression
C2C12	Immortalised murine myoblasts	ATCC[e]	C3H mice strain	Tetraploid (Not Confirmed)

1.2 Cell Culture Conditions

With exception of C2C12 murine myoblasts and 293FT cells, maintained in Dulbecco's Modified Eagle Medium (DMEM; Gibco) complete medium [10% heat-inactivated Fetal Bovine Serum (FBS; Gibco) 1% Penicillin-Streptomycin (PS; 10000 U/mL, Gibco)], all cell lines were maintained in RPMI complete medium [10% FBS and 1% PS RPMI 1640 (Gibco)] at 37°C in a humidified incubator in the presence of 5% CO_2. When reached a confluence of 70-80%, media was removed from the plates and cells were washed once with Phosphate Buffered Saline (PBS). 0.05% Trypsin-EDTA (Gibco) was added to dissociate cells from the plates. Trypsin was neutralized with complete media and detached cells were collected in tubes and centrifuged at 1200 rpm for 5 min. Pellets were resuspended in the correspondent media and cells seeded at the dilution chosen according to the experimental procedure to follow.

1.3 Cell thawing and cryopreserving procedures

For cryopreserving, cells were harvested as previously described and pellets resuspended in freezing medium [90% FBS; 10% dimethyl sulfoxide (DMSO)]. Cryotubes were placed in freezing chambers containing RT isopropanol, to gradually reduce the temperature, and immediately stored at -80°C for at least 24 h. Vials were then moved to liquid N2 tanks at -196°C for long-term storage.

Cryopreserved cells were rapidly thawed by maintaining the vials in agitation at 37°C in a water bath. After the addition of complete media, cells were transferred to tubes and centrifuged at 1200 rpm for 5 min. Pellets were resuspended in complete media and cells were seeded in 100 mm plates (p100).

1.4 Cell pelleting

For the obtention of pellets, cells were harvested as previously described and centrifuged for 10 min at 1800 rpm. After washing with PBS, cells were transferred to Eppendorf tubes and centrifuged again for 10 min at 1800 rpm. PBS was aspirated and pellets were stored at -80°C or immediately used for the following experimental procedure.

1.5 Cell counting

For cell counting, after pelleting and resuspending in complete media, 10 µL of cell suspension was loaded into a Kova Glasstic Slide chamber (ThermoFisher). The average of 4 independent counting areas was considered for confluence calculation. Viable and dead cells were distinguished by the addition to the cell suspension of Trypan Blue (Sigma-Aldrich), a dye that can diffuse to the cytoplasm of non-viable cells, in which membrane integrity is lost, producing a blue staining. Only viable, clear cells were considered when counting for experiment seeding.

1.6 Treatment conditions

For all the following experimental procedures, cells were seeded in 6 well plates in the correspondent complete media, at the adequate dilution to achieve a confluence of 60-70% at the time of the treatment.

1.6.1 Arginine deprivation

The day after seeding, media was aspirated, and cells washed twice with PBS to remove the residual arginine present in the seeding media. Then, 10% FBS 1% PS SILAC RPMI

1640 Flex Media (Gibco), with the addition of 10 mM glucose (Gibco) and 40 mg/L L-Lysine (Gibco), was added to the cells. Control cells were treated with the same media, with the addition of 200 mg/L Arginine (Gibco). After 24, 48 and 72 h from the media change, cells were collected and counted as previously described. Pellets were obtained and stored at -80°C or immediately used for the following experimental procedure.

1.6.2 Serum deprivation

The day after seeding, media was removed, and cells were washed twice with PBS to remove the residual FBS present in the seeding media. Then, RPMI was added to the cells. After 24 h, cells were collected and counted, and pellets were obtained and stored at -80°C or immediately used for protein extraction.

1.6.3 PDK1 and S6K1 inhibitors

The day after seeding, media was removed, and cells were washed once with PBS. Then, complete media containing different concentration of the inhibitors was added to the cells [1 µM or 10 µM BX912 (SantaCruz Biotechnology), 10 µM or 20 µM PF-4708671 (Sigma-Aldrich) and 2,5 µM or 5 µM OSU03012 (SantaCruz Biotechnology)]. BX912 is a small competitive inhibitor of the 3-phosphoinositide dependent protein kinase 1 (PDK1) that binds the ATP-binding pocket to inhibit phosphorylation, therefore affecting AKT signalling and cell growth. OSU03012 is a derivative of the Celecoxib, a cyclooxygenase-2 (COX2) inhibitor, lacking COX2 inhibitory activity. It is a potent inhibitor of PDK1 and suppress cell proliferation in a wide range of tumor cell lines. PF-4708671 is a P70 ribosomal S6 kinase (S6K1) inhibitor that acts preventing S6 phosphorylation without affecting the activity of S6K2 isoform, producing the inhibition of cell growth and proliferation. All the inhibitors were dissolved in DMSO (Sigma-Aldrich). Cells treated with the higher concentration of DMSO used for each treatment were used as a control. After 24, 48 and 72 h from the treatment, cells were collected and counted to determine the effect of the inhibitors on cell proliferation, and pellets were obtained and used to perform protein expression analysis and confirm S6K1 and PDK1 inhibition.

2. Plasmid amplification

The plasmids used for this study have been amplified from commercially available vectors, according to the procedure described below.

2.1 Bacteria transformation

First, 50 µL of Escherichia Coli DH5α competent bacteria for subcloning (Invitrogen) were mixed with 50 µg of the chosen vector in polypropylene tubes and incubated on ice for 30 min. After that, tubes were transferred to a 42°C water bath for 45 sec to produce a heat shock and returned to ice for 2 min. Then, 250 µL of SOC (Super Optimal broth with Catabolite repression, ThermoFisher) media were added and tubes were incubated at 37°C for 1 h in a shaking incubator. Afterward, 50 µL of the culture were seeded on LB (Luria-Broth)- agar plates containing 100 µg/mL ampicillin to let the colonies form and grow overnight in a dry incubator at 37°C.

2.2 Bacterial culture

For the amplification of the plasmid DNA, high density liquid bacterial cultures were established. Using a sterile pipette tip, single colonies were isolated from the LB-agar plates and transferred to polypropylene tubes containing 5 mL of LB media in the presence of 100 µg/mL ampicillin and let grow overnight at 37°C in a shaking incubator. Afterwards, an aliquot of 3 mL of the culture was used to verify the presence of the vector of interest using the NucleoSpin Plasmid Mini Preparation kit (Macherey-Nagel), according to manufacturer instructions. The DNA concentration and quality were determined at NanoDrop. After confirming the presence and the purity of the plasmid, 0,5 mL of the initial culture were inoculated in 200 mL of LB media with the addition of 100 µg/mL ampicillin and let grow overnight at 37°C in a shaking incubator. The day after, the plasmid was purified using the maxiprep EndoFree Plasmid Maxi kit (Qiagen), following the manufacturer instructions. The concentration and quality of the plasmid DNA obtained were tested at NanoDrop.

2.3 Restriction digest analysis

For plasmid verification, inserts and backbones maps were analysed to search for restriction cut sites that allowed plasmid linearization or its cut in multiple specific sized fragments.

The digestion was performed by incubating 500 ng of DNA with 0.5 µL of the chosen restriction enzyme and 2 µL of the correspondent buffer, in a final volume of 20 µL in nuclease-free water at 37 °C for 1 to 2 h. The resulting fragments were then analysed by gel electrophoresis.

2.4 Electrophoresis of nucleic acids

To separate DNA fragments by size, after restriction digest, samples were loaded to agarose gels at different concentration (0.8-1%, depending on the expected fragments size), in the presence of 0.2 µg/µL ethidium bromide for DNA visualization under ultraviolet (UV) light. Electrophoresis was performed in 1X Tris-Acetic Acid-EDTA (TAE) buffer at constant voltage of 100 V for approximately 1 h. A molecular weight ladder was loaded as a reference for DNA fragments size determination.

3. Transient transfection

To perform transient transfection, cells were seeded in 6 well plates at the adequate confluence, depending on the selected cell line. The day after, once cells reached the confluence of 70%, 50 nM of short interfering RNA (siRNA) or 4 µg of the plasmid of interest were mixed together with the correspondent transfection agent: 4 µL of Dharmafect (ThermoFisher) for the transient silencing, or Lipofectamine 2000 (Invitrogen), for the transient introduction, in a final volume of 400 µL of RPMI for each condition. After 20 min, the mix was added to the cells in antibiotic-free-growing media. After 6 h, media was discarded and replaced by fresh correspondent complete media, to preserve cells from the transfection agent toxicity. Cells were collected after 24, 48 and 72 h from the transfection to proceed with the selected experimental procedure.

siRNA sequences employed in this study were obtained from bibliographic analysis of previous publications and purchased from Sigma-Aldrich or Origene. A non-specific siRNA sequence (siNT, Non-Targeting) was used as transfection control. All siRNA sequences used for this study are listed in the **Table M2**.

All the plasmid used to perform transient introduction are listed in the **Table M3** displayed in the section 4.

Table M2: List of siRNA sequences used for transient silencing.

siRNA	Sequence
siNT	UAAGGCUAUGAGAGAUAC
siPAX3-FOXO1	GGCCUCUCACCUCAGAAUUCAAU
siASS1 Pool	Mix of 3 siRNA duplexes Sequences not disclosed

4. Stable transfection and clone selection

To perform stable transfection, cells were seeded in 6 well plates in complete media. The day after, 4 µg of the plasmids of interest and 10 µL of Lipofectamine 2000 were mixed together in a final volume of 500 µL of media for each condition, incubated at RT for 20 min and added to the cells, in antibiotic-free 10% FBS media. After 6h, media was discarded and replaced by fresh complete media. After 24 h, media containing the correspondent antibiotic concentration was added to the cells, to start the selection process. Several vials of the resistant pool obtained were frozen and stored as described above, and pellets were collected to proceed with protein expression analysis and check the presence of the protein of interest.

For lentivirus-mediated stable transduction, highly transfectable embryonic human kidney 293FT cells were used as packaging cells for the generation of viral particles and seeded in T75 flasks in complete media. The day after, cells were co-transfected with 6 µg of the plasmid of interest, 3 µg of psPAX plasmid and 3 µg of pMD2.G plasmid for viral particles generation, mixed with 30 µL of Lipofectamine 2000 in a final volume of 1.5 mL for each condition. Complexes were incubated at RT for 20 min and added to the cells in antibiotic-free 10%FBS DMEM. The day after, media was changed to fresh complete DMEM. After 24 h, viral particles were collected in tubes and centrifuged at 1200 rpm for 5 min to pellet any packaging cell material collected. The supernatant was then filtered using 0.42 µm pores sterile filters and added to the cells to transduce, previously seeded in 6 well plates in complete media. Viral supernatant was diluted at different concentrations in 10% FBS DMEM in the presence of 10 µg/mL Polybrene (SantaCruz Biotechnology) to facilitate the infection. After 48-72 h, media was changed to complete media containing the appropriate antibiotic concentration, to start the selection process. Resistant cells populations were expanded, and stocks were frozen and stored or harvested for RNA and protein expression analysis.

The adequate antibiotic concentration for each cell line was previously determined by growing cells in the presence of increasing amounts of antibiotic, to determine the lowest concentration at which the 100% of cell death is produced after 15 days from seeding. For the stable introduction of PAX3-FOXO1 plasmid, the concentration of Neomycin (Geneticin G418; Gibco) set for the selection was 1000 µg/mL for both C2C12 and RD cells. For the stable introduction of luciferase (Luc) plasmid, RH4 cells were grown in the presence of 100 µg/mL Hygromycin (Invitrogen).

For clonal selection, positive transfected pools were seeded in 96 well plates at a dilution of 1 cell per well in selection media, that was changed every 48-72 h. After 15-30 days,

clones that reached confluence were passaged to obtain enough material to check the selection efficiency. Cellular pellets were obtained and used for RNA and protein extraction, to confirm the stable introduction of the plasmid of interest by Real-Time quantitative PCR (qPCR) and Western Blot (WB).

All the plasmids used for this study are listed in the **Table M3**.

Table M3: List of the vectors used to achieve stable expression of the proteins of interest. The application, acquisition and correspondent antibiotic resistance are specified.

[a]Department of Oncology and Children's Research Center, University Children's Hospital, Zurich, Switzerland; [b]Josep Carreras Leukaemia Research Institute (IJC), Badalona, Spain.

Plasmid	Application	Acquisition	Resistance
CMV	Control	Dr. Beat Schäfer[a]	Neomycin
PAX3-FOXO1	PAX3-FOXO1 introduction	Dr. Beat Schäfer[a]	Neomycin
psPAX	Viral packaging generation	Dr. Manel Esteller[b]	-
pMD2.G	Viral envelope generation	Dr. Manel Esteller[b]	-
CMV	Control	VectorBuilder customed design	Neomycin
PAX3-FOXO1	PAX3-FOXO1 introduction	VectorBuilder customed design	Neomycin
LUC	Luciferase introduction	VectorBuilder customed design	Hygromycin

5. CRISPR-Cas9-mediated silencing

To achieve stable silencing, Homology Directed Repair (HDR)-mediated CRISPR Knockout kit (Origene) was used. This system ensures the simultaneous knockout of the gene of interest and the knockin of a functional donor cassette with a reporter gene and a selection marker. The target sequence is cloned in 2 pCas Guide vectors (gRNA), that can produce the specific cleavage and the consequent interruption of protein coding activity. Once the targeted break is produced, the donor cassette containing the resistance to Puromycin and the Green Fluorescence Protein (GFP) reporter gene is inserted in the genome via HDR (**Figure M1**).

For the stable silencing of ASS1, RH4 cells were seeded in 6 well plates in complete media the day before the transfection, to obtain a confluence of 70% on the following day. Cells were then co-transfected separately with 10 µL of Lipofectamine 2000, 1 µg of each gRNA vector (G1 and G2) or the scramble control vector (SCR) and 1 µg of the donor vector, in a final volume of 500 µL of RPMI. Complexes were incubated at RT for 20 min and added to the cells in antibiotic-free 10% FBS RPMI. 48 h post-transfection, cells were passaged and split 7 times for around 2 weeks to dilute out cells containing the donor vector in the episomal form. Then, selection with 0.6 µg/mL Puromycin was applied. Transfected pools culture was amplified, stocks were collected, and pellets were harvested to confirm the silencing by RNA and protein expression analysis.

Clonal selection was performed by seeding the selected pools in 96 well plates at the dilution of 1 cell per well in selection media, as previously described. Resistant clones were isolated and tested for RNA and protein expression to confirm the silencing of the gene of interest and perform the functional characterization of the cellular population.

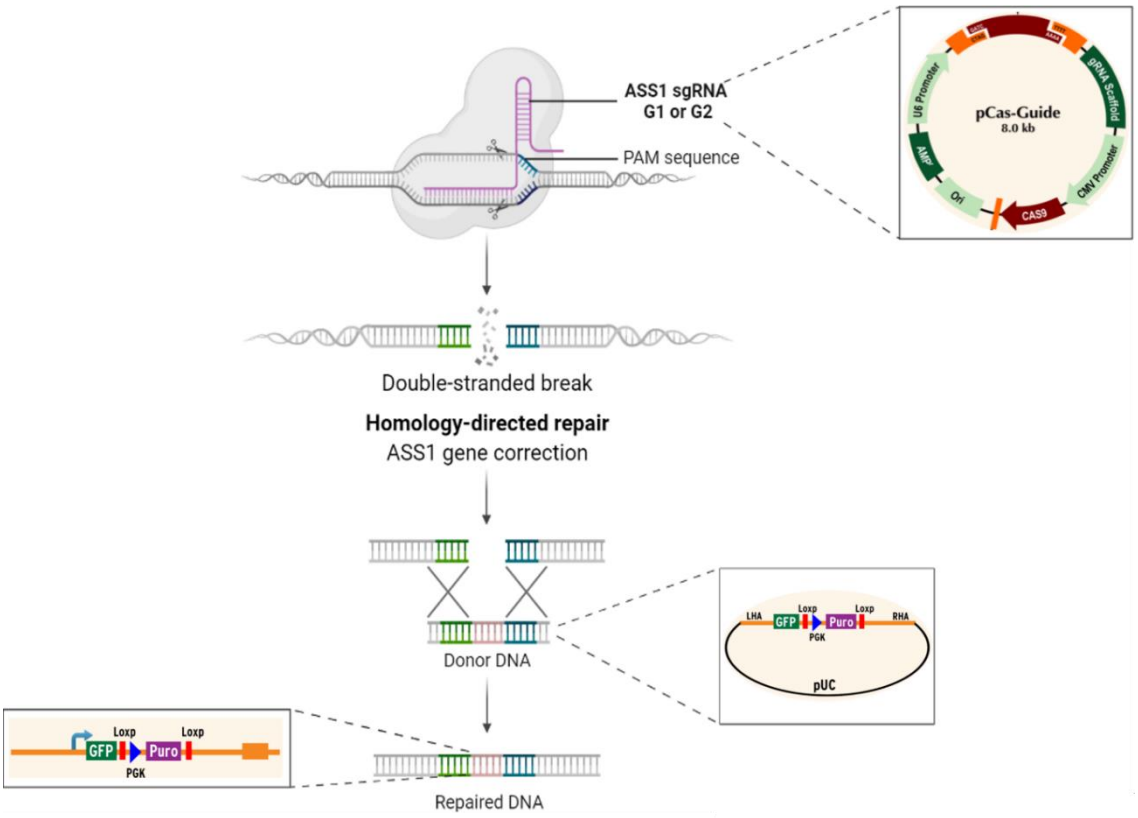

Figure M1: Schematic representation of CRISPR-Cas9-mediated ASS1 silencing. Modified from OriGene CRISPR Knockout Kit Manual using BioRender.com[190].

6. Gene expression analysis

6.1 RNA extraction

For the obtention of the total RNA, cellular pellets were thawed on ice and resuspended in the lysis buffer provided by the NucleoSpin RNA Kit (Macherey-Nagel). The extraction was performed according to manufacturer instructions. RNA concentration and quality were determined at NanoDrop. An absorbance ratio of 2-2.2 at 260/280 nm was set as reference to consider the sample as free of contaminants from the extraction process. RNA extracts were stored at -80°C or immediately used for retro-transcription.

6.2 cDNA obtention by retro-transcription

The cDNA was obtained through reverse transcription reaction, using the system of Oligo dT primers, that specifically anneal to the mRNA poly(A) tails. 500-2000 ng of RNA were mixed with 1 µL of Oligo-dT primers (Invitrogen), 2 µL of Dithiothreitol (DTT; Invitrogen) as a reducing agent for optimal enzyme activity, 1 µL of 10 mM deoxyribonucleotide triphosphates (dNTPs; Invitrogen), 4 µL of First-Strand reaction buffer (Invitrogen), 1 µL of MMLV reverse transcriptase (Invitrogen) in a final volume of 20 µL in nuclease-free water. Samples were then transferred to a thermocycler and submitted to one cycle at 37°C for 1 h, followed by one cycle at 95°C for 5 min and cooling down at 4°C. cDNA was stored at -20°C or directly used for gene expression analysis through qPCR.

6.3 Quantitative Real-Time PCR (qPCR)

For gene expression analysis, qPCR reaction mix was prepared mixing 10 ng of cDNA, 5 µL of MasterMix PCR buffer (ThermoFisher) and 0.5 µL of the commercial Taqman probe of interest (ThermoFisher), in a final volume of 10 µL in nuclease-free water. Samples were loaded in triplicate to 384 well plates and the reaction was conducted according to the LightCycler 480 II thermocycler (Roche) following protocol: 1 cycle of 2 min at 50°C, 1 cycle of 10 min at 95°C and 40 cycles of 15 sec at 95°C followed by 1 min at 60°C. To calculate gene expression levels, the Pfaffl ΔΔCT mathematic method was applied[281] and quantification was based on the fold-differences as compared to the gene expression of a control sample. The obtained values for each gene expression were normalized to the housekeeping gene β-actin, to correct variations related to RNA amount and quality.

The Taqman probes employed for this study are: PAX3-FOXO1 (Hs03024825_ft), ASS1 (Hs01597989_g1), MYL1 (Hs00984899_M1), EEF1A2 (Hs00951278_m1), HTN3 (Hs00264790_m1) and ACTB (Hs99999903_m1).

6.4 Transcriptomic analysis

To identify differences in gene expression across sample groups, Affimetrix ClariomD microarray (Applied Biosystem) was performed at the Institut Hospital del Mar d'Investigacions Mèdiques (IMIM). RNA extraction was performed as previously described, and quality and quantity of the samples were determined at NanoDrop. 1 µg of RNA for each sample in triplicate was sent to the External Service MARGenomics Laboratory Unit of IMIM, where the quality control and quantification were tested again before performing the microarray experiment.

The bioinformatic analysis of the results obtained was performed in R (v.3.5.2), using RMA normalization (oligo package) and differential expression analysis using Limma (limma package). Significant differences were defined as p-value ≤ 0.005 and absolute $\log_2$ fold change ≥ 0.8 and differentially expressed gene were ranked according to these two parameters. Genes with the lowest p-value and highest absolute fold change values were selected as candidate targets for the *in vitro* array validation through qPCR.

7. Protein expression analysis

7.1 Protein extraction and quantification

Cellular pellets were submitted to lysis using 30-80 µL of Radioimmunoprecipitation (RIPA) buffer (ThermoFisher), with the addition of 1 tab of Complete miniProtease Inhibitor Cocktail (SigmaAldrich) and 1 tab of PhosStop Phosphatase Inhibitor Cocktail (Roche) for 10 mL of RIPA buffer. Once resuspended, pellets were incubated on ice for 30 min. Afterwards, 2 cycles of 7 sec of sonication at 100% amplitude, with a 7 sec incubation on ice in between, were performed. Finally, pellets were centrifuged at 13000 rpm for 20 min at 4°C and the supernatant containing the total protein extract was collected in a new Eppendorf tube. For quantification, 1 µL of the extracts was diluted 1:25 in Elix water. 200 µL of A:B buffers mix (1:50) from Pierce BCA Protein Assay kit (ThermoFisher) were added to the extracts and loaded to a 96 well plate. After 30 min incubation at 37°C, absorbance was read at 562 nm and concentration determined by extrapolation from a standard curve generated by a series of dilutions at known

concentration (0 – 2000 µg/µL) of Bovine Serum Albumin (BSA; ThermoFisher). After quantification, protein extracts were stored at 80°C or directly used for WB analysis.

7.2 Western Blot (WB)

For protein expression analysis, Mini-Protean Tetra Cell system (Bio-Rad) was used to perform WB. 25-50 µg of protein extract were mixed with 10 µL of loading buffer [5% 2-mercaptoethanol (Bio-Rad) in 2X Laemmli buffer (Bio-Rad)] and denatured through incubation at 95°C for 10 min. To perform electrophoresis, samples were then loaded to SDS-acrylamide gels, together with the pre-stained protein ladder Precision Plus Protein All Blue Standards (Bio-Rad). Depending on the molecular weight of the protein of interest, for separating gels, different concentrations of acrylamide were used (6-12%); for stacking gels, 4% acrylamide was used. Electrophoresis was performed in 1X running buffer (Tris-Glycine-SDS buffer; BioRad) at a constant voltage of 120 V for 80-120 min. Proteins were then transferred to 0,2 µm pores nitrocellulose membranes through wet electroblotting at 400 mA for 70-85 min at 4°C in 1X transfer buffer (Tris-Glycine buffer; BioRad) with the addition of 20% methanol. Membranes were blocked in a solution of 5% non-fat milk in 0,1% Tween PBS (PBS-T) for 1 h on a rocking platform and then incubated with the optimised primary antibody concentration, as detailed in the **Table M4**, in blocking solution overnight on a rocking platform. Following incubation, membranes were washed 3 times with PBS-T for 5 min and incubated with HPR-conjugated secondary antibody in blocking solution (**Table M4**), for 1 h on a rocking platform at RT. Finally, membranes were washed again with PBS-T for 10 min and incubated with 1 mL of Pierce ECL WB substrate (ThermoFisher) or in alternative with ECL Prime WB Detection Reagent (GE Healthcare), when better sensitivity was required, and chemiluminescence detected using Amersham Imager 600. When needed, the intensity of the bands obtained was quantified by analysing the images using the software ImageJ (Fiji).

Table M4: List of the primary and secondary antibodies used for WB protein expression analysis. Commercial reference, dilution and molecular weight of the detected bands are specified. Mo: mouse; Rb: Rabbit.

Primary Antibody	Supplier ID	Dilution	Secondary Antibody	Molecular Weight
α-Tubulin	Sigma Aldrich #T6199	1:10000	Mo 1:20000	54 kDa
β-Actin	Abcam #ab49900	1:10000	HRP-Conjugated	42 kDa
ASS1	Cell Signaling #70720	1:5000	Rb 1:10000	47 kDa
FOXO1	Cell Signaling #2880	1:2000	Rb 1:4000	78-82 kDa
ERK1/2	Cell Signaling #4695	1:2000	Rb 1:5000	42 kDa
p-ERK1/2 (Thr202/Tyr204)	Cell Signaling #4376	1:1000	Rb 1:2000	42 kDa
mTOR	Cell Signaling #2983	1:1000	Rb 1:2000	289 kDa
p-mTOR (Ser2448)	Cell Signaling #2971	1:1000	Rb 1:2000	289 kDa
AKT	Cell Signaling #9272	1:2000	Rb 1:5000	60 kDa
p-AKT (Ser473)	Cell Signaling #4060	1:2000	Rb 1:5000	60 kDa
S6	Cell Signaling #2217	1:5000	Rb 1:10000	32 kDa
p-S6	Cell Signaling #4858	1:2000	Rb 1:4000	32 kDa
S6K1 (Ser235/236)	Cell Signaling #9202	1:1000	Rb 1:2000	70-85 kDa
p-S6K1 (Thr389)	Cell Signaling #9205	1:1000	Rb 1:2000	70-85 kDa

8. Metabolomic analysis

Metabolomic analysis was performed at Prof. Eyal Gottlieb's laboratory, during a secondment spent at the Ruth and Bruce Rappaport Faculty of Medicine of Technion-Israel Institute of Technology (Haifa, Israel). Cells were plated using the corresponding

complete media. The day after, media was changed for Modified DMEM-F12, containing 5% FBS, 2.5 mM glucose, 100 mM Pyruvate, 200 mM Glutamine. After 24 h, metabolites extraction was performed both from the conditioned media (CM) and the cells (**Figure M2**), using the metabolites extraction mix, a polar solvent composed by 50% Methanol, 30% Acetonitrile and 20% water, stored at -20°C before use. 980 µL of extraction mix were added to 20 µL of CM (1:50 dilution) and vortexed for 10 min at 4 °C. Then, extracts were centrifuged at maximum speed for 10 min at 4 °C. The supernatants were transferred to glass HPLC vials and kept at -75 °C until the utilization. After media aspiration, cells were washed three times with cold PBS and a volume of approximately 0.5-1 mL of extraction mix per 10^6 cells was added to the wells. The cell culture plates were then placed on a rocking shaker at 4 °C for 5 min. The extraction solutions were then transferred to Eppendorf tubes and centrifuged at maximum speed for 10 min at 4 °C. The supernatants were transferred to glass HPLC vials and kept at -75 °C until the utilization. The extracts were analysed using Q Exactive Orbitrap (ThermoFisher) liquid chromatography coupled with mass spectrometry (LC/MS) system and the results were analysed using TraceFinder 4.1 software (ThermoFisher).

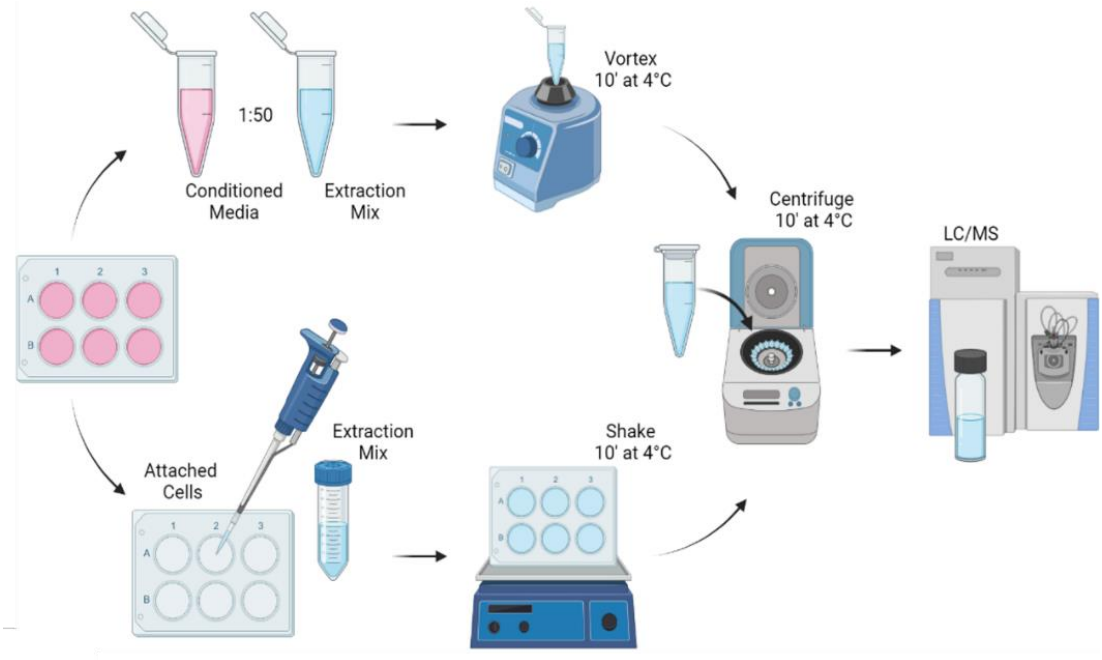

Figure M2: Schematic representation of metabolites extraction protocol from CM and attached cells. Created with BioRender.com[190].

For the analysis, the mass and the retention times of the metabolites found in the samples were compared with an existing database of 171 standards metabolites for the identification of the compounds of interest. For each one of them, the peak area of the

extracted ion chromatogram at the correspondent retention time is determined and metabolic changes are detected by comparison of peak areas among different samples. Normalization among conditions was achieved by cell number.

9. Histological analysis

Tissues processing for histological analysis was performed by the Histology facility of the CMRB – Centre de Medicina Regenerativa de Barcelona (L'Hospitalet de Llobregat). Samples were embedded in paraffin and sections 3 µm thick were cut using a microtome, placed on glass slides onto water at 40°C and let dry at RT until used for immunohistochemistry procedure, as detailed in section 10, or for Haematoxylin and Eosin (H&E) staining. To that purpose, sections were incubated overnight at 60°C to facilitate the dewaxing procedure, that was realized by placing the slides in xylene (10 min x3), ethanol (100% 5 min x3; 96% 5 min x3; 70% 5 min x1) and Elix water. Afterwards, sections were stained with Harris Haematoxylin (Sigma-Aldrich) for 1 min and washed with tap water for 5 min. After a quick passage in Acid Alcohol (1% hydrochloric acid in 70% ethanol) and a wash in tap water for 5 min, samples were stained with Eosin (Sigma-Aldrich) for 1 min and washed again in water for 5 min. Then, sections were submitted to dehydration process by quick washing in ethanol (70% x1, 96% x3, 100% x3), followed by quick washing in xylene (x3). Finally, coverslips were placed on top of a drop of DePeX non-aqueous mounting media (Sigma-Aldrich), avoiding bubbles formation. Once dried, samples were observed at the optical microscope Eclipse 80i (Nikon).

10. Immunohistochemistry

Before starting with the immunohistochemistry (IHC) procedure, slides were placed at 60°C overnight to facilitate the ~~following~~ dewaxing process, performed as previously described. Heat-induced epitope retrieval (HIER) was achieved by boiling the samples in a pressure cooker at 240°C for 10 min in sodium citrate buffer pH 6.0 (1.81 mM citric acid; 0.82 mM sodium citrate). Once de-pressurized and cooled down, slides were washed twice in PBS for 5 min and incubated for 15 min in a 3% hydrogen peroxide solution in methanol, to quench endogenous peroxidase activity. After washing in tap water for 15 min and PBS for 5 min, to reduce non-specific interactions with the primary antibodies, blocking was performed by incubating the samples in Antibody Diluent solution (Dako) for 30 min in a humidity chamber. 200 µL of primary antibodies dilution,

prepared in the same blocking solution as specified in the **Table M5**, were added to the slides, and incubated at 4°C overnight. The day after, primary antibody solutions were discarded, and samples washed three times in PBS for 5 min. Then, samples were incubated 30 min at RT with 200 µL of Biotinylated Link Universal solution (Dako) in a humidity chamber. After 3 washes of 5 min in PBS, and 30 min incubation in Streptavidin-Horseradish Peroxidase solution (Dako), Diaminobenzidine (DAB) chromogen solution (Dako) was added to the slides and the intensity of the staining was monitored under a light microscope, to follow the formation of coloured precipitates in correspondence of the antigen expression sites. The reaction was stopped by placing the slides in Milli-Q water. Finally, samples were counterstained with Harris haematoxylin for 1 min, washed in tap water and maintained in Milli-Q water for 5 min, to then proceed with the dehydration process as described in the previous section. Coverslips were mounted using DePeX mounting media and sections were observed at optical microscope Eclipse 80i (Nikon).

11. Immunofluorescence

Cells were seeded in Millicell EZ Slide 4 wells chambers (Merck), at the adequate dilution to obtain a confluence of 70-80% on the following day. The next day, cells were washed twice with 1 mL of PBS for 5 min, carefully removing the liquid from the chambers with a pipette. Cells were then fixed with a solution of 4% paraformaldehyde (PFA) for 20 min at RT. After 3 washes of 5 min with PBS, cell membranes permeabilization was achieved by 15 min incubation in a solution of 0.1% Triton-X100 in PBS at RT. Then, cells were washed again three times for 5 min in PBS and incubated in blocking solution (10% FBS in PBS) in a humidity chamber for 20 min at RT. Finally, primary antibodies diluted in blocking solution as specified in the **Table M5**, were added to the cells, and incubated overnight at 4°C in a humidity chamber. The day after, cells were washed three times for 5 min in PBS and incubated with the corresponding secondary antibody solution (**Table M5**) for 1 h. Cells were washed first with PBS for 10 min twice and then with water for 10 min twice. Prolong Gold antifade reagent with DAPI (Invitrogen) was used for nuclear staining and coverslip mounting. Slides were finally observed at the confocal microscope TCS SP5 DMI6000 (Leica) and images analysed using ImageJ software.

Table M5: List of the antibodies used for IHC and IF staining. For each primary and secondary antibody, commercial reference and dilution are specified.

Primary Antibody	Supplier ID	Dilution	Secondary Antibody (IF)
ASS1	Cell Signaling #70720	1:1500	AlexaFluor 488 #70720 Rb 4 µg/mL
FOXO1	Cell Signaling #2880	1:100	AlexaFluor 488 #70720 Rb 4 µg/mL

12. Proliferation assay

To determine their proliferative capacity, cells were seeded in complete media in 6 well plates at the adequate dilution for each cell line, treatment and condition. After 24, 48 and 72 h from seeding, cells were harvested and counted as described in the section 1.5. Pellets were collected and stored at -80°C for RNA and protein expression analysis.

13. Migration assay

To evaluate cell migratory capacity, Boyden chambers system was employed. According to this principle, cells are seeded on top of a permeable membrane insert. In the bottom part of the chambers, a chemoattractant agent is placed, to induce cell directional migration by the chemotactic gradient. Following an incubation period, cells that have passed through the membrane pores are fixed, stained and counted to quantify and compare the migratory capacity among different conditions.

To perform migration assay, cells previously seeded in complete media, were harvested and centrifuged for 5 min at 1200 rpm. Then, pellets were washed with RPMI to remove any residual FBS, in this case used as chemotactic agent, and centrifuged again for 5 min at 1200 rpm. Cells were resuspended in RPMI, counted and seeded on top of Transwell chambers (Corning) at a confluence of 150000 cells/ insert. 500 µL of complete media for each condition were pipetted in 24 well plates and inserts placed in contact with the media. After 24 h at 37°C in humidified incubator in the presence of 5% CO_2, the inserts were collected and washed with PBS. A cotton swab was used to remove cells that did not migrate from the upper compartment of the membranes. Migrated cells on the bottom site of the inserts were then fixed with 70% ethanol for 30 min and stained with 2% Cristal Violet in 20% methanol solution in water for 20 min. After washing with

PBS, membranes were carefully cut and mounted on a slide for observation at optical microscope. Manual counting of migrated cells was realized using ImageJ software.

14. *In vivo* assay

14.1 Animals maintenance

Female Athymic Nude-Foxn1nu mice at 6-7 weeks of age were purchased from Envigo and maintained under Specific Pathogen Free (SPF) conditions in individually ventilated cages, at 18-22°C with 60-70% relative humidity and 12 h light/dark cycles. Animals were fed ad libitum with Teklad irradiated diet (Envigo) and filtered water was available at all time.

Animal care procedures were followed according to the Association for Assessment and Accreditation of Laboratory Animal Care International (AAALAC) guidelines. All the procedures employed are described in the protocol n. 9745, deposited by Dr. O. Martinez Tirado and approved by the Ministry of Climate Action, Food and Rural Agenda of the Generalitat de Catalunya.

14.2 Orthotopic metastatic assay

RH4 SCR, G2_2 and G1_4 ASS1 CRISPR clones were priorly transfected to stably express the luciferase enzyme, for cell visualization through *In Vivo* Imaging System (IVIS).

Cells were tested for Mycoplasma absence and luciferase activity was confirmed at IVIS prior to the inoculation. Two days before inoculation, media was changed to antibiotic-free media. After 48 h, cells at exponential growth were harvested, counted and resuspended at a concentration of $5x10^6$ cells/ 100 µL of PBS per animal. Cells were then injected in the gastrocnemius muscle of the hind limb. After the inoculation, mice general wellness and weight was monitored every 48 h. Tumor development was followed by measurement with a digital caliper or once a week by IVIS imaging, after the intraperitoneal injection of 150 mg/kg D-luciferin. Once the tumors reached the critical volume of approximately 800 mm^3, mice were anaesthetised in an induction chamber with a mix of 5% isoflurane and 2% oxygen and surgical resection was performed to carefully remove the tumoral mass. After the extraction, the wound was sutured, and the analgesic Buprenorfin was injected to the mice. In addition, the analgesic Meloxicam was injected two consecutive days after surgery. During the following days, all the mice were

completely recovered and active. IVIS lectures were performed on weekly basis to detect metastasis development[282].

After 90 days from the cell inoculation, or when the end point was set depending on the appearance of a recurrence tumor, mice were euthanized by cervical dislocation. Lungs perfusion with 4% PFA solution was performed. All the organs were examined to detect signs of visible metastasis. Lungs, lymph nodes and other organs suspicious of metastasis presence were then embedded in paraffin and submitted to histological analysis and H&E staining, as described in the section 9.

15. Statistical analysis

Unless specified, all the experiments were performed in triplicate. Results are shown as the average of the obtained values ± standard deviation (SD). One-way or 2way-analysis of variance (ANOVA) for multiple comparisons were used for statistical analysis, considering significant differences when pValue ≤ 0.05. All analyses were performed using GraphPad Prism 9 Software or Microsoft Excel 16.0 version.

16. Figures composition

When not otherwise specified by citing the bibliographic source, figures have been created using the Servier Medical Art: SMART figures database (Creative Commons Attribution 3.0 Unported License) and BioRender website tools and templates (BioRender.com[190]).

17. Equipment and reagents

All the equipment, materials and reagents used for this work are listed in the following sections.

17.1 Equipment list

Amersham Imager 600, Amersham

Analogic Thermoblock, VWR

Benchtop centrifuge 5804, Eppendorf

Benchtop Centrifuge 5810R, Eppendorf

Cell Culture Incubator HERAcell 150, Thermo Scientific

Confocal microscope TCS SP5 DMI6000, Leica

Fluorescence microscope Eclipse 80i, Nikon

Gel Doc System, Bio-Rad

Horizontal gel electrophoresis system, BioRad

Inverted microscope IX70, Olympus

IVIS Lumina XR, PerkinElmer

Mice caging system, Allentown

Microcentrífuge CT15E/CT15RE, VWR

Microcentrífuge Galaxy MiniStar, VWR

Q Exactive Orbitrap mass spectrometer, ThermoFisher

Spectrophotometer Nanodrop ND-100, ThermoFisher

Thermal cycler 2720, Applied Biosystem

Thermal cycler LightCycler 480 II, Roche

Ultrasonic processor UP50H Ultrasonic Processor, Hielscher

Vertical gel electrophoresis MiniProtean Tetra Cell system, BioRad

Vertical laminarflow bench CV-100, Telstar

Vibrating platform shaker Titramax 100/101/1000, Heidolph

Vortex mixer ECN444-1378, VWR

17.2 Consumable materials

Bacteriological Petri dishes with lid, Fisher Scientific #10720052

Conical flat cap microtube 0.5 mL, Sarstedt #72699

Conical flat cap microtube 1.5 mL, Sarstedt #72690

Conical round cap microtube 0.2 mL, Nirco #4095.9N

Coverslips 12 mm diameter, Menzel-Gläsen #631-0713

Coverslips 24 x 60 mm, Menzel-Gläsen #MZ3016

Cryotubes 1,6 mL Quickseal screw cap, Sarstedt #72.380

Kova glasstic slide, Fisher Scientific #10298483

Lightcycler 480 multiwell plate 384, Roche Diagnostics #04729749001

LightCycler 480 Sealing foils, Roche Diagnostics #04729757001

Microscope slide SuperFrost Plus, VWR #631-0108

Millicell EZ Slide 4 wells, Merck #PEZGS0416

Round bottom polypropylene tube 14 mL, Cultek #45352059

Screw cap tube 15 mL, Sarstedt #62.554.502

Screw cap tube 50 mL, Sarstedt #62.547.254

Serological pipet 10 mL, Jet Biofil #GSP010010

Serological pipet 25 mL, Jet Biofil #GSP010025

Serological pipet 5 mL, Jet Biofil #GSP010005

TC-treated culture dish 100 mm, Cultek #430167

TC-treated culture dish 150 mm, Cultek #430599

Tissue culture plate 12 wells, Jet Biofil #TCP011012

Tissue culture plate 24 wells, Jet Biofil #TCP011024

Tissue culture plate 6 wells, Jet Biofil #TCP011006

Tissue culture plate 96 wells, Jet Biofil #TCP011096

Transwell Permeable Supports, Cultek #3422

17.3 Kits and reagents

2-mercaptoetanol, Merck #8.057.400.250

30%Acrylamide/Bis solution 29:1, Bio-Rad #161-0156

Agarose SeaKem, Cambrex #50005

Ammonium sulfate, Sigma-Aldrich #A5132

Ampicillin, Sigma-Aldrich #A9518-5G

Antibody diluent, Dako #52022

ASS1 human gene knockout kit via CRISPR HDR mediated, Origene # N201130

Bacto-agar, Difco #0140-01

Biotinylated Link Universal solution, Dako #K0675

BX-912, SantaCruz Biotechnology #CAS 702674-56-4

Citric acid monohydrate, Merck #1002440500

Complete mini–Protease Inhibitor Cocktail Tablets, Sigma-Aldrich #11836170001

Cristal violet, Sigma-Aldrich #C3886-25G

DharmaFECT 1 Transfection Reagent, Fisher Scientific #W9945D

Diaminobenzidine, Dako #K3468

Dimethyl sulfoxide, Sigma-Aldrich #D2650-100 mL

D-Luciferine firefly potassium salt, Biosynth #I82201G

DMEM High glucose, pyruvate, ThermoFisher Scientific #41966

DMEM/F12, no glutamine, ThermoFisher Scientific #21331-020

dNTPs 10 mM MIX, Life Technologies #18427-013

DPX mounting media, Merck #100579

Dulbecco's PBS 10X w/o calcium w/o magnesium, Biowest #X0515-500

ECL Prime Western Blotting Detection Reagent, GE Healthcare #RPN2232

EndoFree Plasmid Maxi kit, Qiagen #12362

Eosin, Sigma-Aldrich #HT110232

Ethanol 96%, Merck #50.651.071.000

Ethanol absolute, Merck #1.00983.2500

Ethiudium Bromide solution, Sigma-Aldrich #E1510-10 mL

Fetal Bovine Serum qualified, Life Technologies #10270-106

GeneRuler 1kb DNA ladder, #SM0313

Geneticin G-418 Sulfate, Life Technologies #11811-031

Glucose solution, ThermoFisher Scientific #A2494001

Harris Haematoxylin, Sigma-Aldrich #HHS80-2.5L

Hoechst 33342, Life Technologies #H3570

Hydrochloric acid, Merck #1.00317.1000

Hydrogen peroxide solution, Sigma-Aldrich #H1009-500 mL

Hygromycin B, ThermoFisher Scientific #10687010

Isopropanol, Merck #1.09634.2500

Laemmli buffer, Bio-Rad #161-0737

L-Arginine, Merck Life Science #A8094

LB Broth, Acumedia #7290A

L-Glutamine, ThermoFisher Scientific #25030024

Lipofectamine 2000, Life Technologies #11668030

Liquid DAB and substrate chromogen system, Dako #K3468

L-Lysine, Merck Life Science #L8662

Methanol, Merck #106009

Methanol, Panreac #141091.1214

M-MLV Reverse Transcriptase 200 U/µL, Invitrogen #28025013

Nitrocellulose membrane 0,2 µm, Bio-Rad #162-0112

Nuclease free water, Cell Signaling #12931S

NucleoSpin Plasmid kit, Macherey-Nagel #740588.250

NucleoSpin RNA kit, Macherey-Nagel #740955.50

Oligo-dT Primer, Life Technologies #18418-012

OSU03012, SantaCruz Biotechnology #CAS 742112-33-0

Penicillin/Streptomycin, Life Technologies #15140-122

PF-4708671, Sigma-Aldrich #559273-10MG

PFA solution 4%, VWR #1004969010

PhosStop Phosphatase Inhibitor Cocktail Tablets, Roche #04906845001

Pierce BCA Protein Assay, Thermo Fisher Scientific #23225

Pierce Bovine Serum Albumin Standard Ampules, 2 mg/mL, ThermoFisher Scientific #23209

Pierce ECL Western Blotting Substrate, ThermoFisher Scientific #4832106

Polybrene, SantaCruz Biotechnology #SC-1324220

Ponceau S solution, Applichem A2935

Precision Plus Protein All Blue Prestained Protein Standards, BioRad #1610373

ProLong Gold antifade mountant with DAPI, Life Technologies # P36941

Puromycin, Sigma-Aldrich #P8833

RIPA lysis and extraction buffer, ThermoFisher Scientific #89900

RPMI 1640 GlutaMAX supplement, ThermoFisher Scientific #61870044

SDS 10%, Applichem #A0676

SILAC RPMI 1640 Flex Media, no glucose, no phenol red, ThermoFisher Scientific #A2494201

SOC media, Life Technologies #46-0700

Sodium citrate dihydrate, Sigma-Aldrich #S1804

Sodium Pyruvate solution, Merck Life Science #S8636

Streptavidin-Horseradish Peroxidase solution, Dako #K0675

Subcloning Efficiency DH5α competent cells, Life Technologies #18265-017

TAE buffer 50X, Severn Biotech #20-6001-10

TaqMan 2X Universal PCR MasterMix, Life Technologies #4324018

Tris-glycine buffer 10X, Bio-Rad #161-0771

Tris-glycine-SDS buffer 10X, Bio-Rad #161-0772

Triton X-100, Merck #1.086.031.000

Trypan Blue 0.4%, Sigma-Aldrich #T8154

Trypsin-EDTA solution, Life Technologies #25300-054

Tween-20, Sigma-Aldrich #P1379-500 mL

Xylene, Merck #1.08681.2500

RESULTS

1. PAX3-FOXO1 introduction in C2C12 murine myoblasts

With the aim to establish a cellular model for the study of ARMS metabolism, we started transfecting C2C12 murine myoblasts with the fusion protein PAX3-FOXO1, both transiently and stably. We used a lentiviral plasmid bearing the fusion protein construct, Neomycin resistance gene and the Green Fluorescent Protein (GFP) as a reporter. Cells transfected with an empty vector (CMV) were used as control.

Following transient transfection with Lipofectamine 2000, we were able to obtain a considerable expression of PAX3-FOXO1 after 24 and 48 h from the transfection, while it resulted to be almost undetectable after 72 h (**Figure R1**).

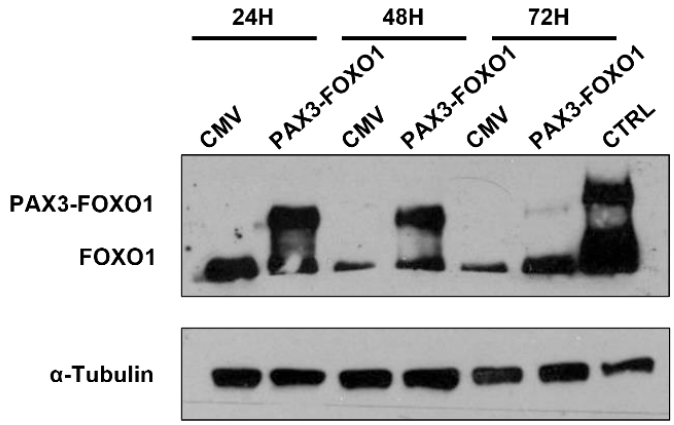

Figure R1: Representative WB analysis showing PAX3-FOXO1 expression levels after 24, 48 and 72 h from its transient introduction in C2C12 myoblasts. Cells transfected with the empty vector (CMV) were used as transfection control. Parental RH4 cells were used as positive control (CTRL) for PAX3-FOXO1 expression. α-Tubulin was used as loading control.

To achieve the stable expression of PAX3-FOXO1 in C2C12 cells, we performed a viral transduction using the same construct employed for the transient transfection. As shown in **Figure R2A**, different ratios of viral supernatant and media were used, to set the best experimental conditions for PAX3-FOXO1 introduction. Unfortunately, we were not able to obtain the stable expression of the fusion protein in C2C12 myoblasts, neither after lentiviral transduction (**Figure R2A-B**), nor performing the stable transfection of the same plasmid with Lipofectamine 2000, followed by antibiotic selection using the correspondent Neomycin concentration (**Figure R2B**).

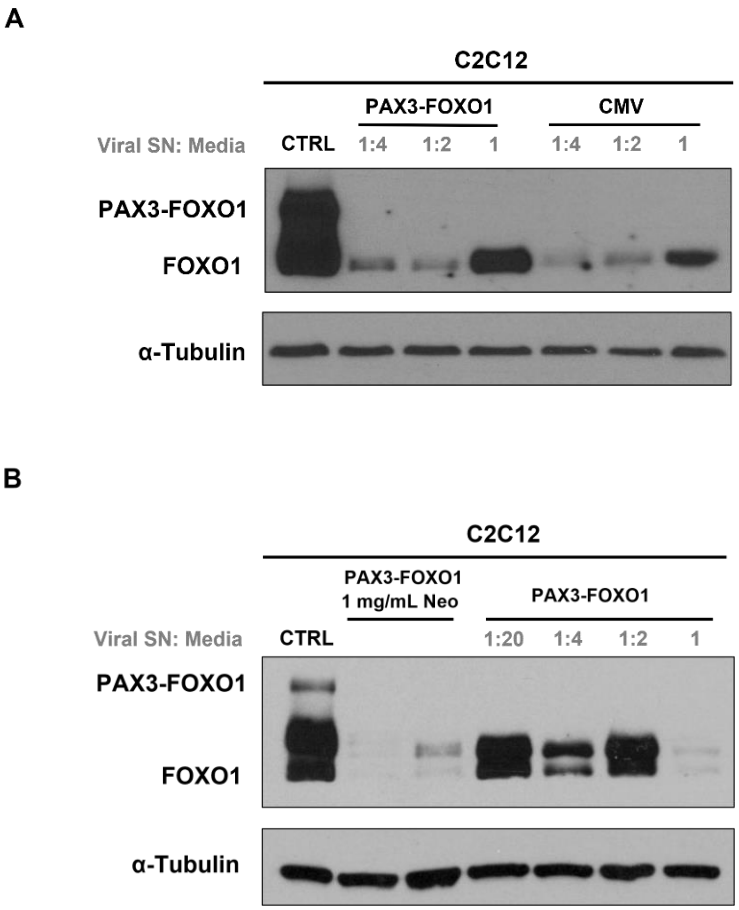

Figure R2: A. Representative WB analysis showing PAX3-FOXO1 expression after lentiviral transduction of C2C12 cells with different ratios of viral supernatant (SN) and complete media. **B**. Representative WB analysis showing PAX3-FOXO1 expression after its stable transfection in C2C12 cells, followed by selection with 1 mg/mL Neomycin, and the lentiviral transduction of the same cells with different ratios of PAX3-FOXO1 viral SN and complete media. C2C12 transiently transfected with the fusion protein were used as positive control (CTRL). Cells transfected with CMV empty vector were used as transfection control. α-Tubulin was used as loading control.

2. PAX3-FOXO1 introduction in RD cell line

Given the difficulties encountered in generating a murine muscle cell line stably expressing PAX3-FOXO1, we decided to switch to another model for the study of the fusion protein-related changes in the RMS cellular context, based on the stable transfection of PAX3-FOXO1 in the fusion-negative Embryonal RMS (ERMS) cell line RD. We performed viral transduction of RD cells using different viral particles concentrations. We obtained a heterogeneous pool of RD cells stably expressing PAX3-

FOXO1 fusion protein (**Figure R3A**), from which we isolated several clones characterized by the higher expression of our protein of interest (**Figure R3B**). Selection was performed using 1 mg/mL Neomycin concentration. RD cells were compared to PAX3-FOXO1-transfected 293FT cells, epithelial cells from human embryonic kidney employed for the viral particle's generation. Using liquid chromatography coupled with mass spectrometry techniques (LC-MS), the metabolomic profile of PAX3-FOXO1-expressing clones will be compared to the parental RD cells metabolome, to individuate possible changes induced by the expression of the fusion protein.

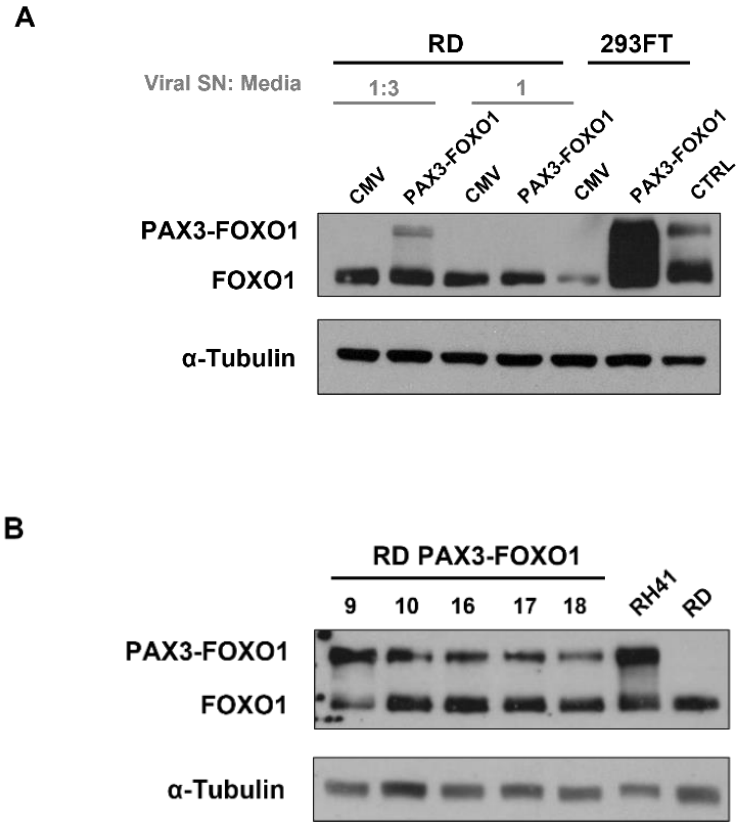

Figure R3: A. Representative WB analysis showing RD and 293FT cells transduced with a control vector (CMV) or PAX3-FOXO1. For RD transduction, different ratios of viral SN and complete media were used. C2C12 cells transiently transfected with the fusion protein were used as positive control (CTRL). **B**. Representative WB analysis showing RD clones (RD PAX3-FOXO1) isolated from the positive pool shown in **A**. ARMS RH41 cells were used as positive control for PAX3-FOXO1 expression. Parental RD cells were used as negative control. α-Tubulin was used as loading control.

3. PAX3-FOXO1 silencing in RH4 cell line

To generate another tool for the study of the effects induced by PAX3-FOXO1 on ARMS metabolism, we performed the transient silencing of the fusion-positive RMS cell line RH4 using a siRNA against PAX3-FOXO1 (siPAX3-FOXO1) or a control siRNA (siNT). The transient silencing of the fusion protein was confirmed by WB analysis (**Figure R4**) after 24, 48 and 72 h from the transfection with Dharmafect, using 50 nM siRNA concentration. Together with the other established cellular models, PAX3-FOXO1-silenced RH4 cells represent a useful tool to further investigate the role played by the fusion protein in modulating ARMS metabolism.

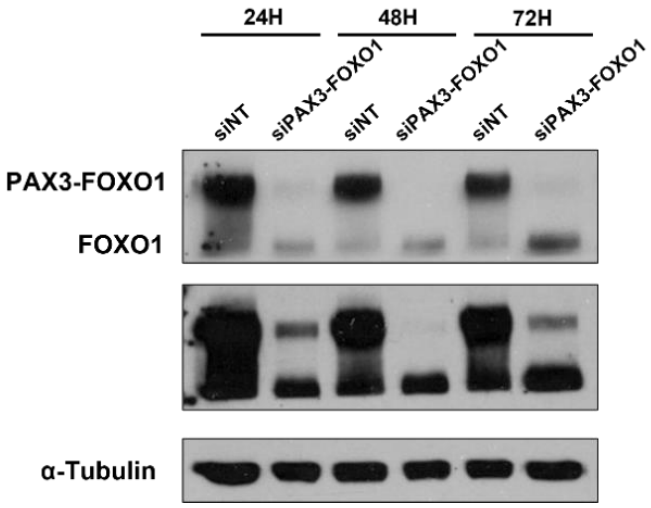

Figure R4: Representative WB analysis showing RH4 cells transfected with the control siRNA (siNT) or a siRNA against PAX3-FOXO1 (siPAX3-FOXO1) after 24, 48 and 72 h from the transfection. Two different exposures times of the same image are shown. α-Tubulin was used as loading control.

4. Metabolomic analysis of PAX3-FOXO1-expressing cells

To study PAX3-FOXO1 role in ARMS metabolic context, we performed metabolomic analysis at Prof. Eyal Gottlieb laboratory, during a secondment spent at the Ruth and Bruce Rappaport Faculty of Medicine at Technion Institute (Haifa, Israel). The aim of our experiments was to evaluate changes in the abundance of the six most exchanged metabolites in the conditioned media (CM) and the cellular extracts of RD cells stably transfected with PAX3-FOXO1 as previously described. Following viral transduction, two

clones characterized by the higher expression of our protein of interest were selected to perform the analysis (RD Clone 9 and RD Clone 17). Using LC-MS technique, extracts from PAX3-FOXO1-expressing clones, RD cells transfected with a control vector (CMV) and parental RD cells were compared, to individuate possible changes in the metabolic profile induced by the fusion protein expression (**Figure R5**). Metabolites extraction was performed both from the CM and the cellular compartment (data not shown).

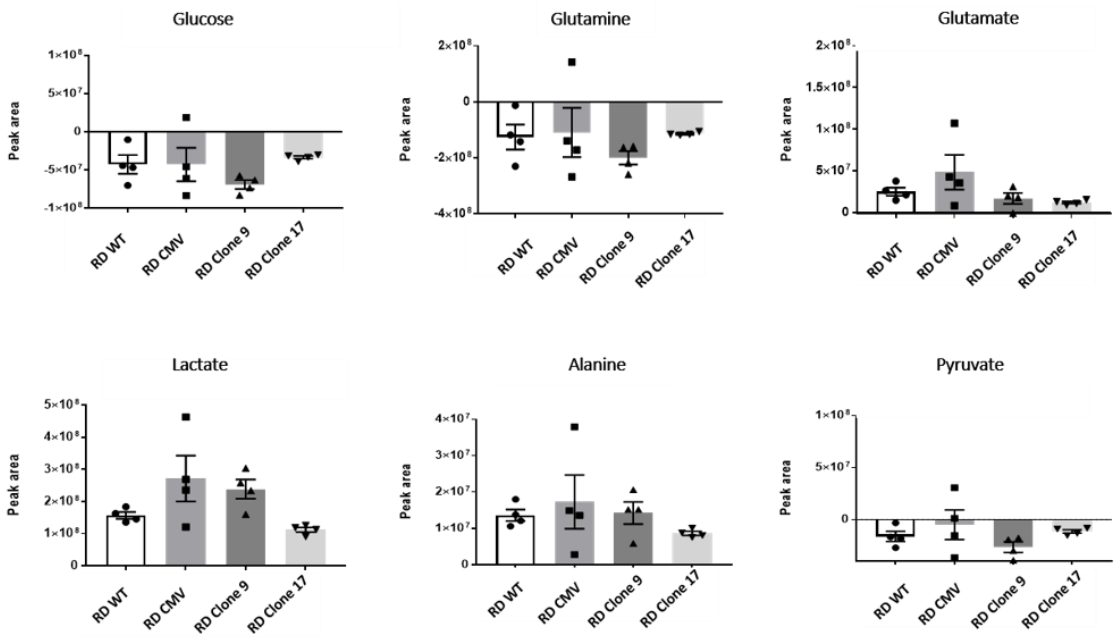

Figure R5: Metabolomic analysis showing the relative levels of glucose, glutamine, glutamate, lactate, alanine and pyruvate in the CM of PAX3-FOXO1-expressing RD clones (RD Clone 9 and RD Clone 17), cells transfected with a control vector (CMV) and parental RD cells (RD WT). Normalization among conditions was performed by cell counting.

No significative differences were observed among the levels of the six most exchanged metabolites (glucose, glutamine, glutamate, alanine and pyruvate) in the extracts obtained from the CM of the four cell types.

5. Transcriptomic analysis of PAX3-FOXO1-expressing cells

Given the lack of significative changes among the profiles compared in the metabolomic study shown in the previous section, we decided to perform a transcriptomic analysis

using a script previously established by our group. We interrogated publicly available data with the aim to identify differences in metabolic genes expression related to the fusion protein presence. We selected three publication[97,283,284] from which four lists of genes were analyzed, comparing the profile of parental ARMS cells silenced or not for PAX3-FOXO1 expression, ARMS and ERMS primary tumors as well as ARMS tumors and normal muscle cells. More than 50 de-regulated genes were found in common between the sets obtained with our analysis (**Figure R6**). Among them, we found that the expression of the Argininosuccinate Synthase 1 (ASS1) was significatively upregulated at transcriptional level by PAX3-FOXO1. The complete list of de-regulated genes is shown in the Annex I (**Table A1**).

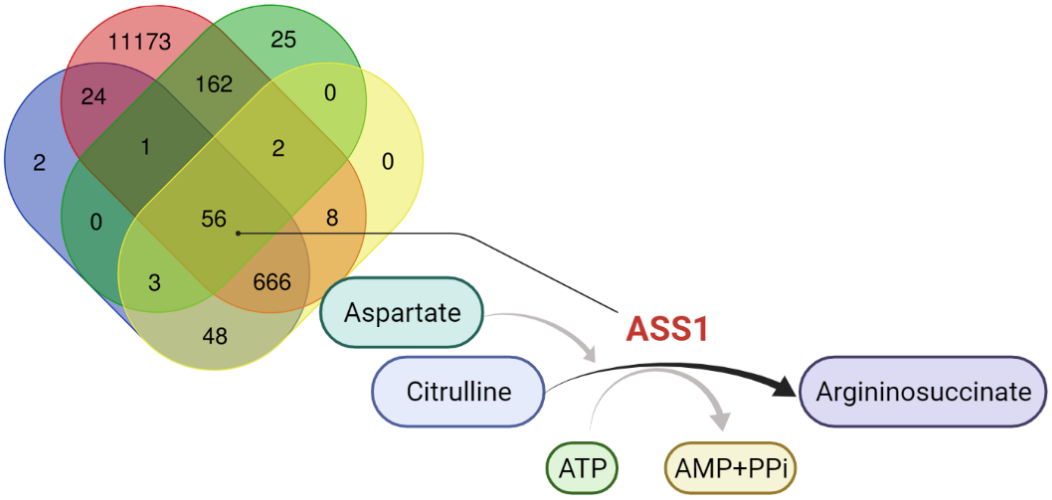

Figure R6: Schematic representation of the Venn diagram showing the relation between the 4 sets of genes analysed by transcriptomics, based on the expression of PAX3-FOXO1 fusion protein, and the biochemical reaction catalysed by ASS1 enzyme for the synthesis of argininosuccinate. Created with BioRender.com[190].

ASS1 is a key enzyme of the urea cycle that catalyzes the formation of arginosuccinate from aspartate, citrulline and ATP. Together with the Argininosuccinate Lyase (ASL), it is responsible for the biosynthesis of arginine in most body tissues. Both up- and down-regulation of ASS1 have been associated to increased proliferation in tumor cells, tumor development, metastasis and drug resistance[225]. In particular, many types of sarcomas have been described as ASS1-deficient tumors[238] and a clinical trial using arginine deprivation strategy in ASS1-deficient adult sarcomas is actually ongoing. Therefore, we

decided to further study ASS1 upregulation in ARMS as it could represent a unique metabolic signature of this specific pediatric malignancies.

6. ASS1 is overexpressed in ARMS and partially correlates with PAX3-FOXO1 expression

To confirm the fusion protein mediated ASS1 upregulation detected with our transcriptomic analysis, we interrogated our previous metabolomics results to check the levels of urea cycle intermediates. As shown in **Figure R7A**, RD Clone 9 and RD Clone 17 (RD CL9, RD CL17) presented undetectable levels of citrulline, one of ASS1 substrates. On the contrary, the levels of argininosuccinate, ASS1 main product, resulted to be considerably higher in PAX3-FOXO1-expressing clones than in parental RD and CMV cells, suggesting an increased expression or activity of the enzyme. This was further confirmed by the analysis of several TCA cycle intermediates (**Figure R7B**), which levels resulted to be increased in RD CL9 and RD CL17, in accordance with what expected.

Based on the metabolomic and transcriptomic analysis results obtained, we performed qPCR to evaluate mRNA levels of ASS1 in several ARMS and ERMS cell lines, as well as in PAX3-FOXO1-expressing RD clones (**Figure R8A**), with the aim of verifying the increment of its expression in a fusion-dependent manner. We found that ASS1 mRNA levels were increased in RH4 cells, as well as in the two fusion-positive RD clones analyzed, also at protein level, as shown by WB in the **Figure R8B**. On the contrary, ERMS cell line RD and RH36 as well as A673 Ewing Sarcoma (ES) cell line presented almost undetectable levels of ASS1 mRNA.

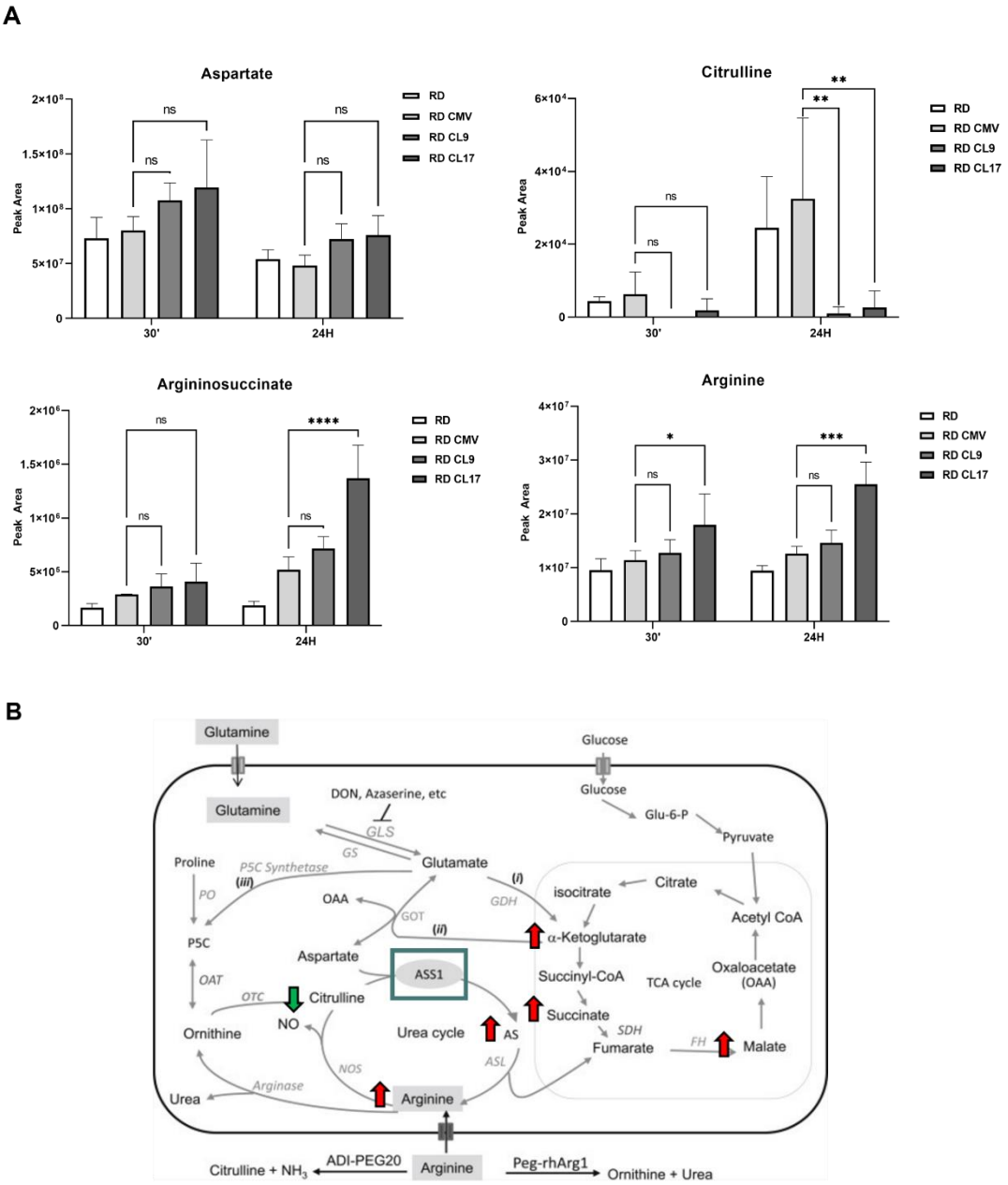

Figure R7: A. Metabolomic analysis showing aspartate, citrulline, argininosuccinate and arginine relative levels in RD parental cells, cells stably expressing PAX3-FOXO1 (RD CL9 and RD CL17) or a control vector (CMV). Metabolites extraction was performed after 30 min and 24 h from the media change. Normalization among conditions was performed by cell counting. Data are expressed as mean ± SD from at least three different experiments. Statistical significance was achieved by 2way ANOVA test (ns: non-significant, *p ≤ 0.05, **p ≤ 0.01, ***p ≤ 0.001, ****p ≤ 0.0001). **B.** Schematic representation of metabolites levels related to ASS1 and arginine metabolism in the same cells (modified from Long *et al*., 2017).

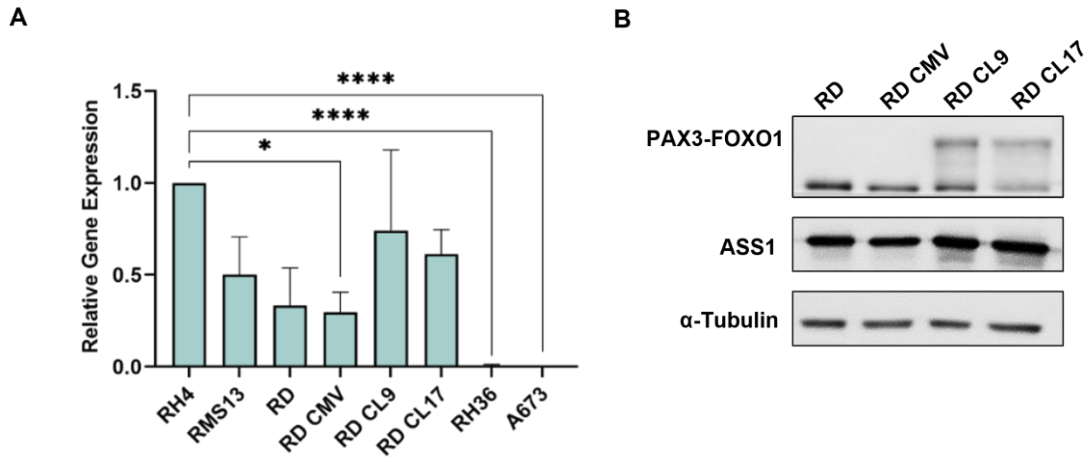

Figure R8: A. qPCR analysis showing relative mRNA levels of ASS1 in different ARMS and ERMS cell lines compared to ES A673 cell line and RD ERMS cell line transfected with PAX3-FOXO1 (RD CL9 and RD CL17) or an empty vector (RD CMV). Obtained values are referred to RH4 ASS1 expression levels. Data are expressed as mean ± SD from at least three different experiments. Statistical significance was achieved by One-way ANOVA test (*p ≤ 0.05, ****p ≤ 0.0001). **B.** Representative WB analysis showing PAX3-FOXO1 and ASS1 expression in parental RD cells, RD transfected with PAX3-FOXO1 (RD CL9 and RD CL17) or an empty vector (CMV). α-Tubulin was used as loading control.

Then, we analyzed ASS1 protein expression in a panel of RMS, ES and Leiomyosarcoma (LMS) cell lines (**Figure R9**).

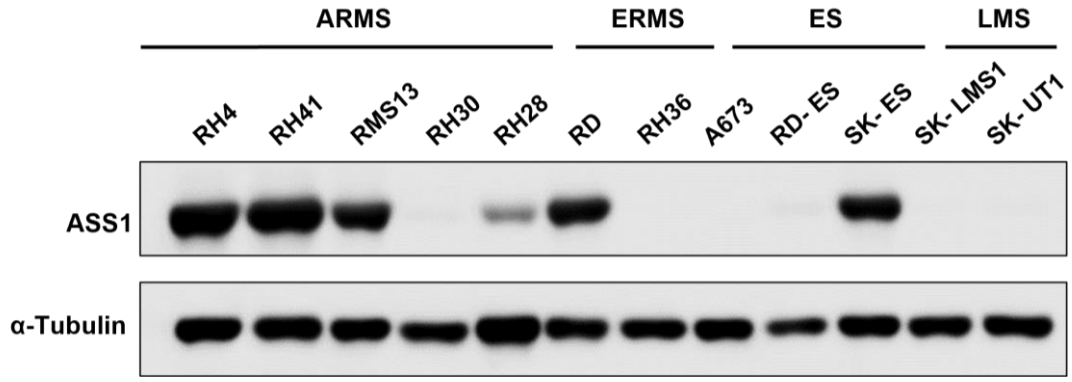

Figure R9. Representative WB analysis showing ASS1 expression in a panel of RMS, ES and LMS cell lines. α-Tubulin was used as loading control.

At protein level, both ARMS and ERMS cell lines showed increased ASS1 expression, mostly independently from PAX3-FOXO1 presence (**Figure R9**). Consistently as described for more than the 80% of primary STS and bone sarcoma tumors[238,239], ASS1 expression resulted to be undetectable or very low in A673 and RD-ES ES cell lines and SK-LMS1 and SK-UT1 LMS cell lines.

ASS1 expression in ARMS was also confirmed by immunohistochemistry staining of ES and ARMS xenograft tumors (**Figure R10**). Tumors derived from RH4 and RH41 cells showed strong ASS1 expression, while tumors originated from A673 cells resulted to be completely negative for ASS1 staining.

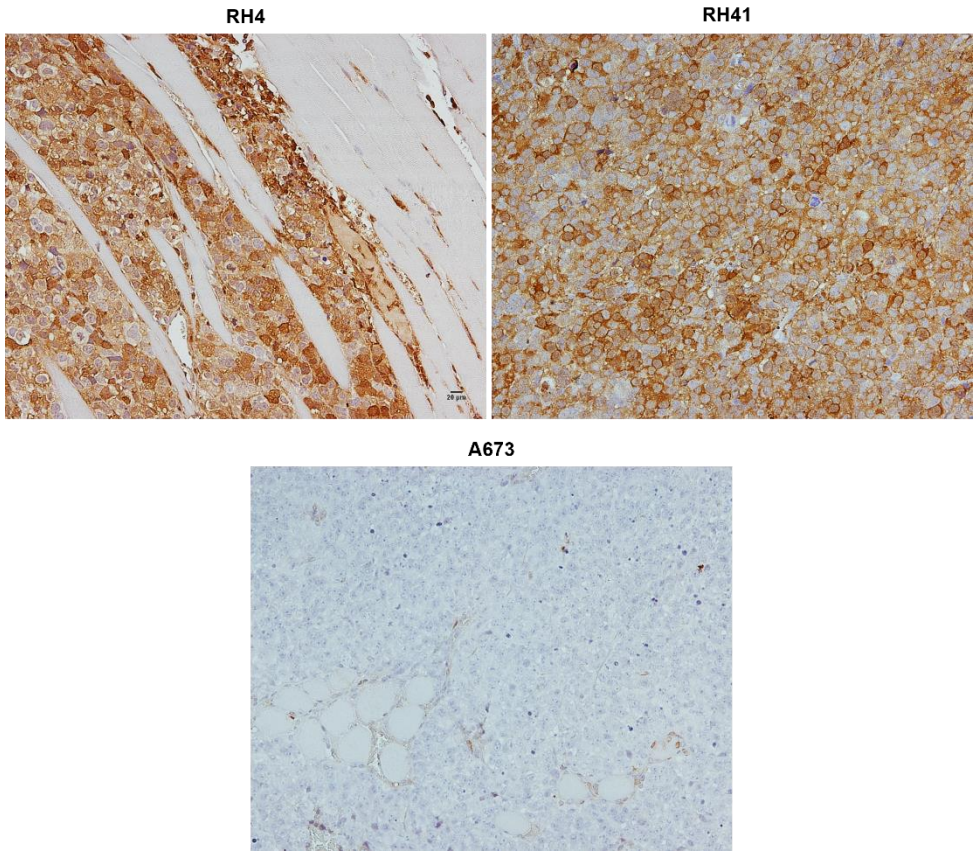

Figure R10: Representative immunohistochemistry staining pictures showing ASS1 expression in xenograft tumors generated from RH4 and RH41 ARMS cell lines and A673 ES cell line. Scale bar: 20 µm.

To better investigate the impact of the fusion protein on ASS1 expression, we employed our model of PAX3-FOXO1 transient introduction in C2C12 cells. As shown in the **Figure R11**, in this case, ASS1 protein levels were not significatively affected by PAX3-FOXO1 ectopic expression.

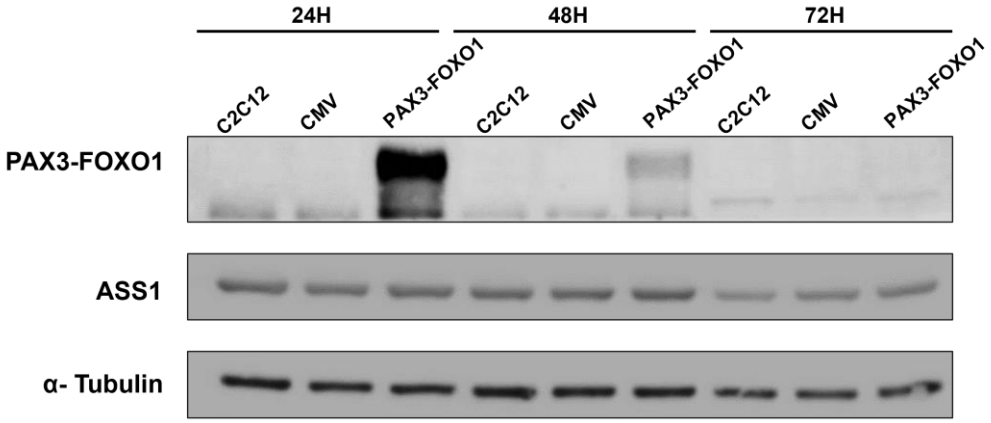

Figure R11: Representative WB analysis showing PAX3-FOXO1 and ASS1 expression in C2C12 cells transiently transfected with PAX3-FOXO1, after 24, 48 and 72 h from the fusion protein introduction. C2C12 transfected with the control vector (CMV) were used as transfection control. α-Tubulin was used as loading control.

Then, we analysed the expression of ASS1 upon PAX3-FOXO1 transient silencing in RH4 cells. At mRNA level, we observed a decrease of ASS1 expression after 48 and 72 h from PAX3-FOXO1 transient silencing (**Figure R12A**).

Contrarily to what expected, when we analysed ASS1 protein level in the same cells, we were not able to observe any significative difference in its expression upon PAX3-FOXO1 silencing (**Figure R12B**), suggesting that probably ASS1 protein levels and stability could be influenced by other factors that do not strictly depend on the fusion protein presence.

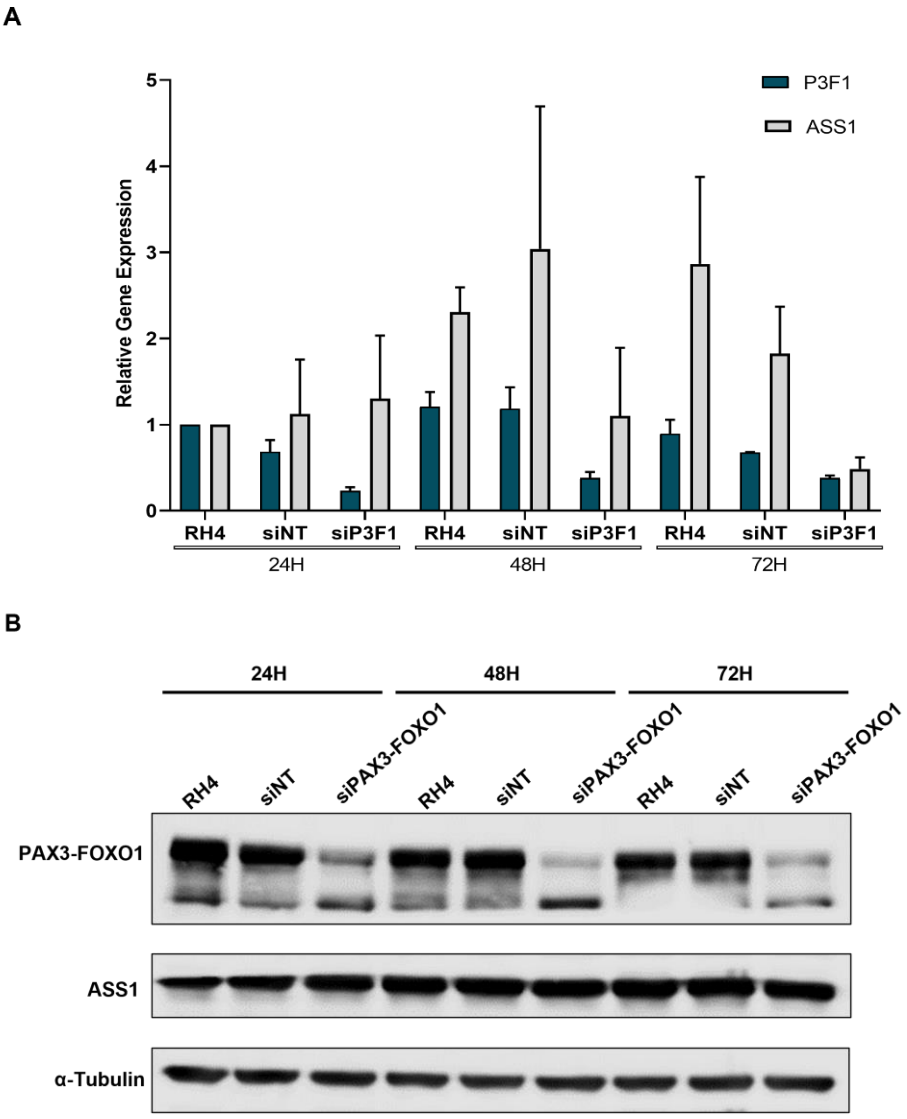

Figure R12: A. qPCR analysis showing PAX3-FOXO1 and ASS1 relative mRNA levels in RH4 cells transiently silenced for the fusion protein expression (siP3F1) after 24, 48 and 72 h from the transfection. Obtained values are referred to RH4 ASS1 and PAX3-FOXO1 expression at 24 h. Data are expressed as mean ± SD from two different experiments. **B.** Representative WB analysis showing PAX3-FOXO1 and ASS1 expression levels in RH4 cells transiently silenced for PAX3-FOXO1 expression at 24, 48 and 72 h from the transfection. Cells transfected with the control siRNA (siNT) were used as transfection control. α-Tubulin was used as loading control.

To further validate this result, we performed the same experiment with other two ARMS cell lines characterized by a high expression of ASS1: RMS13 and RH41 cells. In the case of RMS13 cells, the results obtained were in accordance with what observed for

RH4: at mRNA level, a decrease of ASS1 expression was observed when PAX3-FOXO1 was silenced, while at protein level no significative difference was detected (**Figure R13A-B**).

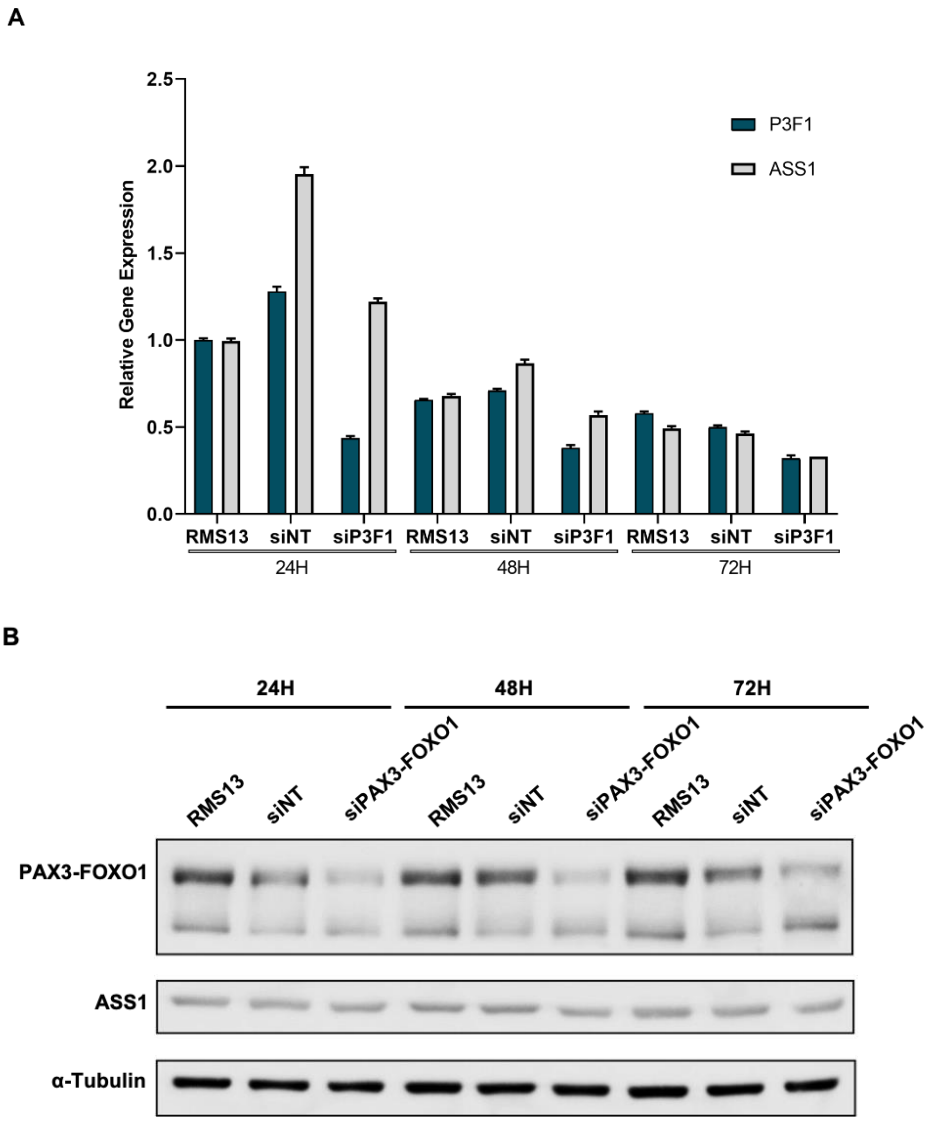

Figure R13: A. qPCR analysis showing PAX3-FOXO1 and ASS1 relative mRNA levels in RMS13 cells transiently silenced for PAX3-FOXO1 expression (siP3F1) at 24, 48 and 72 h after the transfection. Values are referred to RMS13 ASS1 and PAX3-FOXO1 expression at 24 h. Data are expressed as mean ± SD from two different experiments. **B.** Representative WB analysis showing PAX3-FOXO1 and ASS1 expression levels in RMS13 cells transiently silenced for PAX3-FOXO1 expression at 24, 48 and 72 h from the transfection. Cells transfected with the control siRNA (siNT) were used as transfection control. α-Tubulin was used as loading control.

On the other hand, in RH41 cells, ASS1 expression was notably reduced upon PAX3-FOXO1 silencing, not only at mRNA but also at protein level, especially after 72 h from the transfection (**Figure R14A-B**), suggesting that PAX3-FOXO1 impact on ASS1 levels could also be cell line-dependent.

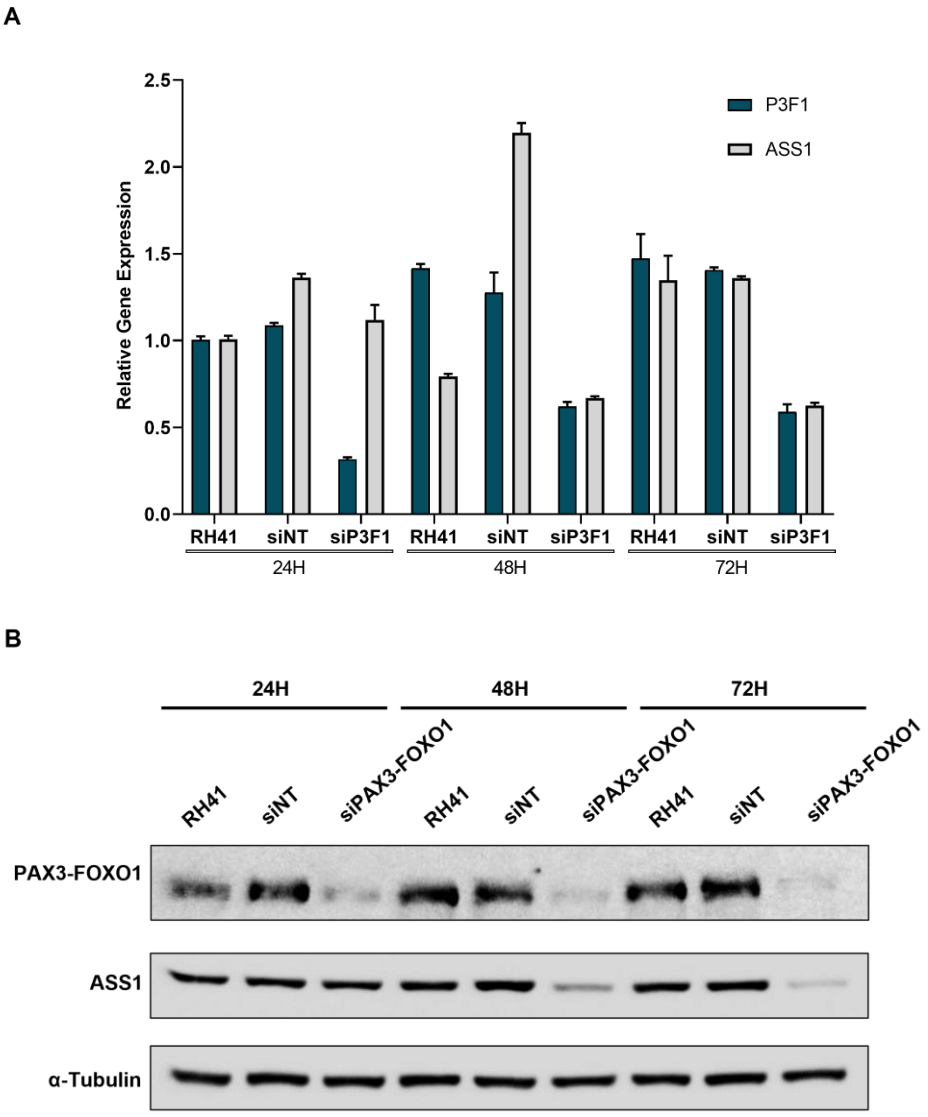

Figure R14: A. qPCR analysis showing PAX3-FOXO1 and ASS1 relative mRNA levels in RH41 cells transiently silenced for PAX3-FOXO1 expression (siP3F1) at 24, 48 and 72 h after the transfection. Values are referred to RH41 ASS1 and PAX3-FOXO1 expression at 24 h. Data are expressed as mean ± SD from two different experiments. **B.** Representative WB analysis showing PAX3-FOXO1 and ASS1 expression levels in RH41 cells transiently silenced for PAX3-FOXO1 expression after 24, 48 and 72 h from the transfection. Cells transfected with the control siRNA (siNT) were used as transfection control. α-Tubulin was used as loading control.

7. ASS1 transient silencing in RH4 cell line

With the aim to assess its role in ARMS biology, we performed transient silencing of ASS1 in RH4 cells, using two different concentrations of the correspondent siRNA pool. ASS1 mRNA levels resulted to be considerably reduced both using 10 nM (**Figure R15A**) and 30 nM (**Figure R15B**) siRNA concentration after 48 and 72 h from the transfection. Surprisingly, at protein level we were not able to observe almost any decrease of ASS1 expression when transfecting cells using 10 nM siRNA (**Figure R16A**). 48 h after the transfection, a 30% and 40% reduction of ASS1 levels was observed when treating cells with 30 nM (**Figure R16B**) and 50 nM siRNA (**Figure R16C**), respectively. After 72 h, ASS1 levels were reduced of a 60% using 30 nM siRNA and almost 70% when the concentration of siRNA employed was 50 nM. In this later case, a significative increase of cell death was observed following the transfection, also in cells treated with the control siRNA, suggesting that a certain level of toxicity was produced by the treatment.

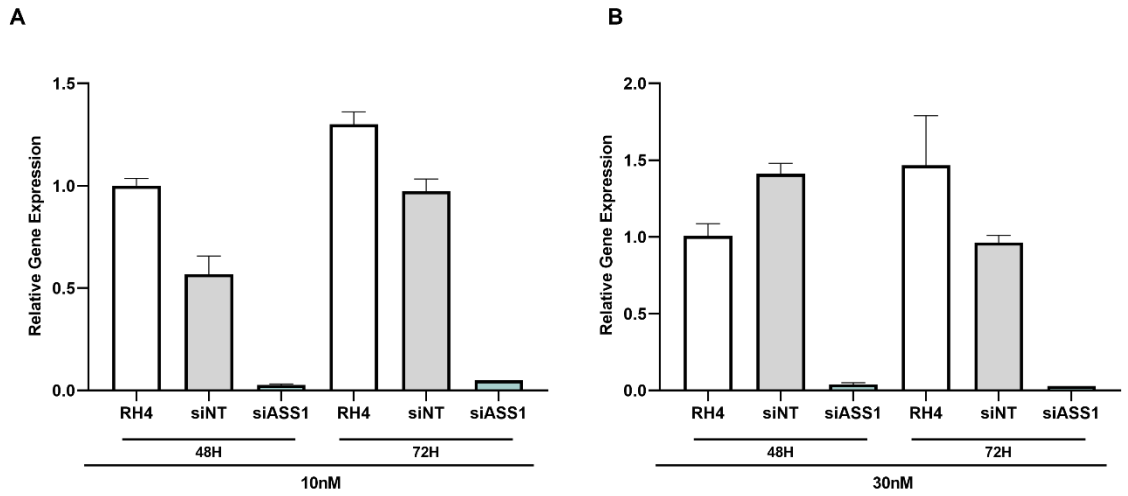

Figure R15: qPCR analysis showing ASS1 relative mRNA levels in RH4 cells transiently silenced for ASS1 expression (siASS1) 48 and 72 h after the transfection using 10 nM (**A**) and 30 nM (**B**) siRNA concentrations. Values are referred to RH4 ASS1 expression at 48 h. Data are expressed as mean ± SD from two different experiments. Cells transfected with the control siRNA (siNT) were used as transfection control.

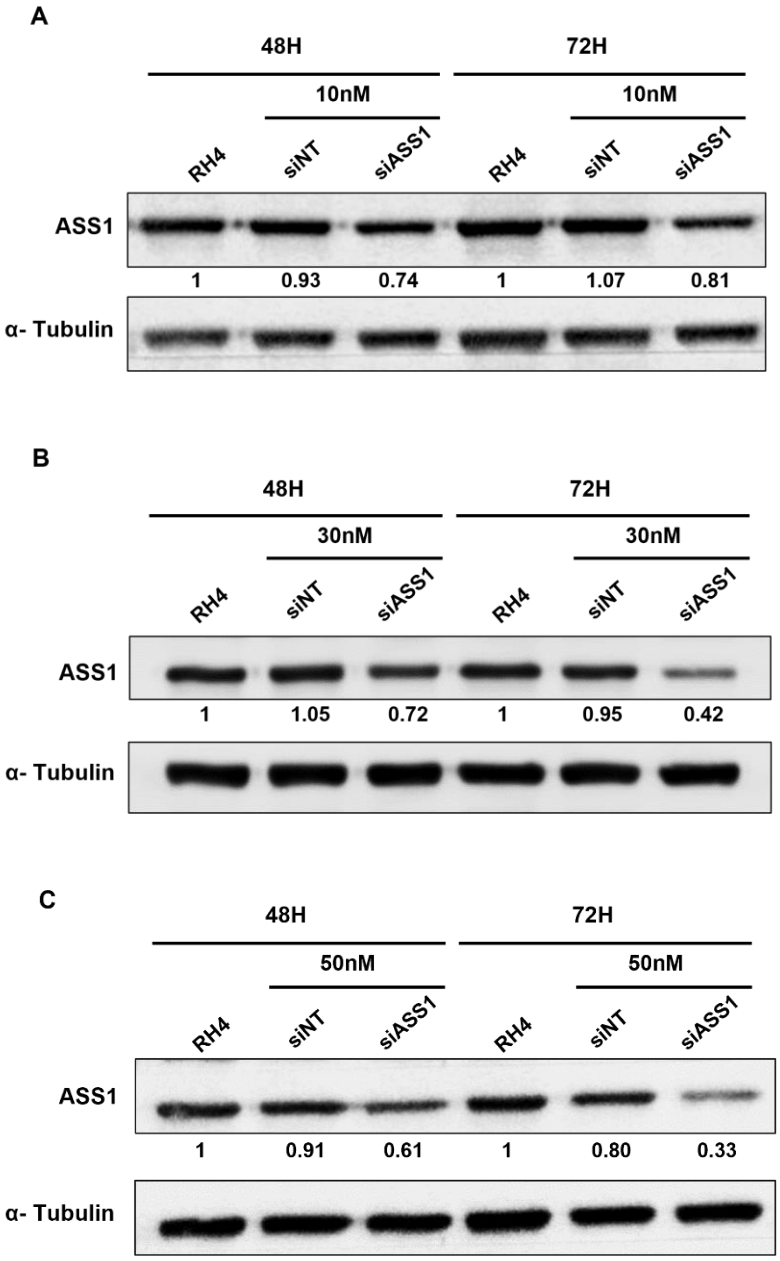

Figure R16: Representative WB analysis showing ASS1 protein levels in RH4 cells transiently silenced for ASS1 expression (siASS1) 48 and 72 h after the transfection, using 10 nM (**A**), 30 nM (**B**) or 50 nM (**C**) siRNA concentrations. Cells transfected with the control siRNA (siNT) were used as transfection control. α-Tubulin was used as loading control.

Given the toxicity observed when treating cells with 50 nM siRNA, we did not employ this condition for the phenotypic characterization of ASS1-silenced cells. However, no significative effect was observed on cell proliferation and migration of RH4 cells upon ASS1 silencing using 30 nM siRNA (data not shown). In our opinion, this was most likely

due to the low efficiency of the silencing and the transitory nature of the treatment, that probably led to the re-expression of the enzyme. On these bases, we decided to perform a stable knockout of ASS1 and study the effects of this protein loss in RH4 cells.

8. ASS1 stable silencing in RH4 cell line through CRISPR-Cas9

To better determine the role played by ASS1 in ARMS cells, we stably downregulated its expression using CRISPR-Cas9 technology, as previously described. We were able to isolate two clones (G2_2 and G1_4) from two pools of cells transfected separately with two different gRNA vectors. Selection was performed using 0.6 µg/mL Puromycin concentration. We compared ASS1 expression of the obtained clones with parental RH4 cells and a pool of cells transfected with a control vector (SCR), both by qPCR (**Figure R17A**) and WB analysis (**Figure R17B**).

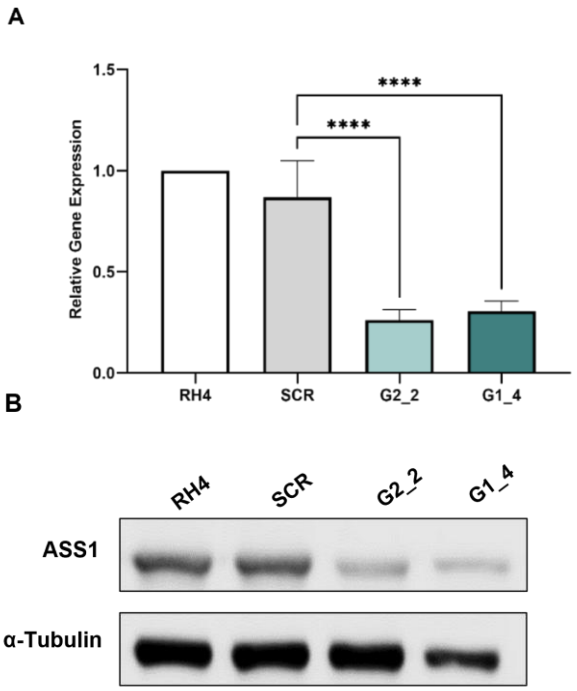

Figure R17: A. qPCR analysis showing relative ASS1 mRNA levels in parental RH4 cells, cells transfected with the control vector (SCR) and two ASS1 CRISPR clones (G2_2 and G1_4). Values are referred to RH4 ASS1 relative expression. Data are expressed as mean ± SD from at least three different experiments. Statistical significance was achieved by One-way ANOVA test (****p ≤ 0.0001). **B.** Representative WB analysis showing ASS1 expression levels in the same cells. α-Tubulin was used as loading control.

As suggested by the residual expression of the protein observed in G2_2 and G1_4 clones, it is probable that we were only able to obtain the monoallelic knockout of ASS1: only one of the two alleles of the gene was targeted and replaced by the GFP-Puro cassette.

ASS1 downregulation was also confirmed by immunofluorescence staining of the same cells, as shown in **Figure R18**. ASS1 was found to be expressed mainly in the cytoplasm of RH4 cells, although nuclear localization was also observed.

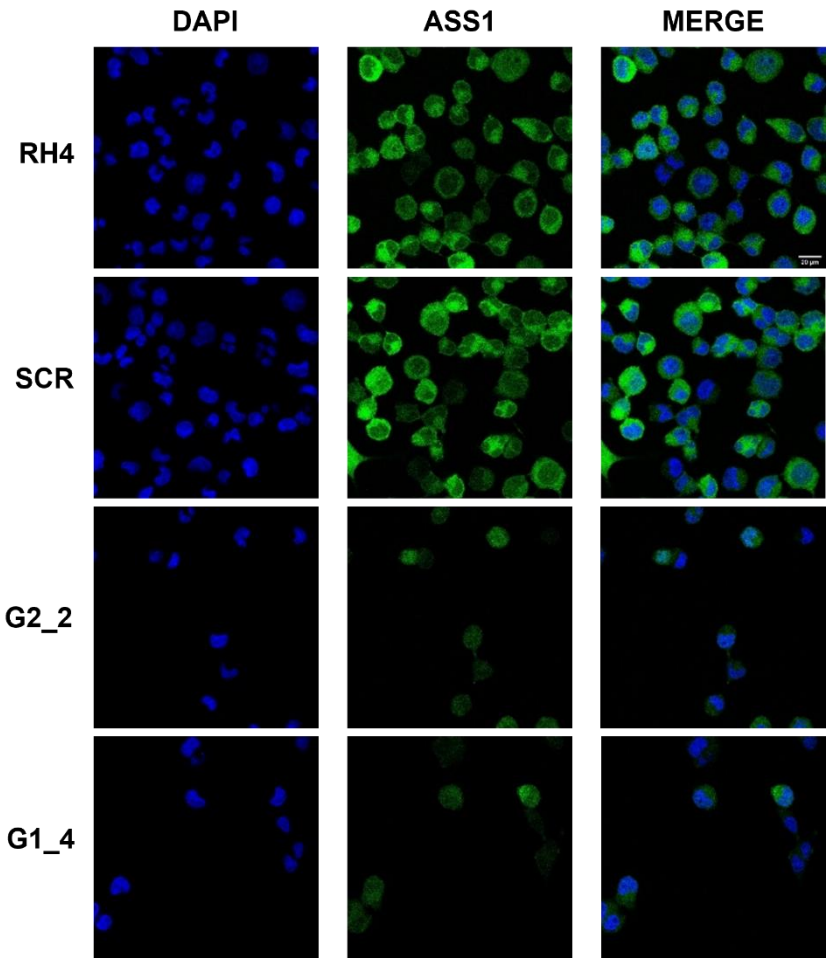

Figure R18: Representative immunofluorescence staining pictures showing ASS1 expression and localization in parental RH4 and SCR cells and in G2_2 and G1_4 ASS1 CRISPR clones. DAPI was used to stain the nuclei. Scale bar: 20 µm.

9. ASS1 downregulation does not affect RH4 cell proliferation *in vitro*

To characterize the phenotype of ASS1-deficient ARMS cells, we proceeded analyzing the proliferative capacity of G2_2 and G1_4 clones, both under basal cell culture conditions (**Figure R19A**) and when cells were grown under the stress of arginine deprivation (**Figure R19B**).

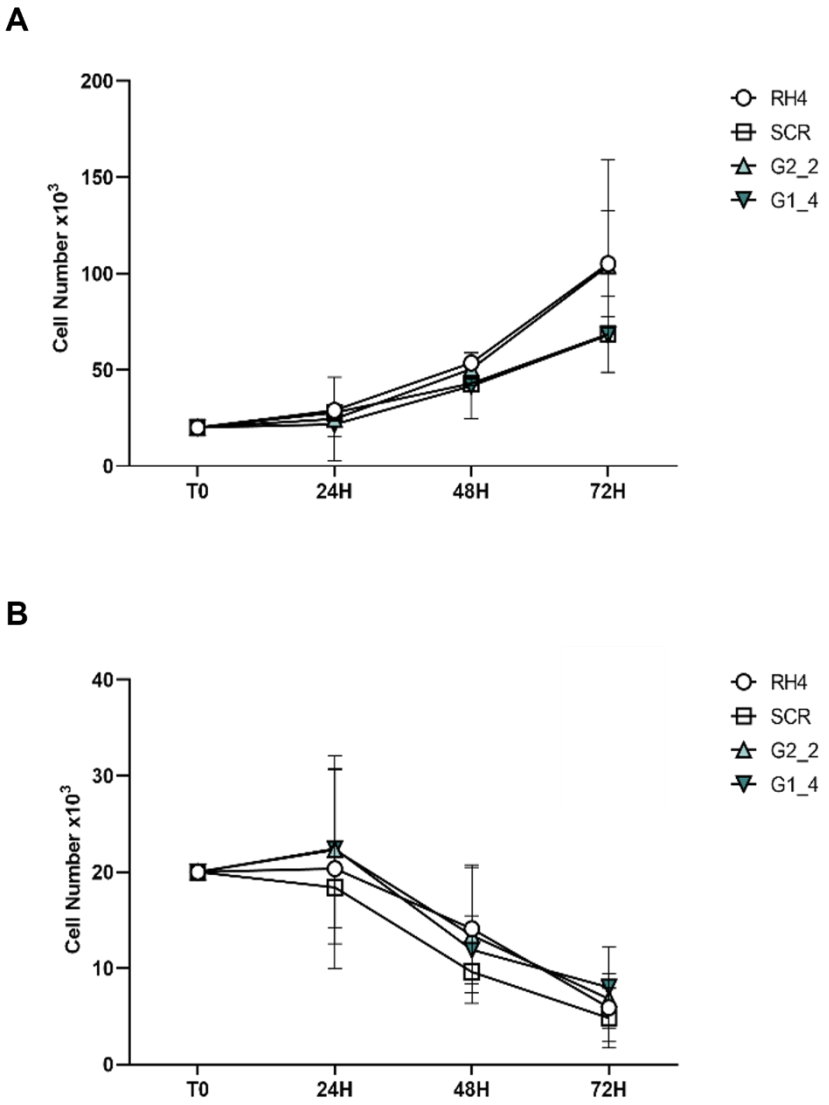

Figure R19: A. Proliferation assay showing of parental RH4, SCR, G2_2 and G1_4 clones cell proliferation, counting after 24, 48 and 72 h from the seeding in the correspondent growing media. **B.** Proliferation assay showing cell proliferation of the same cells, counting after 24, 48 and 72 h under arginine deprivation. Data are expressed as mean ± SD from at least three different experiments.

In both cases, no significative difference was observed when comparing the proliferation rate of parental RH4 or SCR cells with G2_2 and G1_4 clones. This result suggests that ASS1 overexpression is not involved neither in conferring a proliferative advantage to these cells nor in preventing cell death induced by arginine deprivation *in vitro.*

10. ASS1 downregulation impairs RH4 cell migration *in vitro*

Once determined the impact of ASS1 silencing on cell proliferation, we analyzed its effect on the migratory capability of RH4 cells. We performed migration assays in Boyden chambers comparing parental and SCR cells with G2_2 and G1_4 clones. The migratory capability of ASS1-deficient clones resulted to be notably impaired (**Figure R20A-B**), letting us hypothesize that ASS1 could be modulating the metastatic potential of ARMS.

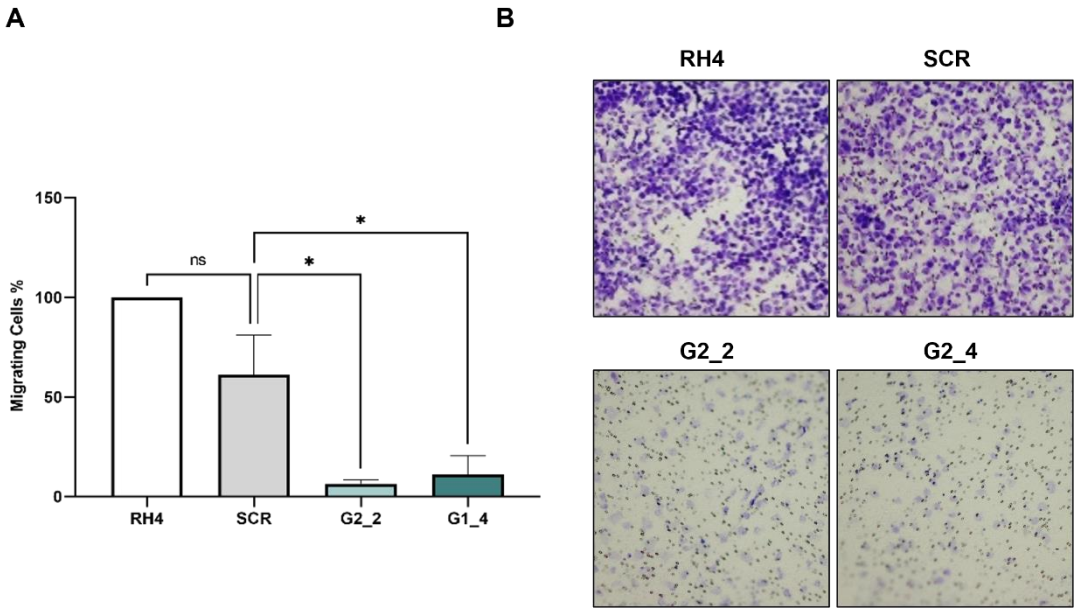

Figure R20: A. Migration assay quantification showing migratory capability of RH4, SCR, G2_2 and G1_4 clones. Obtained values are referred to RH4 percentage of migrated cells. Data are expressed as mean ± SD from at least three different experiments. Statistical significance was achieved by One-way ANOVA test (ns: non-significant, *p ≤ 0.05). **B.** Representative pictures of Boyden chambers membranes stained with Cristal Violet, showing migratory capability of the same cells.

11. ASS1 downregulation inhibits ARMS tumorigenesis *in vivo*

To further study ASS1 role in ARMS tumorigenesis and metastatic spreading, we performed an orthotopic experiment injecting RH4 SCR or G2_2 and G1_4 cells, priorly transfected with luciferase (Luc) as reporter gene, in the gastrocnemius muscles of athymic nude Foxn1nu mice. Before the injection, Luc transfected-cells proliferation was checked, to detect any change in their proliferative capacity after the introduction of the reporter gene (**Figure R21**).

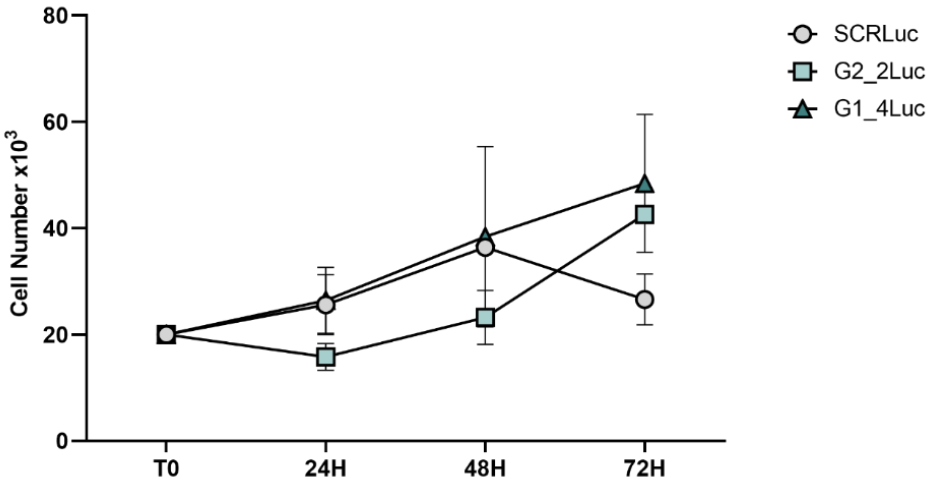

Figure R21: Proliferation assay showing SCRLuc, G2_2Luc and G1_4Luc cell proliferation, counting after 24, 48 and 72 h from the seeding in the correspondent growing media. Data are expressed as mean ± SD from at least three different experiments.

5 x 10^6 cells for each condition were injected in the gastrocnemius muscle of mice right hindlimb, and tumor development was followed by direct measurement and luciferase detection by IVIS. Ten mice were inoculated for each condition, and all of them (10/10) developed primary tumors. Surprisingly, ASS1 downregulation had a dramatic effect on tumor development *in vivo* (**Figure R22**), that resulted to be notably delayed in mice injected with G2_2Luc and G1_4Luc clones when compared to control mice (SCRLuc). The difference in tumor growth was important at the first days post-inoculation. Later, after day 30, the tumors originated from clones G2_2Luc and G1_4Luc injection grew faster, reaching the same tumor volume than the control but showing an evident delay: all the control mice have been operated by day 30, while for the clones G2_2Luc and

G1_4Luc this time was doubled. These results suggest that, differently from what we observed in our *in vitro* proliferation assays, ASS1 can play an important role in favoring tumor development and growth in the *in vivo* context.

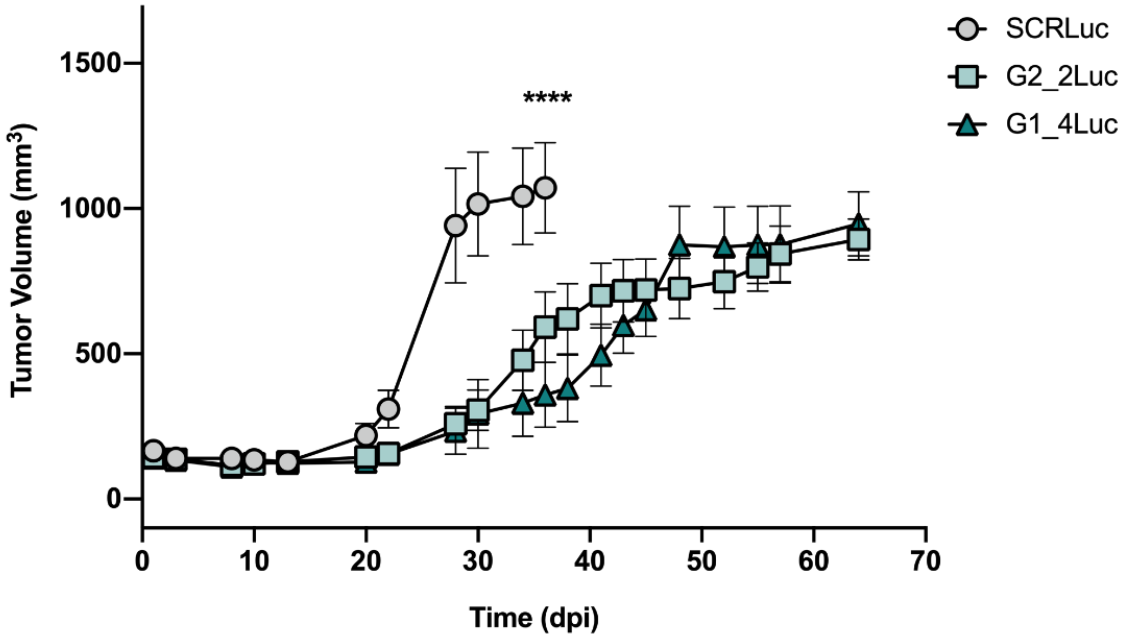

Figure R22: Tumor growth curve showing tumor development in mice injected with SCRLuc, G2_2Luc and G1_4Luc RH4 cells. Data are expressed as mean ± SEM of tumor measurements from 10 animals for each condition, each 3 or 5 days until surgery. Statistical significance was achieved by One-way ANOVA test (****$p \leq 0.0001$).

Once reached the critical volume of approximately 800 mm^3, tumors were extracted and processed for histological analysis. No significative difference was observed among the conditions when tumors were stained with H&E (**Figure R23**).

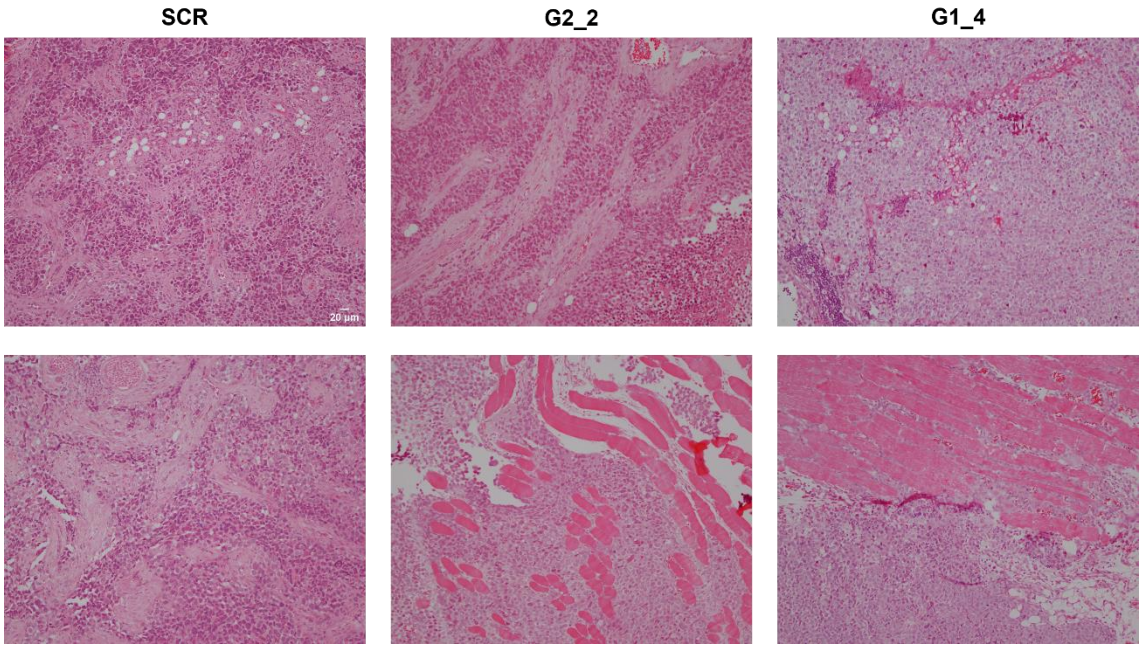

Figure R23: Representative H&E staining pictures showing the histological pattern of xenograft tumors generated from SCRLuc, G2_2Luc and G1_4Luc cells. Scale bar: 20 µm.

After the surgical removal of the tumors, most of the mice developed relapses before any signal of metastatic spreading was detected at IVIS. Therefore, we were not able to observe any significative difference in metastasis formation among the conditions. Only two cases of metastatic spreading in the pelvic lymph nodes area were reported in animals bearing G1_4Luc tumors. This could be possibly due to ASS1 re-expression in these tumors, as confirmed by ASS1 immunohistochemistry staining: at the final point of the assay, G2_2Luc and G1_4Luc tumors presented the same expression level of the enzyme as SCRLuc tumors (**Figure R24**). Moreover, ASS1 re-expression *in vivo* could also explain the rapid tumor growth observed in G2_2Luc and G1_4Luc tumors approximately after 47 days from the injection, even if with a considerable delay when compared to SCRLuc tumors, as shown in **Figure R22**.

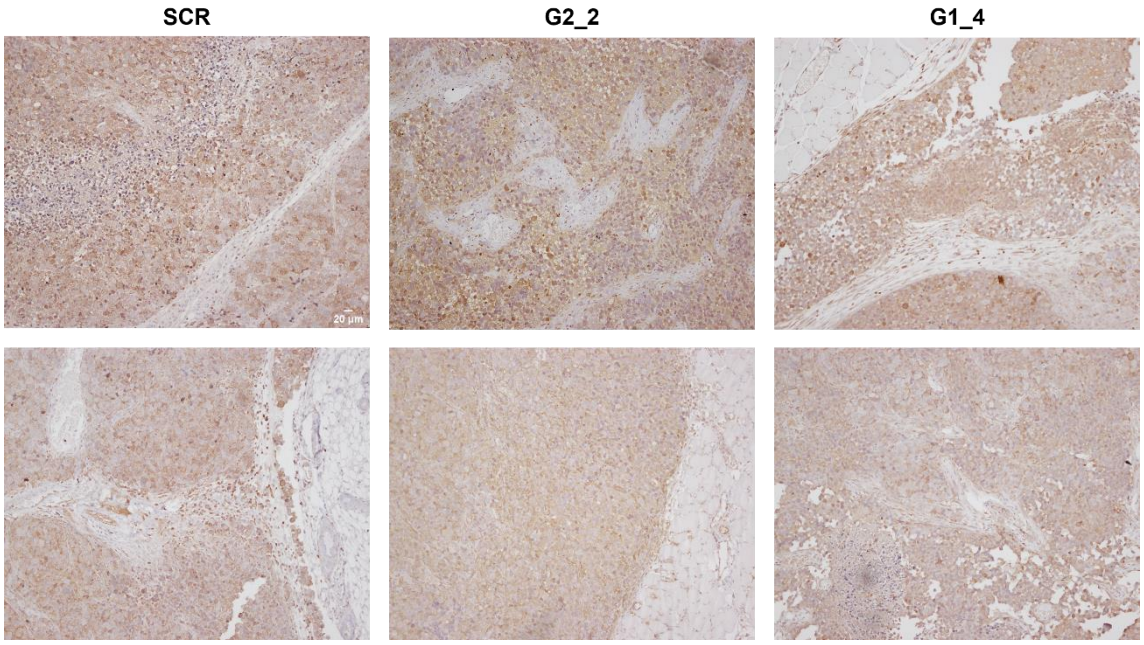

Figure R24: Representative immunohistochemistry staining pictures showing ASS1 expression in xenograft tumors generated from SCRLuc, G2_2Luc and G1_4Luc cells. Scale bar: 20 µm.

ASS1 expression was also assessed by immunohistochemistry in the two G1_4 metastatic samples collected. As shown in **Figure R25**, the positivity for FOXO1 staining in the nuclei confirmed that both pelvic masses were derived from the spreading of PAX3-FOXO1-expressing RH4 G1_4Luc cells. As for their correspondent primary tumors, also the metastatic samples presented high levels of ASS1 expression.

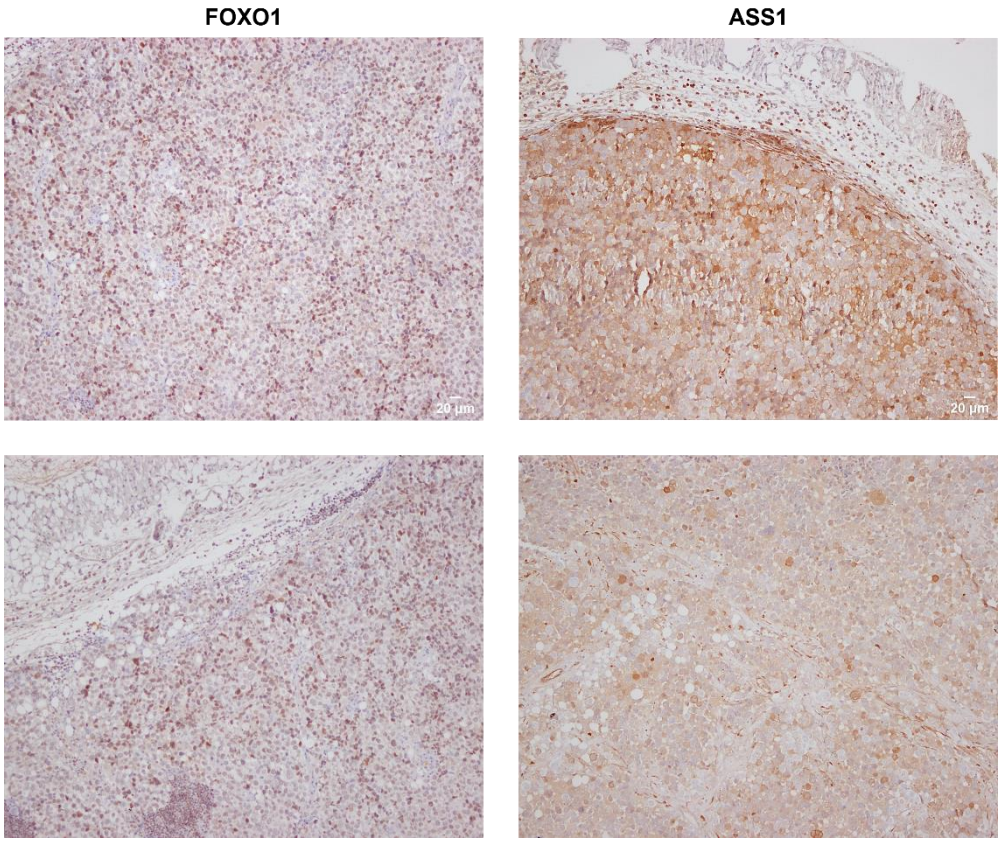

Figure R25: Representative immunohistochemistry staining pictures showing FOXO1 and ASS1 expression in pelvic lymph nodes metastatic tissues generated from G1_4Luc tumors. Scale bar: 20 µm.

12. Pathway analysis of RH4 cells silenced for ASS1 expression

Once established that ASS1 could play a role in ARMS tumorigenesis and metastatic spreading, we decided to focus on the signaling involved in this process. To this purpose, we performed a ClariomD transcriptomics array comparing the profile of parental RH4 and SCR cells versus G2_2 and G1_4 ASS1 clones, to study the impact that the silencing of this enzyme can have on the transcriptional signature of ARMS. The expression of more than 200 genes was found to be differentially regulated upon ASS1 silencing (**Figure R26**). The list of the top 50 de-regulated genes is shown in the Annex I (**Table A2**).

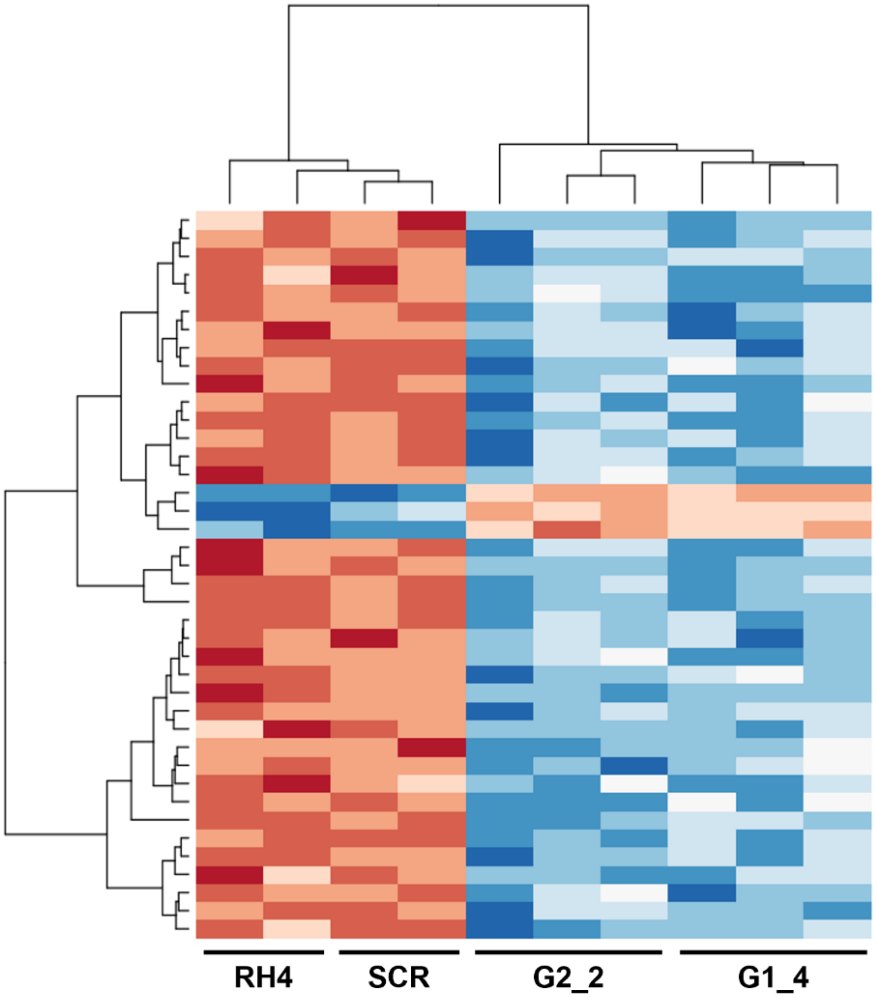

Figure R26: Heatmap showing differentially expressed genes of parental and SCR RH4 cells versus G2_2 and G1_4 ASS1 CRISPR clones. Upregulated genes upon ASS1 silencing are represented in red; downregulated genes are represented in blue.

To validate the results obtained with our *in silico* analysis, we analyzed by qPCR the mRNA levels of several top candidate genes, after selecting them according to fold change and statistical significance. The expression of Myosin Light Chain 1 (MYL1), Histatin 3 (HTN3) and Eukaryotic Translation Elongation Factor 1 Alpha 2 (EEF1A2) was measured in RH4, SCR cells and G2_2 and G1_4 clones, to confirm that ASS1 silencing was actually producing a downregulation of these genes expression (**Figure R27**).

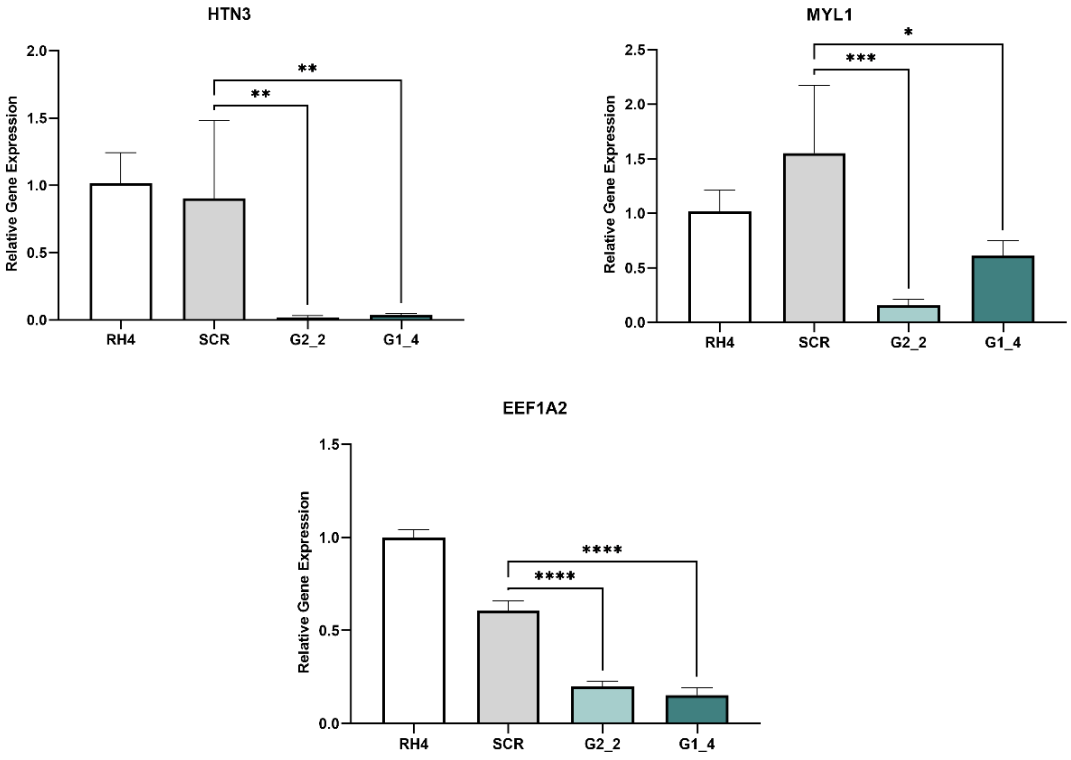

Figure R27: qPCR analysis showing relative HTN3, MYL1 and EEF1A2 gene expression levels in RH4 parental, SCR cells, G2_2 and G1_4 ASS1-CRISPR clones. Values are referred to parental RH4 ASS1 relative expression. Data are expressed as mean ± SD from at least three different experiments. Statistical significance was achieved by One-way ANOVA test (*p ≤ 0.05, **p ≤ 0.01, ***p ≤ 0.001, ****p ≤ 0.0001).

We focused our attention on the elongation factor EEF1A2 as a possible mediator of the phenotype we observed in our model. EEF1A2 has in fact being described to display oncogenic potential in a variety of cancers[285], specifically acting on enhancing cell motility through the activation of AKT[286]. Thus, we analyzed by WB the expression of AKT and its phosphorylated form (Ser473), as well as the activation of the downstream effectors S6K1 and S6, that resulted to be downregulated in G2_2 and G1_4 clones (**Figure R28**), suggesting that this pathway could be involved in regulating ASS1-deficient cells behavior. S6K1 kinase and its main target, the ribosomal protein S6, have been extensively described as master regulators of important basic functions such as protein synthesis and splicing, but also cancer specific mechanisms, including apoptosis inhibition, cell proliferation and cytoskeleton reorganization[287]. Therefore, we also checked the expression of mTOR and its phosphorylated form, as it is considered the main activator of S6K1, but we did not observe significative differences among the

conditions (**Figure R28**), suggesting that the signaling could be regulated by other upstream mediators, such as PDK1. On the other hand, also ERK activation did not seem affected by ASS1 repression (**Figure R28**). This could explain the high proliferation rate maintained by ASS1-deficient clones when compared to parental and SCR RH4 cells.

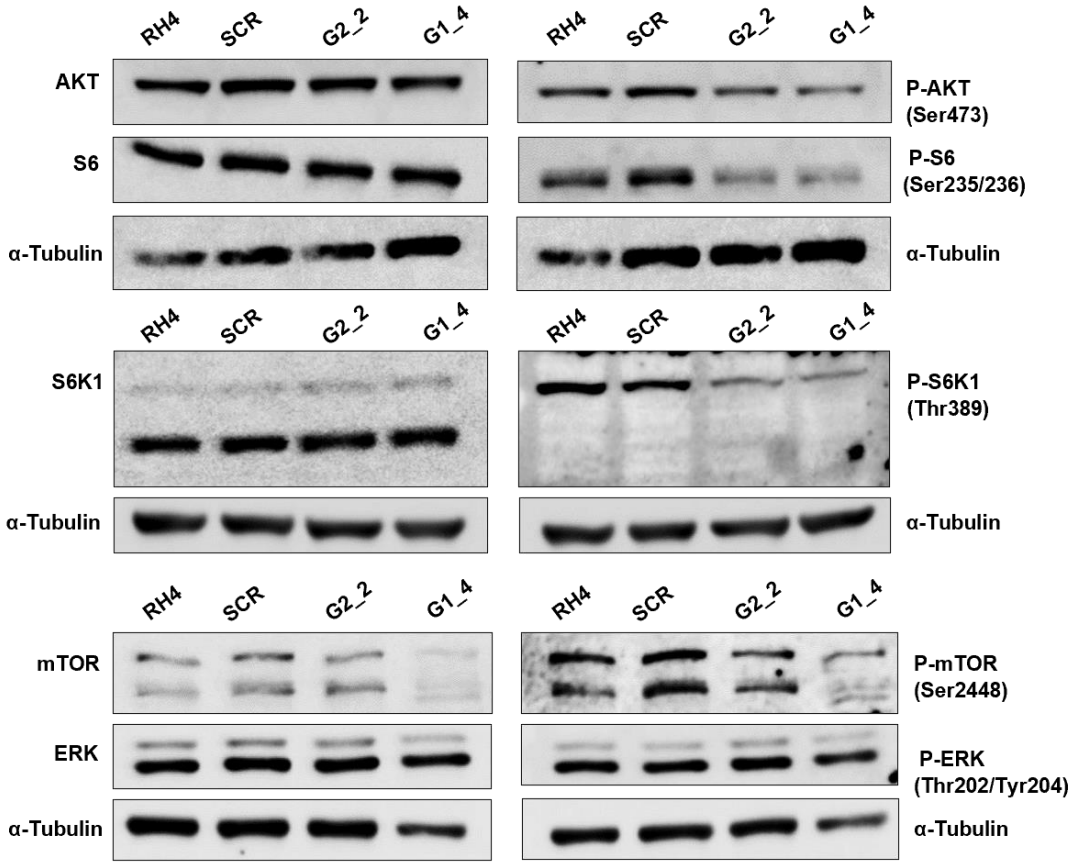

Figure R28: Representative WB analysis showing the expression levels of AKT, S6, S6K1, mTOR, ERK and their respective phosphorylated forms in RH4, SCR, G2_2 and G1_4 cells. α-Tubulin was used as loading control.

To further confirm the involvement of this pathway in ASS1-mediated ARMS aggressive phenotype, we treated RH4 cells with two different PDK1 inhibitors, BX912 and OSU03012, and the S6K1 inhibitor PF-4708671, with the aim to recapitulate the same effects on cell proliferation and migration that we observed when downregulating ASS1 expression. First, we treated RH4 with different concentration of PF-4708671 (10 μM and 20 μM), BX912 (1 μM and 10 μM) and OSU03012 (2.5 μM and 5 μM) and confirmed by WB the inhibition of S6 activation (**Figure R29A-B**).

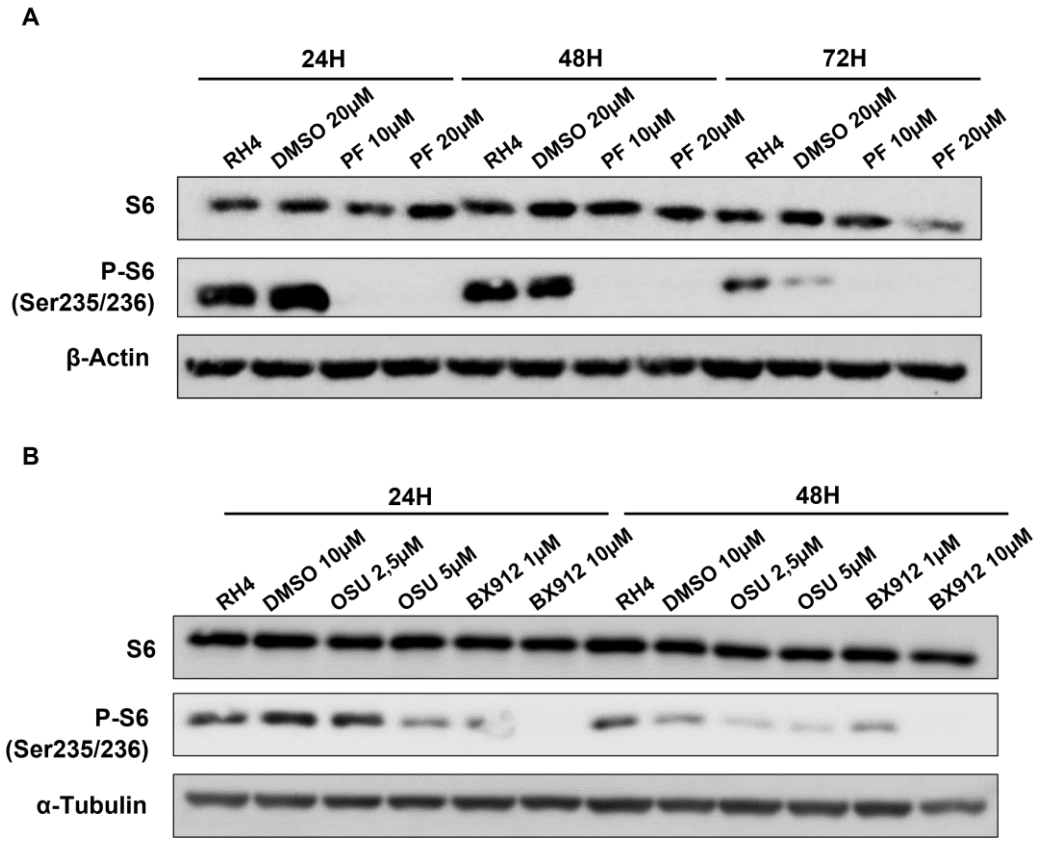

Figure R29: A. Representative WB analysis showing the expression levels of S6 and its phosphorylated form in RH4 cells treated with 10 μM and 20 μM PF-4708671 (PF10μM and PF20μM), after 24, 48 and 72 h from the treatment. Cells treated with 20 μM DMSO were used as control. β-Actin was used as loading control. **B.** Representative WB analysis showing the expression levels of S6 and its phosphorylated form in RH4 cells treated with 2.5 μM and 5 μM OSU03012 (OSU 2.5μM and OSU 5μM) or 1 μM and 10 μM BX912, after 24, 48 and 72 h from the treatment Cells treated with 10 μM DMSO were used as control. α-Tubulin was used as loading control.

Once confirmed the inhibition of S6 downstream activation, we measured RH4 cell proliferation upon the treatment with the three inhibitors. As shown in **Figure R30A**, treating RH4 cells with the S6K1 inhibitor PF-4708671 led to a significative inhibition of cell proliferation at both 1 μM and 10 μM concentrations, after 48 and 72 h from the treatment. The same result was obtained when treating cells with PDK1 inhibitors OSU03012, that caused the stop of cell proliferation at both concentrations employed, after 48 and 72 h from the treatment, and BX912, that considerably affected cell proliferation even after 24 h at the highest concentration tested of 10 μM (**Figure R30B**).

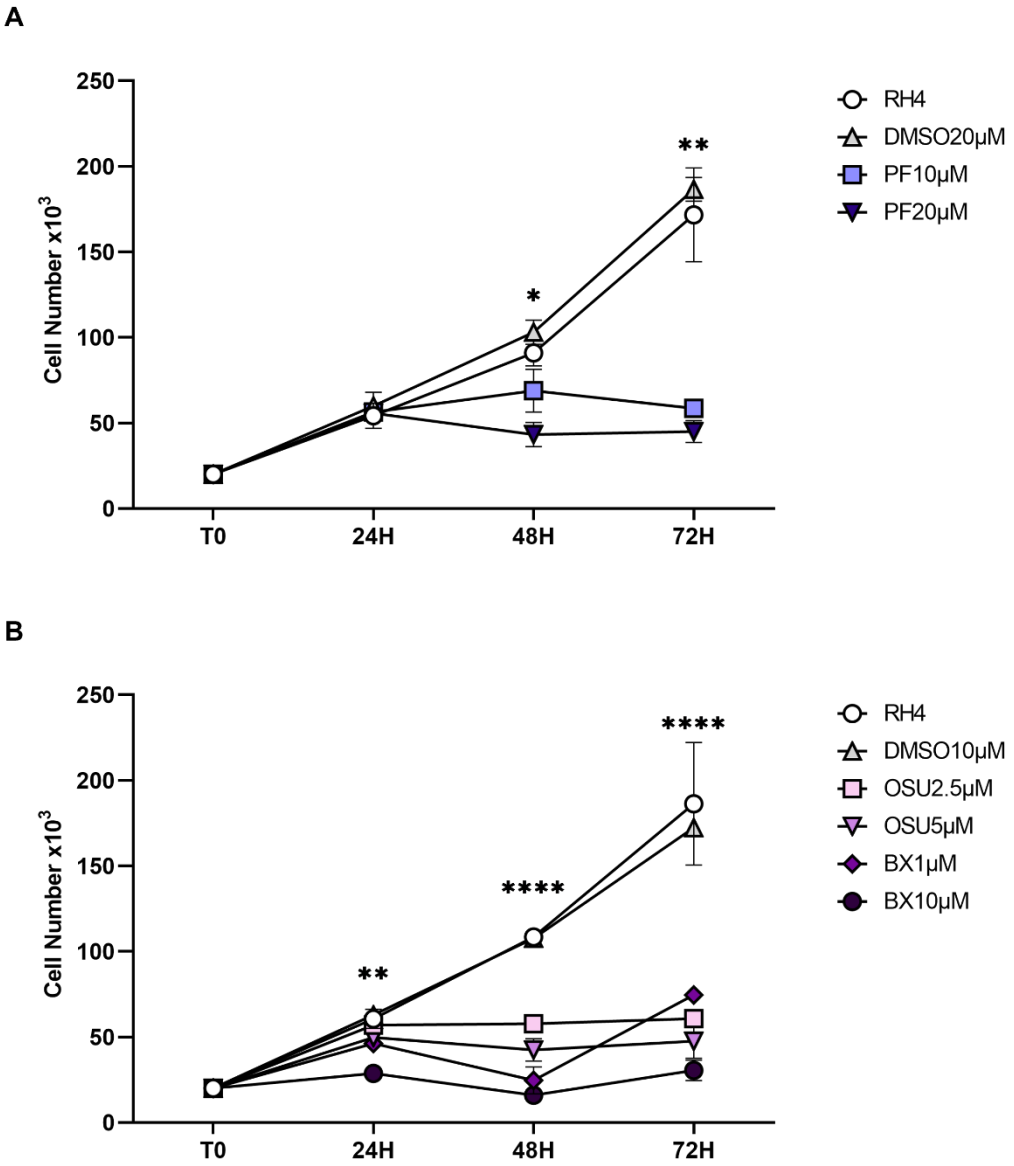

Figure R30: A. Proliferation assay showing RH4 cell proliferation counting after 24, 48 and 72 h from the treatment with PF-4708671 (PF10µM and PF20µM). Data are expressed as mean ± SD from at least three different experiments. Statistical significance (DMSO20µM/ all treatments conditions at 48 and 72 h) was achieved by 2way ANOVA test (*p ≤ 0.05, **p ≤ 0.01). **B.** Proliferation assay showing RH4 cell proliferation counting after 24, 48 and 72 h from the treatment with OSU03012 (OSU 2.5µM and OSU 5µM) or BX912 (BX1µM and BX10µM). Data are expressed as mean ± SD from at least three different experiments. Statistical significance (DMSO 10µM/ BX10µM at 24 h, DMSO 10µM/ all treatments conditions at 48 and 72 h) was achieved by 2way ANOVA test (**p ≤ 0.01, ****p ≤ 0.0001).

Based on these results, migration assay experiments will be performed pre-treating RH4 cells for 24 h with the same inhibitors concentrations tested, to avoid the effect observed on cell proliferation after 48 and 72 h of treatment. In this way, we will be able to evaluate the impact of the pathway inhibition on cellular motility independently from its effect on RH4 proliferative capacity. Further experiments are needed to confirm that PDK1 could be involved in the EEF1A2-mediated phenotype observed in these cells when ASS1 is downregulated and confirm that the inhibition of this pathway can block ASS1 impact on ARMS tumorigenesis and invasiveness.

DISCUSSION

1. Cellular models for the study of ARMS metabolism

Despite all the molecular advances achieved in the past decades, that have enabled a considerable improvement of the molecular and biological understanding of RMS, the successful treatment of young patients affected by this disease still remains a challenge. However, following the implementation of new molecular tools, such as CRISPR-Cas9-based techniques, single-cell gene expression profiling and large-scale DNA sequencing, new therapeutic approaches have emerged as promising alternatives. Given the low incidence of these cancers and the consequent unavailability of clinical specimens, the collaboration among investigators as well as the use of valid *in vitro* and *in vivo* models are essential for the study of RMS.

Since the first observations about cancer cell anomalous metabolic features[145,288], increasing research effort has been focusing on the field, up to recognize metabolism reprogramming as an emerging hallmark of cancer[144]. In order to sustain the increased energy demand for biomass generation and maintenance, tumors have to adjust their metabolism, implementing strategies to increase nutrients uptake and reprogram the reactions to utilize them, as well as to regulate metabolites function in driving gene regulation and interacting with tumor microenvironment[146]. To target metabolism for cancer therapy, it is crucial to uncover the main molecular actors that contribute to reshape the energetic landscape of tumors. So far, very little is known about cancer metabolism in RMS. Our effort with this thesis work was directed towards the identification of new metabolic vulnerabilities of these tumors, especially focusing on the most aggressive fusion-driven ARMS subtype.

First, we aimed to establish several *in vitro* tools for the study of PAX3-FOXO1 role in modulating ARMS metabolism. As a first approach, we induced the fusion protein ectopic expression in C2C12 murine myoblasts. Although the cell of origin of RMS is still not well characterized, all subtypes resemble skeletal myoblasts features, including the expression of adult or embryonal myogenic markers, such as MyoD, myogenin and PAX3/7[289]. Therefore, the most accredited hypothesis sees the mesenchymal stem cell (MSCs) directed towards myogenesis as the putative cell of origin of RMS. Beside the common localization of primary tumors in or near skeletal muscle districts, RMS can also arise in areas that lack muscle tissue, such as the biliary and the genitourinary tract. In this sense, alternative hypotheses have been proposed, according to which RMS can originate from mesenchymal progenitor cells not committed to the myogenic lineage, but to the formation of the stromal components such as fat and fibroblasts[290]. On these bases, an ERMS mouse model originating from the adipocyte lineage through the

constitutive activation of Shh pathway has been described[291]. Furthermore, the more recent possible endothelial derivation of a fusion-negative RMS subtype has been also described[292]. One of our goals was to establish an *in vitro* system that could allow us to reproduce the cellular context in which ARMS arises and study the impact of PAX3-FOXO1 especially on the metabolic rewiring of these tumors. Several cellular systems have been employed to study the fusion protein role *in vitro*. Ren and collaborators have shown that PAX3-FOXO1 introduction is essential for ARMS development in a model of dominant-negative p53 Ras-mutated MSCs, giving rise to tumors that fully resemble human ARMS at histological and transcriptional levels[110]. The introduction of PAX3-FOXO1 has also been described in an immortalized human Duchenne muscular dystrophy myoblast cell line (Dbt)[293], as well as in primary mouse myoblasts using CRISPR-Cas9 technology[294].

C2C12 cellular model has been broadly applied for the *in vitro* pharmaceutical and biomedical research, especially to study skeletal muscle differentiation process[295,296] and metabolism[297], mostly due to the biochemical similarity with human muscle cells and the availability of extensive and documented research protocols. C2C12 cells have been employed also for the preclinical development of a variety of compounds[298], and for the study of RMS oncogenic pathways[299,300], becoming a well-established model to understand this tumors biology. We were able to transiently transfect C2C12 myoblasts with PAX3-FOXO1, originating a tool that could be easily employed for the study of short-term evaluation of the fusion protein-induced changes. However, in our case, obtaining the stable expression of the fusion protein was essential, considering our initial goal to use PAX3-FOXO1-expressing cells for metabolomics studies. Unfortunately, we were not able to obtain a stable transduced pool of C2C12 cells. This could be due to the notorious difficulty of genetically manipulating skeletal muscle cells *in vitro*, especially regarding the methods of gene transfer. As the transient introduction of PAX3-FOXO1 in C2C12 was obtained without any technical problem, we hypothesize that the transduction efficiency was the technical aspect to improve, reconsidering the parameters used for our experiments, such as the virus titration, cells confluency and the infection timing, as well as the features of the plasmids employed.

Considering the importance of achieving the ectopic expression of PAX3-FOXO1 for the study of its impact on ARMS biology, we performed the stable introduction of the fusion protein in the RD ERMS cells. Several studies have employed this fusion-negative cell line to the same purpose[96,301], to study PAX3-FOXO1 role in regulating gene expression. Differently from what experienced with C2C12 transduction, we were able to obtain a pool of RD cells stably expressing PAX3-FOXO1, from which two clones were isolated

and used to perform the following experiments. Nevertheless, the metabolomic analysis performed comparing PAX3-FOXO1-expressing clones with RD parental and CMV-transduced cells, did not give any significative results. In our opinion, this could be due to the tumoral background of parental RD cells, with all the transcriptional and metabolic modifications induced by the high number of mutations and aberrant pathway activation that characterize ERMS tumors. In fact, the wide genomic landscape of ERMS comprises a variety of mutations that can regulate their metabolism, such as the constitutive activation of the RTK/RAS/PI3K axis[302,303] as well as the loss of heterozygosis (LOH) at 11p15.5, that leads to IGF-2 overexpression[82]. The uptake of glucose and amino acids is in fact sustained by the PI3K/AKT pathway[304], consequently promoting the glycolysis and the production of lactate[305], as well as the lipogenesis[306] and the protein synthesis via m-TOR[307]. Loss of p53 activity is also considered one of the main fusion-negative RMS gene signatures that could impact the metabolic landscape of these cancers[308]. It has been described that the uptake of glucose in RD cells is increased due to the upregulation of the glucose transporters GLUT1 and GLUT4 gene expression, directly caused by p53 loss[309]. Moreover, p53 activity can also regulate the expression of the phosphate-activated glutaminase (GLS2), inducing glutamine anapleurosis[310]. Altogether, this evidence suggest that the changes induced at metabolic level by the introduction of PAX3-FOXO1 in RD cells could be unnoticed due to the tumoral genetic background of these cells, that could have masked the effect that the fusion protein alone could have induced.

Furthermore, it is important to underline that the metabolomic analysis of this cellular model was performed during a three-months secondment at Technion Institute in Haifa (Israel). Given the strict window of time to plan the experiments, perform metabolites extraction, LC-MS technique and data interpretation, the analysis of RD clones was prioritized. Due to a lack of time, we were not able to perform the same experiment using the other cellular tools obtained during the first part of this study: PAX3-FOXO1 transient introduction in C2C12 myoblasts could have let us analyse the metabolic profile of non-tumoral cells, in which the main metabolic pathways of interest are not influenced by any oncogenic mutations; on the other hand, it could have been interesting also to integrate the results obtained analysing the metabolic profile of RH4 cells transiently silenced for PAX3-FOXO1 expression with the data referred to PAX3-FOXO1-expressing RD cells. This would have let us confirm the fusion-mediated ASS1 overexpression in the same ARMS cell line used to perform the following experiments of ASS1 silencing. Ultimately, the ideal cellular model to use would have been represented by human skeletal myoblast isolated from healthy tissues. We believe that the introduction of PAX3-FOXO1 in these

primary cells could have allowed to study the changes strictly induced by the presence of the fusion protein in a physiologic cellular context. Thus, the absence of other alterations and the human genetic background could had helped to better correlate the metabolic profile of transfected cells with the fusion protein expression.

PAX3-FOXO1 is considered the true driver of ARMS initiation and progression, due to its enhanced transcriptional activity, that leads to the upregulation of several oncogenic downstream targets[311]. Multiple studies have focused on the epigenetic and transcriptional profile of PAX3-FOXO1-expressing cells[91,94,301,312], but very little is known about the metabolic rewiring related to the fusion protein activity. The metabolism of STS is poorly understood, although some articles have analysed nutrient requirements or "glycolytic versus respiratory" characteristics of STS subtypes[313]. According to this study, ARMS cells show respiration rates and spare glycolytic capacity that appear to be lower than other sarcoma subtypes, suggesting that ATP production in these cells could rely more on glycolysis than mitochondrial respiration. Furthermore, PAX3-FOXO1 has been described to control glucose uptake via the transcriptional upregulation of GLUT4 transporter[314]. In consistence with this, ARMS cells result to be more sensitive to glucose deprivation and treatment with the glycolysis inhibitor 2-deoxyglucose (2-DG) than ERMS cells[315], suggesting that PAX3-FOXO1 could play a role in increasing glucose consumption.

PAX3-FOXO1 has also been described to control the transcription of the phosphatase PTEN[316], that inhibits PI3K downstream pathway. This way, the fusion protein is responsible of sustaining PI3K/AKT/mTOR metabolic axis.

Another interesting transcriptional target of the fusion protein is the carnitine palmitoyltransferase gene (CPT1A). The activity of this mitochondrial enzyme leads to the formation of acyl carnitines and its PAX3-FOXO1-mediated upregulation has been described to increase lipid degradation[317]. The hypothesis suggested by Liu and collaborators sees this mechanism as a source of additional energy to supply ARMS metastatic spreading, unravelling a putative unique signature of fusion-positive RMS metabolism. In this sense, the identification of new metabolic target genes of PAX3-FOXO1 could be extremely important to describe the molecular adaptations of these tumors and hopefully identify new potential vulnerabilities of these aggressive RMS subtype.

With this in mind, we decided to perform a bioinformatic analysis of previously published data and compare gene expression across datasets, based on PAX3-FOXO1

expression, to individuate target genes of the fusion that could possibly play a role in modulating cancer metabolism. The studies we selected for our analysis[97,283,284] compared the profile of parental ARMS cells silenced or not for PAX3-FOXO1 expression, ARMS and ERMS primary tumors as well as ARMS tumors and normal muscle cells. Including different sets of transcriptomic arrays, from patient samples to cell lines, allowed us obtaining a wider source of data to analyze with our bioinformatic tools, especially considering that the amount of published material from RMS studies is reduced, due to the low incidence of these tumors. Thus, it is important to underline that the collaboration among researchers by sharing pre-clinical and clinical data is key for the scientific progress in the field of rare diseases and pediatric cancers.

We focused our attention on the identification of putative metabolic mediators of ARMS phenotype among the 56 upregulated genes we found in common between the lists obtained from our comparisons. Very few genes directly related to metabolic pathways were identified. Among them, the Dihydrofolate reductase (DHFR) called our attention as one of the key regulators of purine synthesis. Its inhibitor Methotrexate was previously employed in a phase II trial for children and adolescents with high-risk metastatic RMS[318], and currently other clinical trials are ongoing to study its efficacy in combination with other chemotherapeutic agents in STS. For this reason, we decided to focus on another interesting candidate, ASS1, especially considering that to date there is no evidence describing its function in RMS, while in contrast it is well established that the majority of STS are ASS1-deficient[238]. Therefore, we selected this target to validate its expression in RMS and study its potential role as a specific metabolic signature of these cancers.

2. ASS1 overexpression in ARMS and its partial correlation with PAX3-FOXO1

Our study suggests that new metabolites can be involved in the metabolic reprogramming of RMS tumor cells, such as the ASS1 pathway intermediates. ASS1 dysregulation is linked to altered arginine metabolism, recognized as one of the most important metabolites for tumor cells proliferation[174]. This amino acid is, in fact, crucial for most of biological functions, and the inability of many cancer types to synthesize it *de novo* has been exploited for several arginine deprivation-based therapeutic strategies. Currently, the use of PEGylated arginine deiminase (ADI-PEG20) for extracellular arginine depletion is being tested in clinical trials for several ASS1-negative tumor types, including STS. Bean and collaborators profiled over 700 specimens from 45 different

STS subtypes and ASS1 negativity was assessed in more than the 90% of the samples[238]. The use of ADI-PEG20 together with the clinically available compound chloroquine, was described as a well-tolerated and wide applicable therapeutic alternative for these untreatable diseases.

Although most sarcoma types have been described as ASS1-deficient, its overexpression in ARMS could be considered as a novel hallmark for these STS subtypes, unrevealing a new metabolic vulnerability that could represent a therapeutic target for the treatment of this pediatric cancer.

Using the model of PAX3-FOXO1 introduction in RD cells, we were able to demonstrate that the relative levels of urea cycle metabolites were reflecting the upregulation of ASS1 upon the fusion protein expression. It is interesting to observe that the protein expression analysis did not confirm such a significative upregulation of the enzyme in terms of protein levels, when comparing parental RD and CMV cells to RD PAX3-FOXO1-expressing clones, suggesting that ASS1 expression could be not exclusively regulated by the fusion protein at transcriptional level. Indeed, other mechanisms controlled by PAX3-FOXO1 could influence its enzymatic activity. That is suggested also by the lack of changes in ASS1 expression at protein level upon PAX3-FOXO1 silencing in RH4 and RMS13 cells, or its introduction in C2C12 myoblasts. It is also interesting to notice that when silencing PAX3-FOXO1 in RH41, the decrease of ASS1 expression at protein level is dramatic. This suggests that the effect of the fusion protein on the enzyme expression could also be cell line dependent.

The lack of correlation between the results obtained with the RNA and protein expression analysis once again could be explained by the fact that other mechanisms may be involved in regulating the activity of the enzyme as well as its stability. Although the bulk of published literature suggests that ASS1 regulation occurs primarily at transcriptional level, some recent findings report that this enzyme activity could be influenced by the interaction with other molecules, such as the NADPH sensor protein HSCARG[319]. Arginine availability in the tumor microenvironment as well as ASS1 subcellular localization, possibly linked to Caveolin-1 expression, may also affect ASS1 activity[320]. Also, it has been shown that human ASS1 can be inactivated by reversible nitrosylation at Cys-132[321] and phosphorylated in response to VEGF treatment by protein kinase A (PKA) in vascular endothelial cells[322], suggesting that other post-translational mechanisms may regulate its enzymatic activity. The main mechanism that regulates ASS1 expression in cancer is the methylation of its promoter[275,323], that leads to its silencing and the consequent tumor auxotrophy for arginine. One of the most common

causes for the failure of treatments that exploit this metabolic vulnerability is ASS1 re-expression: under arginine depletion, c-MYC translocates to the nucleus to bind ASS1 promoter and enhance its transcription[241,324].

Overall, our data show that the increased expression of ASS1 in ARMS cells is not strictly dependent on PAX3-FOXO1 presence, suggesting that arginine synthesis in these tumors could be not only regulated at a transcriptional level by the fusion protein, but also by other effectors, as the arginine availability in the microenvironment or other post-translational mechanisms that could act on ASS1 enzyme stability and activity.

Even though ASS1 upregulation in ARMS could be unrelated to PAX3-FOXO1 presence, it seems clear that this enzyme is overexpressed in most of RMS cell lines, including ERMS RD cells. Although over 70% of cancers have been described as ASS1-deficient[172], there is evidence that ASS1 upregulation may also play a role in enhancing tumor progression and invasion in different malignancies. In gastric cancer, ASS1 overexpression was correlated with a worst prognosis[249]. Furthermore, its silencing led to a considerable reduction of liver metastasis, and arginine depletion inhibited gastric cell lines migration, suggesting that ASS1 could be involved in modulating the invasiveness of these cancers[325]. The mechanism suggested to explain this process indicates that ASS1 could sustain gastric cancer invasion through the inhibition of lysosome activity and cell autophagy, leading to the accumulation of active β-catenin, Snail and Twist[326].

Ovarian cancer has also been described to present high ASS1 expression in comparison with normal surface epithelium[246]. Another interesting mechanism for ASS1 expression regulation has been described in these tumors: the pro-inflammatory cytokine TNF-α co-localizes with ASS1; furthermore, the expression of the enzyme is induced in ovarian cancer cells following stimulation with TNF-α, suggesting a possible correlation between tumor inflammation and arginine metabolism in this cancer type.

In line with what has been described for ovarian cancer, in Caco-2 colon adenocarcinoma cell line, interleukin 1-β (IL-β) has also been addressed as a regulator of ASS1 expression, by activating the transcription factor NF-κB[327]. Interestingly, this mechanism is inhibited by glutamine addition that can reduce p65 levels, suggesting a novel molecular reciprocity between the effects of an amino acid and a cytokine on gene expression[252].

Bateman and collaborators described ASS1 as a colorectal cancer target that, when inhibited, lowers the levels of the tumor suppressing metabolite fumarate, leading to impaired cancer cell glycolytic capacity and lipid metabolism[247]. In these tumors, ASS1

upregulation is driven by a specific mutation of KRAS and its knockdown causes the inhibition of cancer growth in 3D culture systems, that is not rescued by arginine supplementation, confirming that its role is not only essential for arginine *de novo* synthesis, but also to produce the key metabolite fumarate[328].

In line with all the evidence that describe ASS1 as a key oncogenic player, our experiments confirm that it is overexpressed in RMS cell lines and ARMS xenograft tumors at RNA and protein level. It would be interesting to evaluate it in tissue microarrays (TMAs) from RMS primary samples, to validate our findings and possibly correlate its expression with patient outcome and stratification. It would be also crucial to identify the mechanism by which PAX3-FOXO1 regulates ASS1 expression or possibly its activity. Experiments of chromatin immunoprecipitation combined with sequencing (ChIP-Seq) would be ideal to identify sites for PAX3-FOXO1 direct binding to ASS1 promoter and describe its direct function as transcriptional regulator, but also to individuate new interactors that could act as modulators of the enzyme expression in these tumors.

3. ASS1 plays a role in sustaining ARMS tumorigenesis and metastasis

To determine its role in ARMS, we silenced ASS1 expression in RH4 cells first transiently, using a commercially available pool of three specific siRNA sequences. We tried to set up the best experimental conditions to obtain a decrease of ASS1 protein expression, using different siRNA concentrations. Unfortunately, none of the conditions tested gave an enough level of silencing to study its effects on cell behaviour and phenotype. Indeed, when using 50 nM siRNA concentration, even if the level of silencing produced seemed to be adequate, the transfection itself resulted to affect cell viability. On the other hand, when using 30 nM siRNA concentration, no toxicity was observed but the percentage of silencing obtained was not significative, especially when considering the protein levels, that were not matching the RNA decrease. The most reasonable explanation for what we observed is related to the possible slow turnover of the enzyme: for proteins characterized by high stability and half-life, it could be difficult to observe a protein reduction that matches the mRNA decrease. It would be interesting to evaluate ASS1 stability in our model and determine its half-life, treating cells with the protein synthesis inhibitor Cycloheximide (CHX). Indeed, its use represents a well-established technique to measure protein stability in a short window of time, inducing the stop of the translational machinery to observe progressive protein levels decrease upon treatment. While the amount of an unstable protein will decrease in a shorter period of

time, the reduction of a stable protein with a slow turnover will require more time, and possibly the decrease observed will be lower[329,330]. Following CHX treatment, comparing ASS1 levels in ARMS cells to a known protein characterized by a quick turnover rate, would shed light on the lack of correlation between ASS1 mRNA and protein levels and possibly explain the low silencing efficacy we obtained using siRNA.

Given the difficulties encountered in performing ASS1 transient silencing, we decided to move on to the stable downregulation of its expression in RH4 using CRISPR-Cas9 technology. We employed the HDR-mediated DNA reparation system, allowing the simultaneous knockout of ASS1 gene and the knockin of GFP, as reporter gene, and resistance to Puromycin, as selection marker. We were able to obtain the stable downregulation of ASS1 in both pools of cells transfected separately with each gRNA plasmids, G1 and G2, although both cellular populations maintained a certain level of ASS1 protein expression. Thinking that this could have been due to the heterogeneous nature of the two cell populations, we decided to isolate clones from each pool, seeding cells at a density of one cell per well in 96 wells plates. This way, we were able to expand various cell populations originated from a single cell, therefore homogeneous, and analyse ASS1 expression to individuate the clones characterized by the lowest protein levels. Surprisingly, all the clones analysed showed a certain level of ASS1 protein expression. This suggests that most likely we were only able to obtain the monoallelic knockout of ASS1, meaning that of the two gene alleles, only one was effectively targeted. To confirm that, it would be necessary to sequence the edited gene and determine the exact position of the indels in one or both alleles. Once confirmed the monoallelic knockout, it would be interesting to repeat the transfection of CRISPR-Cas9-edited cells using another donor vector, containing a different selection marker from the one employed for the first round of silencing. This way, it would be possible to target the second unedited allele and check if the complete knockout of the enzyme would be compatible with cell viability.

To perform phenotypic assays and study the impact of ASS1 downregulation in RH4, we selected G2_2 and G1_4 clones, as these were the two cell populations characterized by the lowest enzyme expression among all the clones isolated. Despite ASS1 residual expression, this model allowed to describe the impact of ASS1 upregulation on ARMS tumors behaviour. Although it does not seem to be involved in regulating cell proliferation *in vitro*, even when growing cells under the stress of arginine deprivation, we had evidence showing that tumorigenesis *in vivo* was notably delayed upon ASS1 silencing, suggesting that in a context that recapitulates better the tumor features, ASS1 plays an important role in determining tumor growth rate. Nevertheless, also G2_2 and G1_4 cells

injection led to tumor formation in mice. This was most likely due to the ASS1 re-expression observed after 4 weeks from the orthotopic inoculation, as suggested by the staining pattern observed in these xenograft tissues by immunohistochemistry.

To recapitulate *in vivo* the results obtained *in vitro* still remains one of the biggest challenges for cancer research, especially if metabolic therapeutic strategies are involved. The tumor microenvironment and the complex interactions that occur between the extracellular component, the stromal compartment and the malignant cells can affect tumor behaviour and contribute to its adaptation to extreme metabolic landscapes[157]. As previously discussed, the regulation of ASS1 expression can be influenced by many transcriptional and post-translational mechanisms. ASS1 re-expression *in vivo* is has been already shown as a common mechanism for ADI-PEG resistance: positivity to ASS1 staining was documented in tumor biopsies of patients that initially responded to the therapy, but later showed progression[331]. ADI-PEG-resistant melanoma cell lines have been described to present high ASS1 expression consequently to the constitutive c-Myc binding to the ASS1 promoter[276]. Interestingly, these cells also showed enhanced AKT signaling and sensitivity to PI3K/AKT inhibitors, in accordance with the results we obtained with ASS1-expressing ARMS cells.

Several metabolites as hormones, nutrients and immunostimulants have been described to regulate tissue specific ASS1 expression[209]. Concerning arginine, it has been reported that in human epithelial cell lines, arginine concentration in culture can lead to the de-repression of ASS1 transcription, therefore increasing the enzyme levels[332]. In our case, it would have been interesting to evaluate ASS1 protein levels in the RH4 model under the stress of arginine deprivation: although no effect was produced in terms of cell proliferation, it could have been useful to check if the lack of arginine availability was determining the re-expression of the enzyme *in vitro*, to then verify this hypothesis also in the *in vivo* context.

A potentially effective strategy to overcome the differences in terms of nutrient availability between the *in vitro* and *in vivo* conditions is represented using human plasma-like medium (HPLM) for cell culture. This physiologic medium is characterized by a composition that resembles human plasma, with amino acids, nutrients and salt concentration that mimic the body cellular environment[333]. Although its use in cell culture is far from recapitulating *in vitro* the complexity of metabolic interactions that occur *in vivo*, growing cells in HPLM medium represents a well-established method that can be exploited to test cell response to nutrient deprivation in a more accurate manner. Growing cells in a 3D culture system can also represent a useful tool to study metabolic

alterations of solid tumors. Indeed, metabolites gradients *in vivo* can be responsible for the creation of a specific spatial organization, that involves the stroma as well as immune and malignant cells[334]. Therefore, the spatial differential concentration of nutrients can contribute to shape tumor metabolic features and vulnerabilities that would be very difficult to spot in a 2D cell culture system.

Regarding the metastatic process, we demonstrated that ASS1 silencing leads to a significative impairment of RH4 migratory capability in Boyden chambers, as previously described in other cancer types[325,326]. Unfortunately, we were not able to confirm these findings *in vivo*, as, after tumors removal, relapses occurred in mice injected with SCR as well as G2_2 and G1_4 cells, before we were able to detect any metastasis formation through IVIS. The histological analysis of the tumor sections revealed the presence of only two cases of metastatic spreading in the pelvic lymph nodes area of mice bearing G1_4Luc tumors. We attributed this event to ASS1 re-expression in these tumors: our immunohistochemistry analysis confirmed ASS1 positivity not only in G2_2Luc and G1_4Luc tumors, but also in the two G1_4Luc metastatic tissues collected. This result, together with our findings *in vitro*, is in line with our hypothesis that ASS1 contributes to ARMS cells spreading.

ASS1 role in modulating cancer metastasis is strictly dependent on the tumor type. For most cancers that are described as ASS1-negative, its downregulation is associated to poor survival and metastasis. Silberman and collaborators showed that in a cohort of 648 patients across 14 different cancer types, ASS1 downregulation correlated with hypoxia-related gene overexpression and metastasis detection[335]. Furthermore, it has been described that from a bioinformatic analysis of different datasets for breast cancer bone metastasis, ASS1 emerged as one of the most significative validated targets among the downregulated genes, and its overexpression inhibited breast cancer cells motility *in vitro*[336].

Nevertheless, and consistently with our findings, several publications correlated ASS1 overexpression with increased tumor invasion. According to a very recent study, ASS1 depletion in SW-1116 colorectal cancer cells has been described to decrease cell migration, while its stable introduction in ASS1-deficient Caco-2 cells led to an increase in cell motility *in vitro*. Furthermore, a correlation between ASS1 upregulation, lymph node and distant metastasis, and shorter overall survival was established, suggesting that the enzyme could be considered as a novel biomarker for colorectal cancer diagnosis and prognosis[248]. From in-depth proteomics analysis and *in vitro* validation of endometrial cancer primary samples and sentinel lymph nodes (SLN), ASS1 emerged

as one of the proteins specifically overexpressed in high grade tumors and their corresponding SLN[337]. This data further suggests a possible link between this enzyme and cancer spreading to the lymph nodes. As previously discussed, ASS1 upregulation has also been reported to sustain cell migration in gastric cancer. Using shRNA against ASS1, gastric cancer motility resulted impaired through the suppression of STAT3, leading to the reduction of liver metastasis formation *in vivo*[249]. The molecular mechanism proposed to explain ASS1-mediated gastric cancer invasiveness involves the inhibition of autophagy and lysosome activity, with the consequent accumulation of Snail and Twist[326].

Another interesting aspect that emerged from our results regards ASS1 localization. To confirm the protein knockdown in our clones, we performed immunofluorescence staining of the enzyme and analysed the samples using a confocal microscope. This allowed us to obtain information about ASS1 localization in our cellular model: although mainly present in the cytoplasmatic compartment, ASS1 was also found to localize in the nuclei of RH4 cells.

The bulk of published literature describes ASS1 as a cytoplasmatic enzyme, highly expressed in the liver, but also detected in most human tissues and organs, where its subcellular localization can vary[320].

Cohen and Kuda described for the first time that in the liver, ASS1 localizes around mitochondria, in proximity of the outer membrane cytoplasmic side[338], where it transforms the citrulline that is synthetised on the inner mitochondrial membrane by the ornithine transcarbamoylase[339]. This spatial control avoids the exchange of the substrates and products of these reactions with other cellular and extracellular pools of the same metabolites.

If in the liver ASS1 main role is related to the urea cycle, in the other human tissue its function is mainly oriented to arginine synthesis, for the consequent production of nitric oxide[340]. Indeed, ASS1 has been described to co-localize with both neuronal nitric oxide synthase (nNOS) in the gastrointestinal tract[341], and with the epithelial isoform of the enzyme (eNOS), in endothelial cells, where it has been detected in correspondence of the plasma membrane structures caveolae[342] and outside of the Golgi[343].

In cancer, ASS1 has been shown to localize in the cytoplasm[249,344]. Nevertheless, consistently with our results, the Human Protein Atlas reports the uncertain additional location of ASS1 in the nucleoplasm of A-431 epidermoid carcinoma cell line and MCF7 breast adenocarcinoma cell line[345].

It is well established that nutrients from the diets, genetic mutation and interactions with tumor microenvironment can produce changes in the metabolic status of the cancer that can impact histone methylation and therefore gene expression[346]. Indeed, many chromatin-modifying enzyme often require cofactors for their function that are proceeding from metabolic reactions, demonstrating the existence of a strict cooperation between epigenetics and metabolism for cancer progression[347]. Less is known about the role played by the direct translocation of metabolic enzymes inside the nucleus. ATP-citrate lyase (ACLY) has been described to localize in the nuclei of different human cancer cell types, such as glioblastoma and colon carcinoma[348] indicating that the production of acetyl-CoA can be involved in regulating gene expression.

Another enzyme that was described to translocate to the nucleus is the pyruvate dehydrogenase complex (PDC). During the S phase, under serum deprivation, mitochondrial stress or growth factors stimulation, it has been observed that PDC nuclear levels increase, while a simultaneous decrease of the enzyme is observed in the mitochondria[349]. As for ACLY, PDC activity in the nucleus is upregulated in various tumor types and can contribute to sustain cancer growth and progression by increasing acetyl-CoA formation, therefore impacting histone acetylation and cell cycle progression.

Another important example of a metabolic enzyme translocation to the nucleus is represented by the glycolytic isozyme M2 of pyruvate kinase (PKM2), described for the first time on 1988 by Guminska and collaborators in Ehrlich ascites tumor and Morris hepatoma 7777[350]. Since then, an extensive bulk of literature has described a variety of nuclear PKM2 interactors and targets, such as the poly-ADP-ribose (PAR), as well as STAT3 different histone proteins and β-catenin, defining the role of nuclear PMK2 as key for cancer cell proliferation[351]. Interestingly, nuclear PMK2 has been identified also as an important player in cancer metastasis: sirtuin 6 (SIRT6)-mediated suppression of pro-oncogenic PMK2 inhibits hepatocellular carcinoma spreading *in vivo*[352].

Apart from their role in metabolic pathways, there is growing evidence that metabolic enzymes may exhibit non-canonical or “moonlighting” functions, as gene expression regulation following nuclear translocation. Together with genetic mutations and changes in the enzymatic activity, the spatial re-distribution of metabolic enzymes could be crucial for the energetic rewiring of cancer[353]. Our study reports for the first time the putative nuclear localization of ASS1 in RH4 ARMS cells. Although further experiments are needed to confirm this result and verify the possible interaction with nuclear proteins and chromatin, we believe that this data may suggest a “moonlighting” function of ASS1 in ARMS, which can explain its upregulation and pro-tumorigenic role. Our hypothesis is

further supported by the lack of significative changes in cell proliferation when growing cells in the absence of arginine: ASS1 upregulation in ARMS may not be directed related to support arginine synthesis and metabolism, and its alternative subcellular compartmentalization may regulate cancer progression through alternative non-metabolic interactions.

4. EEF1A2 is involved in mediating ASS1 role in ARMS by activating AKT signaling

In the last part of our study, we focused our attention on understanding the signaling produced by ASS1 overexpression in ARMS. We performed a transcriptomic array comparing parental RH4 or SCR cells with the two ASS1-deficient clones selected for our *in vitro* experiments. The bioinformatic results obtained showed that the expression of more than 200 genes resulted de-regulated upon ASS1 silencing. Although the *in silico* analysis did not display any specific pathway affected, we identified several downregulated genes that could be responsible of mediating the observed phenotype. We proceeded ranking the de-regulated genes according to their fold-change and the statistical significance of the differences observed. Among the top targets identified, we selected and validated the elongation factor EEF1A2 as one of the most interesting candidates for our study. The Eukaryotic Elongation Factor 1 alpha (EEF1A) is the second most abundant protein in eukaryotic cells after actin and is a key regulator of protein synthesis: by binding to amino-acylated tRNAs, it determines their recruitment to the ribosomes[354]. Two isoforms of EEF1A have been identified, namely EEF1A1 and EEF1A2, characterized by 92% sequence identity[355]. In addition to its canonical function, EEF1A2 has been largely described to be ectopically overexpressed in different cancer types, acting as an oncogene by regulating cytoskeleton modification, apoptosis, tumor progression and metastasis[285].

In breast cancer, EEF1A2 was described to be strongly upregulated in primary neoplasms and metastasis[356], sustaining tumorigenesis through the activation of PI3K and AKT[286]. Furthermore, in ovarian cancer, EEF1A2 plays a role in favouring tumorsphere formation *in vitro*[357] and its overexpression correlates with poor prognosis[285]. Also, lung cancer, hepatocellular carcinoma and pancreatic cancer cells have shown to be characterized by high EEF1A2 expression[354], confirming the oncogenic role of this protein in a wide spectrum of malignancies.

Regarding the mechanism by which EEF1A2 is involved in sustaining tumorigenesis, the most validated hypothesis sees the involvement of AKT as the main target of the

elongation factor. Indeed, EEF1A2 ectopic expression has been described to induce cytoskeletal remodeling through PI3K-mediated AKT activation, that leads to filopodia formation and increased cell motility[286]. Moreover, siRNA-mediated silencing of EEF1A2 has shown to reduce phosphorylated-AKT levels, while its overexpression induces AKT phosphorylation in human colorectal cancer[358], osteosarcoma[359], in which also mTOR activation was observed, and pancreatic cancer, with the AKT-mediated upregulation of the matrix metalloproteinase 9 (MMP9)[360].

We found that EEF1A2 gene expression was significatively downregulated in G2_2 and G1_4 ASS1 clones, suggesting that it could be involved in mediating the aggressive phenotype associated with ASS1 overexpression. It would be interesting to assess EEF1A2 levels in ARMS cell lines and tumors samples, to validate its oncogenic role in these cancers. Furthermore, in line with the literature discussed above, we found that together with EEF1A2, also AKT, S6K1 and S6 phosphorylated forms were decreased upon ASS1 silencing, in accordance with the evidence that described AKT activation as downstream EEF1A2 oncogenic signaling.

However, further experiments are needed to elucidate the ultimate molecular mechanism that links ASS1 and EEF1A2 overexpression in ARMS, as well as the downstream mediators involved in the metastatic behaviour of these tumors. Recent advances suggest that EEF1A2 could be directly involved in activating AKT and mTOR signaling: its ectopic introduction in U2OS osteosarcoma cells promotes mTOR phosphorylation at Ser2448 and Ser2441 residues, as well as AKT phosphorylation at Thr308 and Ser437, while its silencing in MG63 neuroblastoma cells induces the opposite effect[359]. Moreover, EEF1A2 silencing in SH-SY5Y neuroblastoma cells has been reported to induce a slight reduction of mTORC1 and mTORC2 mRNA levels, as well as a decrease of AKT and mTOR protein phosphorylation, suggesting that this mechanism could be mediating the cell death phenotype observed following EEF1A2 silencing in these cells[361]. In our case, mTOR Ser2448-phosphorylation did not seem to be affected by ASS1 silencing. We also performed immunoprecipitation assays to identify a possible spatial interaction between ASS1 and Rictor, as part of mTORC2, or Raptor, as mTORC1 component, in our RH4 cellular model, but our results did not show any interaction between them (data not shown). Therefore, we hypothesized that other factors could be responsible for S6K1 downstream induction, such as PDK1. However, mTOR phosphorylation is a very complex process. Ser2448 residue has been largely used in the past as a marker of mTOR activation. Nevertheless, more recent studies show that actually this residue does not represent a AKT target for mTOR activation; on the contrary, S6K1 can phosphorylate Ser2448, inducing a negative feedback loop.

Therefore, Ser2448 phosphorylated levels alone do not represent a good marker to evaluate mTOR activity, that should be assessed also looking at the downstream effectors S6K1 and 4EBP1362. In our case, S6K1 and S6 phosphorylated forms were found to be decreased upon ASS1 silencing. Furthermore, arginine has been broadly described as a direct mTOR activator[172]. Therefore, it is not possible to firmly conclude that mTOR is not involved in the mechanism we proposed.

To verify whether PDK1 was alternatively involved in activating the downstream pathway, we decided to perform experiments treating RH4 cells with PDK1 and S6K1 inhibitors trying to recapitulate the effects resulting from ASS1 downregulation in these cells and confirm this pathway involvement in the establishment of ASS1-mediated ARMS aggressive behaviour.

PDK1 is a protein kinase described to be constitutively active in several different cancer types, being involved in signaling pathways that are often dysregulated in tumors, such as PI3K/AKT axis and MAPK cascade[363]. Indeed, AKT and S6K1 represent two of the main targets for PDK1 activity[364]. It would be interesting to evaluate its expression levels in ARMS cell lines to verify the existence of a direct connection between the ASS1 enzyme and the kinase activity in these tumors.

S6K1 was identified for the first time as the mitogen-inducible kinase that phosphorylates the ribosomal protein S6[365]. Since then, several other substrates of S6K1 phosphorylation have been described, defining its role as crucial in a variety of important cellular processes, such as cell death, gene expression regulation and protein translation[366]. S6 is an evolutionarily conserved component of the 40S small ribosomal subunit. It has been extensively characterized as a key player of fundamental cellular functions, as protein synthesis and splicing, DNA repair and cell differentiation, but also cancer specific features: it is involved in inhibiting apoptosis, sustaining cell proliferation, and remodeling the cytoskeleton to promote cancer migration[367]. All this evidence sustains our hypothesis that this pathway could be involved in promoting ASS1-mediated ARMS tumorigenesis and aggressiveness.

To verify PDK1 and S6K1 involvement in ASS1-mediated phenotype and reproduce the effects observed in ASS1-downregulated cells, we planned to treat our cells with two PDK1 inhibitors, BX912 and OSU03012, and the S6K1 inhibitor PF-4708671. We set up the experimental conditions and confirmed the inhibition of S6 downstream activation using different inhibitor concentrations. Unfortunately, we were only able to test RH4 cell proliferation upon treatments, as due to time reasons, we were not able to perform migration assays and test the effects on cell motility. This would have allowed us to verify

if the same reduction of cell migration observed after ASS1 silencing was also recapitulated following PDK1 or S6K1 inhibition, independently from the effect on RH4 proliferative capacity.

Further experiments are needed to confirm that PDK1 could be involved in the EEF1A2-mediated phenotype observed in ARMS cells when ASS1 is downregulated and confirm that the inhibition of this pathway can block ASS1 impact on ARMS tumorigenesis and invasiveness.

The results we collected with the *in vivo* assay strongly suggest that ASS1 expression in ARMS sustains tumor development and growth. That is also confirmed by its re-expression in silenced cells *in vivo* and the following tumor size increase. Overall, our results suggest that the inhibition of ASS1 could represent a potential effective strategy to counteract ARMS tumorigenesis and progression. Bateman and collaborators have demonstrated that treating colorectal cancer cells with the specific ASS1 inhibitor N-methyl-DL-aspartic acid (MDLA) not only reduces cell proliferation and survival, but also induces changes in the metabolomic profile of the tumor, leading to the decrease of fumarate and impairing glycolytic capacity and lipid metabolism[247]. ASS1 inhibition with MDLA has also shown to be affecting serine and glycine production, leading to a decrease in purine synthesis: tumors with high ASS1 levels, indeed, present purine-rich mutational signature, that is associated to a poor response to immunotherapy. Targeting ASS1 activity can revert this phenotype and improve cancer sensitivity to immune cell therapy[279]. Another interesting aspect to consider in that ASS1 levels have been described to potentially change during tumor progression: the analysis of a cohort of more than 600 breast primary tumors showed that cancers that developed metastasis presented significatively higher ASS1 levels, in comparison to the tumors that did not generate metastatic foci[279]. Therefore, tumors characterized by low ASS1 expression, that can be targeted with arginine deprivation-based strategies, can potentially progress to metastasis that do express ASS1 to sustain cell survival in nutrient-depleted microenvironment.

5. Final resume

New insights into tumor metabolic liabilities have definitively provided valid therapeutic strategies to target cancer. The main aim of this thesis was focused on the identification of new molecular actors that can re-shape ARMS metabolism in order to favour tumor progression and metastasis.

In the first part of this study, we have generated different cellular tools that allowed us to compare the impact of PAX3-FOXO1 expression or silencing on ARMS metabolism. Following the fusion protein ectopic expression in the RD ERMS cell line, we were able to obtain the metabolomic profile of the transduced cells and study PAX3-FOXO1 role in the metabolic context. The lack of significative results let us conclude that for the study of PAX3-FOXO1 impact on cellular metabolism, the integration of more than one cellular model would have facilitated the interpretation of the metabolomics data obtained. Indeed, taking advantage from the access to publicly available ARMS and ERMS datasets, we were able to perform a further bioinformatic analysis and finally identify a putative transcriptional target of PAX3-FOXO1, the urea cycle enzyme ASS1, which upregulation was later confirmed also in our metabolomic sets of data previously collected.

Despite the lack of a clear correlation with the expression of the fusion protein in RMS cell lines, ASS1 resulted to be clearly overexpressed in PAX3-FOXO1-positive cells. To better address its potential role in regulating ARMS metabolism, we silenced its expression using CRISPR-Cas9 in RH4 cells. ASS1 downregulation led to the inhibition of ARMS migratory capacity *in vitro* and caused a significative delay in tumorigenesis *in vivo*. This data suggest that the enzyme could represent a novel molecular target that could be exploited to block ARMS tumor progression and invasion. Furthermore, to our knowledge, this is the first study showing nuclear ASS1 localization in cancer cells, unravelling a possible “moonlighting” function of this enzyme that could represent a unique targetable feature of these tumors.

Analysing the transcriptomic profile of cells silenced for ASS1 expression, we were also able to identify a possible molecular mediator of the phenotype observed in ASS1-deficient cells: the elongation factor EEF1A2, extensively described in literature to display oncogenic activity in cancer, resulted to be transcriptionally downregulated upon ASS1 silencing. Consequently, AKT phosphorylation was also found to decrease, together with the activation of S6K1 and S6 downstream effectors. Further experiments are needed to better describe the upstream signaling involved and the precise mechanism that links ASS1 to EEF1A2 downregulation.

In conclusion, our work shed light on the role played by ASS1, a novel putative transcriptional target of PAX3-FOXO1, in contributing to ARMS tumorigenesis and invasiveness. The identification of new PAX3-FOXO1 targets involved in metabolic processes could be useful to better understand the molecular mechanisms underlying the features of fusion-positive RMS. Collecting detailed and complete information about

ARMS metabolic landscape, will hopefully lead to identify and test new altered metabolic mediators as therapeutic targets.

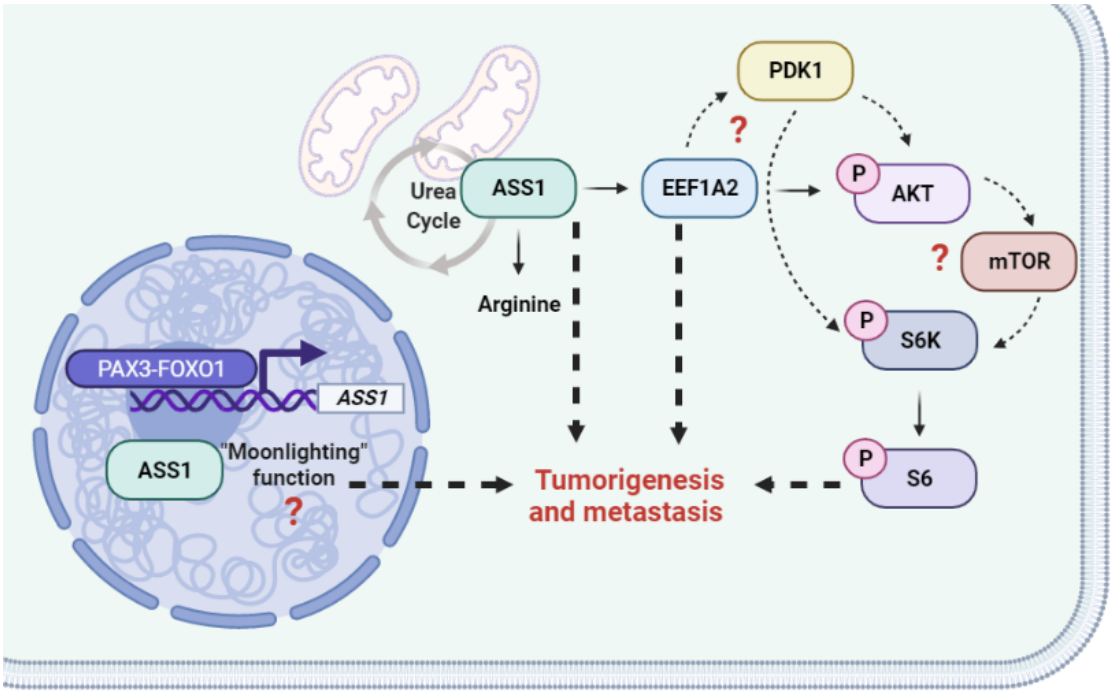

Figure D1: Schematic representation of ASS1 role in sustaining ARMS tumorigenesis and metastatic potential. Created with BioRender.com[190]

CONCLUSIONS

1. Urea cycle enzyme ASS1 expression is upregulated by PAX3-FOXO1 at transcriptional level in ARMS.
2. Fusion protein-expressing RD cells present lower levels of ASS1 substrate Citrulline as well as higher levels of its product Argininosuccinate.
3. ASS1 is highly expressed in most RMS cell lines, contrary to other STS cell lines.
4. PAX3-FOXO1 regulates *ASS1* mRNA levels but the silencing or overexpression of the fusion protein does not affect significatively ASS1 protein expression.
5. CRISPR-Cas9-mediated ASS1 silencing inhibits RH4 cell migration *in vitro* and delays tumorigenesis *in vivo.*
6. ASS1-silenced RH4 cells re-express ASS1 *in vivo*, leading to tumor formation and lymph nodes metastatic spreading.
7. The elongation factor EEF1A2 expression is decreased upon ASS1 silencing in RH4 cells.
8. ASS1 silencing leads to a reduction of AKT, S6K1 and S6 phosphorylation, but not mTOR, suggesting that PDK1 could be involved in activating the signaling.

BIBLIOGRAPHY

1. Bourcier, K. *et al.* Basic Knowledge in Soft Tissue Sarcoma. *Cardiovasc. Intervent. Radiol.* **42**, 1255–1261 (2019).

2. Siegel, R. L., Miller, K. D., Fuchs, H. E. & Jemal, A. Cancer Statistics, 2021. *CA. Cancer J. Clin.* **71**, 7–33 (2021).

3. Gamboa, A. C., Gronchi, A. & Cardona, K. Soft-tissue sarcoma in adults: An update on the current state of histiotype-specific management in an era of personalized medicine. *CA. Cancer J. Clin.* **70**, 200–229 (2020).

4. Sbaraglia, M., Bellan, E. & Dei Tos, A. P. The 2020 WHO Classification of Soft Tissue Tumours: News and perspectives. *Pathologica* **113**, 70–84 (2021).

5. MacDonald, D. *Positron Emission Tomography*. *Oral and Maxillofacial Radiology: A Diagnostic Approach* (2013). doi:10.1002/9781118786734.ch7

6. Jain, S., Xu, R., Prieto, V. G. & Lee, P. Molecular classification of soft tissue sarcomas and its clinical applications. *Int. J. Clin. Exp. Pathol.* **3**, 416–429 (2010).

7. Gilbert, N. F., Cannon, C. P., Lin, P. P. & Lewis, V. O. Soft-tissue sarcoma. *J. Am. Acad. Orthop. Surg.* **17**, 40–47 (2009).

8. Meyer, M. & Seetharam, M. First-Line Therapy for Metastatic Soft Tissue Sarcoma. *Curr. Treat. Options Oncol.* **20**, 6 (2019).

9. Monograph, S. P. Cancer Incidence and Survival among Children and Adolescents: United States SEER Program 1975-1995. (2014).

10. Oberlin, O. *et al.* Prognostic factors in metastatic rhabdomyosarcomas: Results of a pooled analysis from United States and European Cooperative Groups. *J. Clin. Oncol.* **26**, 2384–2389 (2008).

11. STOUT, A. P. RHABDOMYOSARCOMA OF THE SKELETAL MUSCLES. *Ann. Surg.* **123**, (1946).

12. HORN, R. C. J. & ENTERLINE, H. T. Rhabdomyosarcoma: a clinicopathological study and classification of 39 cases. *Cancer* **11**, 181–199 (1958).

13. Wang-Wuu, S., Soukup, S., Ballard, E., Gotwals, B. & Lampkin, B. Chromosomal analysis of sixteen human rhabdomyosarcomas. *Cancer Res.* **48**, 983–987 (1988).

14. Douglass, E. C. *et al.* A specific chromosomal abnormality in rhabdomyosarcoma. *Cytogenet. Cell Genet.* **45**, 148–155 (1987).

15. Barr, F. G. *et al.* Rearrangement of the PAX3 paired box gene in the paediatric solid tumour alveolar rhabdomyosarcoma. *Nat. Genet.* **3**, 113–117 (1993).

16. Galili, N. *et al.* Fusion of a fork head domain gene to PAX3 in the solid tumour alveolar rhabdomyosarcoma. *Nat. Genet.* **5**, 230–235 (1993).

17. Howlader N, Noone AM, Krapcho M, Miller D, Brest A, Yu M, Ruhl J, Tatalovich Z, Mariotto A, Lewis DR, Chen HS, Feuer EJ, C. K. (eds). *SEER Cancer Statistics Review, 1975-2018, National Cancer Institute. Bethesda, MD, https://seer.cancer.gov/csr/1975_2018/, based on November 2020 SEER data submission, posted to the SEER web site, April 2021*.

18. Shern, J. F., Yohe, M. E. & Khan, J. Pediatric Rhabdomyosarcoma. *Crit. Rev. Oncog.* **20**, 227–243 (2015).

19. Pastore, G. *et al.* Childhood soft tissue sarcomas incidence and survival in European children (1978-1997): report from the Automated Childhood Cancer Information System project. *Eur. J. Cancer* **42**, 2136–2149 (2006).

20. Perez, E. A. *et al.* Rhabdomyosarcoma in children: a SEER population based study. *J. Surg. Res.* **170**, e243-51 (2011).

21. Furlong, M. A., Mentzel, T. & Fanburg-Smith, J. C. Pleomorphic rhabdomyosarcoma in adults: a clinicopathologic study of 38 cases with emphasis on morphologic variants and recent skeletal muscle-specific markers. *Mod. Pathol. an Off. J. United States Can. Acad. Pathol. Inc* **14**, 595–603 (2001).

22. Ognjanovic, S., Linabery, A. M., Charbonneau, B. & Ross, J. A. Trends in childhood rhabdomyosarcoma incidence and survival in the United States, 1975-2005. *Cancer* **115**, 4218–4226 (2009).

23. Crist, W. *et al.* The Third Intergroup Rhabdomyosarcoma Study. *J. Clin. Oncol. Off. J. Am. Soc. Clin. Oncol.* **13**, 610–630 (1995).

24. Crist, W. M. *et al.* Intergroup rhabdomyosarcoma study-IV: results for patients with nonmetastatic disease. *J. Clin. Oncol. Off. J. Am. Soc. Clin. Oncol.* **19**, 3091–3102 (2001).

25. Sung, L. *et al.* Late events occurring five years or more after successful therapy for childhood rhabdomyosarcoma: a report from the Soft Tissue Sarcoma Committee of the Children's Oncology Group. *Eur. J. Cancer* **40**, 1878–1885 (2004).

26. Meza, J. L., Anderson, J., Pappo, A. S. & Meyer, W. H. Analysis of prognostic factors in patients with nonmetastatic rhabdomyosarcoma treated on intergroup rhabdomyosarcoma studies III and IV: the Children's Oncology Group. *J. Clin. Oncol. Off. J. Am. Soc. Clin. Oncol.* **24**, 3844–3851 (2006).

27. Davicioni, E. *et al.* Molecular classification of rhabdomyosarcoma--genotypic and phenotypic determinants of diagnosis: a report from the Children's Oncology Group. *Am. J. Pathol.* **174**, 550–564 (2009).

28. Sultan, I., Qaddoumi, I., Yaser, S., Rodriguez-Galindo, C. & Ferrari, A. Comparing adult and pediatric rhabdomyosarcoma in the surveillance, epidemiology and end results program, 1973 to 2005: an analysis of 2,600 patients. *J. Clin. Oncol. Off. J. Am. Soc. Clin. Oncol.* **27**, 3391–3397 (2009).

29. Martin-Giacalone, B. A., Weinstein, P. A., Plon, S. E. & Lupo, P. J. Pediatric Rhabdomyosarcoma: Epidemiology and Genetic Susceptibility. *J. Clin. Med.* **10**, (2021).

30. Grufferman, S., Schwartz, A. G., Ruymann, F. B. & Maurer, H. M. Parents' use of cocaine and marijuana and increased risk of rhabdomyosarcoma in their children. *Cancer Causes Control* **4**, 217–224 (1993).

31. Rumrich, I. K. *et al.* Maternal Smoking and the Risk of Cancer in Early Life - A Meta-Analysis.

PLoS One **11**, e0165040 (2016).

32. Grufferman, S., Ruymann, F., Ognjanovic, S., Erhardt, E. B. & Maurer, H. M. Prenatal X-ray exposure and rhabdomyosarcoma in children: a report from the children's oncology group. *Cancer Epidemiol. biomarkers Prev. a Publ. Am. Assoc. Cancer Res. cosponsored by Am. Soc. Prev. Oncol.* **18**, 1271–1276 (2009).

33. Lupo, P. J. *et al.* Perinatal and familial risk factors for soft tissue sarcomas in childhood through young adulthood: A population-based assessment in 4 million live births. *Int. J. cancer* **146**, 791–802 (2020).

34. Lupo, P. J. *et al.* Association Between Birth Defects and Cancer Risk Among Children and Adolescents in a Population-Based Assessment of 10 Million Live Births. *JAMA Oncol.* **5**, 1150–1158 (2019).

35. Sankaran, H. *et al.* The Role of Childhood Infections and Immunizations on Childhood Rhabdomyosarcoma: A Report From the Children's Oncology Group. *Pediatr. Blood Cancer* **63**, 1557–1562 (2016).

36. Lupo, P. J. *et al.* Maternal and birth characteristics and childhood rhabdomyosarcoma: a report from the Children's Oncology Group. *Cancer Causes Control* **25**, 905–913 (2014).

37. Oddsberg, J. Environmental factors in the etiology of esophageal atresia. *J. Pediatr. Gastroenterol. Nutr.* **52 Suppl 1**, S4-5 (2011).

38. Skapek, S. X. *et al.* Rhabdomyosarcoma. *Nat. Rev. Dis. Prim.* **5**, 1 (2019).

39. Ognjanovic, S., Olivier, M., Bergemann, T. L. & Hainaut, P. Sarcomas in TP53 germline mutation carriers: a review of the IARC TP53 database. *Cancer* **118**, 1387–1396 (2012).

40. Kratz, C. P. *et al.* Cancer spectrum and frequency among children with Noonan, Costello, and cardio-facio-cutaneous syndromes. *Br. J. Cancer* **112**, 1392–1397 (2015).

41. Crucis, A. *et al.* Rhabdomyosarcomas in children with neurofibromatosis type I: A national historical cohort. *Pediatr. Blood Cancer* **62**, 1733–1738 (2015).

42. Kratz, C. P., Rapisuwon, S., Reed, H., Hasle, H. & Rosenberg, P. S. Cancer in Noonan, Costello, cardiofaciocutaneous and LEOPARD syndromes. *Am. J. Med. Genet. C. Semin. Med. Genet.* **157C**, 83–89 (2011).

43. Stewart, D. R. *et al.* Neoplasm Risk Among Individuals With a Pathogenic Germline Variant in DICER1. *J. Clin. Oncol. Off. J. Am. Soc. Clin. Oncol.* **37**, 668–676 (2019).

44. Miller, R. W. & Rubinstein, J. H. Tumors in Rubinstein-Taybi syndrome. *Am. J. Med. Genet.* **56**, 112–115 (1995).

45. Kohashi, K. *et al.* Alterations of RB1 gene in embryonal and alveolar rhabdomyosarcoma: special reference to utility of pRB immunoreactivity in differential diagnosis of rhabdomyosarcoma subtype. *J. Cancer Res. Clin. Oncol.* **134**, 1097–1103 (2008).

46. Shuman, C., Beckwith, J. B. & Weksberg, R. Beckwith-Wiedemann Syndrome. in (eds. Adam, M. P. et al.) (1993).

47. Egas-Bejar, D. & Huh, W. W. Rhabdomyosarcoma in adolescent and young adult patients: current perspectives. *Adolesc. Health. Med. Ther.* **5**, 115–125 (2014).

48. Paulino, A. C. & Okcu, M. F. Rhabdomyosarcoma. *Curr. Probl. Cancer* **32**, 7–34 (2008).

49. Dasgupta, R., Fuchs, J. & Rodeberg, D. Rhabdomyosarcoma. *Semin. Pediatr. Surg.* **25**, 276–283 (2016).

50. Dasgupta, R. & Rodeberg, D. A. Update on rhabdomyosarcoma. *Semin. Pediatr. Surg.* **21**, 68–78 (2012).

51. Jawad, N. & McHugh, K. The clinical and radiologic features of paediatric rhabdomyosarcoma. *Pediatr. Radiol.* **49**, 1516–1523 (2019).

52. Norman, G. *et al.* An emerging evidence base for PET-CT in the management of childhood rhabdomyosarcoma: systematic review. *BMJ Open* **5**, e006030 (2015).

53. SlidesGo. Available at: https://slidesgo.com/.

54. Skapek, S. X. *et al.* Rhabdomyosarcoma. *Nat. Rev. Dis. Prim.* **5**, 14–16 (2019).

55. Agaram, N. P. Evolving classification of rhabdomyosarcoma. *Histopathology* **80**, 98–108 (2022).

56. Stuart, A. & Radhakrishnan, J. Rhabdomyosarcoma. *Indian J. Pediatr.* **71**, 331–337 (2004).

57. Dziuba, I., Kurzawa, P., Dopierała, M., Larque, A. B. & Januszkiewicz-Lewandowska, D. Rhabdomyosarcoma in children - current pathologic and molecular classification. *Polish J. Pathol. Off. J. Polish Soc. Pathol.* **69**, 20–32 (2018).

58. Wachtel, M. *et al.* Subtype and prognostic classification of rhabdomyosarcoma by immunohistochemistry. *J. Clin. Oncol. Off. J. Am. Soc. Clin. Oncol.* **24**, 816–822 (2006).

59. Leuschner, I. *et al.* p53 and mdm-2 expression in Rhabdomyosarcoma of childhood and adolescence: clinicopathologic study by the Kiel Pediatric Tumor Registry and the German Cooperative Soft Tissue Sarcoma Study. *Pediatr. Dev. Pathol. Off. J. Soc. Pediatr. Pathol. Paediatr. Pathol. Soc.* **6**, 128–136 (2003).

60. Parham, D. M. & Barr, F. G. Classification of Rhabdomyosarcoma and its molecular basis. *Adv. Anat. Pathol.* **20**, 387–397 (2013).

61. Wachtel, M. *et al.* Gene expression signatures identify rhabdomyosarcoma subtypes and detect a novel t(2;2)(q35;p23) translocation fusing PAX3 to NCOA1. *Cancer Res.* **64**, 5539–5545 (2004).

62. Davicioni, E. *et al.* Identification of a PAX-FKHR Gene Expression Signature that Defines Molecular Classes and Determines the Prognosis of Alveolar Rhabdomyosarcomas. *Cancer Res.* **66**, 6936–6946 (2006).

63. Nishio, J. *et al.* Use of a novel FISH assay on paraffin-embedded tissues as an adjunct to diagnosis of alveolar rhabdomyosarcoma. *Lab. Invest.* **86**, 547–556 (2006).

64. Arnold, M. A. & Barr, F. G. Molecular diagnostics in the management of rhabdomyosarcoma. *Expert Rev. Mol. Diagn.* **17**, 189–194 (2017).

65. Missiaglia, E. *et al.* PAX3/FOXO1 fusion gene status is the key prognostic molecular marker in

rhabdomyosarcoma and significantly improves current risk stratification. *J. Clin. Oncol. Off. J. Am. Soc. Clin. Oncol.* **30**, 1670–1677 (2012).

66. Skapek, S. X. *et al.* PAX-FOXO1 fusion status drives unfavorable outcome for children with rhabdomyosarcoma: a children's oncology group report. *Pediatr. Blood Cancer* **60**, 1411–1417 (2013).

67. World Health Organization. *Soft Tissue and Bone Tumours WHO Classification of Tumours, 5th Edition, Volume 3*. (2020).

68. Xia, S. J., Pressey, J. G. & Barr, F. G. Molecular pathogenesis of rhabdomyosarcoma. *Cancer Biol. Ther.* **1**, 97–104 (2002).

69. Dias, P. *et al.* Strong immunostaining for myogenin in rhabdomyosarcoma is significantly associated with tumors of the alveolar subclass. *Am. J. Pathol.* **156**, 399–408 (2000).

70. Schürch, W. *et al.* Pleomorphic soft tissue myogenic sarcomas of adulthood. A reappraisal in the mid-1990s. *Am. J. Surg. Pathol.* **20**, 131–147 (1996).

71. Li, G. *et al.* Cytogenetic and real-time quantitative reverse-transcriptase polymerase chain reaction analyses in pleomorphic rhabdomyosarcoma. *Cancer Genet. Cytogenet.* **192**, 1–9 (2009).

72. Gaffney, E. F., Dervan, P. A. & Fletcher, C. D. Pleomorphic rhabdomyosarcoma in adulthood. Analysis of 11 cases with definition of diagnostic criteria. *Am. J. Surg. Pathol.* **17**, 601–609 (1993).

73. Folpe, A. L., McKenney, J. K., Bridge, J. A. & Weiss, S. W. Sclerosing rhabdomyosarcoma in adults: report of four cases of a hyalinizing, matrix-rich variant of rhabdomyosarcoma that may be confused with osteosarcoma, chondrosarcoma, or angiosarcoma. *Am. J. Surg. Pathol.* **26**, 1175–1183 (2002).

74. Leuschner, I. Spindle cell rhabdomyosarcoma: histologic variant of embryonal rhabdomyosarcoma with association to favorable prognosis. *Curr. Top. Pathol.* **89**, 261–272 (1995).

75. Parham, D. M. & Ellison, D. A. Rhabdomyosarcomas in adults and children: an update. *Arch. Pathol. Lab. Med.* **130**, 1454–1465 (2006).

76. Malempati, S. & Hawkins, D. S. Rhabdomyosarcoma: review of the Children's Oncology Group (COG) Soft-Tissue Sarcoma Committee experience and rationale for current COG studies. *Pediatr. Blood Cancer* **59**, 5–10 (2012).

77. Arnold, M. A. *et al.* Histology, Fusion Status, and Outcome in Alveolar Rhabdomyosarcoma With Low-Risk Clinical Features: A Report From the Children's Oncology Group. *Pediatr. Blood Cancer* **63**, 634–639 (2016).

78. Williamson, D. *et al.* Fusion gene-negative alveolar rhabdomyosarcoma is clinically and molecularly indistinguishable from embryonal rhabdomyosarcoma. *J. Clin. Oncol. Off. J. Am. Soc. Clin. Oncol.* **28**, 2151–2158 (2010).

79. Parham, D. M. & Barr, F. G. Classification of rhabdomyosarcoma and its molecular basis. *Adv. Anat. Pathol.* **20**, 387–397 (2013).

80. Sorensen, P. H. B. *et al.* PAX3-FKHR and PAX7-FKHR gene fusions are prognostic indicators in

alveolar rhabdomyosarcoma: a report from the children's oncology group. *J. Clin. Oncol. Off. J. Am. Soc. Clin. Oncol.* **20**, 2672–2679 (2002).

81. Davis, R. J., D'Cruz, C. M., Lovell, M. A., Biegel, J. A. & Barr, F. G. Fusion of PAX7 to FKHR by the variant t(1;13)(p36;q14) translocation in alveolar rhabdomyosarcoma. *Cancer Res.* **54**, 2869–2872 (1994).

82. Shern, J. F. *et al.* Comprehensive genomic analysis of rhabdomyosarcoma reveals a landscape of alterations affecting a common genetic axis in fusion-positive and fusion-negative tumors. *Cancer Discov.* **4**, 216–231 (2014).

83. Goulding, M. D., Chalepakis, G., Deutsch, U., Erselius, J. R. & Gruss, P. Pax-3, a novel murine DNA binding protein expressed during early neurogenesis. *EMBO J.* **10**, 1135–1147 (1991).

84. Jostes, B., Walther, C. & Gruss, P. The murine paired box gene, Pax7, is expressed specifically during the development of the nervous and muscular system. *Mech. Dev.* **33**, 27–37 (1990).

85. Accili, D. & Arden, K. C. FoxOs at the crossroads of cellular metabolism, differentiation, and transformation. *Cell* **117**, 421–426 (2004).

86. Barr, F. G. Gene fusions involving PAX and FOX family members in alveolar rhabdomyosarcoma. *Oncogene* **20**, 5736–5746 (2001).

87. del Peso, L., González, V. M., Hernández, R., Barr, F. G. & Núñez, G. Regulation of the forkhead transcription factor FKHR, but not the PAX3-FKHR fusion protein, by the serine/threonine kinase Akt. *Oncogene* **18**, 7328–7333 (1999).

88. Bennicelli, J. L., Edwards, R. H. & Barr, F. G. Mechanism for transcriptional gain of function resulting from chromosomal translocation in alveolar rhabdomyosarcoma. *Proc. Natl. Acad. Sci. U. S. A.* **93**, 5455–5459 (1996).

89. Davis, R. J. & Barr, F. G. Fusion genes resulting from alternative chromosomal translocations are overexpressed by gene-specific mechanisms in alveolar rhabdomyosarcoma. *Proc. Natl. Acad. Sci. U. S. A.* **94**, 8047–8051 (1997).

90. Gryder, B. E. *et al.* PAX3-FOXO1 establishes myogenic super enhancers and confers BET bromodomain vulnerability. *Cancer Discov.* **7**, 884–899 (2017).

91. Böhm, M. *et al.* Helicase CHD4 is an epigenetic coregulator of PAX3-FOXO1 in alveolar rhabdomyosarcoma. *J. Clin. Invest.* **126**, 4237–4249 (2016).

92. Linardic, C. M. PAX3-FOXO1 fusion gene in rhabdomyosarcoma. *Cancer Lett.* **270**, 10–18 (2008).

93. Khan, J. *et al.* cDNA microarrays detect activation of a myogenic transcription program by the PAX3-FKHR fusion oncogene. *Proc. Natl. Acad. Sci. U. S. A.* **96**, 13264–13269 (1999).

94. Barber, T. D. *et al.* Identification of target genes regulated by PAX3 and PAX3-FKHR in embryogenesis and alveolar rhabdomyosarcoma. *Genomics* **79**, 278–284 (2002).

95. Schaaf, G. J. *et al.* Full transcriptome analysis of rhabdomyosarcoma, normal, and fetal skeletal muscle: statistical comparison of multiple SAGE libraries. *FASEB J.* **19**, 404–406 (2005).

96. Mercado, G. E. *et al.* Identification of PAX3-FKHR-regulated genes differentially expressed

between alveolar and embryonal rhabdomyosarcoma: focus on MYCN as a biologically relevant target. *Genes. Chromosomes Cancer* **47**, 510–520 (2008).

97. Ebauer, M., Wachtel, M., Niggli, F. K. & Schafer, B. W. Comparative expression profiling identifies an in vivo target gene signature with TFAP2B as a mediator of the survival function of PAX3/FKHR. *Oncogene* **26**, 7267–7281 (2007).

98. Taulli, R. *et al.* Validation of met as a therapeutic target in alveolar and embryonal rhabdomyosarcoma. *Cancer Res.* **66**, 4742–4749 (2006).

99. Libura, J. *et al.* CXCR4-SDF-1 signaling is active in rhabdomyosarcoma cells and regulates locomotion, chemotaxis, and adhesion. *Blood* **100**, 2597–2606 (2002).

100. Jankowski, K. *et al.* Both hepatocyte growth factor (HGF) and stromal-derived factor-1 regulate the metastatic behavior of human rhabdomyosarcoma cells, but only HGF enhances their resistance to radiochemotherapy. *Cancer Res.* **63**, 7926–7935 (2003).

101. Diomedi-Camassei, F. *et al.* Clinical significance of CXC chemokine receptor-4 and c-Met in childhood rhabdomyosarcoma. *Clin. cancer Res. an Off. J. Am. Assoc. Cancer Res.* **14**, 4119–4127 (2008).

102. Marshall, A. D., van der Ent, M. A. & Grosveld, G. C. PAX3-FOXO1 and FGFR4 in alveolar rhabdomyosarcoma. *Mol. Carcinog.* **51**, 807–815 (2012).

103. Scheidler, S., Fredericks, W. J., Rauscher, F. J. 3rd, Barr, F. G. & Vogt, P. K. The hybrid PAX3-FKHR fusion protein of alveolar rhabdomyosarcoma transforms fibroblasts in culture. *Proc. Natl. Acad. Sci. U. S. A.* **93**, 9805–9809 (1996).

104. Lam, P. Y., Sublett, J. E., Hollenbach, A. D. & Roussel, M. F. The oncogenic potential of the Pax3-FKHR fusion protein requires the Pax3 homeodomain recognition helix but not the Pax3 paired-box DNA binding domain. *Mol. Cell. Biol.* **19**, 594–601 (1999).

105. Kikuchi, K. *et al.* Effects of PAX3-FKHR on malignant phenotypes in alveolar rhabdomyosarcoma. *Biochem. Biophys. Res. Commun.* **365**, 568 (2008).

106. Anderson, J., Ramsay, A., Gould, S. & Pritchard-Jones, K. PAX3-FKHR induces morphological change and enhances cellular proliferation and invasion in rhabdomyosarcoma. *Am. J. Pathol.* **159**, 1089–1096 (2001).

107. Xia, S. J. & Barr, F. G. Analysis of the transforming and growth suppressive activities of the PAX3-FKHR oncoprotein. *Oncogene* **23**, 6864–6871 (2004).

108. Lagutina, I., Conway, S. J., Sublett, J. & Grosveld, G. C. Pax3-FKHR knock-in mice show developmental aberrations but do not develop tumors. *Mol. Cell. Biol.* **22**, 7204–7216 (2002).

109. Keller, C. *et al.* Alveolar rhabdomyosarcomas in conditional Pax3:Fkhr mice: cooperativity of Ink4a/ARF and Trp53 loss of function. *Genes Dev* **18**, 2614–2626 (2004).

110. Ren, Y. X. *et al.* Mouse mesenchymal stem cells expressing PAX-FKHR form alveolar rhabdomyosarcomas by cooperating with secondary mutations. *Cancer Res.* **68**, 6587–6597 (2008).

111. Naini, S. *et al.* Defining the cooperative genetic changes that temporally drive alveolar rhabdomyosarcoma. *Cancer Res.* **68**, 9583–9588 (2008).

112. Weber-Hall, S. *et al.* Gains, losses, and amplification of genomic material in rhabdomyosarcoma analyzed by comparative genomic hybridization. *Cancer Res.* **56**, 3220–3224 (1996).

113. Marshall, A. D. & Grosveld, G. C. Alveolar rhabdomyosarcoma - The molecular drivers of PAX3/7-FOXO1-induced tumorigenesis. *Skelet. Muscle* **2**, 1 (2012).

114. Ragazzini, P. *et al.* Amplification of CDK4, MDM2, SAS and GLI genes in leiomyosarcoma, alveolar and embryonal rhabdomyosarcoma. *Histol. Histopathol.* **19**, 401–411 (2004).

115. Reichek, J. L. *et al.* Genomic and clinical analysis of amplification of the 13q31 chromosomal region in alveolar rhabdomyosarcoma: a report from the Children's Oncology Group. *Clin. cancer Res. an Off. J. Am. Assoc. Cancer Res.* **17**, 1463–1473 (2011).

116. Williamson, D. *et al.* Role for amplification and expression of glypican-5 in rhabdomyosarcoma. *Cancer Res.* **67**, 57–65 (2007).

117. Scrable, H. *et al.* A model for embryonal rhabdomyosarcoma tumorigenesis that involves genome imprinting. *Proc. Natl. Acad. Sci. U. S. A.* **86**, 7480–7484 (1989).

118. Visser, M. *et al.* Allelotype of pediatric rhabdomyosarcoma. *Oncogene* **15**, 1309–1314 (1997).

119. Zhan, S., Shapiro, D. N. & Helman, L. J. Activation of an imprinted allele of the insulin-like growth factor II gene implicated in rhabdomyosarcoma. *J. Clin. Invest.* **94**, 445–448 (1994).

120. Zhang, M., Linardic, C. M. & Kirsch, D. G. RAS and ROS in rhabdomyosarcoma. *Cancer Cell* **24**, 689–691 (2013).

121. Paulson, V. *et al.* High-resolution array CGH identifies common mechanisms that drive embryonal rhabdomyosarcoma pathogenesis. *Genes. Chromosomes Cancer* **50**, 397–408 (2011).

122. Shern, J. F. *et al.* Genomic Classification and Clinical Outcome in Rhabdomyosarcoma: A Report From an International Consortium. *J. Clin. Oncol. Off. J. Am. Soc. Clin. Oncol.* **39**, 2859–2871 (2021).

123. Agaram, N. P. *et al.* Recurrent MYOD1 mutations in pediatric and adult sclerosing and spindle cell rhabdomyosarcomas: evidence for a common pathogenesis. *Genes. Chromosomes Cancer* **53**, 779–787 (2014).

124. Agaram, N. P. *et al.* MYOD1-mutant spindle cell and sclerosing rhabdomyosarcoma: an aggressive subtype irrespective of age. A reappraisal for molecular classification and risk stratification. *Mod. Pathol. an Off. J. United States Can. Acad. Pathol. Inc* **32**, 27–36 (2019).

125. Rudzinski, E. R. *et al.* Pathology of childhood rhabdomyosarcoma: A consensus opinion document from the Children's Oncology Group, European Paediatric Soft Tissue Sarcoma Study Group, and the Cooperative Weichteilsarkom Studiengruppe. *Pediatr. Blood Cancer* **68**, e28798 (2021).

126. Raney, R. B. *et al.* The Intergroup Rhabdomyosarcoma Study Group (IRSG): Major Lessons From the IRS-I Through IRS-IV Studies as Background for the Current IRS-V Treatment Protocols. *Sarcoma* **5**, 9–15 (2001).

127. Haduong, J. H. *et al.* An update on rhabdomyosarcoma risk stratification and the rationale for current and future Children's Oncology Group clinical trials. *Pediatr. Blood Cancer* **69**, e29511 (2022).

128. Chen, C., Dorado Garcia, H., Scheer, M. & Henssen, A. G. Current and Future Treatment Strategies for Rhabdomyosarcoma. *Front. Oncol.* **9**, 1458 (2019).

129. Maurer, H. M. *et al.* The Intergroup Rhabdomyosarcoma Study-I. A final report. *Cancer* **61**, 209–220 (1988).

130. Maurer, H. M. *et al.* The Intergroup Rhabdomyosarcoma Study-II. *Cancer* **71**, 1904–1922 (1993).

131. Bisogno, G. *et al.* Addition of dose-intensified doxorubicin to standard chemotherapy for rhabdomyosarcoma (EpSSG RMS 2005): a multicentre, open-label, randomised controlled, phase 3 trial. *Lancet. Oncol.* **19**, 1061–1071 (2018).

132. Lager, J. J. *et al.* Pooled analysis of phase II window studies in children with contemporary high-risk metastatic rhabdomyosarcoma: a report from the Soft Tissue Sarcoma Committee of the Children's Oncology Group. *J. Clin. Oncol. Off. J. Am. Soc. Clin. Oncol.* **24**, 3415–3422 (2006).

133. Miwa, S. *et al.* Recent Advances and Challenges in the Treatment of Rhabdomyosarcoma. *Cancers (Basel).* **12**, (2020).

134. Giannikopoulos, P. & Parham, D. M. Rhabdomyosarcoma: How Advanced Molecular Methods Are Shaping the Diagnostic and Therapeutic Paradigm. *Pediatr. Dev. Pathol. Off. J. Soc. Pediatr. Pathol. Paediatr. Pathol. Soc.* **24**, 395–404 (2021).

135. Li, S. Q. *et al.* Targeting wild-type and mutationally activated FGFR4 in rhabdomyosarcoma with the inhibitor ponatinib (AP24534). *PLoS One* **8**, e76551 (2013).

136. Yohe, M. E. *et al.* MEK inhibition induces MYOG and remodels super-enhancers in RAS-driven rhabdomyosarcoma. *Sci. Transl. Med.* **10**, eaan4470 (2018).

137. Mangoni, M. *et al.* Enhancement of Soft Tissue Sarcoma Cell Radiosensitivity by Poly(ADP-ribose) Polymerase-1 Inhibitors. *Radiat. Res.* **190**, 464–472 (2018).

138. Yan, C. *et al.* Visualizing Engrafted Human Cancer and Therapy Responses in Immunodeficient Zebrafish. *Cell* **177**, 1903-1914.e14 (2019).

139. Dang, C. V, Reddy, E. P., Shokat, K. M. & Soucek, L. Drugging the 'undruggable' cancer targets. *Nat. Rev. Cancer* **17**, 502–508 (2017).

140. Rengaswamy, V., Zimmer, D., Süss, R. & Rössler, J. RGD liposome-protamine-siRNA (LPR) nanoparticles targeting PAX3-FOXO1 for alveolar rhabdomyosarcoma therapy. *J. Control. release Off. J. Control. Release Soc.* **235**, 319–327 (2016).

141. Bharathy, N. *et al.* The HDAC3-SMARCA4-miR-27a axis promotes expression of the PAX3:FOXO1 fusion oncogene in rhabdomyosarcoma. *Sci. Signal.* **11**, (2018).

142. Dagher, R. *et al.* Pilot trial of tumor-specific peptide vaccination and continuous infusion interleukin-2 in patients with recurrent Ewing sarcoma and alveolar rhabdomyosarcoma: an inter-institute NIH study. *Med. Pediatr. Oncol.* **38**, 158–164 (2002).

143. Orentas, R. J. *et al.* Identification of cell surface proteins as potential immunotherapy targets in 12 pediatric cancers. *Front. Oncol.* **2**, 194 (2012).

144. Hanahan, D. & Weinberg, R. A. Hallmarks of cancer: the next generation. *Cell* **144**, 646–674 (2011).

145. Warburg, O., Wind, F. & Negelein, E. THE METABOLISM OF TUMORS IN THE BODY. *J. Gen. Physiol.* **8**, 519–530 (1927).

146. Pavlova, N. N. & Thompson, C. B. The Emerging Hallmarks of Cancer Metabolism. *Cell Metab.* **23**, 27–47 (2016).

147. Hay, N. Reprogramming glucose metabolism in cancer: can it be exploited for cancer therapy? *Nat. Rev. Cancer* **16**, 635–649 (2016).

148. Vazquez, A. *et al.* Cancer metabolism at a glance. *J. Cell Sci.* **129**, 3367–3373 (2016).

149. Hensley, C. T., Wasti, A. T. & DeBerardinis, R. J. Glutamine and cancer: cell biology, physiology, and clinical opportunities. *J. Clin. Invest.* **123**, 3678–3684 (2013).

150. Pavlova, N. N., Zhu, J. & Thompson, C. B. The hallmarks of cancer metabolism: Still emerging. *Cell Metab.* **34**, 355–377 (2022).

151. Hirschey, M. D. *et al.* Dysregulated metabolism contributes to oncogenesis. *Semin. Cancer Biol.* **35 Suppl**, S129–S150 (2015).

152. Bergers, G. & Fendt, S.-M. The metabolism of cancer cells during metastasis. *Nat. Rev. Cancer* **21**, 162–180 (2021).

153. Liu, Y. & Cao, X. Characteristics and Significance of the Pre-metastatic Niche. *Cancer Cell* **30**, 668–681 (2016).

154. Fong, M. Y. *et al.* Breast-cancer-secreted miR-122 reprograms glucose metabolism in premetastatic niche to promote metastasis. *Nat. Cell Biol.* **17**, 183–194 (2015).

155. Elia, I., Doglioni, G. & Fendt, S.-M. Metabolic Hallmarks of Metastasis Formation. *Trends Cell Biol.* **28**, 673–684 (2018).

156. Park, J. H., Pyun, W. Y. & Park, H. W. Cancer Metabolism: Phenotype, Signaling and Therapeutic Targets. *Cells* **9**, (2020).

157. Martínez-Reyes, I. & Chandel, N. S. Cancer metabolism: looking forward. *Nat. Rev. Cancer* **21**, 669–680 (2021).

158. Wu, G. *et al.* Arginine metabolism and nutrition in growth, health and disease. *Amino Acids* **37**, 153–168 (2009).

159. Szefel, J., Danielak, A. & Kruszewski, W. J. Metabolic pathways of L-arginine and therapeutic consequences in tumors. *Adv. Med. Sci.* **64**, 104–110 (2019).

160. Brosnan, M. E. & Brosnan, J. T. Renal arginine metabolism. *J. Nutr.* **134**, 2791S-2795S; discussion 2796S-2797S (2004).

161. Zou, S., Wang, X., Liu, P., Ke, C. & Xu, S. Arginine metabolism and deprivation in cancer therapy.

Biomed. Pharmacother. **118**, 109210 (2019).

162. Patil, M. D., Bhaumik, J., Babykutty, S., Banerjee, U. C. & Fukumura, D. Arginine dependence of tumor cells: targeting a chink in cancer's armor. *Oncogene* **35**, 4957–4972 (2016).

163. Feun, L. *et al.* Arginine deprivation as a targeted therapy for cancer. *Curr. Pharm. Des.* **14**, 1049–1057 (2008).

164. Scott, L., Lamb, J., Smith, S. & Wheatley, D. N. Single amino acid (arginine) deprivation: rapid and selective death of cultured transformed and malignant cells. *Br. J. Cancer* **83**, 800–810 (2000).

165. Rodriguez, P. C., Quiceno, D. G. & Ochoa, A. C. L-arginine availability regulates T-lymphocyte cell-cycle progression. *Blood* **109**, 1568–1573 (2007).

166. Lu, Y. *et al.* Overexpression of arginine transporter CAT-1 is associated with accumulation of L-arginine and cell growth in human colorectal cancer tissue. *PLoS One* **8**, e73866 (2013).

167. Abdelmagid, S. A., Rickard, J. A., McDonald, W. J., Thomas, L. N. & Too, C. K. L. CAT-1-mediated arginine uptake and regulation of nitric oxide synthases for the survival of human breast cancer cell lines. *J. Cell. Biochem.* **112**, 1084–1092 (2011).

168. Ban, H. *et al.* Arginine and Leucine regulate p70 S6 kinase and 4E-BP1 in intestinal epithelial cells. *Int. J. Mol. Med.* **13**, 537–543 (2004).

169. Fujiwara, T. *et al.* L-arginine stimulates fibroblast proliferation through the GPRC6A-ERK1/2 and PI3K/Akt pathway. *PLoS One* **9**, e92168 (2014).

170. Pi, M., Nishimoto, S. K. & Quarles, L. D. GPRC6A: Jack of all metabolism (or master of none). *Mol. Metab.* **6**, 185–193 (2017).

171. Chen, C.-L. *et al.* Arginine is an epigenetic regulator targeting TEAD4 to modulate OXPHOS in prostate cancer cells. *Nat. Commun.* **12**, 2398 (2021).

172. Chen, C.-L., Hsu, S.-C., Ann, D. K., Yen, Y. & Kung, H.-J. Arginine Signaling and Cancer Metabolism. *Cancers (Basel).* **13**, (2021).

173. Bredt, D. S. Endogenous nitric oxide synthesis: biological functions and pathophysiology. *Free Radic. Res.* **31**, 577–596 (1999).

174. Keshet, R. & Erez, A. Arginine and the metabolic regulation of nitric oxide synthesis in cancer. *DMM Dis. Model. Mech.* **11**, (2018).

175. Ciani, E., Severi, S., Contestabile, A., Bartesaghi, R. & Contestabile, A. Nitric oxide negatively regulates proliferation and promotes neuronal differentiation through N-Myc downregulation. *J. Cell Sci.* **117**, 4727–4737 (2004).

176. Villalobo, A. Nitric oxide and cell proliferation. *FEBS J.* **273**, 2329–2344 (2006).

177. Lopez-Rivera, E. *et al.* Inducible nitric oxide synthase drives mTOR pathway activation and proliferation of human melanoma by reversible nitrosylation of TSC2. *Cancer Res.* **74**, 1067–1078 (2014).

178. Du, Q. *et al.* Nitric oxide production upregulates Wnt/β-catenin signaling by inhibiting Dickkopf-1.

Cancer Res. **73**, 6526–6537 (2013).

179. Fukumura, D., Kashiwagi, S. & Jain, R. K. The role of nitric oxide in tumour progression. *Nat. Rev. Cancer* **6**, 521–534 (2006).

180. Terzuoli, E. *et al.* Linking of mPGES-1 and iNOS activates stem-like phenotype in EGFR-driven epithelial tumor cells. *Nitric oxide Biol. Chem.* **66**, 17–29 (2017).

181. Dai, F. *et al.* Extracellular polyamines-induced proliferation and migration of cancer cells by ODC, SSAT, and Akt1-mediated pathway. *Anticancer. Drugs* **28**, 457–464 (2017).

182. Samoilenko, O. A., Milinevska, O. A., Karnaushenko, O. V, Shlyakhovenko, V. A. & Zaletok, S. P. Effect of polyamine metabolism inhibitors on Lewis lung carcinoma growth and metastasis. *Exp. Oncol.* **37**, 151–153 (2015).

183. Samal, K. *et al.* AMXT-1501, a novel polyamine transport inhibitor, synergizes with DFMO in inhibiting neuroblastoma cell proliferation by targeting both ornithine decarboxylase and polyamine transport. *Int. J. cancer* **133**, 1323–1333 (2013).

184. Mayeur, C. *et al.* Effects of agmatine accumulation in human colon carcinoma cells on polyamine metabolism, DNA synthesis and the cell cycle. *Biochim. Biophys. Acta* **1745**, 111–123 (2005).

185. Wolf, C. *et al.* Molecular basis for the antiproliferative effect of agmatine in tumor cells of colonic, hepatic, and neuronal origin. *Mol. Pharmacol.* **71**, 276–283 (2007).

186. Dudkowska, M. *et al.* Agmatine modulates the in vivo biosynthesis and interconversion of polyamines and cell proliferation. *Biochim. Biophys. Acta* **1619**, 159–166 (2003).

187. Jahani, M., Noroznezhad, F. & Mansouri, K. Arginine: Challenges and opportunities of this two-faced molecule in cancer therapy. *Biomed. Pharmacother.* **102**, 594–601 (2018).

188. Cao, Y., Feng, Y., Zhang, Y., Zhu, X. & Jin, F. L-Arginine supplementation inhibits the growth of breast cancer by enhancing innate and adaptive immune responses mediated by suppression of MDSCs in vivo. *BMC Cancer* **16**, 343 (2016).

189. Geiger, R. *et al.* L-Arginine Modulates T Cell Metabolism and Enhances Survival and Anti-tumor Activity. *Cell* **167**, 829-842.e13 (2016).

190. BioRender. Available at: https://biorender.com/.

191. RATNER, S. & PETRACK, B. Biosynthesis of urea. III. Further studies on arginine synthesis from citrulline. *J. Biol. Chem.* **191**, 693–705 (1951).

192. ROCHOVANSKY, O. & RATNER, S. Biosynthesis of ureas. IX. Further studies on mechanism of argininosuccinate synthetase reaction. *J. Biol. Chem.* **236**, 2254–2260 (1961).

193. SCHUEGRAF, A., RATNER, S. & WARNER, R. C. Free energy changes of the argininosuccinate synthetase reaction and of the hydrolysis of the inner pyrophosphate bond of adenosine triphosphate. *J. Biol. Chem.* **235**, 3597–3602 (1960).

194. Beaudet, A. L. *et al.* Dispersion of argininosuccinate-synthetase-like human genes to multiple autosomes and the X chromosome. *Cell* **30**, 287–293 (1982).

195. Su, T. S., Bock, H. G., O'Brien, W. E. & Beaudet, A. L. Cloning of cDNA for argininosuccinate synthetase mRNA and study of enzyme overproduction in a human cell line. *J. Biol. Chem.* **256**, 11826–11831 (1981).

196. Takiguchi, M., Matsubasa, T., Amaya, Y. & Mori, M. Evolutionary aspects of urea cycle enzyme genes. *Bioessays* **10**, 163–166 (1989).

197. Freytag, S. O., Beaudet, A. L., Bock, H. G. & O'Brien, W. E. Molecular structure of the human argininosuccinate synthetase gene: occurrence of alternative mRNA splicing. *Mol. Cell. Biol.* **4**, 1978–1984 (1984).

198. Engel, K., Höhne, W. & Häberle, J. Mutations and polymorphisms in the human argininosuccinate synthetase (ASS1) gene. *Hum. Mutat.* **30**, 300–307 (2009).

199. Su, T. S. & Lin, L. H. Analysis of a splice acceptor site mutation which produces multiple splicing abnormalities in the human argininosuccinate synthetase locus. *J. Biol. Chem.* **265**, 19716–19720 (1990).

200. Ratner, S. Argininosuccinate synthetase of bovine liver: chemical and physical properties. *Proc. Natl. Acad. Sci. U. S. A.* **79**, 5197–5199 (1982).

201. Karlberg, T. *et al.* Structure of human argininosuccinate synthetase. *Acta Crystallogr. D. Biol. Crystallogr.* **64**, 279–286 (2008).

202. Goto, M., Nakajima, Y. & Hirotsu, K. Crystal structure of argininosuccinate synthetase from Thermus thermophilus HB8. Structural basis for the catalytic action. *J. Biol. Chem.* **277**, 15890–15896 (2002).

203. Kato, H., Oyamada, I., Mizutani-Funahashi, M. & Nakagawa, H. New radioisotopic assays of argininosuccinate synthetase and argininosuccinase. *J. Biochem.* **79**, 945–953 (1976).

204. Gornall, A. G. Nitrogen Study in the Ornithine Cycle of Urea Formation. *Can. Med. Assoc. J.* **47**, 421–423 (1942).

205. Morris, S. M. J. Regulation of enzymes of urea and arginine synthesis. *Annu. Rev. Nutr.* **12**, 81–101 (1992).

206. Keshet, R., Szlosarek, P., Carracedo, A. & Erez, A. Rewiring urea cycle metabolism in cancer to support anabolism. *Nat. Rev. Cancer* **18**, 634–645 (2018).

207. Goodwin, B. L., Solomonson, L. P. & Eichler, D. C. Argininosuccinate synthase expression is required to maintain nitric oxide production and cell viability in aortic endothelial cells. *J. Biol. Chem.* **279**, 18353–18360 (2004).

208. Xie, L. & Gross, S. S. Argininosuccinate synthetase overexpression in vascular smooth muscle cells potentiates immunostimulant-induced NO production. *J. Biol. Chem.* **272**, 16624–16630 (1997).

209. Husson, A., Brasse-Lagnel, C., Fairand, A., Renouf, S. & Lavoinne, A. Argininosuccinate synthetase from the urea cycle to the citrulline-NO cycle. *Eur. J. Biochem.* **270**, 1887–1899 (2003).

210. Saheki, T., Katsunuma, T. & Sase, M. Regulation of urea synthesis in rat liver. Changes of

ornithine and acetylglutamate concentrations in the livers of rats subjected to dietary transitions. *J. Biochem.* **82**, 551–558 (1977).

211. Snodgrass, P. J. & Lin, R. C. Induction of urea cycle enzymes of rat liver by amino acids. *J. Nutr.* **111**, 586–601 (1981).

212. Tomomura, M., Tomomura, A., Dewan, M. A. & Saheki, T. Long-chain fatty acids suppress the induction of urea cycle enzyme genes by glucocorticoid action. *FEBS Lett.* **399**, 310–312 (1996).

213. Ah Mew, N. *et al.* Urea Cycle Disorders Overview. in (eds. Adam, M. P. et al.) (1993).

214. Summar, M. L. *et al.* The incidence of urea cycle disorders. *Mol. Genet. Metab.* **110**, 179–180 (2013).

215. Summar, M. Current strategies for the management of neonatal urea cycle disorders. *J. Pediatr.* **138**, S30-9 (2001).

216. Kölker, S. *et al.* The phenotypic spectrum of organic acidurias and urea cycle disorders. Part 2: the evolving clinical phenotype. *J. Inherit. Metab. Dis.* **38**, 1059–1074 (2015).

217. Beaudet, A. L., O'Brien, W. E., Bock, H. G., Freytag, S. O. & Su, T. S. The human argininosuccinate synthetase locus and citrullinemia. *Adv. Hum. Genet.* **15**, 161-196,291-292 (1986).

218. Posset, R. *et al.* Impact of Diagnosis and Therapy on Cognitive Function in Urea Cycle Disorders. *Ann. Neurol.* **86**, 116–128 (2019).

219. Berning, C. *et al.* Investigation of citrullinemia type I variants by in vitro expression studies. *Hum. Mutat.* **29**, 1222–1227 (2008).

220. Quinonez, S. C. & Thoene, J. G. Citrullinemia Type I. in (eds. Adam, M. P. et al.) (1993).

221. Häberle, J. *et al.* Structure of the human argininosuccinate synthetase gene and an improved system for molecular diagnostics in patients with classical and mild citrullinemia. *Hum. Genet.* **110**, 327–333 (2002).

222. Gao, H.-Z. *et al.* Identification of 16 novel mutations in the argininosuccinate synthetase gene and genotype-phenotype correlation in 38 classical citrullinemia patients. *Hum. Mutat.* **22**, 24–34 (2003).

223. Zielonka, M. *et al.* Early prediction of phenotypic severity in Citrullinemia Type 1. *Ann. Clin. Transl. Neurol.* **6**, 1858–1871 (2019).

224. Atlas, T. H. P. No Title. Available at: https://www.proteinatlas.org/ENSG00000130707-ASS1/pathology.

225. Delage, B. *et al.* Arginine deprivation and argininosuccinate synthetase expression in the treatment of cancer. *International Journal of Cancer* **126**, 2762–2772 (2010).

226. Liu, Q. *et al.* Reduced expression of argininosuccinate synthetase 1 has a negative prognostic impact in patients with pancreatic ductal adenocarcinoma. *PLoS One* **12**, e0171985 (2017).

227. Yoon, C.-Y. *et al.* Renal cell carcinoma does not express argininosuccinate synthetase and is

highly sensitive to arginine deprivation via arginine deiminase. *Int. J. cancer* **120**, 897–905 (2007).

228. Szlosarek, P. W. *et al.* In vivo loss of expression of argininosuccinate synthetase in malignant pleural mesothelioma is a biomarker for susceptibility to arginine depletion. *Clin. cancer Res. an Off. J. Am. Assoc. Cancer Res.* **12**, 7126–7131 (2006).

229. Ensor, C. M., Holtsberg, F. W., Bomalaski, J. S. & Clark, M. A. Pegylated arginine deiminase (ADI-SS PEG20,000 mw) inhibits human melanomas and hepatocellular carcinomas in vitro and in vivo. *Cancer Res.* **62**, 5443–5450 (2002).

230. Dillon, B. J. *et al.* Incidence and distribution of argininosuccinate synthetase deficiency in human cancers: a method for identifying cancers sensitive to arginine deprivation. *Cancer* **100**, 826–833 (2004).

231. Sahu, D. *et al.* Argininosuccinate Synthetase 1 Loss in Invasive Bladder Cancer Regulates Survival through General Control Nonderepressible 2 Kinase-Mediated Eukaryotic Initiation Factor 2α Activity and Is Targetable by Pegylated Arginine Deiminase. *Am. J. Pathol.* **187**, 200–213 (2017).

232. Allen, M. D. *et al.* Prognostic and therapeutic impact of argininosuccinate synthetase 1 control in bladder cancer as monitored longitudinally by PET imaging. *Cancer Res.* **74**, 896–907 (2014).

233. Khare, S. *et al.* ASS1 and ASL suppress growth in clear cell renal cell carcinoma via altered nitrogen metabolism. *Cancer Metab.* **9**, 40 (2021).

234. Wu, L. *et al.* Expression of argininosuccinate synthetase in patients with hepatocellular carcinoma. *J. Gastroenterol. Hepatol.* **28**, 365–368 (2013).

235. Du, D. *et al.* Metabolic dysregulation and emerging therapeutical targets for hepatocellular carcinoma. *Acta Pharm. Sin. B* **12**, 558–580 (2022).

236. Kelly, M. P. *et al.* Arginine deiminase PEG20 inhibits growth of small cell lung cancers lacking expression of argininosuccinate synthetase. *Br. J. Cancer* **106**, 324–332 (2012).

237. Kim, R. H. *et al.* Arginine deiminase as a novel therapy for prostate cancer induces autophagy and caspase-independent apoptosis. *Cancer Res.* **69**, 700–708 (2009).

238. Bean, G. R. *et al.* A metabolic synthetic lethal strategy with arginine deprivation and chloroquine leads to cell death in ASS1-deficient sarcomas. *Cell Death Dis.* **7**, 1–11 (2016).

239. Kobayashi, E. *et al.* Reduced argininosuccinate synthetase is a predictive biomarker for the development of pulmonary metastasis in patients with osteosarcoma. *Mol. Cancer Ther.* **9**, 535–544 (2010).

240. Miyamoto, T. *et al.* Argininosuccinate synthase 1 is an intrinsic Akt repressor transactivated by p53. *Sci. Adv.* **3**, e1603204 (2017).

241. Tsai, W.-B. *et al.* Resistance to arginine deiminase treatment in melanoma cells is associated with induced argininosuccinate synthetase expression involving c-Myc/HIF-1alpha/Sp4. *Mol. Cancer Ther.* **8**, 3223–3233 (2009).

242. Nicholson, L. J. *et al.* Epigenetic silencing of argininosuccinate synthetase confers resistance to

platinum-induced cell death but collateral sensitivity to arginine auxotrophy in ovarian cancer. *Int. J. cancer* **125**, 1454–1463 (2009).

243. Syed, N. *et al.* Epigenetic status of argininosuccinate synthetase and argininosuccinate lyase modulates autophagy and cell death in glioblastoma. *Cell Death Dis.* **4**, e458 (2013).

244. Wheatley, D. N. Controlling cancer by restricting arginine availability--arginine-catabolizing enzymes as anticancer agents. *Anticancer. Drugs* **15**, 825–833 (2004).

245. Rabinovich, S. *et al.* Diversion of aspartate in ASS1-deficient tumours fosters de novo pyrimidine synthesis. *Nature* **527**, 379–383 (2015).

246. Szlosarek, P. W. *et al.* Aberrant regulation of argininosuccinate synthetase by TNF-alpha in human epithelial ovarian cancer. *Int. J. cancer* **121**, 6–11 (2007).

247. Bateman, L. A. *et al.* Argininosuccinate Synthase 1 is a Metabolic Regulator of Colorectal Cancer Pathogenicity. *ACS Chem. Biol.* **12**, 905–911 (2017).

248. Jia, H. *et al.* Snail enhances arginine synthesis by inhibiting ubiquitination-mediated degradation of ASS1. *EMBO Rep.* **22**, 1–18 (2021).

249. Shan, Y.-S. *et al.* Increased expression of argininosuccinate synthetase protein predicts poor prognosis in human gastric cancer. *Oncol. Rep.* **33**, 49–57 (2015).

250. Yuan, J., Zhang, F. & Niu, R. Multiple regulation pathways and pivotal biological functions of STAT3 in cancer. *Sci. Rep.* **5**, 17663 (2015).

251. Amara, S. *et al.* Critical role of SIK3 in mediating high salt and IL-17 synergy leading to breast cancer cell proliferation. *PLoS One* **12**, e0180097 (2017).

252. Brasse-Lagnel, C. *et al.* Glutamine and interleukin-1beta interact at the level of Sp1 and nuclear factor-kappaB to regulate argininosuccinate synthetase gene expression. *FEBS J.* **274**, 5250–5262 (2007).

253. Mao, Y., Shi, D., Li, G. & Jiang, P. Citrulline depletion by ASS1 is required for proinflammatory macrophage activation and immune responses. *Mol. Cell* **82**, 527-541.e7 (2022).

254. DeBerardinis, R. J. & Chandel, N. S. Fundamentals of cancer metabolism. *Sci. Adv.* **2**, e1600200 (2016).

255. Olivares, O., Däbritz, J. H. M., King, A., Gottlieb, E. & Halsey, C. Research into cancer metabolomics: Towards a clinical metamorphosis. *Semin. Cell Dev. Biol.* **43**, 52–64 (2015).

256. Dang, L. *et al.* Cancer-associated IDH1 mutations produce 2-hydroxyglutarate. *Nature* **462**, 739–744 (2009).

257. Garcia-Bermudez, J., Williams, R. T., Guarecuco, R. & Birsoy, K. Targeting extracellular nutrient dependencies of cancer cells. *Mol. Metab.* **33**, 67–82 (2020).

258. Siegel, S. E. *et al.* Pediatric-Inspired Treatment Regimens for Adolescents and Young Adults With Philadelphia Chromosome-Negative Acute Lymphoblastic Leukemia: A Review. *JAMA Oncol.* **4**, 725–734 (2018).

259. Douer, D., Gökbuget, N., Stock, W. & Boissel, N. Optimizing use of L-asparaginase-based treatment of adults with acute lymphoblastic leukemia. *Blood Rev.* **53**, 100908 (2022).

260. Luengo, A., Gui, D. Y. & Vander Heiden, M. G. Targeting Metabolism for Cancer Therapy. *Cell Chem. Biol.* **24**, 1161–1180 (2017).

261. Savaraj, N. *et al.* The relationship of arginine deprivation, argininosuccinate synthetase and cell death in melanoma. *Drug Target Insights* **2**, 119–128 (2007).

262. Bowles, T. L. *et al.* Pancreatic cancer cell lines deficient in argininosuccinate synthetase are sensitive to arginine deprivation by arginine deiminase. *Int. J. cancer* **123**, 1950–1955 (2008).

263. Khalil, N. & Abi-Habib, R. J. [HuArgI (co)-PEG5000]-induced arginine deprivation leads to autophagy dependent cell death in pancreatic cancer cells. *Invest. New Drugs* **38**, 1236–1246 (2020).

264. Fultang, L., Vardon, A., De Santo, C. & Mussai, F. Molecular basis and current strategies of therapeutic arginine depletion for cancer. *Int. J. cancer* **139**, 501–509 (2016).

265. Miyazaki, K. *et al.* Potent growth inhibition of human tumor cells in culture by arginine deiminase purified from a culture medium of a Mycoplasma-infected cell line. *Cancer Res.* **50**, 4522–4527 (1990).

266. Abou-Alfa, G. K. *et al.* Phase III randomized study of second line ADI-PEG 20 plus best supportive care versus placebo plus best supportive care in patients with advanced hepatocellular carcinoma. *Ann. Oncol. Off. J. Eur. Soc. Med. Oncol.* **29**, 1402–1408 (2018).

267. Ott, P. A. *et al.* Phase I/II study of pegylated arginine deiminase (ADI-PEG 20) in patients with advanced melanoma. *Invest. New Drugs* **31**, 425–434 (2013).

268. Tsai, H.-J. *et al.* A Phase II Study of Arginine Deiminase (ADI-PEG20) in Relapsed/Refractory or Poor-Risk Acute Myeloid Leukemia Patients. *Sci. Rep.* **7**, 11253 (2017).

269. Tsai, H.-J. *et al.* Phase I study of ADI-PEG20 plus low-dose cytarabine for the treatment of acute myeloid leukemia. *Cancer Med.* **10**, 2946–2955 (2021).

270. Yau, T. *et al.* A phase 1 dose-escalating study of pegylated recombinant human arginase 1 (Peg-rhArg1) in patients with advanced hepatocellular carcinoma. *Invest. New Drugs* **31**, 99–107 (2013).

271. Yau, T. *et al.* Preliminary efficacy, safety, pharmacokinetics, pharmacodynamics and quality of life study of pegylated recombinant human arginase 1 in patients with advanced hepatocellular carcinoma. *Invest. New Drugs* **33**, 496–504 (2015).

272. De Santo, C. *et al.* Metabolic therapy with PEG-arginase induces a sustained complete remission in immunotherapy-resistant melanoma. *J. Hematol. Oncol.* **11**, 68 (2018).

273. Khadeir, R., Szyszko, T. & Szlosarek, P. W. Optimizing arginine deprivation for hard-to-treat cancers. *Oncotarget* **8**, 96468–96469 (2017).

274. Locke, M. *et al.* Inhibition of the Polyamine Synthesis Pathway Is Synthetically Lethal with Loss of Argininosuccinate Synthase 1. *Cell Rep.* **16**, 1604–1613 (2016).

275. Delage, B. *et al.* Promoter methylation of argininosuccinate synthetase-1 sensitises lymphomas to arginine deiminase treatment, autophagy and caspase-dependent apoptosis. *Cell Death Dis.* **3**, e342 (2012).

276. Long, Y. *et al.* Arginine deiminase resistance in melanoma cells is associated with metabolic reprogramming, glucose dependence, and glutamine addiction. *Mol. Cancer Ther.* **12**, 2581–2590 (2013).

277. Glazer, E. S. *et al.* Phase II study of pegylated arginine deiminase for nonresectable and metastatic hepatocellular carcinoma. *J. Clin. Oncol. Off. J. Am. Soc. Clin. Oncol.* **28**, 2220–2226 (2010).

278. Yang, T.-S. *et al.* A randomised phase II study of pegylated arginine deiminase (ADI-PEG 20) in Asian advanced hepatocellular carcinoma patients. *Br. J. Cancer* **103**, 954–960 (2010).

279. Keshet, R. *et al.* Targeting purine synthesis in ASS1-expressing tumors enhances the response to immune checkpoint inhibitors. *Nat. cancer* **1**, 894–908 (2020).

280. Monti, E. & Fanzani, A. Uncovering metabolism in rhabdomyosarcoma. *Cell Cycle* **15**, 184–195 (2016).

281. Pfaffl, M. W. A new mathematical model for relative quantification in real-time RT-PCR. *Nucleic Acids Res.* **29**, e45 (2001).

282. López-Alemany, R. & Tirado, O. M. Metastasis Assessment in Ewing Sarcoma Using Orthotopic Xenografts. *Methods Mol. Biol.* **2226**, 201–213 (2021).

283. Sun, W. *et al.* Distinct methylation profiles characterize fusion-positive and fusion-negative rhabdomyosarcoma. *Mod. Pathol.* **28**, 1214–1224 (2015).

284. No Title. https://www.ncbi.nlm.nih.gov/geo/query/acc.cgi?acc

285. Lee, M. H. & Surh, Y. J. eEF1A2 as a putative oncogene. *Ann. N. Y. Acad. Sci.* **1171**, 87–93 (2009).

286. Amiri, A. *et al.* eEF1A2 activates Akt and stimulates Akt-dependent actin remodeling, invasion and migration. *Oncogene* **26**, 3027–3040 (2007).

287. Tavares, M. R. *et al.* The S6K protein family in health and disease. *Life Sci.* **131**, 1–10 (2015).

288. WARBURG, O. On the origin of cancer cells. *Science* **123**, 309–314 (1956).

289. Merlino, G. & Helman, L. J. Rhabdomyosarcoma--working out the pathways. *Oncogene* **18**, 5340–5348 (1999).

290. Hettmer, S. & Wagers, A. J. Muscling in: Uncovering the origins of rhabdomyosarcoma. *Nat. Med.* **16**, 171–173 (2010).

291. Hatley, M. E. *et al.* A mouse model of rhabdomyosarcoma originating from the adipocyte lineage. *Cancer Cell* **22**, 536–546 (2012).

292. Drummond, C. J. *et al.* Hedgehog Pathway Drives Fusion-Negative Rhabdomyosarcoma Initiated From Non-myogenic Endothelial Progenitors. *Cancer Cell* **33**, 108-124.e5 (2018).

293. Pandey, P. R. *et al.* PAX3–FOXO1 is essential for tumour initiation and maintenance but not recurrence in a human myoblast model of rhabdomyosarcoma. *Journal of Pathology* **241**, 626–637 (2017).

294. Lagutina, I. V. *et al.* Modeling of the Human Alveolar Rhabdomyosarcoma Pax3-Foxo1 Chromosome Translocation in Mouse Myoblasts Using CRISPR-Cas9 Nuclease. *PLoS Genet.* **11**, 1–24 (2015).

295. McMahon, D. K. *et al.* C2C12 cells: biophysical, biochemical, and immunocytochemical properties. *Am. J. Physiol.* **266**, C1795-802 (1994).

296. Chen, X., Sun, Y., Zhang, T., Roepstorff, P. & Yang, F. Comprehensive Analysis of the Proteome and PTMomes of C2C12 Myoblasts Reveals that Sialylation Plays a Role in the Differentiation of Skeletal Muscle Cells. *J. Proteome Res.* **20**, 222–235 (2021).

297. Wong, C. Y., Al-Salami, H. & Dass, C. R. C2C12 cell model: its role in understanding of insulin resistance at the molecular level and pharmaceutical development at the preclinical stage. *J. Pharm. Pharmacol.* **72**, 1667–1693 (2020).

298. Wong, C. Y., Al-Salami, H. & Dass, C. R. C2C12 cell model: its role in understanding of insulin resistance at the molecular level and pharmaceutical development at the preclinical stage. *J. Pharm. Pharmacol.* **72**, 1667–1693 (2020).

299. Kohsaka, S. *et al.* A recurrent neomorphic mutation in MYOD1 defines a clinically aggressive subset of embryonal rhabdomyosarcoma associated with PI3K-AKT pathway mutations. *Nat. Genet.* **46**, 595–600 (2014).

300. Choo, F. *et al.* Functional impact and targetability of PI3KCA, GNAS, and PTEN mutations in a spindle cell rhabdomyosarcoma with MYOD1 L122R mutation. *Cold Spring Harb. Mol. case Stud.* **8**, (2022).

301. Ahn, E. H., Mercado, G. E., Laé, M. & Ladanyi, M. Identification of target genes of PAX3-FOXO1 in alveolar rhabdomyosarcoma. *Oncol. Rep.* **30**, 968–978 (2013).

302. Stratton, M. R., Fisher, C., Gusterson, B. A. & Cooper, C. S. Detection of point mutations in N-ras and K-ras genes of human embryonal rhabdomyosarcomas using oligonucleotide probes and the polymerase chain reaction. *Cancer Res.* **49**, 6324–6327 (1989).

303. Shukla, N. *et al.* Oncogene mutation profiling of pediatric solid tumors reveals significant subsets of embryonal rhabdomyosarcoma and neuroblastoma with mutated genes in growth signaling pathways. *Clin. Cancer Res.* **18**, 748–757 (2012).

304. Edinger, A. L. & Thompson, C. B. Akt maintains cell size and survival by increasing mTOR-dependent nutrient uptake. *Mol. Biol. Cell* **13**, 2276–2288 (2002).

305. Elstrom, R. L. *et al.* Akt stimulates aerobic glycolysis in cancer cells. *Cancer Res.* **64**, 3892–3899 (2004).

306. Bauer, D. E., Hatzivassiliou, G., Zhao, F., Andreadis, C. & Thompson, C. B. ATP citrate lyase is an important component of cell growth and transformation. *Oncogene* **24**, 6314–6322 (2005).

307. Gingras, A. C., Raught, B. & Sonenberg, N. Regulation of translation initiation by FRAP/mTOR.

Genes Dev. **15**, 807–826 (2001).

308. Chen, X. *et al.* Targeting Oxidative Stress in Embryonal Rhabdomyosarcoma. *Cancer Cell* **24**, 710–724 (2013).

309. Schwartzenberg-Bar-Yoseph, F., Armoni, M. & Karnieli, E. The tumor suppressor p53 down-regulates glucose transporters GLUT1 and GLUT4 gene expression. *Cancer Res.* **64**, 2627–2633 (2004).

310. Suzuki, S. *et al.* Phosphate-activated glutaminase (GLS2), a p53-inducible regulator of glutamine metabolism and reactive oxygen species. *Proc. Natl. Acad. Sci. U. S. A.* **107**, 7461–7466 (2010).

311. Ramadan, F., Fahs, A., Ghayad, S. E. & Saab, R. Signaling pathways in Rhabdomyosarcoma invasion and metastasis. *Cancer Metastasis Rev.* **39**, 287–301 (2020).

312. Gryder, B. E. *et al.* PAX3-FOXO1 Establishes Myogenic Super Enhancers and Confers BET Bromodomain Vulnerability. *Cancer Discov.* **7**, 884–899 (2017).

313. Issaq, S. H., Teicher, B. A. & Monks, A. Bioenergetic properties of human sarcoma cells help define sensitivity to metabolic inhibitors. *Cell Cycle* **13**, 1152–1161 (2014).

314. Armoni, M. *et al.* PAX3/forkhead homolog in rhabdomyosarcoma oncoprotein activates glucose transporter 4 gene expression in vivo and in vitro. *J. Clin. Endocrinol. Metab.* **87**, 5312–5324 (2002).

315. Ramírez-Peinado, S. *et al.* 2-Deoxyglucose induces Noxa-dependent apoptosis in alveolar rhabdomyosarcoma. *Cancer Res.* **71**, 6796–6806 (2011).

316. Li, H. G. *et al.* PAX3 and PAX3-FKHR promote rhabdomyosarcoma cell survival through downregulation of PTEN. *Cancer Lett.* **253**, 215–223 (2007).

317. Liu, L., Wang, Y. D., Wu, J., Cui, J. & Chen, T. Carnitine palmitoyltransferase 1A (CPT1A): a transcriptional target of PAX3-FKHR and mediates PAX3-FKHR-dependent motility in alveolar rhabdomyosarcoma cells. *BMC Cancer* **12**, 1–12 (2012).

318. Pappo, A. S. *et al.* A phase II trial of high-dose methotrexate in previously untreated children and adolescents with high-risk unresectable or metastatic rhabdomyosarcoma. *J. Pediatr. Hematol. Oncol.* **19**, 438–442 (1997).

319. Zhao, Y. *et al.* An NADPH sensor protein (HSCARG) down-regulates nitric oxide synthesis by association with argininosuccinate synthetase and is essential for epithelial cell viability. *J. Biol. Chem.* **283**, 11004–11013 (2008).

320. Haines, R. J., Pendleton, L. C. & Eichler, D. C. Argininosuccinate synthase: At the center of arginine metabolism. *Int. J. Biochem. Mol. Biol.* **2**, 8–23 (2011).

321. Hao, G., Xie, L. & Gross, S. S. Argininosuccinate synthetase is reversibly inactivated by S-nitrosylation in vitro and in vivo. *J. Biol. Chem.* **279**, 36192–36200 (2004).

322. Corbin, K. D., Pendleton, L. C., Solomonson, L. P. & Eichler, D. C. Phosphorylation of argininosuccinate synthase by protein kinase A. *Biochem. Biophys. Res. Commun.* **377**, 1042–1046 (2008).

323. Huang, H.-Y. *et al.* ASS1 as a novel tumor suppressor gene in myxofibrosarcomas: aberrant loss via epigenetic DNA methylation confers aggressive phenotypes, negative prognostic impact, and therapeutic relevance. *Clin. cancer Res. an Off. J. Am. Assoc. Cancer Res.* **19**, 2861–2872 (2013).

324. Prudner, B. C. *et al.* Arginine starvation and docetaxel induce c-Myc–driven HENT1 surface expression to overcome gemcitabine resistance in AsS1-negative tumors. *Clin. Cancer Res.* **25**, 5122–5134 (2019).

325. Shan, Y. S. *et al.* Argininosuccinate synthetase 1 suppression and arginine restriction inhibit cell migration in gastric cancer cell lines. *Sci. Rep.* **5**, 1–10 (2015).

326. Tsai, C. Y. *et al.* Argininosuccinate synthetase 1 contributes to gastric cancer invasion and progression by modulating autophagy. *FASEB J.* **32**, 2601–2614 (2018).

327. Brasse-Lagnel, C., Lavoinne, A., Fairand, A., Vavasseur, K. & Husson, A. IL-1beta stimulates argininosuccinate synthetase gene expression through NF-kappaB in Caco-2 cells. *Biochimie* **87**, 403–409 (2005).

328. Doubleday, P. F., Fornelli, L., Ntai, I. & Kelleher, N. L. Oncogenic KRAS creates an aspartate metabolism signature in colorectal cancer cells. *FEBS J.* **288**, 6683–6699 (2021).

329. Buchanan, B. W., Lloyd, M. E., Engle, S. M. & Rubenstein, E. M. Cycloheximide Chase Analysis of Protein Degradation in Saccharomyces cerevisiae. *J. Vis. Exp.* (2016). doi:10.3791/53975

330. Kao, S.-H. *et al.* Analysis of Protein Stability by the Cycloheximide Chase Assay. *Bio-protocol* **5**, (2015).

331. Feun, L. & Savaraj, N. Pegylated arginine deiminase: a novel anticancer enzyme agent. *Expert Opin. Investig. Drugs* **15**, 815–822 (2006).

332. Jackson, M. J., Allen, S. J., Beaudet, A. L. & O'Brien, W. E. Metabolite regulation of argininosuccinate synthetase in cultured human cells. *J. Biol. Chem.* **263**, 16388–16394 (1988).

333. Cantor, J. R. The Rise of Physiologic Media. *Trends Cell Biol.* **29**, 854–861 (2019).

334. Carmona-Fontaine, C. *et al.* Metabolic origins of spatial organization in the tumor microenvironment. *Proc. Natl. Acad. Sci. U. S. A.* **114**, 2934–2939 (2017).

335. Silberman, A. *et al.* Acid-Induced Downregulation of ASS1 Contributes to the Maintenance of Intracellular pH in Cancer. *Cancer Res.* **79**, 518–533 (2019).

336. Zhang, Y., He, W. & Zhang, S. Seeking for Correlative Genes and Signaling Pathways With Bone Metastasis From Breast Cancer by Integrated Analysis. *Front. Oncol.* **9**, 138 (2019).

337. Aboulouard, S. *et al.* In-depth proteomics analysis of sentinel lymph nodes from individuals with endometrial cancer. *Cell reports. Med.* **2**, 100318 (2021).

338. Cohen, N. S. & Kuda, A. Argininosuccinate synthetase and argininosuccinate lyase are localized around mitochondria: an immunocytochemical study. *J. Cell. Biochem.* **60**, 334–340 (1996).

339. Watford, M. Channeling in the urea cycle: a metabolon spanning two compartments. *Trends Biochem. Sci.* **14**, 313–314 (1989).

340. Wu, G. & Morris, S. M. J. Arginine metabolism: nitric oxide and beyond. *Biochem. J.* **336 (Pt 1**, 1–17 (1998).

341. Daniel, E. E., Wang, Y. F., Salapatek, A. M., Mao, Y. K. & Mori, M. Arginosuccinate synthetase, arginosuccinate lyase and NOS in canine gastrointestinal tract: immunocytochemical studies. *Neurogastroenterol. Motil. Off. J. Eur. Gastrointest. Motil. Soc.* **12**, 317–334 (2000).

342. Flam, B. R., Hartmann, P. J., Harrell-Booth, M., Solomonson, L. P. & Eichler, D. C. Caveolar localization of arginine regeneration enzymes, argininosuccinate synthase, and lyase, with endothelial nitric oxide synthase. *Nitric oxide Biol. Chem.* **5**, 187–197 (2001).

343. Fulton, D. *et al.* Targeting of endothelial nitric-oxide synthase to the cytoplasmic face of the Golgi complex or plasma membrane regulates Akt- versus calcium-dependent mechanisms for nitric oxide release. *J. Biol. Chem.* **279**, 30349–30357 (2004).

344. Edfors, F. *et al.* Gene-specific correlation of RNA and protein levels in human cells and tissues. *Mol. Syst. Biol.* **12**, 883 (2016).

345. ASS1 ProteinAtlas. Available at: https://www.proteinatlas.org/ENSG00000130707-ASS1/subcellular.

346. Tran, T. Q., Lowman, X. H. & Kong, M. Molecular Pathways: Metabolic Control of Histone Methylation and Gene Expression in Cancer. *Clin. cancer Res. an Off. J. Am. Assoc. Cancer Res.* **23**, 4004–4009 (2017).

347. Kinnaird, A., Zhao, S., Wellen, K. E. & Michelakis, E. D. Metabolic control of epigenetics in cancer. *Nat. Rev. Cancer* **16**, 694–707 (2016).

348. Wellen, K. E. *et al.* ATP-citrate lyase links cellular metabolism to histone acetylation. *Science* **324**, 1076–1080 (2009).

349. Sutendra, G. *et al.* A nuclear pyruvate dehydrogenase complex is important for the generation of acetyl-CoA and histone acetylation. *Cell* **158**, 84–97 (2014).

350. Gumińska, M., Stachurska, M. B. & Ignacak, J. Pyruvate kinase isoenzymes in chromatin extracts of Ehrlich ascites tumour, Morris hepatoma 7777 and normal mouse and rat livers. *Biochim. Biophys. Acta* **966**, 207–213 (1988).

351. He, Y. *et al.* Nuclear localization of metabolic enzymes in immunity and metastasis. *Biochim. Biophys. acta. Rev. cancer* **1868**, 359–371 (2017).

352. Bhardwaj, A. & Das, S. SIRT6 deacetylates PKM2 to suppress its nuclear localization and oncogenic functions. *Proc. Natl. Acad. Sci. U. S. A.* **113**, E538-47 (2016).

353. Pan, C., Li, B. & Simon, M. C. Moonlighting functions of metabolic enzymes and metabolites in cancer. *Mol. Cell* **81**, 3760–3774 (2021).

354. Abbas, W., Kumar, A. & Herbein, G. The eEF1A Proteins: At the Crossroads of Oncogenesis, Apoptosis, and Viral Infections. *Front. Oncol.* **5**, 75 (2015).

355. Mills, A. & Gago, F. On the Need to Tell Apart Fraternal Twins eEF1A1 and eEF1A2, and Their Respective Outfits. *Int. J. Mol. Sci.* **22**, (2021).

356. Tomlinson, V. A. L. *et al.* Translation elongation factor eEF1A2 is a potential oncoprotein that is overexpressed in two-thirds of breast tumours. *BMC Cancer* **5**, 113 (2005).

357. Pinke, D. E., Kalloger, S. E., Francetic, T., Huntsman, D. G. & Lee, J. M. The prognostic significance of elongation factor eEF1A2 in ovarian cancer. *Gynecol. Oncol.* **108**, 561–568 (2008).

358. Pellegrino, R. *et al.* EEF1A2 inactivates p53 by way of PI3K/AKT/mTOR-dependent stabilization of MDM4 in hepatocellular carcinoma. *Hepatology* **59**, 1886–1899 (2014).

359. Yang, J. *et al.* Effect of activation of the Akt/mTOR signaling pathway by EEF1A2 on the biological behavior of osteosarcoma. *Ann. Transl. Med.* **9**, 158 (2021).

360. Xu, C., Hu, D. M. & Zhu, Q. EEF1A2 promotes cell migration, invasion and metastasis in pancreatic cancer by upregulating MMP-9 expression through Akt activation. *Clin. Exp. Metastasis* **30**, 933–944 (2013).

361. Khwanraj, K. & Dharmasaroja, P. Neuroblastoma Cell Death Induced by eEF1A2 Knockdown Is Possibly Mediated by the Inhibition of Akt and mTOR Phosphorylation. *Int. J. Hematol. stem cell Res.* **15**, 221–229 (2021).

362. Figueiredo, V. C., Markworth, J. F. & Cameron-Smith, D. Considerations on mTOR regulation at serine 2448: implications for muscle metabolism studies. *Cell. Mol. Life Sci.* **74**, 2537–2545 (2017).

363. Gagliardi, P. A., Puliafito, A. & Primo, L. PDK1: At the crossroad of cancer signaling pathways. *Semin. Cancer Biol.* **48**, 27–35 (2018).

364. Pullen, N. *et al.* Phosphorylation and activation of p70s6k by PDK1. *Science* **279**, 707–710 (1998).

365. Jenö, P., Ballou, L. M., Novak-Hofer, I. & Thomas, G. Identification and characterization of a mitogen-activated S6 kinase. *Proc. Natl. Acad. Sci. U. S. A.* **85**, 406–410 (1988).

366. Sridharan, S. & Basu, A. Distinct Roles of mTOR Targets S6K1 and S6K2 in Breast Cancer. *Int. J. Mol. Sci.* **21**, (2020).

367. Yi, Y. W., You, K. S., Park, J.-S., Lee, S.-G. & Seong, Y.-S. Ribosomal Protein S6: A Potential Therapeutic Target against Cancer? *Int. J. Mol. Sci.* **23**, (2021).

ANNEX I

Table A1: List of the 56 de-regulated genes upon PAX3-FOXO1 expression or silencing, obtained following the integration of bioinformatic analysis outcomes of previously published data[97,283,284]

Gene Symbol	Gene Name
SLC46A3	solute carrier family 46 member 3
CHD7	chromodomain helicase DNA binding protein 7
JADE1	jade family PHD finger 1
TNFAIP3	TNF alpha induced protein 3
CCP110	centriolar coiled-coil protein 110
ARRB1	arrestin beta 1
ABAT	4-aminobutyrate aminotransferase
CDH3	cadherin 3
SKP2	S-phase kinase associated protein 2
PPP1R16B	protein phosphatase 1 regulatory subunit 16B
VAV3	vav guanine nucleotide exchange factor 3
NCOA1	nuclear receptor coactivator 1
NXPE3	neurexophilin and PC-esterase domain family member 3
DFFB	DNA fragmentation factor subunit beta
IL4R	interleukin 4 receptor
TLE1	TLE family member 1, transcriptional corepressor
PEG3	paternally expressed 3
DAPK1	death associated protein kinase 1
PIPOX	pipecolic acid and sarcosine oxidase
NBPF1	NBPF member 1
SIRT2	sirtuin 2
TOX3	TOX high mobility group box family member 3
MN1	MN1 proto-oncogene, transcriptional regulator
ALDH1A3	aldehyde dehydrogenase 1 family member A3
ZFYVE16	zinc finger FYVE-type containing 16
PKP1	plakophilin 1
CEP104	centrosomal protein 104
CRMP1	collapsin response mediator protein 1
JAKMIP2	janus kinase and microtubule interacting protein 2
NKAIN1	sodium/potassium transporting ATPase interacting 1
IFI16	interferon gamma inducible protein 16
PRKAR2B	protein kinase cAMP-dependent type II regulatory subunit beta
CNR1	cannabinoid receptor 1
MICAL1	microtubule associated monooxygenase, calponin and LIM domain containing 1
DISC1	DISC1 scaffold protein

TFAP2A	transcription factor AP-2 alpha
TFAP2B	transcription factor AP-2 beta
ATP8B4	ATPase phospholipid transporting 8B4
GCA	grancalcin
WSCD1	WSC domain containing 1
SRD5A1	steroid 5 alpha-reductase 1
AP1S2	adaptor related protein complex 1 subunit sigma 2
BCL11A	BAF chromatin remodeling complex subunit BCL11A
FOXF1	forkhead box F1
MCAM	melanoma cell adhesion molecule
ZNF804A	zinc finger protein 804A
SULF1	sulfatase 1
POU4F1	POU class 4 homeobox 1
ASS1	argininosuccinate synthase 1
BMP5	bone morphogenetic protein 5
MED13L	mediator complex subunit 13L
DHFR	dihydrofolate reductase
NELL1	neural EGFL like 1
SLCO3A1	solute carrier organic anion transporter family member 3A1
ACKR3	atypical chemokine receptor 3
FGFR2	fibroblast growth factor receptor 2

Table A2: List of the top 50 de-regulated genes upon ASS1 downregulation in RH4 cells. Probe Set ID: Affimetrix ClariomD microarray probe identity; logFC: logarithmic fold change of the gene expression.

Probe Set ID	logFC	PValue	Gene Symbol	Gene Title
TC0400007771.hg.1	-4.57	1.45E-09	HTN3	histatin 3
TC0400007770.hg.1	-2.91	2.92E-09	STATH	statherin
TC0X00008207.hg.1	-2.28	5.75E-10	AGTR2	angiotensin II receptor, type 2
TC0400008556.hg.1	-2.24	6.05E-03	MYOZ2	myozenin 2
TC0100015819.hg.1	-1.82	6.15E-03	S100A10	S100 calcium binding protein A10
TC0300011391.hg.1	-1.77	4.59E-05	ADAMTS9	ADAM metallopeptidase with thrombospondin type 1 motif 9
TC0500013298.hg.1	-1.71	2.97E-06	C1QTNF3	C1q and tumor necrosis factor related protein 3
TC0900011854.hg.1	-1.70	2.71E-06	TMEM8C	transmembrane protein 8C
TC0400010944.hg.1	-1.70	5.50E-06	CSN2	casein beta
TC0100018271.hg.1	-1.61	3.40E-07	OLFML3	olfactomedin like 3
TC0200015607.hg.1	-1.51	2.58E-04	MYL1	myosin light chain 1
TC0200010447.hg.1	-1.51	6.45E-07	CASP8	caspase 8, apoptosis-related cysteine peptidase
TC0900008953.hg.1	-1.48	1.55E-08	ASS1	argininosuccinate synthase 1
TC0800012319.hg.1	-1.44	2.78E-04	LINC01111	long intergenic non-protein coding RNA 1111
TC0100015826.hg.1	-1.43	4.88E-03	TCHH	trichohyalin
TC0100013534.hg.1	-1.39	4.58E-02	LAPTM5	lysosomal protein transmembrane 5
TC0500010835.hg.1	-1.37	3.73E-06	PLK2	polo-like kinase 2
TC0200015194.hg.1	-1.37	1.35E-06	TFPI	tissue factor pathway inhibitor (lipoprotein-associated coagulation inhibitor)
TC2000009813.hg.1	-1.36	1.89E-06	EEF1A2	eukaryotic translation elongation factor 1 alpha 2
TC1900009752.hg.1	-1.33	4.66E-04	PRDX2	peroxiredoxin 2
TC1000008955.hg.1	-1.31	4.04E-06	PLEKHS1	pleckstrin homology domain containing, family S member 1

TC0300011454.hg.1	-1.30	2.50E-03	LMOD3	leiomodin 3 (fetal)
TC0400008345.hg.1	-1.28	2.14E-05	SGMS2	sphingomyelin synthase 2
TC0300011849.hg.1	-1.28	5.97E-06	ABI3BP	ABI family, member 3 (NESH) binding protein
TC0500011418.hg.1	-1.27	3.55E-06	MEF2C	myocyte enhancer factor 2C
TC2200008036.hg.1	-1.24	1.33E-03	USP41	ubiquitin specific peptidase 41
TC0300007013.hg.1	-1.21	1.67E-06	ARPP21	Camp-regulated phosphoprotein 21kDa
TC1700009850.hg.1	-1.14	4.53E-05	PMP22	peripheral myelin protein 22
TC0400008813.hg.1	-1.14	1.52E-03	MGST2	microsomal glutathione S-transferase 2
TC1400010785.hg.1	-1.14	2.57E-04	LINC01550	long intergenic non-protein coding RNA 1550
TC1600006510.hg.1	-1.12	2.67E-05	LMF1-AS1	LMF1 antisense RNA 1
TC0100006864.hg.1	-1.12	7.51E-08	DRAXIN	dorsal inhibitory axon guidance protein
TC1000011904.hg.1	-1.10	1.03E-04	ABLIM1	actin binding LIM protein 1
TC1200006604.hg.1	-1.10	2.32E-03	CD9	CD9 molecule
TC1000012482.hg.1	-1.09	5.69E-07	ENTPD1	ectonucleoside triphosphate diphosphohydrolase 1
TC1500010160.hg.1	-1.09	6.43E-04	CTSH	cathepsin H
TC0700007034.hg.1	-1.08	1.17E-05	CREB5	Camp responsive element binding protein 5
TC0400007542.hg.1	-1.07	3.92E-05	KIT	v-kit Hardy-Zuckerman 4 feline sarcoma viral oncogene homolog
TC0700008657.hg.1	-1.07	2.09E-06	LRRC17	leucine rich repeat containing 17
TC1700006946.hg.1	-1.07	3.39E-05	HS3ST3B1	heparan sulfate (glucosamine) 3-O-sulfotransferase 3B1
TC1500007829.hg.1	-1.06	1.50E-04	LOXL1	lysyl oxidase-like 1
TC1100008886.hg.1	-1.05	4.15E-04	TMEM133	transmembrane protein 133
TC2100006854.hg.1	-1.05	2.83E-04	MAP3K7CL	MAP3K7 C-terminal like
TC0700010420.hg.1	-1.04	2.20E-06	ASS1P11	argininosuccinate synthetase 1 pseudogene 11
TC0500007384.hg.1	-1.04	7.91E-08	ASS1P9	argininosuccinate synthetase 1 pseudogene 9

TC0100016794.hg.1	-1.03	5.04E-06	B3GALT2	UDP-Gal:betaGlcNAc beta 1,3-galactosyltransferase 2
TC1700010015.hg.1	-1.03	2.56E-05	B9D1	B9 protein domain 1
TC1300009980.hg.1	-1.02	4.59E-04	LMO7	LIM domain 7
TC1700012359.hg.1	-1.01	2.45E-04	COX10-AS1	COX10 antisense RNA 1

ANNEX II

During the development of this doctoral thesis, the PhD candidate contributed to the elaboration of the scientific article detailed below:

Olga Almacellas-Rabaiget, Paola Monaco, Juan Huertas-Martinez, Silvia García-Monclús, Mariona Chicón-Bosch, Susana Maqueda-Marcos, Isabel Fabra-Heredia, David Herrero-Martín, Santiago Rello-Varona, Enrique de Alava, Roser López-Alemany, Paloma H. Giangrande, Oscar M. Tirado. LOXL2 promotes oncogenic progression in alveolar rhabdomyosarcoma independently of its catalytic activity. Cancer Letters, Volume 474, 2020, Pages 1-14, ISSN 0304-3835, https://doi.org/10.1016/j.canlet.2019.12.040.

Cancer Letters 474 (2020) 1–14

Contents lists available at ScienceDirect

Cancer Letters

journal homepage: www.elsevier.com/locate/canlet

Original Articles

LOXL2 promotes oncogenic progression in alveolar rhabdomyosarcoma independently of its catalytic activity

Olga Almacellas-Rabaiget[a], Paola Monaco[a], Juan Huertas-Martinez[a], Silvia García-Monclús[a], Mariona Chicón-Bosch[a], Susana Maqueda-Marcos[a], Isabel Fabra-Heredia[a], David Herrero-Martín[a,b], Santiago Rello-Varona[a,1], Enrique de Alava[b,c], Roser López-Alemany[a], Paloma H. Giangrande[d], Oscar M. Tirado[a,b,e,*]

[a] Sarcoma Research Group, Oncobell Program, Bellvitge Biomedical Research Institute (IDIBELL), L'Hospitalet de Llobregat, Barcelona, Spain
[b] CIBERONC, Carlos III Institute of Health (ISCIII), Madrid, Spain
[c] Laboratory of Molecular Pathology, Instituto de Biomedicina de Sevilla (IBiS), Hospital Universitario Virgen Del Rocío/CSIC/Universidad de Sevilla, Sevilla, Spain
[d] Department of Internal Medicine, Molecular and Cellular Biology Program, Abboud Cardiovascular Research Center, Holden Comprehensive Cancer Center, University of Iowa, Iowa City, IA, USA
[e] Institut Català D'Oncologia (ICO), L'Hospitalet de Llobregat, Barcelona, Spain

ARTICLE INFO

Keywords:
LOXL2
Alveolar rhabdomyosarcoma
Cell migration
Cell invasion
Metastasis
Vimentin

ABSTRACT

Rhabdomyosarcoma (RMS) is the most common soft tissue malignancy in childhood and adolescence. Patients with the most aggressive histological variant have an unfavorable prognosis due to a high metastasis incidence. Lysyl oxidase-like 2 (LOXL2) is a lysyl oxidase, member of a family of extracellular matrix (ECM) crosslinking enzymes that recently have emerged as important regulators of tumor progression and metastasis. We report that LOXL2 is overexpressed in RMS, suggesting a potential role for LOXL2 in RMS oncogenic progression. Consistently, transient and stable LOXL2 knockdown decreased cell migratory and invasive capabilities in two ARMS cell lines. Furthermore, introduction of LOXL2 in RMS non-expressing cells using wild type or mutated (catalytically inactive) constructs resulted in increased cell migration, cell invasion and number and incidence of spontaneous lung metastasis *in vivo*, independently of its catalytic activity. To further study the molecular mechanism associated with LOXL2 expression, a pull-down assay on LOXL2-transfected cells was performed and analyzed by mass spectrometry. The intermediated filament protein vimentin was validated as a LOXL2-interactor. Thus, our results suggest an oncogenic role of LOXL2 in RMS by regulating cytoskeleton dynamics and cell motility capabilities.

1. Introduction

Rhabdomyosarcoma (RMS) is a heterogeneous family of pediatric soft tissue tumors associated with the skeletal muscle lineage [1], accounting for approximately 40% of all soft tissue sarcomas in children and adolescents [2]. RMS comprises two main histological subtypes: alveolar (ARMS) and embryonal (ERMS) [3]. ERMS is the most common subtype, accounting for approximately 70–80% of RMS cases. Each subtype is associated with distinct genetic and molecular alterations [2,4]. Point mutations and loss of heterozygosity on the short arm of chromosome 11 (the 11p15.5 region) are commonly associated with ERMS [3,5]. In contrast, ARMS is linked with acquired specific chromosomal translocations t(2;13)(q35;q14) and t(1;13)(p36;q14), that result in the chimeric transcription factors PAX3-FOXO1 and PAX7-FOXO1, respectively [4,6]. ARMS shows a more aggressive behavior than ERMS and is associated with an unfavorable prognosis, which is partially attributable to its propensity for early dissemination, poor response to therapy and frequent relapses following therapy [7].

LOXL2 is a member of the lysyl oxidase family of proteins currently comprising five members: LOX and four LOX-like proteins, LOXL1–4 [8]. They are secreted copper-dependent amine oxidases, with a traditional role of catalyzing the covalent crosslinking of collagen and elastin in the extracellular matrix (ECM), through oxidative deamination of peptidyl lysine residues [8]. LOX proteins share a highly

* Corresponding author. Laboratori d'Oncologia Molecular, Institut d'Investigació Biomédica de Bellvitge (IDIBELL), Hospital Duran i Reynals, 3ª Planta, Gran Via 199, 08908, L'Hospitalet de Llobregat, Barcelona, Spain.
E-mail address: omartinez@idibell.cat (O.M. Tirado).
[1] Present address: Cell Biology Department, Universidad Complutense de Madrid - UCM, Calle José Antonio Novais 12, 28040 Madrid, Spain.

https://doi.org/10.1016/j.canlet.2019.12.040
Received 10 September 2019; Received in revised form 5 December 2019; Accepted 21 December 2019

Abbreviations

ARMS	alveolar rhabdomyosarcoma
Chro. Fr	chromatinic fraction
CM	conditioned media
Cyt. Fr	cytoplasmic fraction
ECM	extracellular matrix
EMT	epithelial-to-mesenchymal transition
ERMS	embryonal rhabdomyosarcoma
IF	immunofluorescence
LOX	lysyl oxidase
LOXL2	lysyl oxidase-like 2
MS	mass spectrometry
Nuc. Fr	nuclear fraction
RMS	rhabdomyosarcoma
TMA	tissue microarray
Wh. Lys	whole lysate
wt	wild type

conserved C-terminal amine oxidase catalytic domain. However, they differ at its N-terminus: LOX and LOXL1 have a pro-domain whereas LOXL2-4 have four scavenger receptor cysteine-rich (SRCR) domains [9]. LOX is catalytically activated in the ECM when bone morphogenetic protein-1 (BMP-1) cleaves the LOX pro-domain [10]. On the contrary, LOXL2 undergoes proteolytic processing of the first two SRCR domains at the N-terminus upon secretion. The processing site is unique to LOXL2 in the LOX-family of proteins. PACE4 is the major protease described that processes extracellular LOXL2. The processing of LOXL2 does not seem to be essential for its activity, suggesting a different mechanism for regulation of LOX and LOXL2 catalytic activity [11].

Apart from their role in ECM remodeling, several members of the family have recently appeared as important regulators of tumor progression [12,13]. In particular, a growing body of evidence has implicated LOXL2 in the promotion of cancer cell migration, cell invasion, metastasis and the malignant transformation of solid tumors; a correlation between high LOXL2 expression and poor prognosis in patients has been established [14,15]. However, LOXL2 has a complex role and more research is needed to better understand its mechanisms of action, which could be dependent or independent of its enzymatic activity, and at the same time, on its intra- or extracellular form [14,15].

Here, we show that LOXL2 is expressed in most RMS cells lines and through gain- and loss-of-function experiments we demonstrate that LOXL2, independently of its catalytic activity, is essential for the aggressive properties of ARMS. Additionally, our results strongly suggest that LOXL2 interacts with vimentin, increasing its proteolysis, which seems to be partially dependent on another novel LOXL2-interactor, calpain-2. Consequently, LOXL2 could be a regulator of cell motility, possibly due to remodeling of the cytoskeleton. Altogether, blocking LOXL2 expression or function may be of therapeutic use for the treatment of ARMS.

2. Materials and methods

2.1. Cell culture and transfection

RMS cell lines: RH4 and RH30 (gift from Dr. Peter Houghton), RH28, RMS13, RH36 and RUCH2 (gift from Dr. Beat Schäfer), CW9019 (gift from Dr. Frederic Barr), RH41, RD and A204 (bought from Leibniz Institute DSMZ, Braunschweig, Germany). Ewing Sarcoma (ES) cell lines: A673 (gift from Dr. Heinrich Kovar), RH1 (gift from Dr. Peter Houghton), RD-ES (bought from Leibniz Institute DSMZ) and A4573 (gift from Dr. Santiago Ramón y Cajal). Authenticity of the cell lines was routinely confirmed by STR profiling analysis done at qGenomics SL (Esplugues de Llobregat, Barcelona, Spain).

Cell lines were cultured in complete media: RPMI 1640-GlutaMAX (RPMI; Life Technologies, Carlsbad, CA, USA) supplemented with 10% heat-inactivated fetal bovine serum (FBS, Life Technologies) and 1% penicillin-streptomycin (Life Technologies). All cell lines were incubated at 37 ˚C in a humidified atmosphere of 5% CO_2 in air and checked regularly for mycoplasma infection. Exponentially growing cells were used for all experiments.

To analyze secretory proteins, cells were seeded and 24 h later complete media was replaced by RPMI for 48 h. Conditioned media (CM) was collected and concentrated 20-fold by filtration in Centricon 10 K (Amicon Ultra-15 centrifugal filters, Millipore, Burlington, MA, USA) at 4 ˚C.

For stable transfections, Lipofectamine 2000 (Life Technologies) was used following the manufacturer's protocol. RH4 and CW9019 cells stably expressing pRS-shLOXL2 vector (Origene, Rockville, MD, USA #TG311699) were selected with 0.6 μg/mL and 0.25 μg/mL of puromycin (Sigma-Aldrich, St. Louis, MO, USA), respectively. RH28 transfected cells stably expressing pCDNA3-LOXL2wt FLAG tagged vector or pCDNA3-LOXL2oxmut FLAG tagged vector (gifts from Dr. Sandra Peiró) were selected with 1.2 mg/mL of neomycin (Life Technologies). Antibiotic-resistant pools and individual clones were isolated for further analysis and maintained in the presence of antibiotics.

For transient gene silencing, cells were transfected with Dharmafect (GE Healthcare, Chicago, IL, USA) following the manufacturer's protocol and using 100 nM of customized siRNA for LOXL2 (siLOXL2 5′-AGUAAAGAAGCCUGCGUGGUC-3′) and for vimentin (siVIM#1 5′-ACGCCAUCAACACCGAGUUCA-3′ and siVIM#2 5′ACCUUGAACGC AAAGUGGAAUCUUU-3′). In addition, transient transfection for 48–72 h was performed in RH28 cells with pRP-CMV-LOXL2/mCherry vector (constructed at VectorBuilder, en.vectorbuilder.com), using Lipofectamine 2000.

2.2. Clinical material

For testing the expression of LOXL2 in a tissue micro-array (TMA), tumor samples were collected at the Hospital Universitario Virgen del Rocío, Seville, Spain. Written informed consent was obtained from each patient. Staining of LOXL2 in the TMA was scored by a blinded, trained pathologist on a positive-negative scale. LOXL2 staining in tumor xenografts was considered as a positive control. Immunofluorescence (IF) staining of TMA was performed at the Histology Service of the Centre de Medicina Regenerative de Barcelona (CMRB), Hospitalet de Llobregat, Spain, using LOXL2 antibody (LOXL2 1:100 #NBP1-32954 from Novus Biologicals, Centennial, CO, USA).

2.3. Cell treatments

For inhibiting N-glycosylation, cells were seeded, then incubated with tunicamycin (Sigma-Aldrich) 24 h later. Concentrations between 20 and 100 ng/mL and 50–500 ng/mL were used for 48 h in RH4 and CW9019 cell lines, respectively. In addition, tunicamycin was used to induce cell death at 250 ng/mL in RH4 cells for 48 h.

For inhibiting caspases and calpains proteases, the pan-caspase and calpain inhibitors Z-VAD-FMK (Z-VAD) and calpeptin, respectively, were used. Cells were seeded, then incubated with the corresponding drug 24 h later: Z-VAD (APExBIO, Boston, MA, USA) 10–50 μM for 48 h and calpeptin (Sigma-Aldrich) 25–50 μM for 48 h.

2.4. Immunofluorescence

Immunofluorescence (IF) of RMS cells was performed as previously described [16,17]. The primary antibodies used were: LOXL2 1:100

#NBP1-32954 (Novus Biologicals); vimentin 1:10 000 #V6630 and vinculin 1:10 000 #V9131 (Sigma-Aldrich). Photographs were taken with a confocal Leica TCS SP5 microscope (Leica Microsystems, Wetzlar, Germany) or Nikon Eclipse 80i (Nikon, Amstelveen, Netherlands). Images were analyzed with ImageJ software (U. S. National Institutes of Health) or Adobe Photoshop.

2.5. Fractionation of cellular extracts

Cells were lysed in buffer CE at pH 7.6 (10 mM HEPES, 60 mM KCl, 1 mM EDTA, 0.075% NP-40 and 1 mM DTT, supplemented with protease and phosphatase inhibitors [Complete, Mini Protease Inhibitor Cocktail Tablets; PhosStop, Phosphatase Inhibitor Cocktail Tablets, Roche, Basel, Switzerland]) for 5 min. All steps were performed at 4 °C. Samples were then centrifuged at 1,500 rpm for 5 min. Supernatant was collected (cytoplasmic fraction). Pellets were washed with CE buffer without NP-40 and centrifuged again at 1,500 rpm for 5 min. The soluble nucleus was then separated from the pellet by resuspending in NE buffer at pH 8 (10 mM HEPES, 420 mM NaCl, 1 mM $MgCl_2$, 0.2 mM EDTA and 1 mM DTT, supplemented with protease and phosphatase inhibitors). After using a vortex for 10 min, both the nuclear and the previous cytoplasmic fractions were centrifuged at 13 000 rpm for 10 min. The supernatants were the final nuclear (Nuc. Fr.) and cytoplasmic fractions (Cyt. Fr.). Finally, the pellets were resuspended in CHR buffer (2% SDS, 50 mM Tris pH 7.5, 10% glycerol and 1 mM DTT, supplemented with protease and phosphatase inhibitors). After sonication and centrifugation at 13 000 rpm for 10 min, the supernatant was the chromatinic fraction (Chro. Fr.). As a control of each fraction, the following antibodies were used: α-tubulin (Cyt. Fr.); calreticulin (endoplasmatic reticulum, to discard contamination of cytosolic organelles into the Nuc. Fr.); lamin A/C (Nuc. Fr.) and histone-3 (Chro. Fr.).

2.6. Site-directed mutagenesis

Mutagenesis was performed using QuikChange Site-Directed Mutagenesis Kit (Agilent Technologies, Santa Clara, CA, USA) following the manufacturer's protocol. pCDNA3-LOXL2wt FLAG tagged vector was used as a template. To prevent LOXL2 N-glycosylation, potential N-glycosylation Asn (N) residues were changed into Ala (Q): N288, N455 and N644. The forward primers used were: 5′-CACTGGACCCCATGAA GCAGGTCACCTGCGAGAATGG-3′ for N288, 5′-AGGTGCTGGTGGAGA GACAGGGGTCCCTTGTGTGGGG-3′ for N455 and 5′-CTATGACCTGCT GAACCTCCAGGGCACCAAGGTGGCAGAGG-3′ for N644. After mutagenesis, the full cDNA was sequenced to verify the mutations and to confirm the absence of other possible unspecific mutations in the coding sequence.

2.7. Immunoprecipitation

Immunoprecipitation was performed as previously described [16] using magnetic beads coated with Protein G (Millipore). The antibodies used were: vimentin 1:250 #V6630 (Sigma-Aldrich); calpain-1 1:100 #ab39170 and calpain-2 1:100 #ab39165 (Abcam, Cambridge, UK); normal mouse IgG #sc-2025 and normal rabbit IgG #sc-2027 (Santa Cruz Biotechnology, Heidelberg, Germany). Samples were analyzed by Western blot.

2.8. Pull-down

Cells expressing pCDNA3-LOXL2 FLAG tagged vector or an empty pCDNA3 FLAG tagged vector were harvested per standard protocol (from 150 mm culture dishes). Cell pellets were lysed with 500 μL lysis buffer (250 mM KCl, 1 mM EDTA, 1% Triton, 0.05% NP-40, 1 mM DTT, 10% glycerol, 50 mM Tris pH 7.8 supplemented with protease and phosphatase inhibitors) and incubated for 4 h on ice with the Benzonase nuclease (Sigma-Aldrich). Supernatants were collected after centrifugation at 13 000 rpm for 10 min. The purification of immunocomplexes was carried out using the anti-FLAG M2 affinity gel (Sigma-Aldrich). Prior to incubation, 40 μL per sample of anti-FLAG beads were washed thrice in BC100 buffer (100 mM KCl, 0.05 mM EDTA, 0.05% NP-40, 10% glycerol, 1 mM DTT and 10 mM Tris pH 7.8). Protein extracts were then incubated with anti-FLAG beads overnight at 4 °C with agitation. The following day, beads were washed thrice in BC100 buffer and thrice in BC500 buffer (500 mM NaCl, 0.05 mM EDTA, 0.05% NP-40, 10% glycerol, 1 mM DTT and 10 mM Tris pH 7.8). Finally, bound proteins were eluted based on competent binding with 40 μL 200 ng/mL FLAG peptide (Sigma-Aldrich). Eluates were mixed with loading buffer, denaturated 10 min at 100 °C and analyzed by Western blot.

2.9. Mass spectrometry

SDS-PAGE gel bands of interest were excised from gels and washed with 10 mM ammonium bicarbonate and 50% acetonitrile (Sigma-Aldrich). The gel bands were cut and digested with 10 ng/ul trypsin (Promega, Madison, WI, USA), in a buffer containing 50 mM ammonium bicarbonate, at 37 °C for 12–16 h. The digested peptides were recovered by extraction twice with 50 mM ammonium bicarbonate and 70% acetonitrile. The resulting peptides were separated by reverse phase liquid chromatography using a nano-capillary analytical C18 column, and then electrosprayed into an ion-trap mass spectrometer (Amazon ETD Ion Trap [Bruker Daltonics, Billerica, MA, USA] and LTQ Velos-Orbitrap [Thermo Fisher Scientific, Waltham, MA, USA]). Peptide masses were analyzed at full scan MS, and then at MS/MS fragmentation for the most intense peaks. Data were analyzed using the Mascot search engine (matrixscience.com) and the SwissProt (uniprot.com) human database.

2.10. LOXL2 enzymatic activity

LOXL2 enzymatic activity was measured by coupling horseradish peroxidase (HRP) activity to LOXL2 and using the conversion of Amplex Red to resorufin, as previously described [18]. After LOXL2 pull-down, beads were suspended in 50 μL reaction buffer: 50 μM sodium phosphate pH 7.4, 40 mM Amplex Red (Thermo Fisher), 2 U/ml horseradish peroxidase (Sigma-Aldrich) and 4 mM benzylamine (Sigma-Aldrich). Suspended beads were incubated at 37 °C for 4 h. Finally, samples were centrifuged to separate agarose beads from the reaction mix and absorbance was measured on the supernatant by spectrometry (λ = 560 nm).

2.11. Clonogenic assay

For clonogenic assays, 500 cells (for RH4 and CW9019) and 5 000 cells (for RH28) were seeded in 6-well plates. When colonies reached saturation, approximately 14 days after seeding, cells were fixed with cold methanol for 10 min, washed with Dulbecco's phosphate buffered saline (PBS; Biowest, Nuaillé, France), stained with 1% crystal violet (Sigma-Aldrich) for 20 min, and washed with water. Colonies were discolored with a 10% glacial acetic acid solution and crystal violet was quantified by spectrometry (λ = 570 nm).

2.12. Cell viability assay

For viability assays, 1 000 cells (for RH4 and CW9019) and 8 000 cells (for RH28) were seeded in 96-well plates. At 24, 48, 72, and 96 h after seeding, the culture medium was removed and 100 μL of a 1:10 dilution of water-soluble tetrazolium (WST-1, Roche) in the medium was added to each well. After 120 min, cell viability was quantified by spectrometry (λ = 440 nm).

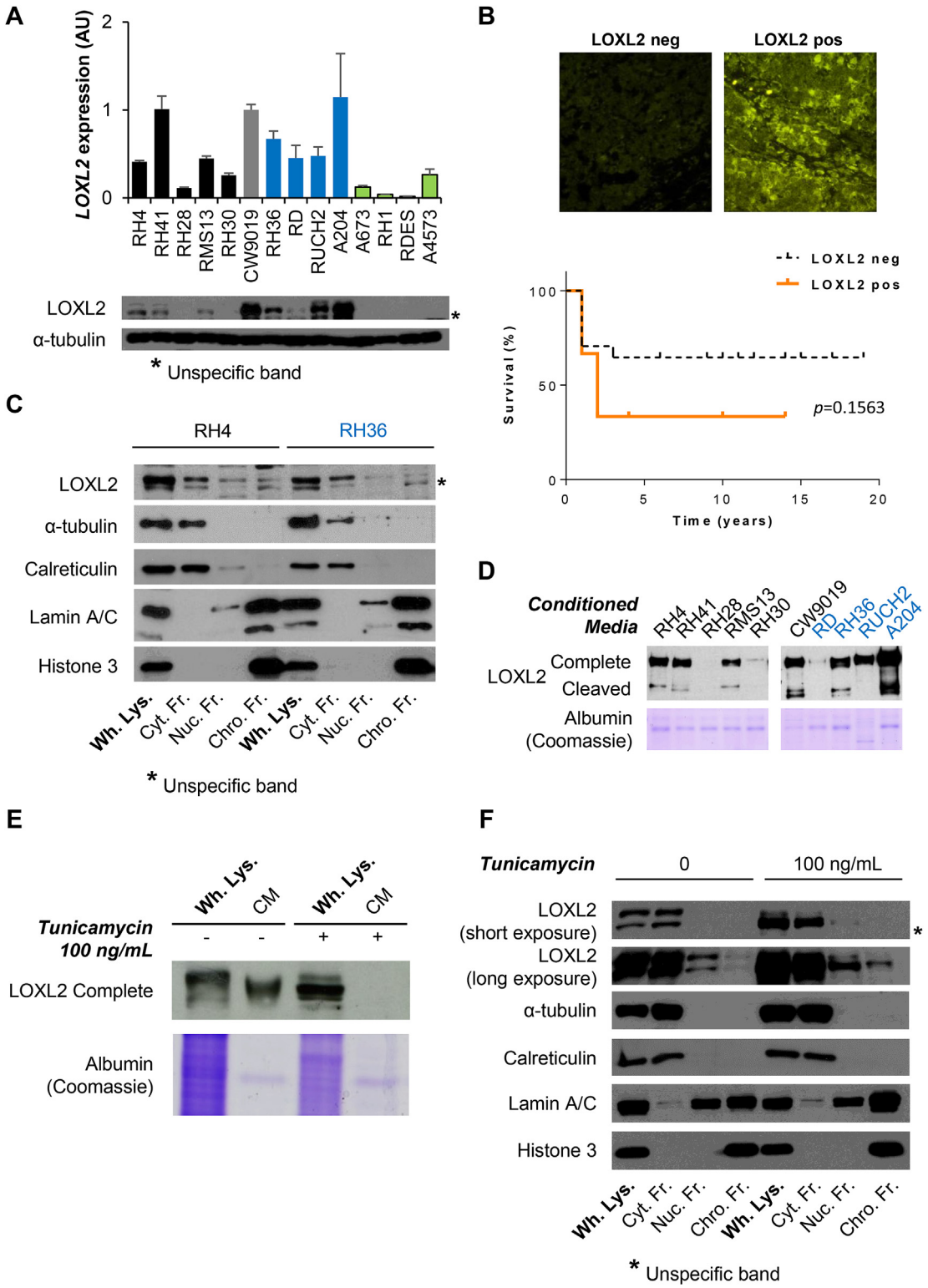

Fig. 1. LOXL2 is expressed in RMS thorough the cell, N-glycosylated and actively secreted. A) Upper: relative expression of *LOXL2* by RT-qPCR in a panel of RMS and ES cell lines. Black bars represent ARMS cells lines, gray bar represents CW9019 (as reference), blue bars represent ERMS, green bars represent ES. Below: representative Western blot indicating protein levels among the same cell lines. B) Upper: representative images of LOXL2 expression evaluated by immunofluorescence in tissue microarray samples (200X magnification). Lower: Kaplan-Meier curve showing differential survival trends among human RMS patients regarding LOXL2 expression (pos = positive; neg = negative). Statistical significance was assessed by Mantel-Cox test; $p = 0.1563$. C) Representative Western blot showing LOXL2 expression in different subcellular fractions in RH4 and RH36 cells. As a control of each fraction was used: α-tubulin (Cyt. Fr.); calreticulin (endoplasmic reticulum); lamin A/C (Nuc. Fr.) and histone-3 (Chro. Fr.). D) Representative Western blot showing LOXL2 expression in conditioned media (CM) in different RMS cell lines. Albumin band in Coomassie stained gels is shown as loading control. E) Representative Western blot showing LOXL2 in both whole lysates (Wh. Lys.) and CM of RH4 cells in control conditions or under treatment with glycosylation inhibitor tunicamycin. Albumin band in Coomassie stained gels is shown as loading control. F) Representative Western blot showing LOXL2 in control conditions or under treatment with tunicamycin in different subcellular fractions of RH4 cells. (For interpretation of the references to color in this figure legend, the reader is referred to the Web version of this article.)

2.13. Transwell migration assay

Cells were harvested per standard protocol. After an additional wash with RPMI, 1.5 × 10^5 cells in 150 μL serum-free medium was added to the top chamber of 8-μm pore polycarbonate transwells (Transwell Permeable Supports, Corning, Corning, NY, USA). Meanwhile, in the bottom chamber, 500 μL complete medium (10% FBS) was added and used as a chemoattractant. After 6 h for RH4 and CW9019, and 48 h for RH28, cells on the upper chamber were removed with a cotton swab. Migrating cells on the membrane underside were fixed for 30 min using 70% ethanol and stained with crystal violet. Transwell membranes were collected and 5 pictures of each transwell were acquired by optical microscopy (100 ×). The number of migrating cells was counted manually using ImageJ. Alternatively, cells were discolored with a 10% glacial acetic acid solution and crystal violet was quantified by spectrometry.

2.14. Matrigel invasion assay

This assay was performed similarly to the migration assay, but transwells were coated with 50 μL cold Matrigel (BD Biosciences, Franklin Lakes, NJ, USA) diluted 1:20 in RPMI and placed in a 37 °C incubator for 6 h. After Matrigel polymerization, cells were seeded, stained, and counted as in the migration assay. Invasion times were 24 h for RH4 and CW9019, and 72 h for RH28.

2.15. Western blot

Protein analysis by Western blot was performed as previously described [17,19]. Primary antibodies used were: LOXL2 1:1 000 #NBP1-32954 (Novus Biologicals); FLAG 1/1 000 #F1804 and vimentin 1:10 000 #V6630 (Sigma-Aldrich); calpain-1 #ab39170, calpain-2 1/1 000 #ab39165, calreticulin 1/1 000 #ab2907 and histone-3 1/10 000 #ab24834 (Abcam); mCherry 1/1 000 #PA5-34974 (Thermo Fisher); and lamin A/C 1/200 #NCL-LAM-A/C (Leica Biosystems). Secondary antibodies used were horseradish peroxidase-conjugated goat anti-rabbit and goat anti-mouse (Life Technologies). Peroxidase activity was detected by enhanced chemiluminescence (Pierce, Thermo Scientific) following the manufacturer's instructions. Immunodetection of α-tubulin (#ab28439) or β-actin (#ab49900) from Abcam was used as loading control.

2.16. RNA extraction, reverse transcription and quantitative real time PCR

Total RNA (2 μg) extracted by using the NucleoSpin RNA kit (Macherey-Nagel, Düren, Germany) was used for cDNA synthesis with SuperScript II Reverse Transcriptase (Life Technologies). Quantitative reverse transcription-PCR (qRT-PCR) was performed under universal cycling conditions on LightCycler 480 II instrument (Roche) using TaqMan PCR Mastermix and TaqMan probes (Life Technologies, *VIM* Hs00958111_m1, *ACTB* 4333762F, *LOX* Hs00942483_m1, *LOXL1* Hs00935937_m1, *LOXL2* Hs00158757_m1, *LOXL3* Hs00261671_m1, *LOXL4* Hs00260059_m1). Cycle threshold (CT) values were normalized to that of β-actin. Relative expression level of the target gene among the different samples was calculated using the ΔΔCT method [20].

2.17. Orthotopic xenograft metastasis assay

This assay was performed as previously described [17]. Briefly, 2 × 10^6 cells resuspended in 100 μL PBS were injected into the gastrocnemius muscles of 6-week-old female athymic nude mice (Hsd:Athymic Nude*Foxn1*^{nu}; Harlan, Indianapolis, IN, USA). Once primary tumor-bearing limbs reached a volume of 800 mm^3, the gastrocnemius muscles were surgically resected. Tumors were fixed in 4% paraformaldehyde and embedded in paraffin. Tumor sections were stained with hematoxylin and eosin or anti-LOXL2 IF was performed. At day 90 after injection, mice were euthanized and lungs were extracted, fixed in 4% paraformaldehyde and embedded in paraffin. Lung sections were stained with hematoxylin and eosin and metastases were counted under an optical microscope. In addition, anti-LOXL2 IF was performed in lung sections (n = 9 for each condition). Animals were cared for according to the Institutional Guidelines for the Care and Use of Laboratory Animals. Ethics approval was provided by a locally appointed ethics committee from IDIBELL, Barcelona, Spain. IDIBELL animal facility abides by the Association for Assessment and Accreditation of Laboratory Animal Care (AAALAC) regulations.

2.18. Proximity ligation assay

This assay was performed using the Duolink In situ Red Starter Kit mouse/rabbit (Merck), following the manufacturer instructions. The primary antibodies used were: LOXL2 1:100 #NBP1-32954 (Novus Biologicals) and vimentin 1:5 000 #V6630 (Sigma-Aldrich). Photographs were taken with a confocal Leica TCS SP5 microscope (Leica Microsystems, Wetzlar, Germany). Images were analyzed with ImageJ software (U. S. National Institutes of Health) or Adobe Photoshop.

2.19. Statistical analysis

Unless otherwise stated, data were analyzed for statistical significance using Student's *t*-test. Fisher's exact test was used for evaluating differences in lung metastasis incidence in mice. Data represented in Kaplan-Meier plots was analyzed with Mantel-Cox test. Experiments were performed thrice; $p \leq 0.05$ was regarded as significant.

3. Results

3.1. LOXL2 is highly expressed, N-glycosylated and secreted in RMS cell lines

LOXL2 has been linked to tumor progression and metastasis in multiple cancer models [14]. To investigate its role in RMS, we first confirmed high and variable LOXL2 expression levels in RMS cell lines compared to other sarcoma cells, at RNA and protein levels (Fig. 1A). We further analyzed LOXL2 expression by IF on a tissue microarray (TMA) containing a panel of 34 RMS patients. Thirty-five percent of samples were positive for LOXL2 (Supplementary Table S1), with a cytoplasmic expression pattern (Fig. 1B upper). Survival information was available for 25 patient samples. Interestingly, in Kaplan-Meier representation those patients with positive LOXL2 expression showed a tendency to worse survival (Fig. 1B lower). However, lack of clinical information did not allow us to establish a statistically significant correlation (Mantel-Cox test, $p = 0.1563$).

LOXL2 belongs to the LOX family, proteins that possess a highly conserved catalytic domain [8]. mRNA expression of LOX members was analyzed by RT-qPCR in RMS cells and one ES cell line (Fig. S1). All other LOX members showed a lower expression than LOXL2, except LOX in two cell lines (CW9019 and A204) and LOXL1, which had higher mRNA levels, even in cells without LOXL2 expression. Accordingly, their mRNA expression was analyzed in RH4 LOXL2 stable silenced model (Fig. S2) and RH28 LOXL2 knock-in model (Fig. S3). No changes in the mRNA of any LOX member were found, confirming an absence of compensatory effect.

We also characterized a cytoplasmic and nuclear LOXL2 localization in several RMS cell lines. The localization was confirmed by subcellular fractionation, indicating that LOXL2 in the nuclei was also associated with the chromatinic fraction (Fig. 1C). Regarding post-translational modification, complete and cleaved LOXL2 forms were detected in the conditioned media (CM) of nearly all RMS cells tested, demonstrating LOXL2 secretion and cleavage (Fig. 1D). Furthermore, treatment with the N-glycosylation inhibitor tunicamycin in RH4 cells suppressed

LOXL2 secretion, confirming that N-glycosylation is essential for LOXL2 secretion (Fig. 1E). Finally, as shown by a light reduction of LOXL2 molecular weight after tunicamycin treatment, this modification was present in all subcellular fractions of RH4 cells (Fig. 1F).

3.2. LOXL2 silencing reduces the clonogenic, viability, migratory and invasive capabilities of ARMS cells

To decipher the involvement of LOXL2 in the progression of ARMS, the most aggressive histological subtype of RMS, we established two silenced models of LOXL2 using RH4 and CW9019 cells by stable transfection with a shRNA against LOXL2 or a shRNA control. Several LOXL2 knockdown clones were selected (RLsh# and CWLsh#) and compared to control transfected cells (SCR; Fig. 2A). LOXL2 knockdown significantly reduced clonogenic capacity in both cell lines (Fig. 2B). Cell viability, as measured by WST1 tetrazolium-based assay, was significantly reduced only in RH4 cells (Fig. 2C). Furthermore, the migratory and invasive capacity of ARMS cells was significantly reduced after stable LOXL2 silencing (Fig. 2D–E). To confirm these results, transient transfection was performed in the same cell lines using a siRNA against LOXL2 or a control siRNA, siNT (Fig. S4A). Transient LOXL2 knockdown in both cell lines significantly reduced both cell viability and migration (Fig. S4B-C). Moreover, vinculin immunolabeling revealed a reduction in focal adhesions after transient LOXL2 silencing (Fig. 2F), concordantly with reduced cell motility.

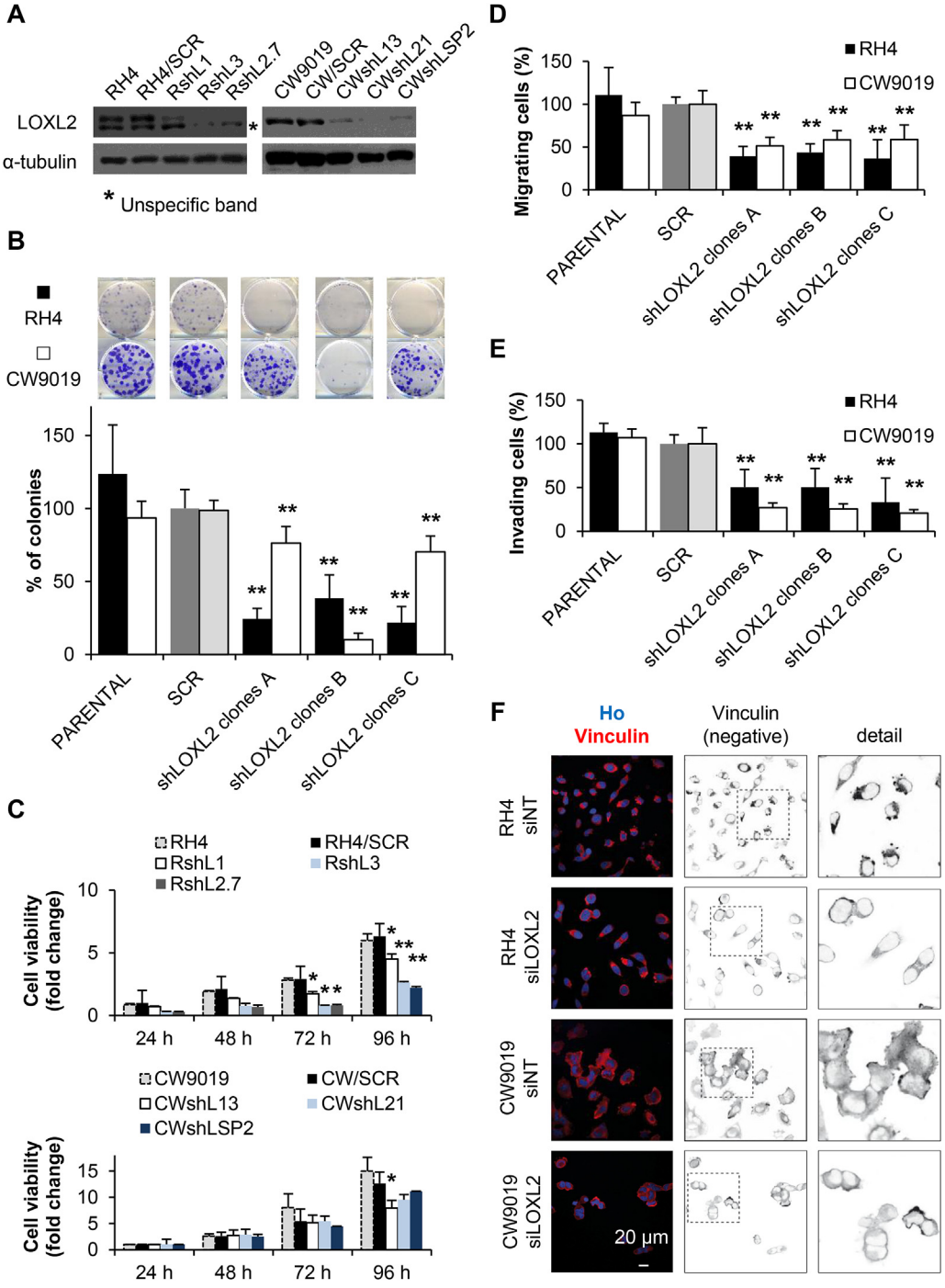

Fig. 2. LOXL2 promotes an oncogenic phenotype in ARMS cells. A) Representative Western blot showing LOXL2 expression in knock-down models generated from RH4 and CW9019 cell lines. SCR = control scrambled sequence; RLsh# and CWLsh# = LOXL2 silenced selected clones. B) Representative images and quantification of clonogenic assays from RH4 and CW9019 models of LOXL2 stable silencing. C) WST-1 tetrazolium-based viability assay in RH4 (above) and CW9019 (below) models of LOXL2 stable silencing. D) Migration assay in Boyden chambers using LOXL2 silenced models. E) Invasion assay in Matrigel-coated Boyden chambers using LOXL2 silenced models. In B, D and E, clones "A", "B" and "C" denote clones RshL1 & CWshL13, RshL3 & CWshL21 and RshL2.7 & CWshLSP2, respectively. In B, C, D and E, SCR models were set as reference (100%). F) Representative images obtained by immunofluorescence showing vinculin intracellular distribution in RH4 and CW9019 cells after transfection for 48 h with non-targeting (siNT) and LOXL2 siRNA (siLOXL2). Nuclei were counterstained with Hoechst 33342 (Ho). "Negative" states the inverted uncolored version of the image. Data are presented as mean ± SD from at least three different experiments. Statistical significance was achieved by Student's *t*-test, $*p \leq 0.05$, $**p \leq 0.01$.

3.3. LOXL2 reintroduction in RMS non-expressing cells increases their oncogenic phenotype in vitro and the formation of spontaneous metastasis in vivo, independently of its catalytic activity

To further demonstrate the role of LOXL2 during the progression of ARMS, we stably transfected RH28, the only ARMS cell line with undetectable LOXL2 levels, with wild type (wt) LOXL2 FLAG tagged construct (RLwt). In addition, cells were transfected with a LOXL2/FLAG catalytically inactive construct (RLoxmut; Fig. 3A) to clarify the implication of LOXL2 enzymatic activity on its function. Individual clones expressing LOXL2 wild type or LOXL2 oxidative mutant (Fig. 3B) were functionally characterized. First, LOXL2 enzymatic activity was determined in pulled-down LOXL2 proteins by coupled fluorimetric assays for H_2O_2 production, confirming the absence of lysyl oxidase activity in the mutants (Fig. S5A-B). Next, LOXL2 cytoplasmic, nuclear and chromatinic localization was determined by subcellular fractionation (Fig. 3C), as well as LOXL2 secretion and processing by Western blot of CM (Fig. 3D). When analyzing the phenotype, all transfected cells, independently of LOXL2 catalytic activity, gained significant viability and clonogenic abilities (Fig. 3E–F).

Moreover, LOXL2 reintroduction resulted in a significant increase of the migratory and invasive capacity of RH28 cells *in vitro* (Fig. 4A–B). Additionally, we performed an orthotopic spontaneous metastasis assay, previously described by our group [17]. A significant increase in

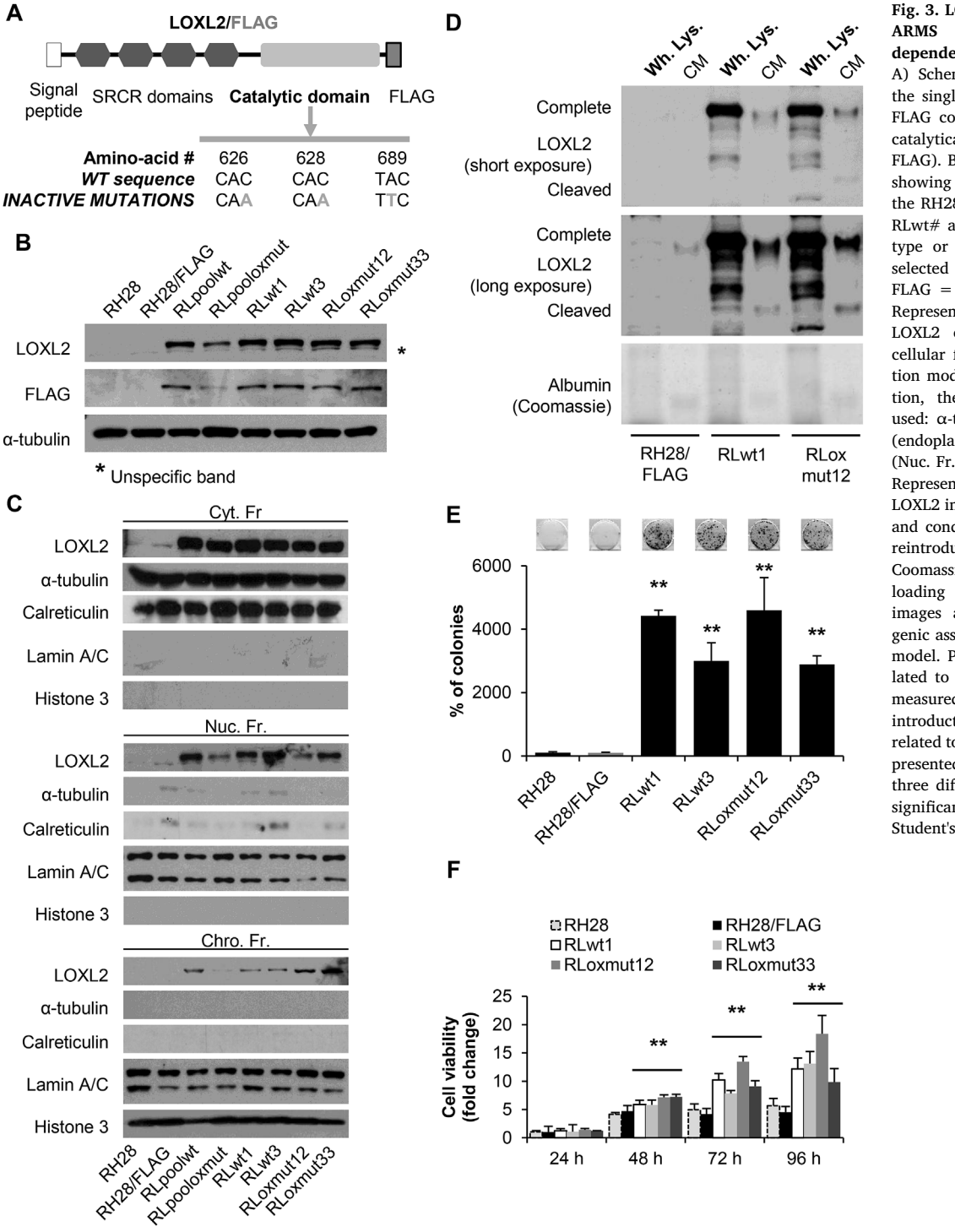

Fig. 3. LOXL2 function in supporting ARMS tumor phenotype is independent of its enzymatic activity. A) Schematic representation showing the single point mutations in LOXL2/FLAG construct to render the protein catalytically inactive (LOXL2oxmut/FLAG). B) Representative Western blot showing LOXL2/FLAG expression in the RH28 reintroduction stable model. RLwt# and RLoxmut# = LOXL2 wild type or catalytically inactive mutant selected clones, respectively; RH28/FLAG = CMV/FLAG empty vector. C) Representative Western blot showing LOXL2 expression in different subcellular fractions in RH28 reintroduction model. As a control of each fraction, the following antibodies were used: α-tubulin (Cyt. Fr.); calreticulin (endoplasmic reticulum); lamin A/C (Nuc. Fr.) and histone-3 (Chro. Fr.). D) Representative Western blot showing LOXL2 in both whole lysates (Wh. Lys.) and conditioned media (CM) in RH28 reintroduction model. Albumin band in Coomassie stained gels is shown as a loading control. E) Representative images and quantification of clonogenic assays from RH28 reintroduction model. Percentage of colonies was related to RH28/FLAG. F) Cell viability measured by WST-1 in RH28 reintroduction model. Fold change was related to RH28/FLAG at 24 h. Data are presented as mean ± SD from at least three different experiments. Statistical significance was achieved by the Student's *t*-test, $^{**}p \leq 0.01$.

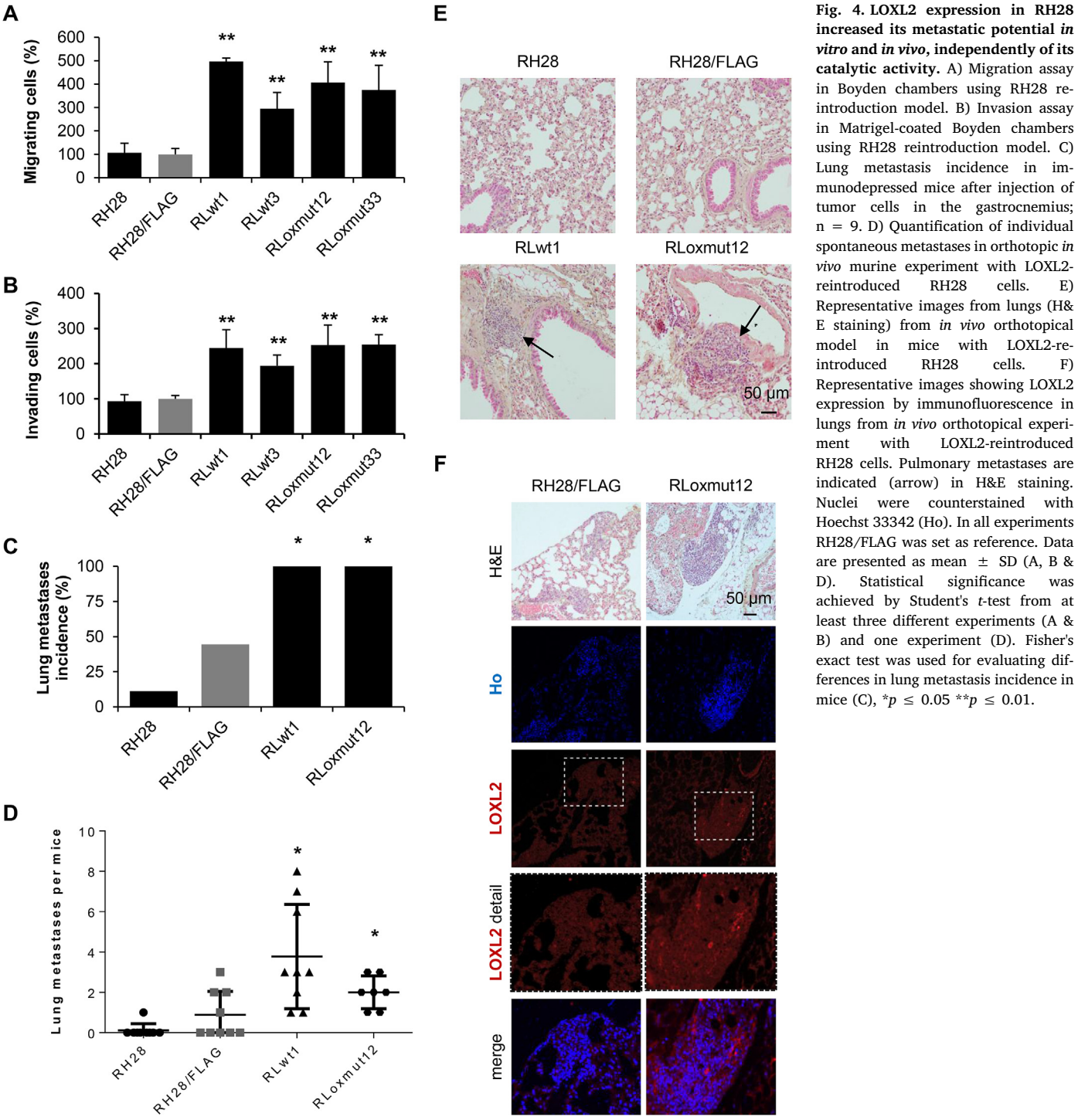

Fig. 4. LOXL2 expression in RH28 increased its metastatic potential *in vitro* and *in vivo*, independently of its catalytic activity. A) Migration assay in Boyden chambers using RH28 re-introduction model. B) Invasion assay in Matrigel-coated Boyden chambers using RH28 reintroduction model. C) Lung metastasis incidence in immunodepressed mice after injection of tumor cells in the gastrocnemius; n = 9. D) Quantification of individual spontaneous metastases in orthotopic *in vivo* murine experiment with LOXL2-reintroduced RH28 cells. E) Representative images from lungs (H&E staining) from *in vivo* orthotopical model in mice with LOXL2-reintroduced RH28 cells. F) Representative images showing LOXL2 expression by immunofluorescence in lungs from *in vivo* orthotopical experiment with LOXL2-reintroduced RH28 cells. Pulmonary metastases are indicated (arrow) in H&E staining. Nuclei were counterstained with Hoechst 33342 (Ho). In all experiments RH28/FLAG was set as reference. Data are presented as mean ± SD (A, B & D). Statistical significance was achieved by Student's *t*-test from at least three different experiments (A & B) and one experiment (D). Fisher's exact test was used for evaluating differences in lung metastasis incidence in mice (C), $*p \leq 0.05$ $**p \leq 0.01$.

the incidence of lung metastasis (Fig. 4C and E) and in the number of metastases per mice was observed (Fig. 4D) when LOXL2-expressing cells were injected. Interestingly, LOXL2 presented a cytoplasmic expression pattern in xenograft tumors (Fig. S6A) and in metastatic lung cells (Fig. 4F). In contrast, non-significant differences were observed regarding tumor growth (Fig. S6B). Altogether, these results strongly suggest that aggressive progression of ARMS cells strongly relies on LOXL2, independently of its catalytic activity.

3.4. A LOXL2 non-secretable mutant increases cell migration and invasion but not its proliferative and clonogenic capabilities

To elucidate LOXL2 intracellular functions, we obtained a LOXL2 non-secretable mutant. As previously shown (Fig. 1E), N-glycosylation is essential for LOXL2 secretion. Three N-glycosylation sites have been predicted for LOXL2, two of which have been confirmed by mass spectrometry (MS) [21]. Taking these into consideration, LOXL2 secretion was avoided by site-directed mutagenesis in its N-glycosylation sites: a double mutant (Lsecmut2x) in the two confirmed N-glycosylation sites and a triple mutant (Lsecmut3x) in all three potential sites were produced. These constructs (Fig. 5A) were stably transfected in

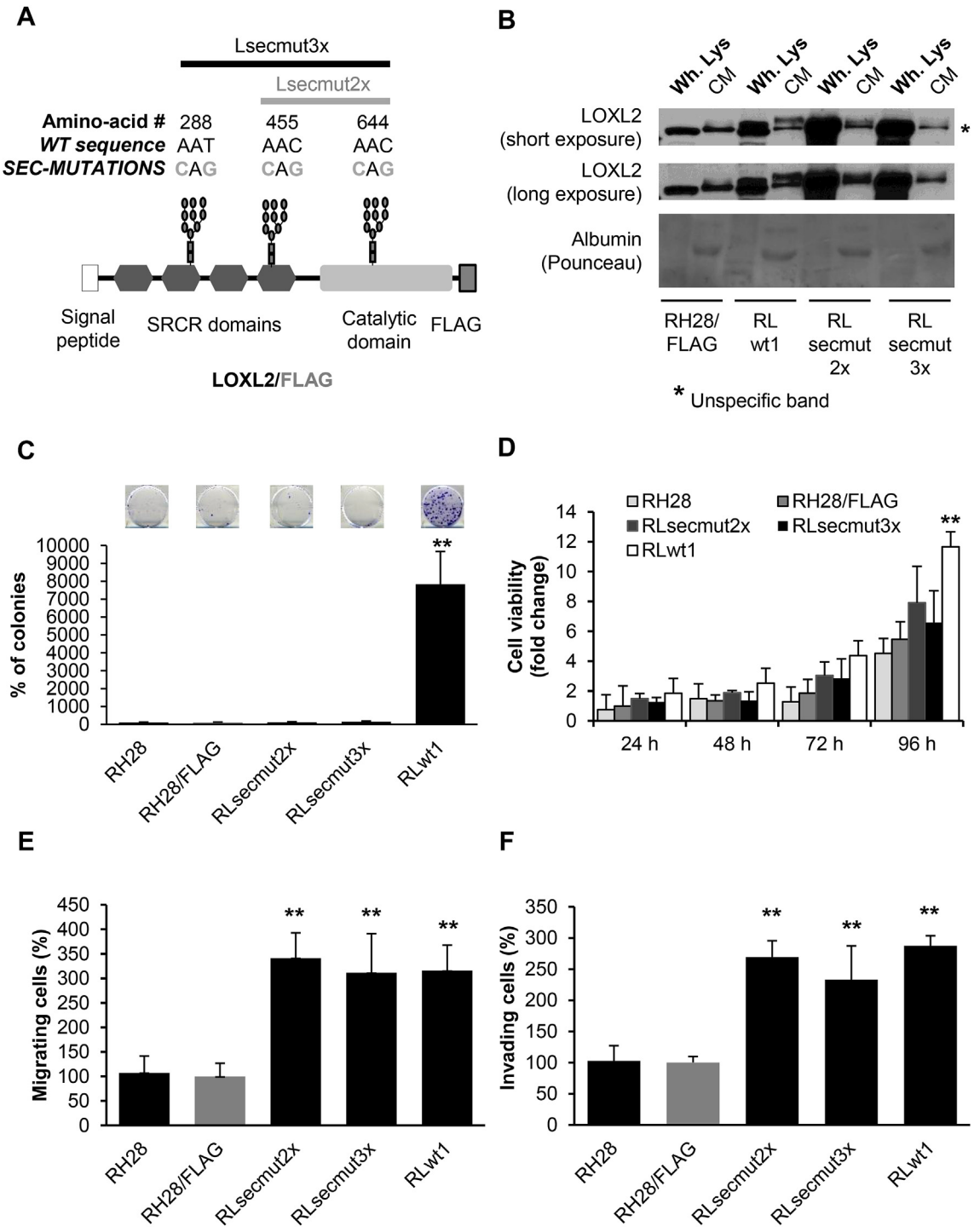

Fig. 5. Non-N-glycosylated and non-secreted LOXL2 is sufficient to increase cell migration and invasion. A) Schematic representation showing the single point mutations in LOXL2/FLAG construct to generate non-secreteable mutants. Secretion was avoided by ablation of the N-glycosylation sites. A double mutant (RLsecmut2x) with N455/644Q and a triple mutant (RLsecmut2x) with N288/455/644Q mutations were obtained. B) Representative Western blot showing LOXL2 in both whole lysates (Wh. Lys.) and conditioned media (CM) in RH28 non-secreted LOXL2 model. Albumin band in Ponceau stained membrane is shown as loading control. C) Representative images and quantification of clonogenic assays from RH28 non-secreted LOXL2 model. D) Viability assay using WST-1 in RH28 non-secreted LOXL2 model. E) Migration assay in Boyden chambers using RH28 non-secreted LOXL2 model. F) Invasion assay in Matrigel-coated Boyden chambers using RH28 non-secreted LOXL2 model. In all experiments RH28/FLAG was set as reference. Data are presented as mean ± SD from at least three different experiments. Statistical significance was achieved by the Student's *t*-test, $^{**}p \leq 0.01$.

RH28 cells and blockage of LOXL2 secretion was partially reached in RLsecmut2x and almost completely achieved in RLsecmut3x pools of cells (Fig. 5B). In contrast to LOXL2 wild type, non-secretable LOXL2 mutant cells were not able to increase clonogenic and proliferative cell rates (Fig. 5C–D). More remarkably, these cells increased cell migratory and invasive capabilities at the same levels as LOXL2 wild type (Fig. 5E–F). These results strongly suggest that intracellular LOXL2 is sufficient to increase cell migration and invasion, processes that are also independent of N-glycosylated protein.

To additionally confirm LOXL2 function, LOXL2 was transiently

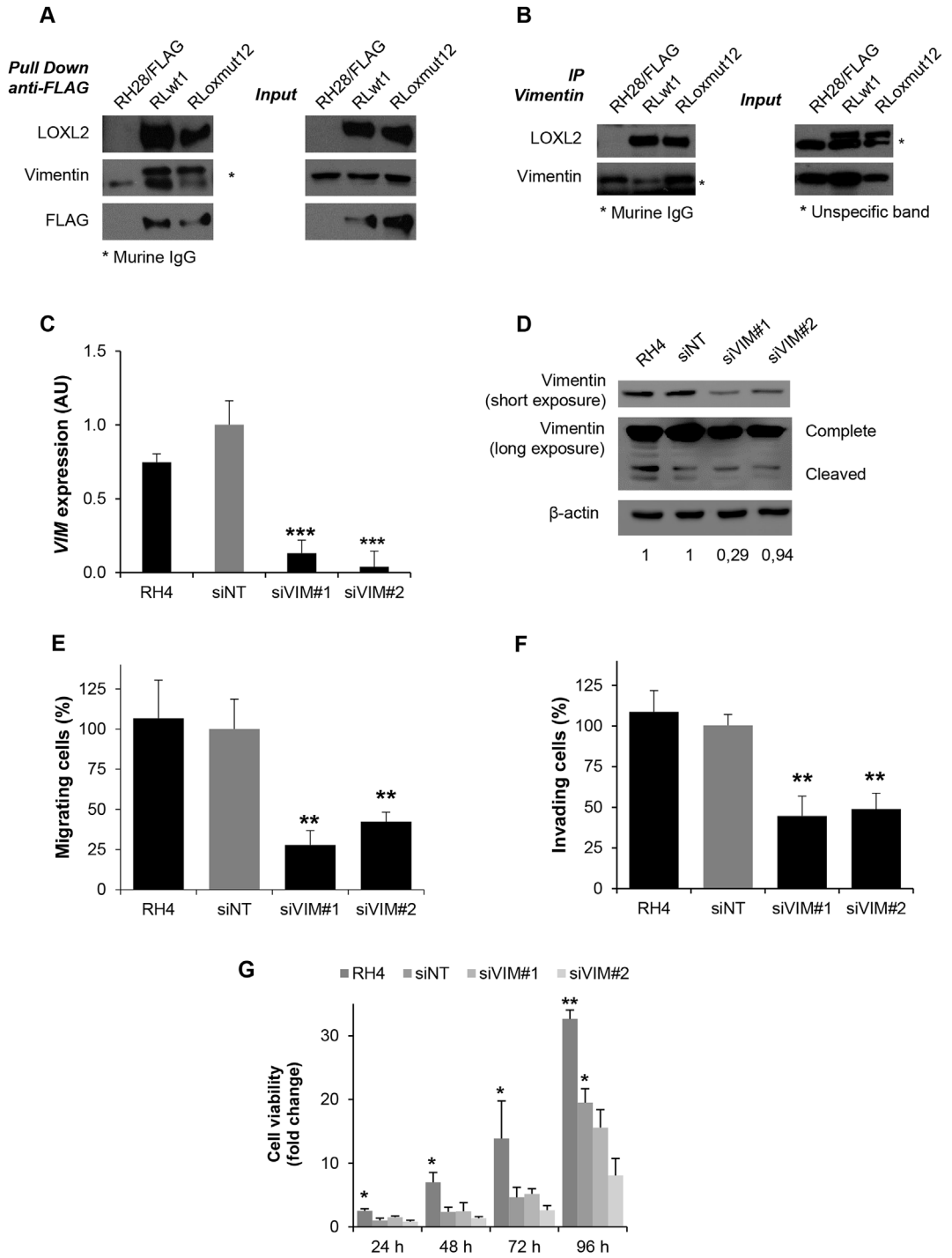

Fig. 6. Vimentin is a novel LOXL2 partner involved in sustaining the RMS cell motility. A) Representative Western blot showing validation of LOXL2-vimentin interaction after pulling down with anti-FLAG M2 affinity gel in two representative clones: RH28-LOXL2/FLAG wt (RLwt1) and oxidation mutant (RLoxmut12). RH28/FLAG cells were used as negative control. Detection of the corresponding LOXL2/FLAG and vimentin proteins in the input fractions is shown in the right panel. B) Representative Western blot showing LOXL2 in immunoprecipitated samples using vimentin antibody in samples from LOXL2-reintroduction RH28 model. Detection of the corresponding vimentin and LOXL2 proteins in the input fractions is shown in the right panel. C) Graphs representing relative mRNA expression levels of vimentin measured by RT-qPCR in RH4 cells transfected with non-targeting (siNT) and vimentin siRNAs (siVIM#1 and siVIM#2). D) Representative Western blot showing vimentin expression in RH4 cells transfected with siNT and vimentin siRNAs. Completed and cleaved vimentin forms are shown. Quantification of vimentin *vs* β-actin expression is indicated. E) Migration assay in Boyden chambers in RH4 cells transfected with siNT and vimentin siRNAs. F) Invasion assay in Matrigel-coated Boyden chambers in RH4 transfected with siNT and vimentin siRNAs. G) WST-1 viability assay in RH4 cells transfected with siNT and vimentin siRNAs. In E, F and G, siNT was set as reference. Data are presented as mean ± SD from at least three different experiments. Statistical significance was achieved by the Student's *t*-test, $*p \leq 0.05$, $**p \leq 0.01$, $***p \leq 0.001$.

silenced in the different RH28 knock-in models (LOXL2 wt, oxmut and secmut3x; Fig. S7A). After siRNA transfection against LOXL2, the increased neoplastic phenotype showed partially reduced clonogenic and viability capabilities (Fig. S7B-C) and was completely abrogated at the control cell level (RH28/FLAG) in cell migration and invasion (Fig. S7D-E).

3.5. Vimentin and calpain-2 are novel LOXL2 interactors: LOXL2 expression increases vimentin cleavage partially due to calpain proteases

To gain insight into the molecular mechanism of LOXL2-mediated oncogenic progression, we attempted to identify LOXL2 potential interactors. Whole cell extracts from RH28 cells overexpressing LOXL2 FLAG-tagged wt (RLwt1) or oxmut (RLoxmut12) were immunoprecipitated with anti-FLAG M2 affinity gel (Fig. 6A) and proteins were identified by mass spectrometry (Supplementary Table S2). Among the proteins found in common between both clones, LOXL2 had the highest coverage. The specific interaction between LOXL2 and the cytoskeleton protein vimentin was validated by pull-down anti-FLAG (Fig. 6A) and immunoprecipitation of vimentin (Fig. 6B). Vimentin is the major intermediate filament protein in mesenchymal cells, considered an epithelial-mesenchymal transition marker. Apart from its role in maintaining cellular integrity and providing resistance against stress, it is also involved in tumor progression [22]. First, we confirmed a high vimentin expression in all RMS cells (Fig. S8A). LOXL2-vimentin interaction was further confirmed by coimmunofluorescence in cells transiently transfected with fluorescent LOXL2 (LOXL2mCherry; Fig. S8B) and by vimentin immunoprecipitation in RH4 cells (Fig. S8C). Furthermore, LOXL-2-vimentin interaction was also confirmed using a Proximity Ligation Assay in RH4 and RH28 cells and stably transfected RH28/FLAG and RLwt1 clones (Fig. S8D). To elucidate the role of vimentin in ARMS, we transiently knocked it down in RH4 cells using two different siRNAs (Fig. 6C–D). Transient silencing of vimentin resulted in a significant decrease in cell migration and invasion (Fig. 6E–F). However, in cell viability assays, a significant reduction was only obtained with one of the two siRNAs used (Fig. 6G). In addition, transient knockdown of vimentin with two specific siRNAs in the RH28 model (Fig. S9) resulted in a significant reduction of cell migration in LOXL2-expressing cells (Fig. S9C).

We observed increased cleavage of vimentin in RH28 LOXL2-transfected cells (Fig. 7A). Vimentin cleavage results in the disassembly of intermediate filaments and could be due to the presence of caspases or calpains [23]. To elucidate which proteases were implicated, RH28 control or LOXL2 wild type transfected cells (RLwt1) were treated with a caspase or calpain inhibitor, Z-VAD and calpeptin, respectively. The results suggested that caspases are not implicated in increased vimentin cleavage (Fig. S10A); instead, calpeptin partially reduced vimentin cleavage (Fig. 7B). The inhibitory effect of both drugs was corroborated (Fig. S10B-C). The typical ubiquitously expressed calpains are calpain-1 and calpain-2 [24]. By pull-down anti-FLAG and immunoprecipitation, we observed an interaction between LOXL2 and calpain-2 (Fig. 7C–D), but not with calpain-1 (Fig. S10D-E). Altogether, our results indicate that LOXL2 expression increases vimentin cleavage, which is at least partially dependent on calpains.

4. Discussion

The present study demonstrates for the first time the role of LOXL2 in ARMS progression and metastasis, highlighting the fact that lysyl oxidase enzymatic activity is not necessary in these processes. Our findings also indicate that intracellular LOXL2 presence is enough to increase cell migration and invasion. Proteomic analysis of LOXL2 partners revealed a specific and novel interaction between LOXL2 and the cytoskeleton intermediate filament protein vimentin. LOXL2 expression increased vimentin proteolysis, which was partially calpain-dependent. Among the two main ubiquitous calpains, we confirmed the

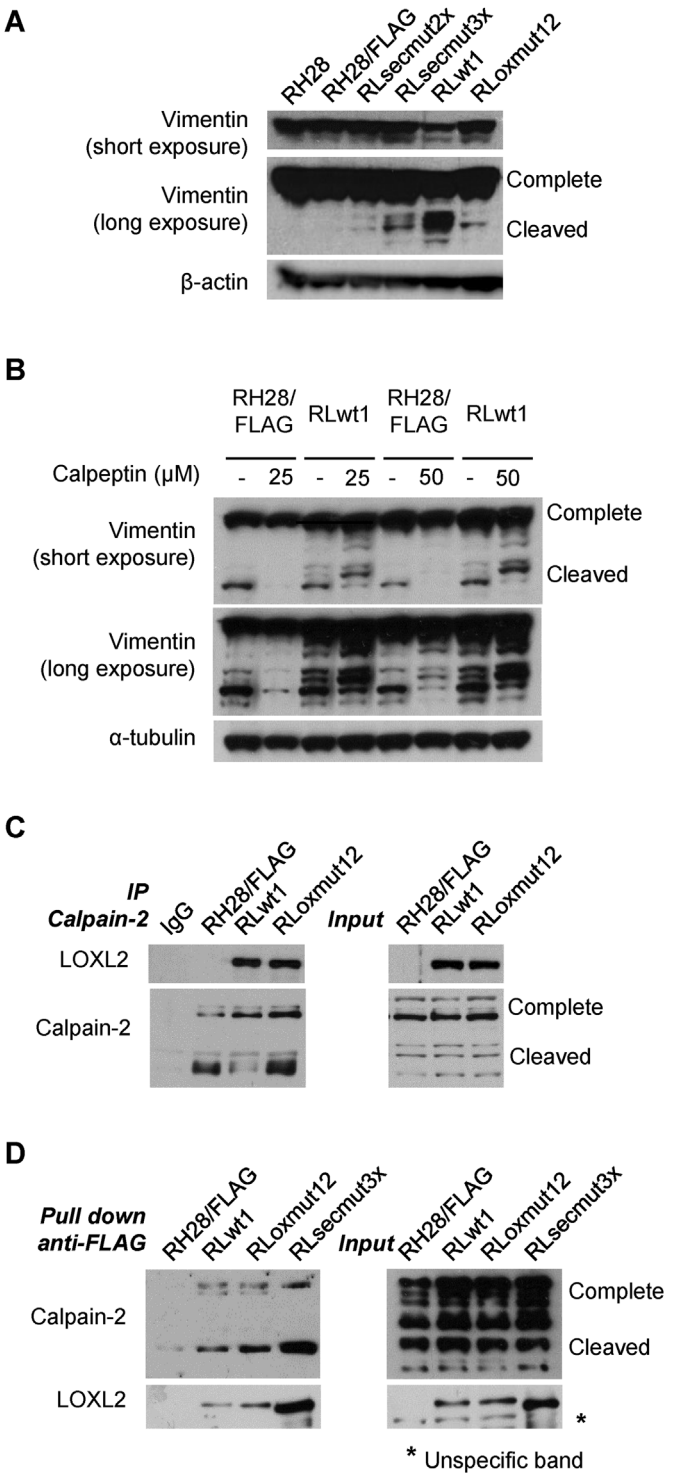

Fig. 7. Calpains are partially responsible for increased cleavage of vimentin in the presence of LOXL2, which interacts with calpain-2. A) Representative Western blot showing vimentin cleavage in different RH28 LOXL2 wild type or mutant models. B) Representative Western blot showing vimentin cleavage in RH28 LOXL2 wild type cells after treatment with calpain inhibitor calpeptin. DMSO (vehicle) is indicated as (−). C) Representative Western blot showing LOXL2 in immunoprecipitated samples using calpain-2 antibody and IgG anti-rabbit in samples from LOXL2-reintroduction RH28 model. Detection of the corresponding LOXL2 and calpain-2 proteins in the input fractions is shown in the right panel. D) Representative Western blot showing calpain-2, complete and cleaved forms, in LOXL2-reintroduced RH28 cells after anti-FLAG pull down. Detection of the corresponding calpain-2 and LOXL2 proteins in the input fractions is shown in the right panel.

interaction between LOXL2 and calpain-2. This increased proteolysis has been related to increased cell motility [23]. Thus, we hypothesize that LOXL2-vimentin interaction and the increased vimentin cleavage, which is partially dependent on calpains, may regulate cytoskeleton dynamics and therefore cell motility. Altogether, our findings suggest a rationale for inhibiting intracellular LOXL2 expression to block ARMS progression.

LOXL2 characterization in ARMS cells reveals high, though variable LOXL2 protein levels compared to ES cells. LOXL2 is a secreted protein that localizes in RMS cell nuclei and cytoplasm, as in multiple other cell types and tissues [8,25]. Due to its complex function and multiple localizations, different correlations between its subcellular distribution and its molecular function and aggressiveness have been established, such us increased cytoplasmic/perinuclear LOXL2 localization and poor prognosis and metastasis [26–28]. Remarkably, LOXL2 staining in tissues from ARMS xenografts or RMS patients is mainly cytoplasmic. In a TMA of RMS human samples, LOXL2 was detected in 35% of the samples showing a tendency towards worse prognosis. In addition, it is important to point out that TMA included different RMS subtypes. When focusing on ARMS samples, positive LOXL2 samples reached 55%. However, lack of clinical information hampered the establishment of a significant correlation with overall survival.

Apart from its role in ECM stabilization, LOXL2 is involved in multiple biological functions related to tumor progression and metastasis in several tumor types. Secreted LOXL2 participates in the remodeling of the ECM of the tumor microenvironment, promoting tumor progression and metastasis [12]. In addition, new intracellular functions of LOXL2 have been described, such as its contribution to the regulation of the epithelial-to-mesenchymal transition [29–31], epithelial cell polarity [25], cell differentiation [26] and cell migration and metastasis [32]. Using cellular models of gain-of-function and loss-of-function we have demonstrated that LOXL2 affects prominently and consistently the migration and invasion *in vitro* and metastasis formation *in vivo*. However, we did not observe a consistent effect on cell viability, since no changes were clearly detected *in vivo*. Our results were in agreement with other reports demonstrating the cell migration, invasion and metastasis promoted by LOXL2 in other tumor entities, without changes in tumor growth [33,34]. Furthermore, transfection of RH28 cells with a LOXL2 catalytically inactive mutant reveals the same competency in increasing the neoplastic phenotype compared to LOXL2 wild type. There is some controversy about the role of LOXL2's catalytic activity. Some functions have been described to be dependent [27,31,35] or independent [25,36,37] on its enzymatic activity. In our model, both LOXL2 wild type and mutant reintroduction increased the neoplastic phenotype of RH28 cells. However, the number of lung metastases in mice injected with LOXL2 wild type cells were slightly higher, but not significantly than LOXL2 mutant cells. Although a role of LOXL2 catalytic activity in tumor microenvironment could not be discarded, a larger number of mice with other clones would be needed to show a significant difference.

LOXL2 contains three predicted N-linked glycosylation sites, two validated by MS in *Drosophila* S2 transfected cells [21], and more recently, all confirmed by MS in HEK transfected cells [38]. In RMS cells, LOXL2 is N-glycosylated in all subcellular fractions and this modification is essential for its secretion. To differentiate between LOXL2 intracellular and extracellular functions, a non-secretable mutant in RH28 cells revealed that cell migration and invasion relies on intracellular LOXL2. In addition, our results underscore the importance of the three glycans in secretion, in contrast to LOXL2 in *Drosophila* S2 cells, where glycans at Asn-455 and Asn-644 are each essential for protein secretion but not at Asn-288 [21,39]. In other models, intracellular LOXL2 is also sufficient to promote EMT [36,39] and increase cell invasion [39].

The present report identifies vimentin as a new LOXL2 partner. RMS cells express high vimentin levels and its expression is important for cell migration and invasion. LOXL2 expression increases vimentin proteolysis, at least partially due to calpains, likely calpain-2, another new LOXL2-interactor. Multiple calpain activating mechanisms have been described: binding to specific membrane phospholipids, interactions with activating proteins, autolysis of the first prodomain, phosphorylation or the unbinding from the endogenous ubiquitous inhibitor Calpastatin [40]. However, how LOXL2-calpain-2 interaction could be affecting calpain-2 activity has not been addressed.

The role of calpains in RMS has been proposed previously, establishing a correlation between calpain expression and cell migratory capacities of RMS cells [41]. In addition, calpain inhibition reduces RMS cell migration and invasion, disturbing actin cytoskeleton organization [41]. Calpains have been related to tumor progression in different tumors and they have an important role in the proteolysis and regulation of cytoskeleton proteins and, therefore, cell motility [42–44]. The relevance of calpain-2 should be confirmed and the role of other members of the family cannot be discarded, though here we have focused on the two calpains that have been more extensively studied and are constitutively expressed [24]. An increase in vimentin proteolysis results in a pool of vimentin fragments that have been correlated to angiogenesis [23] and cell migration and invasion [23,45]. Thus, we hypothesize that LOXL2 increases calpain activity that in turns promotes vimentin proteolysis, which allows an increase in cell motility.

Preliminary data suggests that LOXL2 might be inducing the stem phenotype through activation of the MAPK signaling (data not shown). The exact mechanisms involved in the induction of this putative stem phenotype and its relationship with metastasis will be further explored. We conclude a pro-oncogenic and pro-metastatic role of LOXL2 in ARMS. Therefore, targeting LOXL2-expressing cells may be a new anti-metastatic therapy in ARMS patients, for whom survival decreases drastically with metastatic disease. Until now, the use of LOXL2 inhibitors such as monoclonal antibodies or chemical inhibitors [27,46–48] against the enzymatic activity have not attained expected results [14]. The present analysis of LOXL2 enzymatic function and intracellular LOXL2 role highlights the need for developing specific intracellular inhibitors not focused on the enzymatic activity, such as small molecular inhibitors, since they are likely to have great therapeutic value.

Author contributions

OMT conceived and supervised the study. OA-R designed and performed the main experiments and coordinated the data analysis. PM, MCh-M, SM-M, JH-M, SG-M, IF-H, DH-M and SR-V contributed to the design and conduct of experiments. PHG contributed to the design of experiments. OA-R and RL-A conceived and developed the orthotopical metastasis model. EdA provided the tumor samples. OA-R, RL-A, SR-V, PHG and OMT wrote the manuscript. All authors approved the final manuscript.

Financial support

OMT: *Fundación Alba Pérez lucha contra el cáncer infantil.* Instituto de Salud Carlos III (CES12/021; PI11/00038; PI15/00035; AC14/00026) *and* EU's Fondo Europeo de Desarrollo Regional (FEDER) *"Una manera de hacer Europa*/A way to achieve Europe.*" CERCA Program/Generalitat de Catalunya* (2017SGR332).

OA-R, DH-M: *Fundación Científica de la AECC*.

SG-M, SR-V: *Fundación Alba Pérez lucha contra el cáncer infantil.*

PM: European Union's Horizon 2020 research and innovation program *under Marie Sklodowska-Curie grant agreement ITN*: 766214 – ESR 4.

Declaration of competing interest

The authors declare no potential conflicts of interest.

Acknowledgments

The proteomics analyses were performed in the IDIBELL Clinical Proteomics Unit which is part of the of Proteored, PRB3 and is supported by grant PT17/0019, of the PE I + D + i 2013–2016, funded by ISCIII and ERDF.

Appendix A. Supplementary data

Supplementary data to this article can be found online at https://doi.org/10.1016/j.canlet.2019.12.040.

References

[1] C. De Giovanni, L. Landuzzi, G. Nicoletti, P.-L. Lollini, P. Nanni, Molecular and cellular biology of rhabdomyosarcoma, Future Oncol. 5 (2009) 1449–1475, https://doi.org/10.2217/fon.09.97.
[2] S. Ognjanovic, A.M. Linabery, B. Charbonneau, J.A. Ross, Trends in childhood rhabdomyosarcoma incidence and survival in the United States, 1975-2005, Cancer 115 (2009) 4218–4226, https://doi.org/10.1002/cncr.24465.
[3] E. Davicioni, M.J. Anderson, F.G. Finckenstein, J.C. Lynch, S.J. Qualman, H. Shimada, D.E. Schofield, J.D. Buckley, W.H. Meyer, P.H.B. Sorensen, T.J. Triche, Molecular classification of rhabdomyosarcoma–genotypic and phenotypic determinants of diagnosis: a report from the Children's Oncology Group, Am. J. Pathol. 174 (2009) 550–564, https://doi.org/10.2353/ajpath.2009.080631.
[4] S.J. Xia, J.G. Pressey, F.G. Barr, Molecular pathogenesis of rhabdomyosarcoma, Cancer Biol. Ther. 1 (2002) 97–104, https://doi.org/10.4161/cbt.51.
[5] A.C. Smith, S. Choufani, J.C. Ferreira, R. Weksberg, Growth regulation, imprinted genes, and chromosome 11p15.5, Pediatr. Res. 61 (2007) 43R–47R, https://doi.org/10.1203/pdr.0b013e3180457660.
[6] F.G. Barr, The role of chimeric paired box transcription factors in the pathogenesis of pediatric rhabdomyosarcoma, Cancer Res. 59 (1999) 1711–1715.
[7] J.C. Breneman, E. Lyden, A.S. Pappo, M.P. Link, J.R. Anderson, D.M. Parham, S.J. Qualman, M.D. Wharam, S.S. Donaldson, H.M. Maurer, W.H. Meyer, K.S. Baker, C.N. Paidas, W.M. Crist, Prognostic factors and clinical outcomes in children and adolescents with metastatic rhabdomyosarcoma-a report from the Intergroup Rhabdomyosarcoma Study IV, J. Clin. Oncol. 21 (2003) 78–84, https://doi.org/10.1200/JCO.2003.06.129.
[8] H.-J. Moon, J. Finney, T. Ronnebaum, M. Mure, Human lysyl oxidase-like 2, Bioorg. Chem. 57 (2014) 231–241, https://doi.org/10.1016/j.bioorg.2014.07.003.
[9] K. Csiszar, Lysyl oxidases: a novel multifunctional amine oxidase family, Prog. Nucleic Acid Res. Mol. Biol. 70 (2001) 1–32, https://doi.org/10.1016/S0079-6603(01)70012-8.
[10] J.L. Grimsby, H.A. Lucero, P.C. Trackman, K. Ravid, H.M. Kagan, Role of lysyl oxidase propeptide in secretion and enzyme activity, J. Cell. Biochem. 111 (2010) 1231–1243, https://doi.org/10.1002/jcb.22845.
[11] K. Okada, H.J. Moon, J. Finney, A. Meier, M. Mure, Extracellular processing of lysyl oxidase- like 2 and its effect on amine oxidase activity, Biochemistry 57 (2018) 6973–6983, https://doi.org/10.1021/acs.biochem.8b01008.
[12] Q. Xiao, G. Ge, Lysyl Oxidase, Extracellular matrix remodeling and cancer metastasis, Cancer Microenviron 5 (2012) 261–273, https://doi.org/10.1007/s12307-012-0105-z.
[13] A. Mayorca-Guiliani, J.T. Erler, The potential for targeting extracellular LOX proteins in human malignancy, OncoTargets Ther. 6 (2013) 1729–1735, https://doi.org/10.2147/OTT.S38110.
[14] L. Wu, Y. Zhu, The function and mechanisms of action of LOXL2 in cancer (Review), Int. J. Mol. Med. 36 (2015) 1200–1204, https://doi.org/10.3892/ijmm.2015.2337.
[15] A. Cano, P.G. Santamaría, G. Moreno-Bueno, LOXL2 in epithelial cell plasticity and tumor progression, Future Oncol. 8 (2012) 1095–1108, https://doi.org/10.2217/fon.12.105.
[16] M. Sáinz-Jaspeado, J. Huertas-Martinez, L. Lagares-Tena, J. Martin Liberal, S. Mateo-Lozano, E. de Alava, C. de Torres, J. Mora, X.G. de Muro, O.M. Tirado, EphA2-Induced angiogenesis in ewing sarcoma cells works through bFGF production and is dependent on Caveolin-1, PLoS One 8 (2013) e71449, , https://doi.org/10.1371/journal.pone.0071449.
[17] L. Lagares-Tena, S. García-Monclús, R. López-Alemany, O. Almacellas-Rabaiget, J. Huertas-Martínez, M. Sáinz-Jaspeado, S. Mateo-Lozano, C. Rodríguez-Galindo, S. Rello-Varona, D. Herrero-Martín, O.M. Tirado, Caveolin-1 promotes Ewing sarcoma metastasis regulating MMP-9 expression through MAPK/ERK pathway, Oncotarget 7 (2016) 56889–56903, https://doi.org/10.18632/oncotarget.10872.
[18] A.H. Palamakumbura, P.C. Trackman, A fluorometric assay for detection of lysyl oxidase enzyme activity in biological samples, Anal. Biochem. 300 (2002) 245–251, https://doi.org/10.1006/abio.2001.5464.
[19] S. Garcia-Monclús, R. López-Alemany, O. Almacellas-Rabaiget, D. Herrero-Martín, J. Huertas-Martinez, L. Lagares-Tena, P. Alba-Pavón, L. Hontecillas-Prieto, J. Mora, E. de Álava, S. Rello-Varona, P.H. Giangrande, O.M. Tirado, EphA2 receptor is a key player in the metastatic onset of Ewing sarcoma, Int. J. Cancer 143 (2018) 1188–1201, https://doi.org/10.1002/ijc.31405.
[20] M.W. Pfaffl, A new mathematical model for relative quantification in real-time RT-PCR, Nucleic Acids Res. 29 (2001) e45.
[21] L. Xu, E.P. Go, J. Finney, H.J. Moon, M. Lantz, K. Rebecchi, H. Desaire, M. Mure, Post-translational modifications of recombinant human lysyl oxidase-like 2 (rhLOXL2) secreted from drosophila S2 cells, J. Biol. Chem. 288 (2013) 5357–5363, https://doi.org/10.1074/jbc.C112.421768.
[22] A. Satelli, S. Li, Vimentin in cancer and its potential as a molecular target for cancer therapy, Cell. Mol. Life Sci. 68 (2011) 3033–3046, https://doi.org/10.1007/s00018-011-0735-1.
[23] J.M. Dave, K.J. Bayless, Vimentin as an integral regulator of cell adhesion and endothelial sprouting, Microcirculation 21 (2014) 333–344, https://doi.org/10.1111/micc.12111.
[24] D.E. Goll, V.F. Thompson, H. Li, W. Wei, J. Gong, The calpain system, Physiol. Rev. 83 (2003) 731–801, https://doi.org/10.1152/physrev.00029.2002.
[25] G. Moreno-Bueno, F. Salvador, A. Martín, A. Floristán, E.P. Cuevas, V. Santos, A. Montes, S. Morales, M.A. Castilla, A. Rojo-Sebastián, A. Martínez, D. Hardisson, K. Csiszar, F. Portillo, H. Peinado, J. Palacios, A. Cano, Lysyl oxidase-like 2 (LOXL2), a new regulator of cell polarity required for metastatic dissemination of basal-like breast carcinomas, EMBO Mol. Med. 3 (2011) 528–544, https://doi.org/10.1002/emmm.201100156.
[26] H. Peinado, G. Moreno-Bueno, D. Hardisson, E. Pérez-Gómez, V. Santos, M. Mendiola, J.I. De Diego, M. Nistal, M. Quintanilla, F. Portillo, A. Cano, Lysyl oxidase-like 2 as a new poor prognosis marker of squamous cell carcinomas, Cancer Res. 68 (2008) 4541–4550, https://doi.org/10.1158/0008-5472.CAN-07-6345.
[27] L. Peng, Y.-L. Ran, H. Hu, L. Yu, Q. Liu, Z. Zhou, Y.-M. Sun, L.-C. Sun, J. Pan, L.-X. Sun, P. Zhao, Z.-H. Yang, Secreted LOXL2 is a novel therapeutic target that promotes gastric cancer metastasis via the Src/FAK pathway, Carcinogenesis 30 (2009) 1660–1669, https://doi.org/10.1093/carcin/bgp178.
[28] T.Y. Li, L.Y. Xu, Z.Y. Wu, L. Di Liao, J.H. Shen, X.E. Xu, Z.P. Du, Q. Zhao, E.M. Li, Reduced nuclear and ectopic cytoplasmic expression of lysyl oxidase-like 2 is associated with lymph node metastasis and poor prognosis in esophageal squamous cell carcinoma, Hum. Pathol. 43 (2012) 1068–1076, https://doi.org/10.1016/j.humpath.2011.07.027.
[29] H. Peinado, M.D. Iglesias-de la Cruz, D. Olmeda, K. Csiszar, K.S.K. Fong, S. Vega, M.A. Nieto, A. Cano, F. Portillo, A molecular role for lysyl oxidase-like 2 enzyme in Snail regulation and tumor progression, EMBO J. 24 (2005) 3446–3458, https://doi.org/10.1038/sj.emboj.7600781.
[30] E.P. Cuevas, P. Eraso, M.J. Mazón, V. Santos, G. Moreno-Bueno, A. Cano, F. Portillo, LOXL2 drives epithelial-mesenchymal transition via activation of IRE1-XBP1 signalling pathway, Sci. Rep. 7 (2017) 44988, https://doi.org/10.1038/srep44988.
[31] N. Herranz, N. Dave, A. Millanes-Romero, L. Pascual-Reguant, L. Morey, V.M. Díaz, V. Lórenz-Fonfría, R. Gutierrez-Gallego, C. Jerónimo, A. Iturbide, L. Di Croce, A. García de Herreros, S. Peiró, Lysyl oxidase-like 2 (LOXL2) oxidizes trimethylated lysine 4 in histone H3, FEBS J. 283 (2016) 4263–4273, https://doi.org/10.1111/febs.13922.
[32] P. Hollosi, J.K. Yakushiji, K.S.K. Fong, K. Csiszar, S.F.T. Fong, Lysyl oxidase-like 2 promotes migration in noninvasive breast cancer cells but not in normal breast epithelial cells, Int. J. Cancer 125 (2009) 318–327, https://doi.org/10.1002/ijc.24308.
[33] H.E. Barker, J. Chang, T.R. Cox, G. Lang, D. Bird, M. Nicolau, H.R. Evans, A. Gartland, J.T. Erler, LOXL2-mediated matrix remodeling in metastasis and mammary gland involution, Cancer Res. 71 (2011) 1561–1572, https://doi.org/10.1158/0008-5472.CAN-10-2868.
[34] R. Nishikawa, T. Chiyomaru, H. Enokida, S. Inoguchi, T. Ishihara, R. Matsushita, Y. Goto, I. Fukumoto, M. Nakagawa, N. Seki, Tumour-suppressive microRNA-29s directly regulate LOXL2 expression and inhibit cancer cell migration and invasion in renal cell carcinoma, FEBS Lett. 589 (2015) 2136–2145, https://doi.org/10.1016/j.febslet.2015.06.005.
[35] A. Iturbide, L. Pascual-Reguant, L. Fargas, J.P. Cebrià, B. Alsina, A.G. de Herreros, S. Peiró, LOXL2 oxidizes methylated TAF10 and controls TFIID-dependent genes during neural progenitor differentiation, Mol. Cell 58 (2015) 755–766, https://doi.org/10.1016/j.molcel.2015.04.012.
[36] E.P. Cuevas, G. Moreno-Bueno, G. Canesin, V. Santos, F. Portillo, A. Cano, LOXL2 catalytically inactive mutants mediate epithelial-to-mesenchymal transition, Biol. Open. 3 (2013) 129–137, https://doi.org/10.1242/bio.20146841.
[37] J. Lugassy, S. Zaffryar-Eilot, S. Soueid, A. Mordoviz, V. Smith, O. Kessler, G. Neufeld, The enzymatic activity of lysyl oxidas-like-2 (LOXL2) is not required for LOXL2-induced inhibition of keratinocyte differentiation, J. Biol. Chem. 287 (2012) 3541–3549, https://doi.org/10.1074/jbc.M111.261016.
[38] E.P. Go, H.-J. Moon, M. Mure, H. Desaire, Recombinant human lysyl oxidase-like 2 secreted from human embryonic kidney cells displays complex and acidic glycans at all three N-linked glycosylation sites, J. Proteome Res. 17 (2018) 1826–1832, https://doi.org/10.1021/acs.jproteome.7b00849.
[39] H.J. Moon, J. Finney, L. Xu, D. Moore, D.R. Welch, M. Mure, MCF-7 cells expressing nuclear associated lysyl oxidase-like 2 (LOXL2) exhibit an epithelial-to-Mesenchymal transition (EMT) phenotype and are highly invasive in Vitro, J. Biol. Chem. 288 (2013) 30000–30008, https://doi.org/10.1074/jbc.C113.502310.
[40] D. Moretti, B. Del Bello, G. Allavena, E. Maellaro, Calpains and cancer: friends or enemies? Arch. Biochem. Biophys. 564 (2014) 26–36, https://doi.org/10.1016/j.abb.2014.09.018.
[41] H. Roumes, L. Leloup, E. Dargelos, J.-J. Brustis, L. Daury, P. Cottin, Calpains: markers of tumor aggressiveness? Exp. Cell Res. 316 (2010) 1587–1599, https://doi.org/10.1016/j.yexcr.2010.02.017.
[42] A. Glading, D.A. Lauffenburger, A. Wells, Cutting to the chase: calpain proteases in cell motility, Trends Cell Biol. 12 (2002) 46–54, https://doi.org/10.1016/S0962-8924(01)02179-1.
[43] M.-C. Lebart, Y. Benyamin, Calpain involvement in the remodeling of cytoskeletal anchorage complexes, FEBS J. 273 (2006) 3415–3426, https://doi.org/10.1111/j.1742-4658.2006.05350.x.

[44] S.J. Franco, A. Huttenlocher, Regulating cell migration: calpains make the cut, J. Cell Sci. 118 (2005) 3829–3838, https://doi.org/10.1242/jcs.02562.
[45] B.T. Helfand, M.G. Mendez, S.N.P. Murthy, D.K. Shumaker, B. Grin, S. Mahammad, U. Aebi, T. Wedig, Y.I. Wu, K.M. Hahn, M. Inagaki, H. Herrmann, R.D. Goldman, Vimentin organization modulates the formation of lamellipodia, Mol. Biol. Cell 22 (2011) 1274–1289, https://doi.org/10.1091/mbc.E10-08-0699.
[46] J. Chang, M.C. Lucas, L.E. Leonte, M. Garcia-Montolio, L.B. Singh, A.D. Findlay, M. Deodhar, J.S. Foot, W. Jarolimek, P. Timpson, J.T. Erler, T.R. Cox, J. Chang, M.C. Lucas, L.E. Leonte, M. Garcia-Montolio, L. Babloo Singh, A.D. Findlay, M. Deodhar, J.S. Foot, W. Jarolimek, P. Timpson, J.T. Erler, T.R. Cox, J. Chang, M.C. Lucas, L.E. Leonte, M. Garcia-Montolio, L.B. Singh, A.D. Findlay, M. Deodhar, J.S. Foot, W. Jarolimek, P. Timpson, J.T. Erler, T.R. Cox, Pre-clinical evaluation of small molecule LOXL2 inhibitors in breast cancer, Oncotarget 8 (2017) 26066–26078, https://doi.org/10.18632/oncotarget.15257.
[47] H.M. Rodriguez, M. Vaysberg, A. Mikels, S. McCauley, A.C. Velayo, C. Garcia, V. Smith, Modulation of lysyl oxidase-like 2 enzymatic activity by an allosteric antibody inhibitor, J. Biol. Chem. 285 (2010) 20964–20974, https://doi.org/10.1074/jbc.M109.094136.
[48] V. Barry-Hamilton, R. Spangler, D. Marshall, S. McCauley, H.M. Rodriguez, M. Oyasu, A. Mikels, M. Vaysberg, H. Ghermazien, C. Wai, C.A. Garcia, A.C. Velayo, B. Jorgensen, D. Biermann, D. Tsai, J. Green, S. Zaffryar-Eilot, A. Holzer, S. Ogg, D. Thai, G. Neufeld, P. Van Vlasselaer, V. Smith, Allosteric inhibition of lysyl oxidase–like-2 impedes the development of a pathologic microenvironment, Nat. Med. 16 (2010) 1009–1017, https://doi.org/10.1038/nm.2208.